

INFORMATION TO USERS

This manuscript has been reproduced from the microfilm master. UMI films the text directly from the original or copy submitted. Thus, some thesis and dissertation copies are in typewriter face, while others may be from any type of computer printer.

The quality of this reproduction is dependent upon the quality of the copy submitted. Broken or indistinct print, colored or poor quality illustrations and photographs, print bleedthrough, substandard margins, and improper alignment can adversely affect reproduction.

In the unlikely event that the author did not send UMI a complete manuscript and there are missing pages, these will be noted. Also, if unauthorized copyright material had to be removed, a note will indicate the deletion.

Oversize materials (e.g., maps, drawings, charts) are reproduced by sectioning the original, beginning at the upper left-hand corner and continuing from left to right in equal sections with small overlaps.

Photographs included in the original manuscript have been reproduced xerographically in this copy. Higher quality 6" x 9" black and white photographic prints are available for any photographs or illustrations appearing in this copy for an additional charge. Contact UMI directly to order.

**ProQuest Information and Learning
300 North Zeeb Road, Ann Arbor, MI 48106-1346 USA
800-521-0600**

UMI[®]

**USING COMMERCIAL FINITE ELEMENT CODE CALLED ABAQUS IN
MODELING HYBRID CONSTRAINED LAYERS DAMPING BEAM
STRUCTURE
AND
QUANTITATIVE DETERMINATION OF THE STABILITY OF IMPLANT-BONE
INTERFACE USING RESONANCE FREQUENCY ANALYSIS.**

A Thesis

by

DANIEL DELGADO JR

**Submitted to the Graduate School of the
University of Texas-Pan American
In partial fulfillment of the requirements for the degree of
MASTER OF SCIENCE**

MAY 2002

Major Subject: Mechanical Engineering

UMI Number: 1409777

**Copyright 2002 by
Delgado, Daniel, Jr.**

All rights reserved.

UMI[®]

UMI Microform 1409777

**Copyright 2002 by ProQuest Information and Learning Company.
All rights reserved. This microform edition is protected against
unauthorized copying under Title 17, United States Code.**

**ProQuest Information and Learning Company
300 North Zeeb Road
P.O. Box 1346
Ann Arbor, MI 48106-1346**

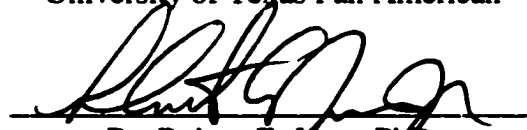
**USING COMMERCIAL FINITE ELEMENT CODE CALLED ABAQUS IN
MODELING HYBRID CONSTRAINED LAYERS DAMPING BEAM
STRUCTURE
AND
QUANTITATIVE DETERMINATION OF THE STABILITY OF IMPLANT-
BONE INTERFACE USING RESONANCE FREQUENCY ANALYSIS.**

**A Thesis
By
DANIEL DELGADO JR.**

Approved as to style and content by:



**Dr. Arturo Fuentes PhD., Chair
Assistant Professor
University of Texas Pan American**



**Dr. Robert E. Jones PhD.
Associate Professor
University of Texas Pan American**



**Dr. Arnold Lumsdaine PhD.
Associate Professor
University of Tennessee at Knoxville**



**Dr. Hashim S. Mahdi PhD.
Chair of the Mechanical Engineering Dept.
University of Texas Pan American**

May 2002

ACKNOWLEDGEMENTS

The author gratefully acknowledge the support of the University of Texas Pan American Mechanical Engineering Department Staff and Faculty have been great to me and I have benefited greatly from all of them and of the Straumann Foundation through the department of Prosthetic dentistry at the University of Texas Health Science Center at San Antonio.

DEDICATION

This thesis is dedicated to my wife

Guadalupe V. Delgado

who has given me invaluable educational opportunities and support.

Copyright ©Daniel Delgado, 2002

All rights reserved

TABLE OF CONTENTS

ACKNOWLEDGEMENTS	iii
DEDICATION	iv
COPYRIGHTS	v
TABLE OF CONTENTS	vi
LIST OF FIGURES	viii
LIST OF TABLES	ix
NOMENCLATURE	x
PREFACE	xi
ABSTRACT	xiii

1.0 CHAPTER 1: USING COMMERCIAL FINITE ELEMENT CODE CALLED ABAQUS IN MODELING HYBRID CONSTRAINED LAYERS DAMPING BEAM STRUCTURE

1.1 Introduction	1
1.2 Technical Background	2
1.3 Finite Elements Modeling	3
1.4 Active Constrained Layer Beam-No Control	7
1.5 Results	8
1.6 Conclusion	8

2.0 CHAPTER 2: QUANTITATIVE DETERMINATION OF THE STABILITY OF IMPLANT-BONE INTERFACE USING RESONANCE FREQUENCY ANALYSIS

2.1 Introduction	10
2.2 Technical Background	11
2.3 Problem Analysis	12
2.4 Results	19
2.5 Conclusion	31

3.0 APPENDICES

A. The ABAQUS Results from GETMAX and RESULT3	32
B. ABAQUS Codes files	37
C. IDEAS FEA Results for Implant Model	41
D. Signal CAL ACE Software Graph Results	48

E. MATHCAD Solution for Theoretical Values.....	154
4.0 REFERENCES	159
5.0 VITA.....	161

LIST OF FIGURES

FIGURE 1-1: TWO DIFFERENT ACTIVE CONSTRAINED LAYER BEAM CONFIGURATIONS	3
FIGURE 1-2: BAZ AND RO ACLD BEAM.....	7
FIGURE 2-1: MEREDITH INSTRUMENTATION DESIGN.....	12
FIGURE 2-2: FIXTURE DESIGN	14
FIGURE 2-3: FIXTURE, ABUTMENT, AND IMPLANT (NOT ASSEMBLED)	14
FIGURE 2-4: TOP VIEW OF THE INSTRUMENTATION.....	15
FIGURE 2-5: INSTRUMENTATION CONFIGURATION	16
FIGURE 2-6: AXIAL MODE	17
FIGURE 2-7: TORSIONAL MODE.....	17
FIGURE 2-8: HIGHER BENDING MODE	18
FIGURE 2-9: LOWER BENDING MODE	18
FIGURE 2-10: FINITE ELEMENT SIMPLIFIED MODEL	20
FIGURE 2-11: ANALYTICAL SIMPLIFIED MODEL	20
FIGURE 2-12: EXPERIMENTAL RESULTS (BRASS MOUNT)	21
FIGURE 2-13: RESPONSE OF BRASS (LEFT) VS ACRYLIC (RIGHT) MOUNT [TORSIONAL MODE].....	23
FIGURE 2-14: TORSION MODE FOR ACRYLIC MOUNTS WITH OVERSIZED PREDRILLED HOLE [0.144 IN]	24
FIGURE 2-15: TORSION MODE FOR ACRYLIC MOUNTS WITH OVERSIZED PREDRILLED HOLE [0.153 IN]	25
FIGURE 2-16: RESPONSE OF IMPLANT WITH ACRYLIC MOUNT WITH OVERSIZED PREDRILLED HOLE (0.144IN.) [LOWER BENDING AND AXIAL MODE].....	25
FIGURE 2-17: RESPONSE OF IMPLANT WITH ACRYLIC MOUNT WITH OVERSIZED PREDRILLED HOLE (0.153IN.) [LOWER BENDING AND AXIAL MODE].....	26
FIGURE 2-18: RESPONSE OF IMPLANT WITH ACRYLIC MOUNT AND OVERSIZED PREDRILLED HOLE (0.144IN.) [HIGHER BENDING AND AXIAL MODE].....	26
FIGURE 2-19: RESPONSE OF IMPLANT WITH ACRYLIC MOUNT WITH OVERSIZED PREDRILLED HOLE (0.153IN.) [HIGHER BENDING AND AXIAL MODE].....	27
FIGURE 2-20: UPPER AND LOWER MOUNTS FOR TABLE 2-6	28
FIGURE 2-21: CURING ACRYLIC MOUNT	28
FIGURE 2-22: EXPERIMENTAL MOUNTS FOR TABLES 2-9—2-11 RESULTS	30
FIGURE 2-23: HALF THREADED MOUNT	30

LIST OF TABLES

TABLE 1-1: MATERIAL PROPERTIES FOR BAZ AND RO BEAM	8
TABLE 1-2: RESULTS FOR ACLD BEAM WITHOUT ACTIVE CONTROL.....	8
TABLE 1-3: RESULTS FOR ACLD BEAM WITH ACTIVE CONTROL.....	8
TABLE 2-1: COMPARISON OF THE FEA AND ANALYTICAL SOLUTION.....	20
TABLE 2-2: FIXTURE'S DIMENSIONS	20
TABLE 2-3: COMPARISON OF THE FEA AND EXPERIMENTAL RESULTS	22
TABLE 2-4: COMPARISON OF THE BRASS AND ACRYLIC MOUNTS	23
TABLE 2-5: COMPARISONS OF NATURAL FREQUENCIES AND DAMPING FACTORS FOR IMPLANTS WITH ACRYLIC MOUNTS WITH DIFFERENT FITS.....	24
TABLE 2-6: ACRYLIC MOUNTS HALF THREADED CASES COMPARISONS.	27
TABLE 2-7: ACRYLIC RESIN CURING TIME FREQUENCIES READINGS	28
TABLE 2-8: HALF THREADED ACRYLIC MOUNT COMPARISONS TO FULL THREADED ACRYLIC MOUNT.....	29
TABLE 2-9: HOLE ON ONE SIDE OF THE IMPLANT COMPARISON TO FULL THREADED ACRYLIC MOUNT.....	29
TABLE 2-10: HOLE ON BOTH SIDES OF THE IMPLANT COMPARISON TO FULL THREADED ACRYLIC MOUNT.....	29
TABLE 2-11: SHORT HALF THREADED ACRYLIC MOUNT COMPARISONS TO FULL THREADED ACRYLIC MOUNT	29

NOMENCLATURE

<p>A = surface area</p> <p>C = capacitance</p> <p>D_{ijkl} = mechanical constitutive tensor</p> <p>D = elastic modulus</p> <p>D^* = dynamic elastic modulus</p> <p>D_1 = elastic storage modulus</p> <p>D_2 = elastic loss modulus</p> <p>E_j = electric field</p> <p>(F) = mechanical force vector</p> <p>G^* = dynamic shear modulus</p> <p>G_1 = shear storage modulus</p> <p>G_2 = shear loss modulus</p> <p>G_p = proportional gain constant</p> <p>[I] = identity matrix</p> <p>K^* = dynamic bulk modulus</p> <p>K_1 = shear bulk modulus</p> <p>K_2 = shear bulk modulus</p> <p>[K] = stiffness bulk modulus</p> <p>$[K_{uu}]$ = mechanical submatrix of the stiffness matrix</p> <p>$[K_{u\phi}]$ = piezoelectric coupling submatrix of the stiffness matrix</p> <p>$[K_{\phi\phi}]$ = electrical submatrix of the stiffness matrix</p> <p>[M] = mass matrix</p>	<p>M = bending moment</p> <p>(Q) = electrical charge vector</p> <p>[T] = transformation matrix</p> <p>W_d = energy loss per cycle</p> <p>W_s = peak energy stored per cycle</p> <p>a = subscript, referring to actuator</p> <p>e_{ijk} = piezoelectric stress coefficients</p> <p>h = thickness of layer</p> <p>p = pressure</p> <p>p_{ij} = dielectric constant (permittivity)</p> <p>q_i = electric displacement</p> <p>s = subscript, referring to sensor</p> <p>u = displacement</p> <p>x = Cartesian dimension</p> <p>ϵ_{ij} = strain tensor</p> <p>η = system loss factor</p> <p>η_m = material loss factor</p> <p>ϕ = electric potential</p> <p>ν = Poisson's ratio</p> <p>ν^* = dynamic Poisson's ratio</p> <p>σ_{ij} = stress tensor</p> <p>ω_r = resonance frequency</p> <p>ω_1, ω_2 = half-power frequencies</p>
--	--

PREFACE

Vibration study and control of structures is among the major research subjects in mechanical engineering and related technical disciplines. Among the most active research in the area, one finds the following two issues. On one hand, conventional structural designs are often unacceptable in coping with modern problems of structural resonance caused by the complex nature of dynamic environments and the requirements of design objectives, including low noise, light weight, long life, and increased reliability. On the other hand, structural dynamic characteristics can be used to infer information of the integrity and the boundary conditions of a structure.

In chapter 1, we focus on controlling vibrations in beam structures and then focus on how to model composite beams in Finite Elements without developing your own Finite Element code. It has been demonstrated that the damping treatments for beam and plate structures are effective, and the vibrational behaviors of the systems considered are influenced by many geometrical and material parameters. Therefore, one approach to solving the high vibration and noise levels of structural resonance problems is to incorporate a high-energy-dissipating mechanism into the structure during fabrication with surface damping treatments. Surface damping treatments are usually classified as extensional or shear damping treatments. Shear damping treatments include Passive Constrained Layer Damping (PCLD) and Active Constrained Layer Damping (ACLD). For a given weight, the shear type of damping treatment is more efficient than the

extensional or unconstrained layer-damping treatment. However, this efficiency is balanced by greater complication in analysis and application.

In extensional damping, the structure is coated on one or both sides with damping materials. Therefore, when it is subjected to cyclic loading, the damping material will be subjected to tension-compression deformation. On the other hand, PCLD systems consist of a stiff constraining layer placed on a viscoelastic material (VEM) layer, providing energy dissipation primarily from shearing in that layer. ACLD systems generally consist of a piece of VEM layer sandwiched between an active piezoelectric layer and a host structure. The main purpose of using a piezoelectric coversheet is its active action that enhances the VEM layer damping ability by increasing the shear angle during operation. However, separate active and passive designs are considered if high active action is needed since the VEM will reduce the active authority of the piezoelectric layer.

In Chapter 2, we develop a quantitative method to establish a standard way to measure stability and osseointegration of implants based on resonance frequency analysis. Among other benefits, these measurements would provide information leading to the prediction of healing time and the implant and the monitoring of the health of the implant's interface.

ABSTRACT

Delgado, Daniel, Using Commercial Finite Element Code Called ABAQUS In Modeling Hybrid Constrained Layers Damping Beam Structure and Quantitative Determination Of The Stability Of Implant-Bone Interface Using Resonance Frequency Analysis. Master of Science (MS), May, 2002, 161 pp., 24 Figures, 14 tables, references, 26 titles.

In Chapter 1, it has been demonstrated that the damping treatments for beam and plate structures are effective, and the vibrational behaviors of the systems considered are influenced by many geometrical and material parameters. This has led to an interest in developing advanced “intelligent” structures. In the past, passive and active damping mechanisms have been used to reduce vibration. The uses of passive constrained layers are limited, but it has dissipative qualities for all the modes of the structure; and the uses of active constrained layers are limited to a single mode control. Recent published papers, many have suggested that a hybrid of active and passive would be the best method to use, but many have to create their own Finite Element Method code to model these hybrids structures and experimentally validate the FEM code. In this chapter we focus on active and passive constrained layers for damping structures, and we have been modeling these structures in a commercial code called ABAQUS. Therefore, the code is going to be validated with experimental and theoretical data of previous paper and determining that the code is accurate to the experimental and theoretical value give the certain material properties, and it can also be used for other structures that are more complex.

In Chapter 2, it is important to have a quantitative method to establish a standard way to measure stability and osseointegration of implants. Among other benefits, these measurements would provide information leading to the prediction of healing time and the implant and the monitoring of the health of the implant's interface.

The dental industry has been looking for non-destructive methods to measure implant integration within the bone. In previous studies, resonance frequency analysis revealed a clear relationship between resonance frequency measurements and stiffness of the implant interface and the effective length of the implant. Earlier studies have examined only one mode of vibration or have suffered from measurement difficulties. Furthermore, no study has evaluated the damping properties of the interface and surrounding tissues.

This chapter describes the development of an instrument capable of capturing and measuring information to characterize the process of dental implant osseointegration.

The parameters needed to measure stability and osseointegration of implants are the stiffness of the implant components (which are a function of their geometry and material composition) and the stiffness and damping properties of the implant-bone interface and surrounding tissues. The instrument developed provides valuable information about the stiffness and damping properties of the implant-bone interface obtained through resonance frequency analysis with torsional, longitudinal and transverse vibration.

Experimental, analytical, and finite element analysis results are presented.

CHAPTER 1

USING COMMERCIAL FINITE ELEMENT CODE CALLED ABAQUS IN MODELING HYBRID CONSTRAINED LAYERS DAMPING BEAM STRUCTURE

1.1 Introduction

There has to be an introduction to the theory and conception behind ACLD and PCLD. According to Lumsdaine (Lumsdaine et. al.), hybrid constrained layer damping have not been model with Finite Element Method commercial code, but using a commercial code would let many studies in ACLD and PCLD to continue without a great deal of investment and getting fully equip with many different testing models. Using Finite Element code, you can also develop many changes of the model without many difficulties than in experimental testing, it can become very expense to change the model. Also, creating you own Finite Element code can be long time consuming task to under take because you have to a good understanding on how Finite Element Method are used, and this will take years of experiences to accomplish. If you do not have the expertise, you can get into a problem that cannot be notices by the code that you create; so you will have an uncertainly on your solution because it my take many different tries to decode and fix all the problems with your code. In using a commercial code, ABAQUS can be a better and easier place to start modeling advanced “intelligent” structures by incorporating sensors, actuators into your model. Controlling mechanical systems has become an increasing interesting by many aerospace industries in advancement studies in space structures. In development of these structures, there has to be a faster way to develop and

test these models. In this chapter, I will try to use a commercial code called ABAQUS in developing models of these advanced structures.

1.2 Technical Background

In reviewing recent papers, the construction of an ACLD layer is as follows. According to Lumsdaine (Lumsdaine et. al.), a piezoelectric ceramic actuator is used as a constraining layer in the place of the simple elastic structure. This can produce additional vibration damping through two means, one active and one passive. Actively, the actuator provides a restoring moment to the base structure, attenuating its motion. This active effect is less than it would be if attached directly to the beam, as it must act through a compliant viscoelastic layer. Passively, the actuator contracts and expands at points in the vibration cycle which induces a greater shearing strain in the damping layer than would be possible in the purely passive case. (Lumsdaine et. al.) The problem is that where would it be the best placement of the actuator and sensor to give the best response. Figure 1-1 shows some examples of two alternative structures of the sensor and the actuator.

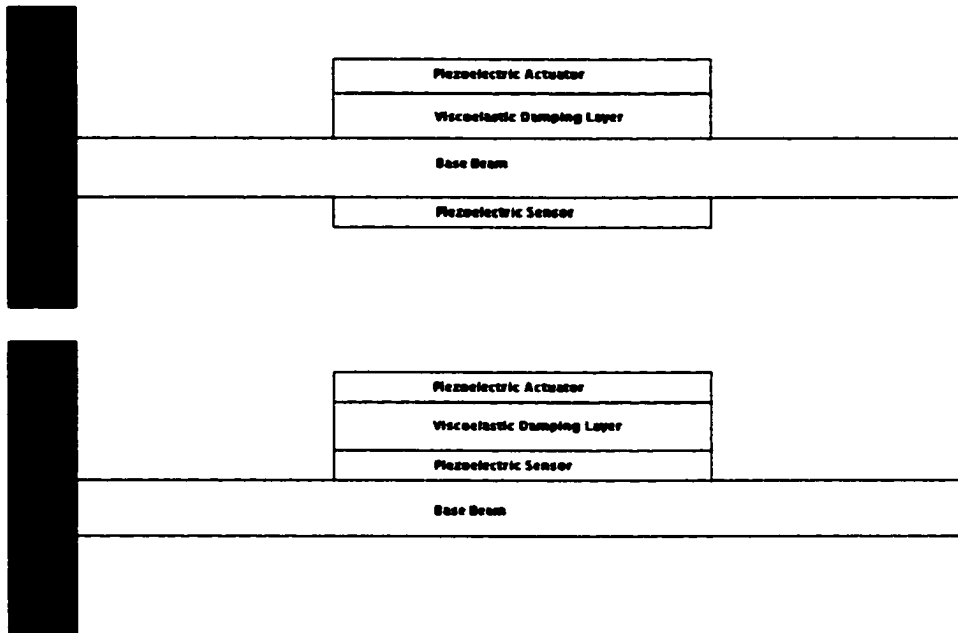


Figure 1-1 Two different Active Constrained Layer Beam Configurations.

1.3 Finite Elements Modeling

In finite elements modeling, the structures should be broken up into three parts. The first one is the basic finite elements equations for a beam structure. The constitutive relationship for beam material can be written as (Lumsdaine et. al.):

$$\sigma_{ij} = D_{ijkl} \epsilon_{kl} \quad (1.1)$$

The finite elements equations can be written as:

$$[M](\ddot{u}) + [K](u) = (F) \quad (1.2)$$

Lumsdaine (Lumsdaine et al) paper derived the following steps to model the structure.

The second one is the basic finite elements equations for piezoelectricity. The constitutive relationship for piezoelectricity material can be written as:

$$\sigma_{ij} = D_{ijkl} \epsilon_{kl} - e_{mij} E_m \quad (1.3)$$

$$q_i = e_{ijk} \varepsilon_{jk} + p_{ij} E_j \quad (1.4)$$

The finite element equation for a piezoelectric structure can be written as:

$$[M](\ddot{u}) + [K_{uu}](u) + [K_{u\phi}](\phi) = (F) \quad (1.5)$$

$$[K_{u\phi}]^T(u) + [K_{\phi\phi}](\phi) = (Q) \quad (1.6)$$

In a static problem, these can be expressed as:

$$\begin{bmatrix} K_{uu} & K_{u\phi} \\ K_{u\phi}^T & K_{\phi\phi} \end{bmatrix} \begin{bmatrix} u \\ \phi \end{bmatrix} = \begin{bmatrix} F \\ Q \end{bmatrix} \quad (1.7)$$

If this is pre-multiplied by a transformation matrix:

$$[T] = [[I] - [K_{u\phi}][K_{\phi\phi}]] \quad (1.8)$$

the following condensed matrix is obtained, with the electric potential degrees of freedom removed:

$$[[K_{uu}] - [K_{u\phi}][K_{\phi\phi}]^{-1}[K_{u\phi}]^T](u) = (F) - [K_{u\phi}][K_{\phi\phi}]^{-1}(Q) \quad (1.9)$$

where the term $[K_{\phi\phi}]^{-1}[K_{u\phi}]^T(Q)$ represents the feedback control force. Given that the electric charge (Q) is zero, in the sensor, Equation (1.6) can be rewritten as:

$$(\phi)_s = -[K_{\phi\phi}]^{-1}[K_{u\phi}]^T(u)_s \quad (1.10)$$

Proportional control is used in the ABAQUS model examined here. In proportional feedback control, the electric potential in the actuator is related to the potential in the sensor through a gain, as in equation below:

$$(\phi)_a = G_p(\phi)_s \quad (1.11)$$

the potential applied to the actuator is given by the following equation:

$$(Q)_a = C(\phi)_a = CG_p(\phi)_s \quad (1.12)$$

where the capacitance is defined as:

$$C = \frac{p_{22}A}{h} \quad (1.13)$$

Inserting equation (1.10) and (1.12) into equation (1.9) yields the finite elements equations of motions:

$$[M](\ddot{u}) + [K^*](u) = (F) \quad (1.14)$$

Here is the user defines finite elements equations:

$$\begin{bmatrix} F_s \\ Q_s \\ F_a \\ Q_a \end{bmatrix} = \begin{bmatrix} 0 & 0 & 0 & 0 \\ 0 & 0 & 0 & 0 \\ 0 & G_p K_{u\phi} & 0 & -K_{u\phi} \\ 0 & G_p K_{\phi\phi} & 0 & -K_{\phi\phi} \end{bmatrix} \begin{bmatrix} u_s \\ \phi_s \\ u_a \\ \phi_a \end{bmatrix} \quad (1.14a)$$

Where $[K^*]$ is:

$$[K^*] = \begin{bmatrix} K_{uu} & K_{u\phi} & 0 & 0 \\ K_{u\phi}^T & K_{\phi\phi} & 0 & 0 \\ 0 & 0 & K_{uu} & K_{u\phi} \\ 0 & 0 & K_{u\phi}^T & K_{\phi\phi} \end{bmatrix}, \text{original form (Lumsdaine et. al.)} \quad (1.14b)$$

$$[K^*] = \begin{bmatrix} 0 & 0 & 0 & 0 \\ 0 & 0 & 0 & 0 \\ 0 & G_p K_{u\phi} & 0 & -K_{u\phi} \\ 0 & G_p K_{\phi\phi} & 0 & -K_{\phi\phi} \end{bmatrix}, \text{new form} \quad (1.15)$$

As mentioned above, ABAQUS has the capability of exporting the elements stiffness matrices. From each element stiffness matrix, the matrices $[K_{u\phi}]$, and $[K_{\phi\phi}]$ are needed to be extracted in order to compute the matrix $[K^*]$.

The third one is the basic finite element equations for viscoelasticity. For linear isotropic viscoelastic materials, the elastic modulus and shear modulus can be written as:

$$D^*(\omega) = D_1(\omega) + iD_2(\omega) \quad (1.16)$$

$$G^*(\omega) = G_1(\omega) + iG_2(\omega) \quad (1.17)$$

Using Equation (1.4) can also be written as:

$$G^*(\omega) = G_1(\omega)[1 + i\eta_m(\omega)] \quad (1.18)$$

D_1 , D_2 , G_1 , and G_2 are the storage and loss modulus for extension and shear, respectively and η_m is the material loss factor. The frequency dependence of these and other material properties will not be explicitly noted.

In harmonic time dependence, it can be shown that the complex bulk modulus is given by:

$$K^* = K_1 + iK_2 = \frac{D^*}{3(1 - 2\nu^*)} \quad (1.19)$$

where “ ν^* ” is the complex Poisson’s ratio defined through:

$$G^* = \frac{D^*}{3(1 - 2\nu^*)} \quad (1.20)$$

Viscoelastic properties can be entered into ABAQUS in several ways. In the Frequency domain, tabular values of G_1 , G_2 , K_1 , and K_2 , are normalized and can be entered as functions of frequency. (Lumsdaine et. al.)

It is important to measure the damping energy lost in a harmonically vibrating structure is the system loss factor, which may be defined by:

$$\eta = \frac{W_s}{2\pi W_d} \quad (1.21)$$

One way of calculating the system loss factor is by the half-power bandwidth method.

$$\eta = \frac{\omega_1^2 - \omega_2^2}{2\omega_r^2} \quad (1.22)$$

where ω_1 and ω_2 are the frequencies at the half power points and ω_r is the resonance frequency. In this problem the damping is light, equation (1.23) can be reduced to:

$$\eta = \frac{\omega_1 - \omega_2}{\omega_r} \quad (1.23)$$

In using ABAQUS, Lumsdaine (Lumsdaine et. al.) created a FORTRAN program to calculate the loss factor from ABAQUS results (see Appendix A for more information).

1.4 Active Constrained Layer Beam-No Control

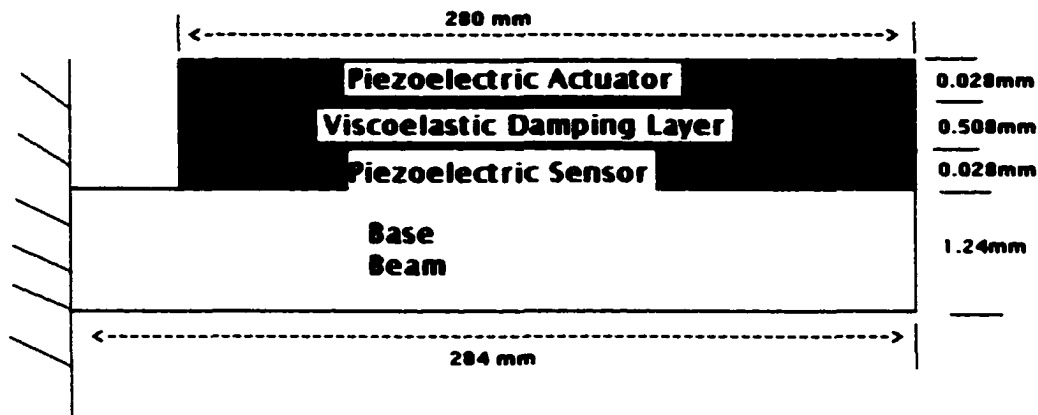


Figure1-2 Baz and Ro ACLD Beam

The results are compared with an ACLD structure examined by Baz and Ro (Baz et. al.) and Veley and Rao (Veley et. al.). The dimensions are shown in Figure1-2. The material properties are in Table1-1. The viscoelastic damping material has a material loss factor of 1.177 at the frequency of 4 Hz. The piezoelectric layers have a piezoelectric stress constant e_{211} of 0.0518 C/m^2 and a permittivity p_{22} of $0.1041 \times 10^{-9} \text{ F/m}$. The results obtained from ABAQUS are compared to with those of Baz and Ro (Baz et. al.) and Veley & Rao (Veley et. al.) in Table 1-2.

Table 1-1 Material Properties for Baz and Ro Beam

	Base Beam (PMMA)	Damping Material (DYAD-606)	Piezo Layer (PVDF)
Density	1240 kg/m ³	1104 kg/m ³	1800 kg/m ³
Elastic Modulus	4.25 GPa	23.7 MPa	2.25 GPa
Poisson's Ratio	0.3	0.4	0.29

Shear Modulus at 4 Hz

1.5 Results

Table 1-2 Results for ACLD Beam without Active Control

	Natural Frequency (Hz)	Loss Factor
Veley and Rao (2D FEM)	4.16	0.0457
Baz and Ro (Theory)	4.04	0.0413
Baz and Ro (experimental)	3.99	0.0419
ABAQUS (2D FEM)	4.18	0.0363

Table 1-3 Results for ACLD Beam with Active Control

	Natural Frequency (Hz)	Loss Factor
Veley and Rao (2D FEM)	4.43	0.131
Baz and Ro (Theory)	4.34	0.134
Baz and Ro (experimental)	4.37	0.102
ABAQUS (2D FEM)	2.63	0.092

Note: See Appendix A for ABAQUS results.

1.6 Conclusions

Using a commercial finite element code, for modeling ACLD structures would make possible to model such structures. This will allow use of finite elements features without having to develop the code from scratch. As you can see using a commercial code ABAQUS can be used to model ACLD structures. Furthermore, their need to be more

research done so to get better results from ABAQUS. Although, introducing active control in ABAQUS could be a trivial matter and may requires some modification.

CHAPTER 2

QUANTITATIVE DETERMINATION OF THE STABILITY OF IMPLANT- BONE INTERFACE USING RESONANCE FREQUENCY ANALYSIS

2.1 Introduction

Vibration study and control of structures are among the major research subjects in mechanical engineering and related technical disciplines. Among the most active research fields in this area, one finds the area of non-destructive evaluation. For a given mechanical structure, mode shapes of oscillation and natural frequencies depend on the structure's dimensions, materials, configuration, and boundary conditions. Thus, resonance frequency analysis can be used to infer information of the boundary conditions of a structure if the other parameters are known. Among many applications, this technique offers a mean to measure stability and osseointegration of implants. Osseointegration has been defined in literature as "a process whereby a clinically a symptomatic rigid fixation of alloplastic materials is achieved and maintained in bone during functional loading" (Zarb et. al.). Currently, there is an interest in enhancing the quality and rate formation around implants by modifying their surface topography or the use of coatings (Hallgren et. al). Thus, among other benefits stability measurements could help define optimal healing conditions and times and allow for ongoing monitoring of the implant-bone interface. Current radiological approaches do not provide much detail about the nature of the interface. Investigators have used resonance frequency analysis and developed a quantitative, non-invasive technique so that changes in implant modal

response can be monitored from a specific point in time. This technique has been used as a research tool and has been commercialized for clinical use.

These implant-bone interface stability studies have examined only one vibration mode or have suffered from measurement difficulties. Furthermore, no study has evaluated the damping properties of the interface and surrounding tissues.

In the present study the goal was to develop an instrument capable of extracting the full range of modal information from the system so that a thorough description of the interface can be developed. The osseointegration analysis can be extended to implants in any part of the human body. Furthermore, similar analysis can be used to measure stability and integrity of other mechanical systems such as composite materials structural elements (Kessler et. al.).

2.2 Technical Background

The use of resonant frequency measurement by Meredith [13-19] to provide a quantitative method for noninvasive diagnosis of implants stability and osseointegration was a significant innovation with great clinical potential. The device is optimized to measure the stiffness of the implant/sensor stack in a particular mode of excitation. The stiffness is driven by three parameters [17]:

1. Implant's stiffness function of implant's components geometry and material composition.
2. Implant-bone interface's stiffness (bond).
3. Stiffness of the surrounding tissues, determined by the trabecular-cortical bone ratio and the bone density, by geometric factors such as the length and diameter of the implant and the nature of the tissues.

Meredith developed this instrument with the configuration shown in Figure 2-1. The cantilever beam, shown in Figure 2-1, oscillates in and out of the page.

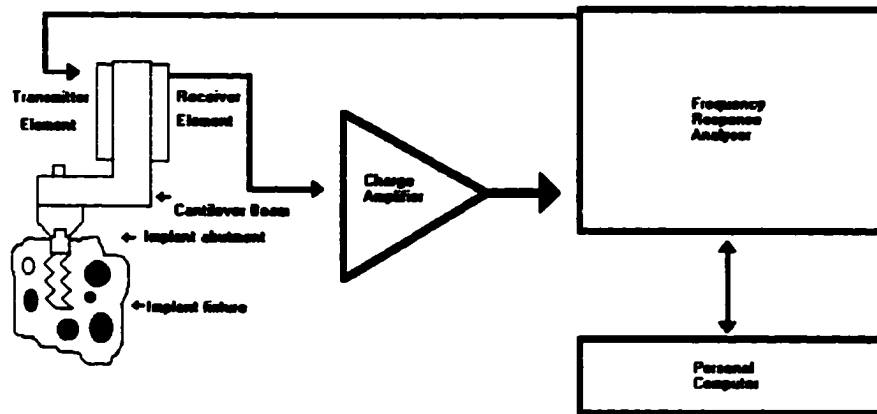


Figure 2-1 Meredith Instrumentation Design

This design is limited in its research potential by two factors. It only measures response in a single mode, which is a combination of two primary modes (oscillation of the cantilever beam and oscillation of the arm supporting the beam). It also cannot provide a complete model of the boundary conditions since it has been optimized for elastic response (stiffness) measurements only. The implant boundary conditions are more complex because bone response contains both elastic and viscoelastic components. Other investigators have approached this problem in various ways (Cawley et. al.). Accelerometers have been bonded directly to the implant or to the mass or hammer used to excite the implant. All of these approaches suffer from difficulties due to transducer limitations or problems in measurement resolution.

2.3 Problem Analysis

The stability of the implant-bone interface is determined by the dynamic modulus and damping of the interface. These properties of the implant's interface will also influence a

dynamic response of a structure attach to it. Therefore, an instrument can be design to capture as much information as possible.

The primary design consideration for this instrument was simplicity of operation since it is being designed for use in a research environment by Dental researchers. Existing accelerometers are generally not capable of measuring responses beyond 25 kHz, but dental implants have natural frequencies far beyond that value in several of their primary modes. To make the frequencies detectable, a fixture design was developed which brought the system natural frequencies into the measurable range for all three primary vibration modes (longitudinal, torsional and transverse vibrations). Theoretical and numerical modeling was done to determine the final dimensions, range of natural frequencies, and damping factors that can be measured with the resulting instrument. Experiments with different boundary conditions were conducted to replicate the process of dental implant osseointegration. The fixture design is shown in Figure 2-2. The fixture, abutment, and dental implant are shown in Figure 2-3. The abutment and the dental implant are made of titanium.

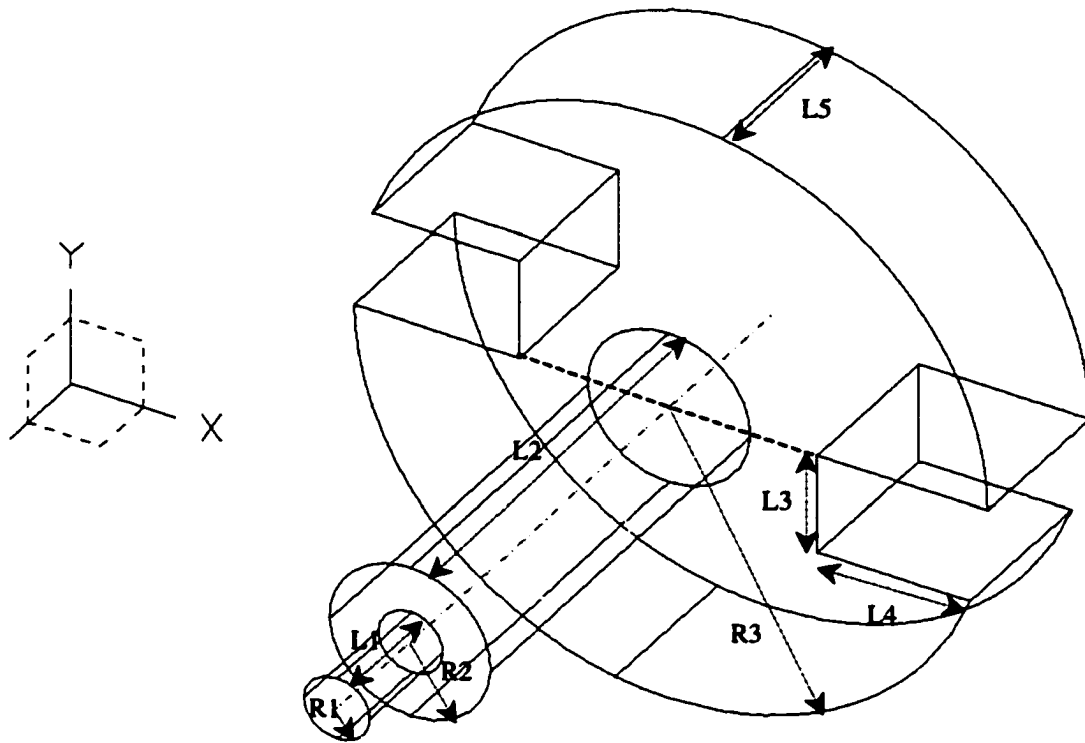


Figure 2-2 Fixture Design

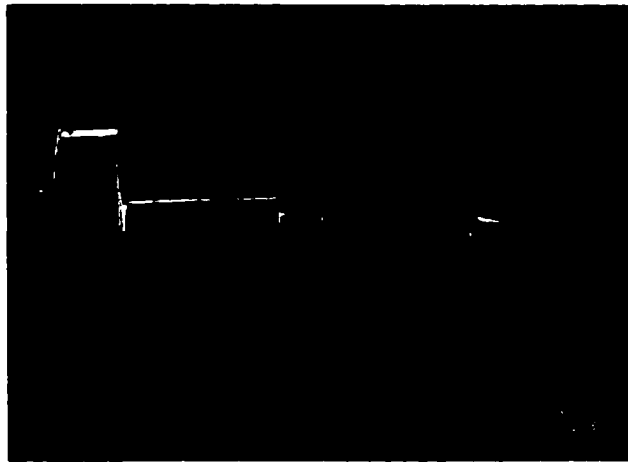


Figure 2-3 Fixture, Abutment, and Implant (Not Assembled)

The prototype fixture was made out of Aluminum for ease of fabrication. It is screwed onto the implant abutment as shown in Figure 2-3. The accelerometer is a Kistler 8614A1000M1. The Aluminum fixture has four piezoceramic elements (PL-055.21 by

Polytec PI) that are attached as shown in Figure 2-4. The piezoceramics are the shakers of the system.



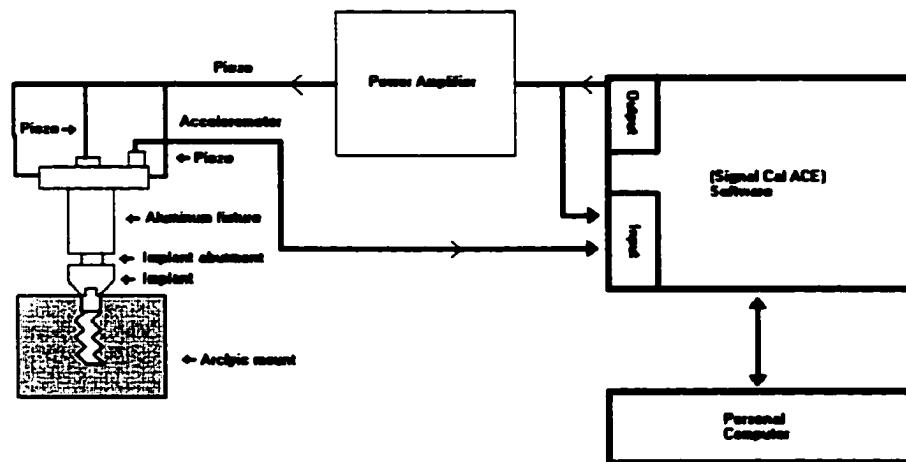
Figure 2-4 Top View of the Instrumentation

The traditional method of measuring the structure's natural frequencies and corresponding damping factors is to excite the structure in the desired mode shape with a sinusoidal wave form and to measure the amplitude of both input and output and their relative phase shift (frequency sweep method). This procedure must be repeated for each frequency that needs to be determined. In our experiments, we have used a frequency domain approach where one measures both the system input and output and then compute their respective frequency spectra. Random vibration (white noise) is sent into the system in order to estimate its transfer function. There is no need to repeat the measurement for each frequency, as was the case of the frequency sweep; this represents the main advantage of this method over the frequency sweep. Care must be taken in setting up the computerized data acquisition system so as to achieve a balance between the upper frequency limit of the spectrum, the frequency resolution, and the time required to collect the samples. The upper frequency limit determines the frequency at which samples must be taken; the Nyquist rule states that a signal must be sampled at a rate twice as high as its

highest frequency component in order to be reproduced. The frequency resolution and sampling time are closely related; the time required for collecting samples equals the number of samples taken divided by the sampling rate. Taking more samples requires longer measurement duration, which could be of concern when taking in-vivo measurements.

The configuration developed for our instrument is shown in Figure 2-5. Because of its ease of use, SignalCAL software from Dataphysics was chosen for control and data acquisition.

The instrument developed provides valuable information about the stiffness and damping properties of the implant-bone interface obtained through resonance frequency analysis with torsional, axial (longitudinal), and transverse vibration. Figures 2-6—2-9 shows the instrument's vibration modes with undistorted (grid) and distorted configurations. For the distorted configuration, dark blue regions experience minimum displacement and red regions experience maximum displacement from original configuration.



Schematic diagram of the instrumentation of the implant by Daniel Delgado

Figure 2-5 Instrumentation Configuration

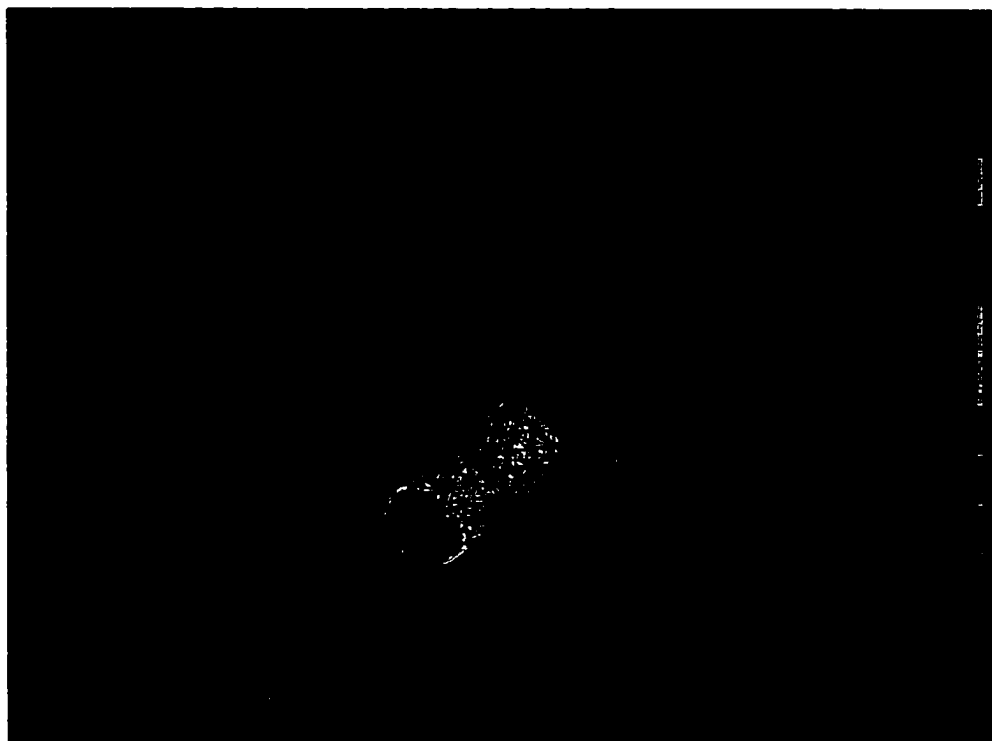


Figure 2-6 Axial Mode

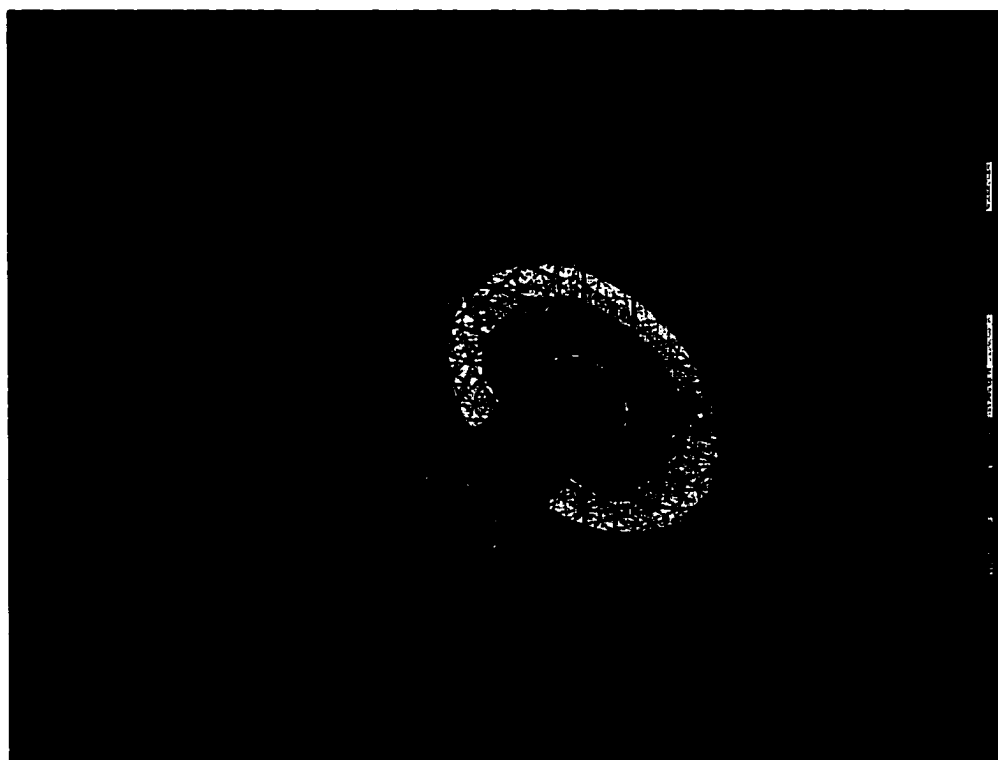


Figure 2-7 Torsional Mode

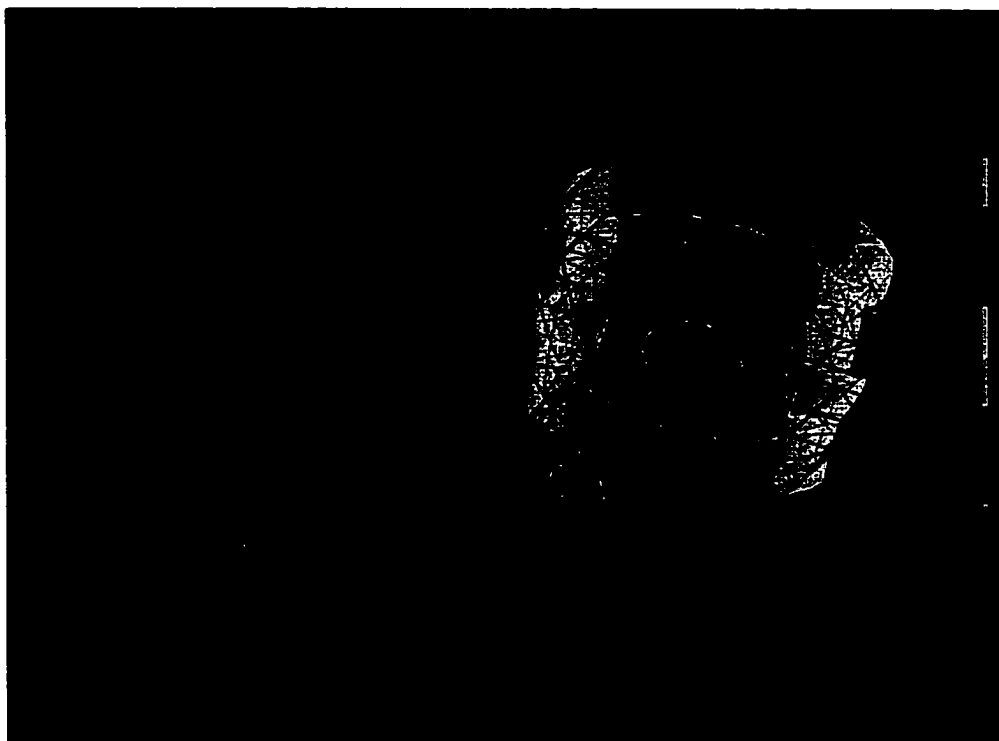


Figure 2-8 Higher Bending Mode

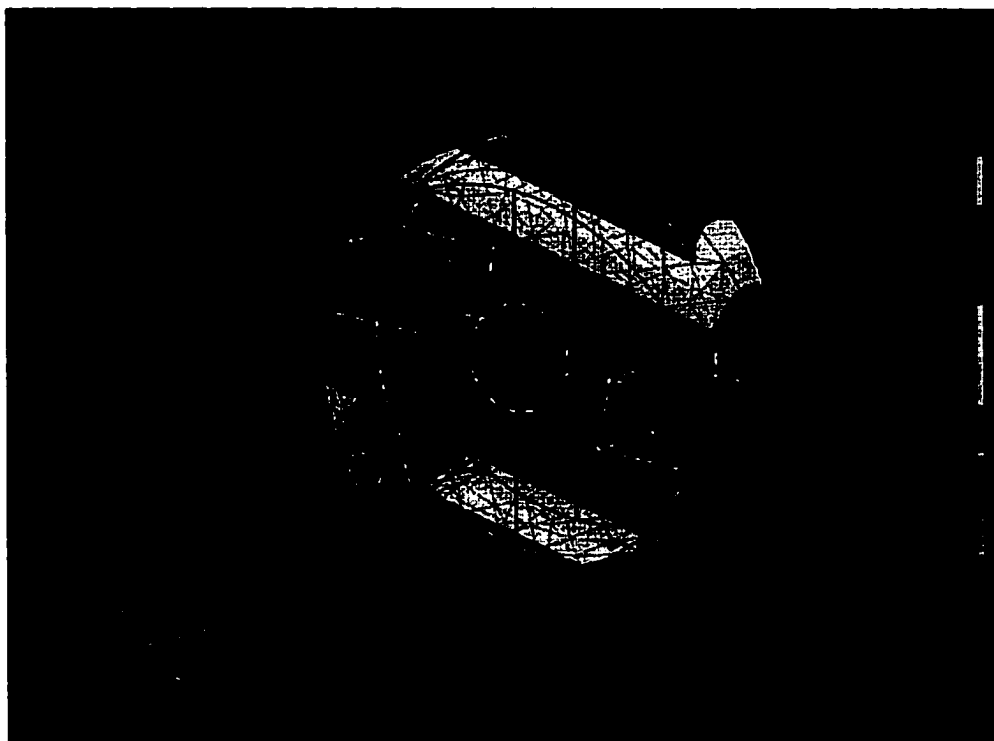


Figure 2-9 Lower Bending Mode

2.4 Results

A solution using finite element analysis (FEA) of a simplified model was compared to a simplified analytical solution to test our computer-generated designs. We used the FEA software called IDEAS to model the instrument. The instrument's simplified model used in our analysis is shown in Figure 2-10. The model consists of a simple beam with disk at the end and fixed at the interface of the implant (lower section). The simplified model for the analytical solution, shown in Figure 2-11, was solved with the following assumptions:

- Equations for torsional vibrations of a uniform shaft
- Equations for longitudinal vibrations of a uniform elastic bar
- Equations for transverse vibrations of a uniform beam
- Mass of the bar is much smaller than the mass of the disk

Table 2-1 presents the comparison between the FE simplified model results and the analytical solution for the analytical simplified model. There is good agreement between the results. However as expected, there are small differences due to the simplifications and assumptions, and the differences are smaller for torsional and transverse vibration than longitudinal vibration.

From the results generated by the FE simplified model, we selected the dimensions for the fixture in our instrumentation. Table 2-2 presents the selected fixture's dimensions (please refer to Figure 2-2 for notation).

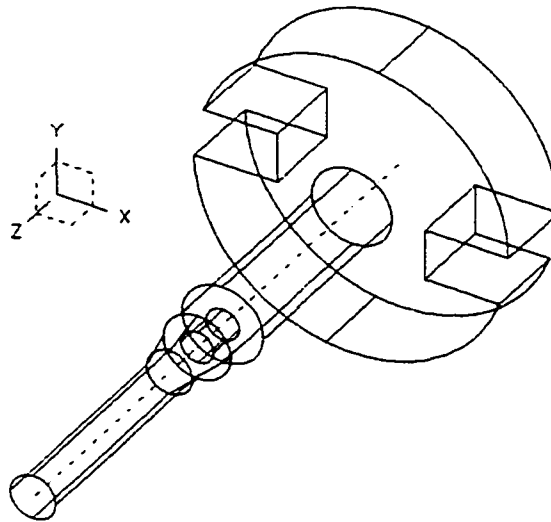


Figure 2-10 Finite Element Simplified Model

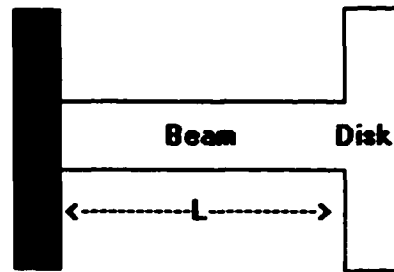


Figure 2-11 Analytical Simplified Model

Table 2-1 Comparison of the FEA and analytical Solution

	Torsional Vibration [Hz]	Transverse Vibration [Hz]	Axial (Longitudinal) Vibration [Hz]
Analytical Solution	3971	3171	26750
FEA Solution	4120	2971	23033
Difference	3.7%	6.3%	13.9%

Table 2-2 Fixture's Dimensions

Dimension	Inches
R1	0.078
R2	0.096
R3	0.375
L1	0.250
L2	0.515
L3	0.125
L4	0.200

L5	0.200
----	-------

Initially, the experimental values were obtained with the implant imbedded in a brass mount in order to simulate the rigid constraint around the implant boundary used in the FEA model. Figure 2-12 shows one of the experimental results obtained by exciting the different mode shapes of oscillations randomly. It is a challenge to excite only one mode oscillation at a time (i.e. the axial mode always appeared in our experimental results). The values of the FEA should be higher than the experimental values because the experimental boundary conditions are not in fact perfectly rigid due to the threading of the mount and because the threaded interface between the transducer and the implant abutment will reduce the resonant frequency of the stack. In addition, the abutment is screwed into the implant. The comparison of results of experimental measurements to FE results from the instrument is presented in Table 2-3. The FE model permitted identification of the first four modes of vibration.

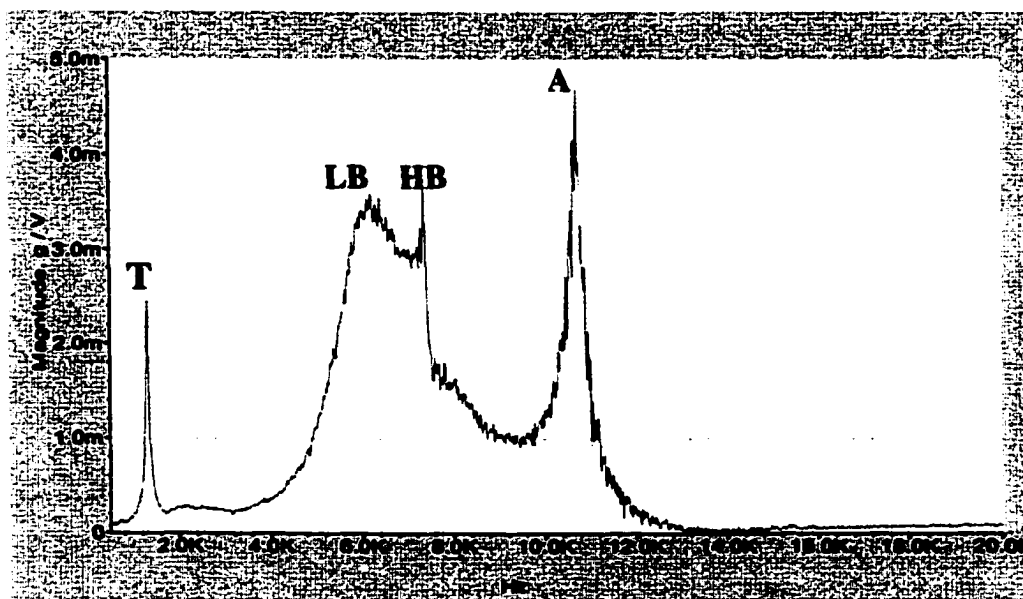


Figure 2-12 Experimental Results (Brass Mount)
[T-torsion, LB-low bending, HB-high bending, A-axial]

Table 2-3 Comparison of the FEA and Experimental Results

TYPE OF VIBRATION	FEA FREQUENCY (Hz)	EXPERIMENTAL FREQUENCY (Hz)	% DIFFERENCE
TORSIONAL MODE	1340	1313	2
LOWER BENDING MODE	9168	7125	22
HIGHER BENDING MODE	10127	8025	21
AXIAL MODE	13872	11025	21

Next, different laboratory experiments were designed and conducted to test the instrumentation's capabilities. To simulate dental operational working conditions, acrylic mounts with stiffness similar to human bones were introduced.

Brass vs. Acrylic Mounts

We obtained the natural frequencies of vibration for the selected modes of oscillation (refer to Figure 2-6—2-9) with brass and acrylic mounts. Changing from the brass mount to an acrylic mount, that is changing the dynamic modulus and damping in the interface, causes the natural frequencies of the different mode of oscillation to shift to the left. This is expected because the acrylic is a softer material than brass (please refer to Figures 2-13, and Table 2-4). The maximum changes in the natural frequencies were experienced in the torsional mode of oscillation. The axial mode of oscillation follows in the magnitude of change between the two different mounts.

We also estimated the viscous damping factors of the systems vibrating in the different modes of oscillation using the respective system's bandwidth. As expected, all viscous damping factors increased for the acrylic mount. However, in the case of torsion the damping factor only increased from 0.0268 to 0.285. The maximum changes in the damping factor were experienced in the bending modes of oscillation. The lower bending

mode shape-damping factor for a given mount was always bigger than for the higher bending due to the dynamics of the mode shapes.

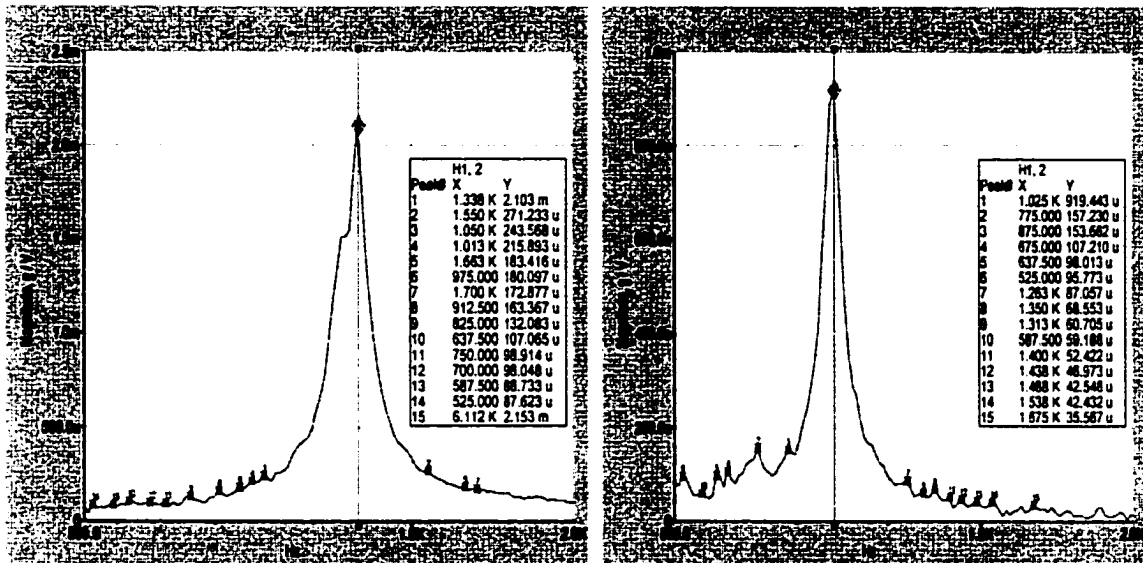


Figure 2-13 Response of Brass (Left) vs Acrylic (Right) Mount [Torsional Mode]

Table 2-4 Comparisons of the Brass and Acrylic Mounts.

Modes	Brass Mount	Acrylic Mount
Torsion	1338	1025
Lower Bending	6000	5800
Higher Bending	7425	6900
Axial	10388	9388

Different fits in Acrylic Mounts

The next experiment consisted in changing conditions in the implant fit in the acrylic mounts. For this purpose a tight and a loose fit were considered by changing the diameter of the hole before tapping. Figures 2-14, 2-15, 2-16, 2-17, 2-18, and 2-19, and Table 2-5 show the shift of the frequency when the hole drilled before tapping is intentionally widened from 0.144in (3.658mm) to 0.153in (3.886mm). All the natural frequencies for the selected modes of oscillation were reduced. The maximum changes in the natural frequencies were experienced in the axial mode of oscillation.

Viscous damping factors are also reported in Table 2-5. The maximum changes in the damping factor were experienced in the bending modes of oscillation. The damping

factor is an estimate by this equation $\lambda = \frac{\omega_2 - \omega_1}{2\omega_n}$

Table 2-5 Comparisons of Natural Frequencies and Damping Factors for Implants with Acrylic Mounts With Different Fits

Mode of Oscillation	Natural Frequencies		Damping Factors	
	Acrylic (0.144 in) Hz	Acrylic (0.153 in) Hz	Acrylic (0.144 in) Hz	Acrylic (0.153 in) Hz
Torsion	1213	1188	0.0221	0.0233
Lower Bending	5763	5313	0.0641	0.0738
Higher Bending	6925	6275	0.0096	0.0166
Axial	9412	7413	0.0252	0.0251

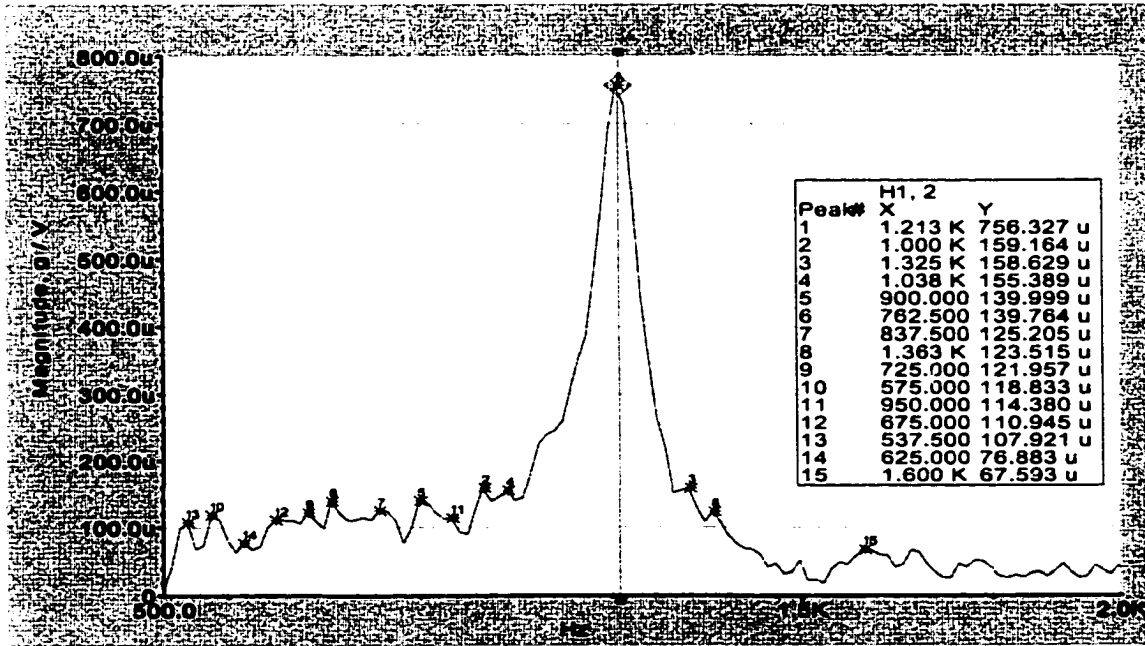


Figure 2-14 Torsion Mode for Acrylic Mounts With Oversized Predrilled Hole [0.144 in]

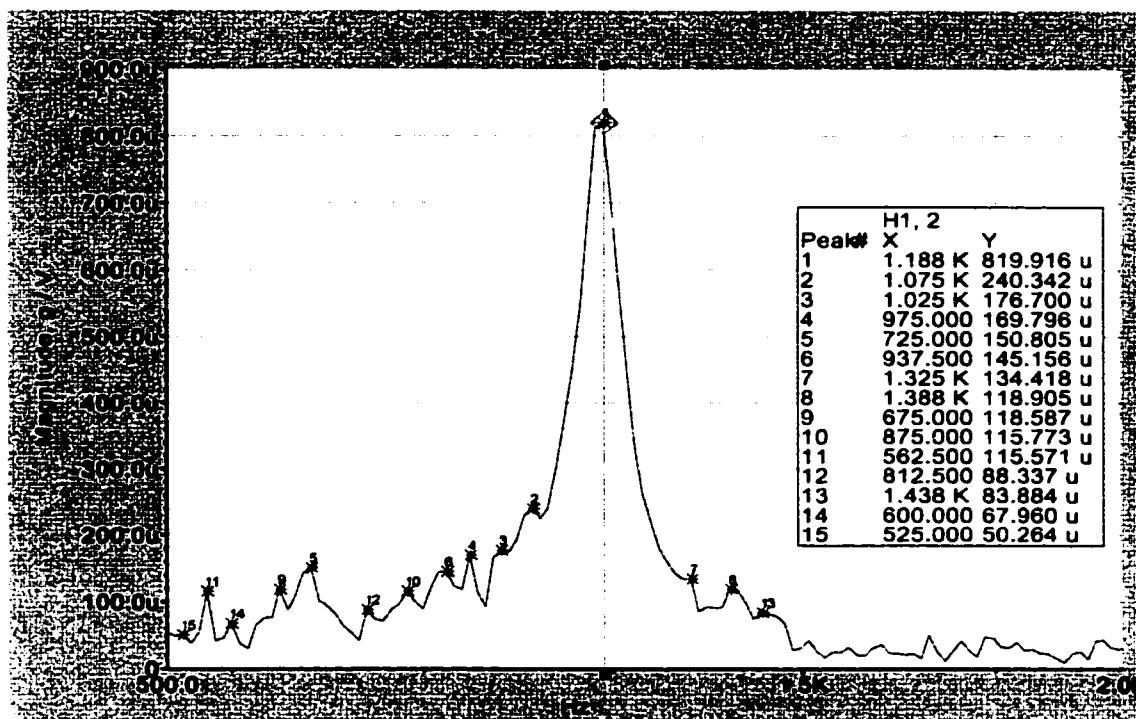


Figure 2-15 Torsion Mode for Acrylic Mounts With Oversized Predrilled Hole [0.153 in]

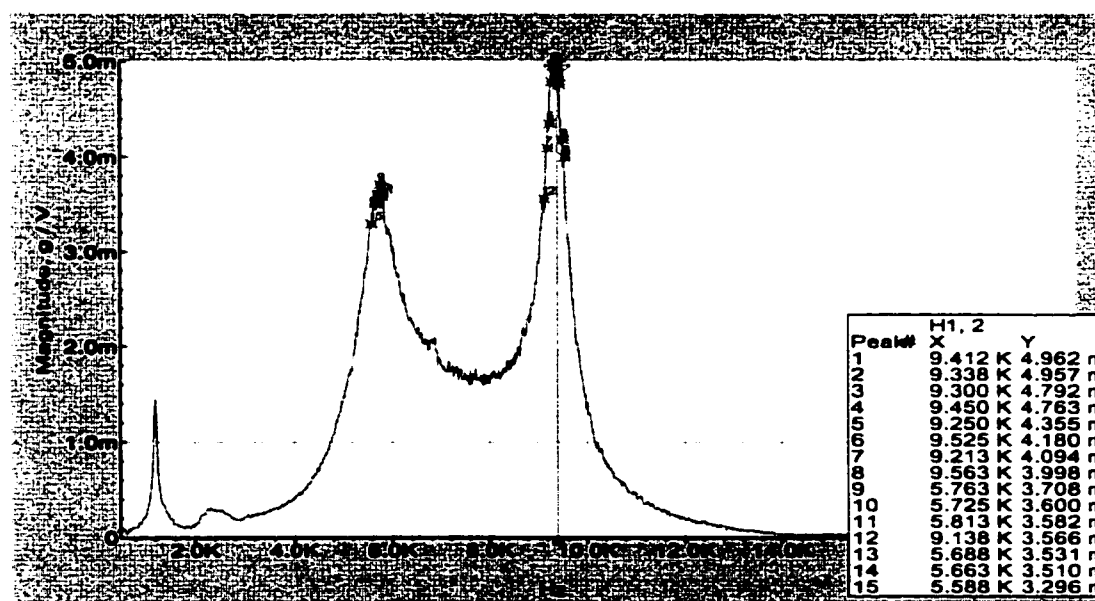


Figure 2-16 Response of Implant with Acrylic Mount with Oversized Predrilled Hole (0.144in.) [Lower Bending and Axial Mode]

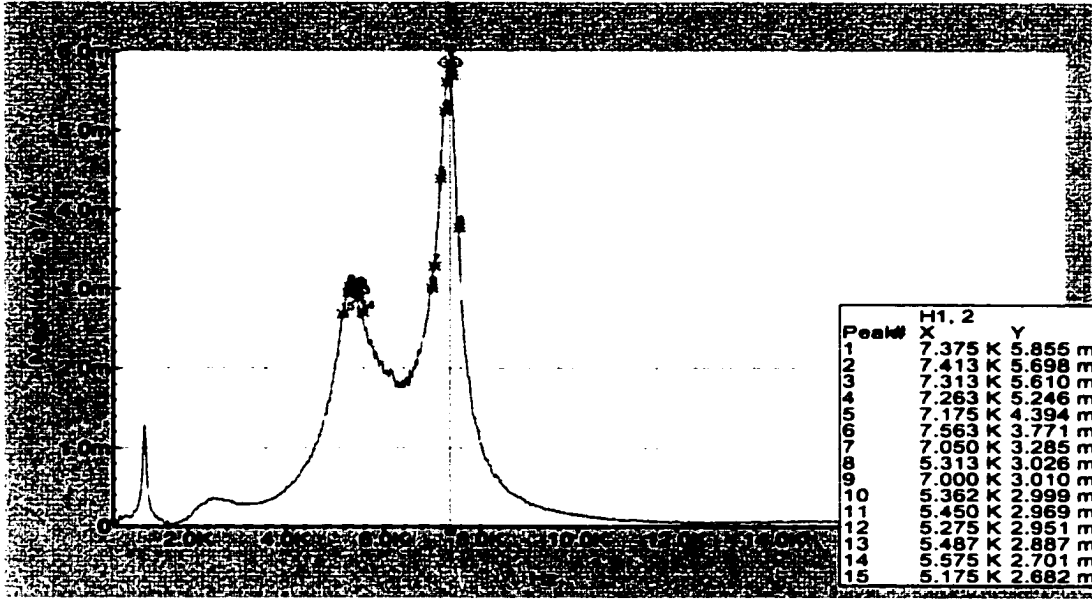


Figure 2-17 Response of Implant with Acrylic Mount with Oversized Predrilled Hole (0.153in.) [Lower Bending and Axial Mode]

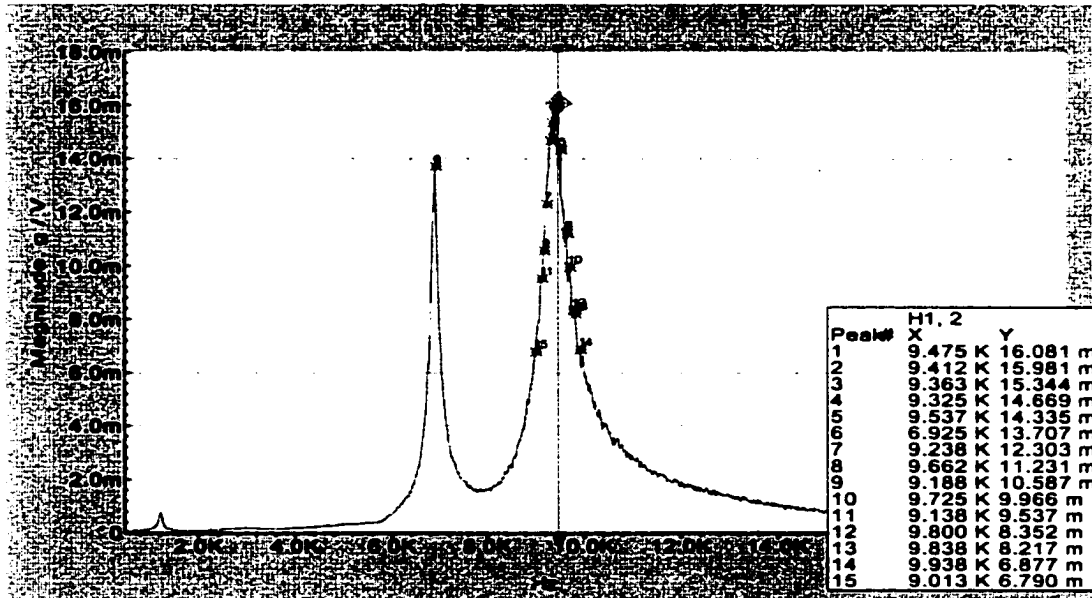


Figure 2-18 Response of Implant with Acrylic Mount and Oversized Predrilled Hole (0.144in.) [Higher Bending and Axial Mode]

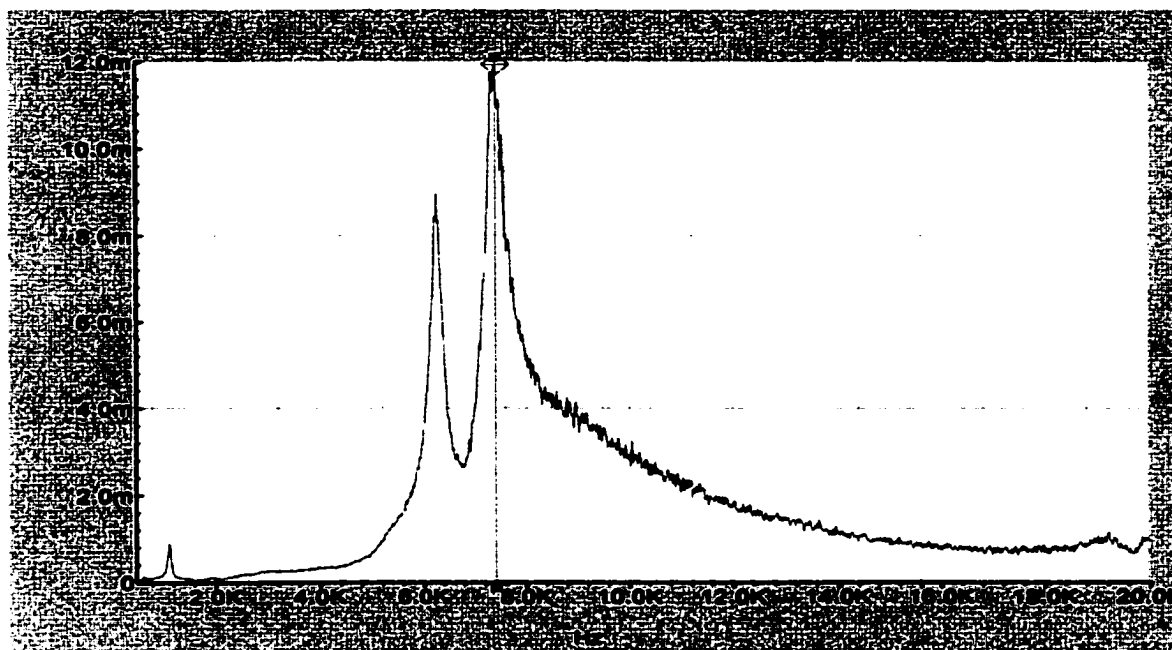


Figure 2-19 Response of Implant with Acrylic Mount with Oversized Predrilled Hole (0.153in.) [Higher Bending and Axial Mode]

Also, we tested half threaded cases in the following table 2-6 that shows the results of the tested. The results shows that the upper and lower threaded mounts the instrument can show that there are differences in frequencies and damping factors.

Table 2-6 Acrylic Mounts Half Threaded Cases Comparisons.

	Natural Frequencies Full Threaded (Hz)	Damping Factors	Natural Frequencies Half Threaded (Hz)	Damping Factors
Mount A Lower Case	787.5	0.1238	537.5	0.0930
Mount B Upper Case	612.5	0.1551	500	0.125



Figure 2-20 Upper and Lower Mounts for Table 2-6

The instrument was also tested in time by inserting the implant in acrylic resin and monitors the curing time and records the results every five minutes. Table 2-7 shows the results of the frequencies response (See Appendix B for more results).

Table 2-7 Acrylic Resin Curing Time Frequencies Readings

Time (min)	Torsional (Hz)	Lower Bending (Hz)	Higher Bending (Hz)	Axial (Hz)
15	300	----	7550	----
20	1262.5	7050	7725	----
25	1525	7413	8525	~9000
30	1637.5	7737	8700	~9500
35	1712.5	7963	8863	~10000
40	1762.5	7862	8825	~10500
45	1787.5	7775	8863	~10750
50	1800	7938	8925	~10900
55	1812.5	7963	9025	~11000
60	1825	9000	9575	~11500



Figure 2-21 Curing Acrylic Mount

As you can see the frequencies response are much higher then the threaded acrylic mounts results. This is because the interface between the implant and the acrylic is now rigid boundary condition.

In the following Tables (2-8—2-11), we decide to create different kinds of problems with the acrylic mounts. As you can see, the instrument demonstrated that it notice the changes in boundary conditions, and the frequency and damping factor changed accordingly to the boundary conditions it had.

Table 2-8 Half Threaded Acrylic Mount Comparisons to Full Threaded Acrylic Mount

	Frequency (Hz) Full Threaded	Damping Factor	Frequency (Hz) Half Threaded	Damping Factor
Torsional	875	0.03543	800	0.04688

Table 2-9 Hole on one side of the implant Comparison to Full Threaded Acrylic Mount

	Frequency (Hz) Full Threaded	Damping Factor	Frequency (Hz) hole in one side	Damping Factor
Torsional	1000	0.01875	1012.5	0.02469

Table 2-10 Hole on both sides of the implant Comparison to Full Threaded Acrylic Mount

	Frequency (Hz) Full Threaded	Damping Factor	Frequency (Hz) hole in both sides	Damping Factor
Torsional	1012.5	0.01852	950	0.03947

Table 2-11 Short Half Threaded Acrylic Mount Comparisons to Full Threaded Acrylic Mount

	Frequency (Hz) Full Threaded	Damping Factor	Frequency (Hz) Half Threaded	Damping Factor
Torsional	1000	0.01875	887.5	0.0845

In table 2-8, we decide to spit the acrylic mount in half to show a half threaded on half the implant's threading. This shows that the instrument can show the frequency changes and the damping factor changes. In table 2-9 and 2-10, there is no difference between the Frequencies but the damping factor did change and it lets know that there is something wrong. In Figure 2-21 and 2-22, it shows the experiment setup for the results.

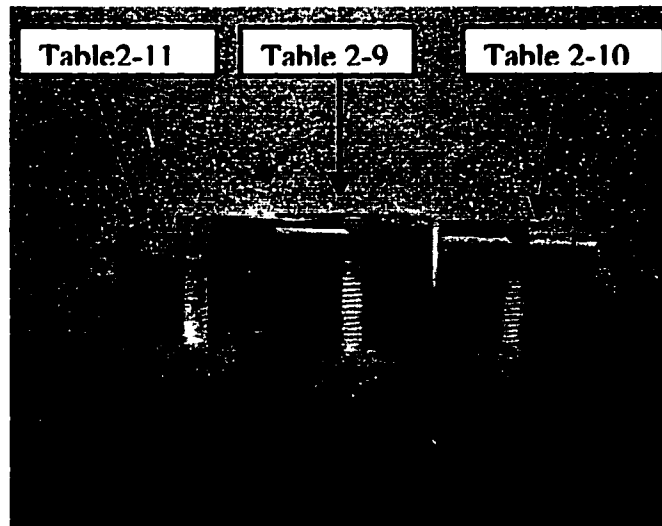


Figure 2-22 Experimental Mounts for tables 2-9—2-11 results.

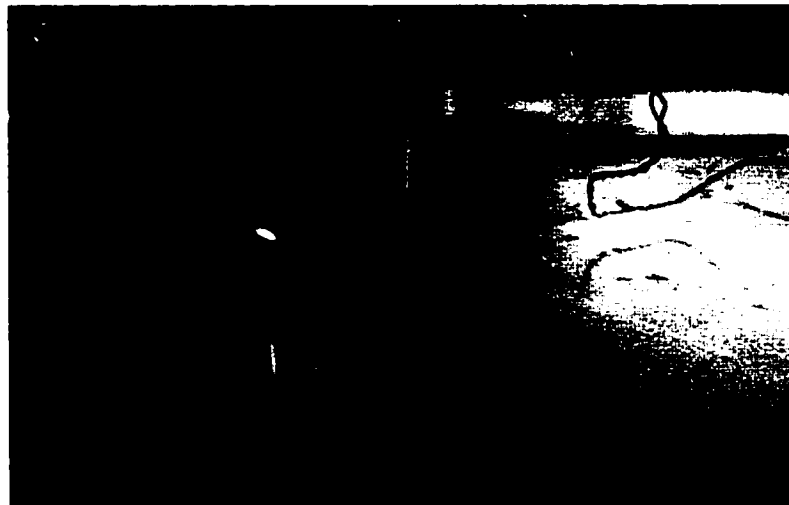


Figure 2-23 Half Threaded Mount

2.5 Conclusion

In summary, a new instrument for resonance frequency analysis of osseointegrating dental implants has been developed. The instrument is capable of capturing and measuring information to characterize the process of dental implant osseointegration. It can detect changes in the boundary conditions (i.e. modulus reduction, damping reduction, and contact area reduction). The measured natural frequencies of the transducer design correspond fairly well to predictions of both an analytical model and FEA. Changes in boundary conditions and excitation modes indicate that the identification of the first four peaks with particular modes of vibration is correct. Variations in the boundary conditions of the implant were detected by resonance frequency analysis. Thus, the instrument offers the potential to use multiple mode shapes of oscillation, natural frequencies, and damping measurements to develop a more complete picture of the implant-bone interface.

By reducing the effective length of the fixture in the instrumentation, one may increase the difference between different boundary conditions. However, reducing the size also implies that the structure's natural frequencies will increase. Thus, for simplicity of operation there is a need for accelerometers capable of measuring responses greater than 25 KHz. Meanwhile, more detailed research may be conducted in laboratories using a laser doppler vibrometer or a similar system.

The osseointegration analysis can be extended to implants in any part of the human body. Furthermore, similar analysis can be used to measure stability and integrity of other mechanical systems such as composite materials structural elements.

APPENDIX A

THE ABAQUS RESULTS FROM GETMAX AND RESULT3

asmeloss81400 results

Here is the results of gain of 1.

hermes% getmax.x**4.5798802137161D-03 4.000000000000****1.2028781216563D-02 4.183333333333****2.7863245685130D-03 4.500000000000****hermes% result3.x****max def: 0.01202878****max freq: 0.41833333E+01****low def: 0.00457988****high def: 0.00278632****half def: 0.00850563****low freq: 0.41104425E+01****high freq: 0.42624600E+01****loss factor: 0.363388E-01**

Here is the results of gain of -1

hermes% getmax.x**4.3598241545943D-03 4.000000000000****1.2034121673808D-02 4.200000000000****2.8735472459135D-03 4.500000000000****hermes% result3.x****max def: 0.01203412****max freq: 0.42000000E+01****low def: 0.00435982****high def: 0.00287355****half def: 0.00850941****low freq: 0.41212849E+01****high freq: 0.42728150E+01**

loss factor: 0.360786E-01

Here is the results of gain of -240

hermes% getmax.x

5.7146580475667D-04 4.00000000000000

1.1711991166967D-02 5.30000000000000

4.2264938688296D-04 7.00000000000000

result3.x

max def: 0.01171199

max freq: 0.53000000E+01

low def: 0.00057147

high def: 0.00042265

half def: 0.00828163

low freq: 0.55459826E+01

high freq: 0.56471737E+01

loss factor: 0.190927E-01

Here is the results of gain of 240

hermes% getmax.x

2.5508375309407D-03 2.00000000000000

1.2140699623333D-02 2.62500000000000

3.5381462132829D-03 3.00000000000000

hermes% result3.x

max def: 0.01214070

max freq: 0.26250000E+01

low def: 0.00255084

high def: 0.00353815

half def: 0.00858477

low freq: 0.25041230E+01

high freq: 0.27459077E+01

loss factor: 0.921084E-01

Here is the results of gain of 100

hermes% getmax.x

1.0559382325236D-03 2.5000000000000

1.2048138901623D-02 3.6200000000000

1.5870771949785D-03 4.2500000000000

hermes% result3.x

max def: 0.01204814

max freq: 0.36200000E+01

low def: 0.00105594

high def: 0.00158708

half def: 0.00851932

low freq: 0.35347655E+01

high freq: 0.37085498E+01

loss factor: 0.480067E-01

Here is the results of gain of 250

hermes% getmax.x

1.3489250957154D-03 1.0000000000000

1.1994763304539D-02 2.5600000000000

8.5393616692868D-04 4.0000000000000

hermes% result3.x

max def: 0.01199476

max freq: 0.25600000E+01

low def: 0.00134893

high def: 0.00085394

half def: 0.00848158

low freq: 0.24098196E+01

high freq: 0.26587458E+01

loss factor: 0.972368E-01

APPENDIX B
ABAQUS CODE FILES

***HEADING**

Veley & Rao ACLD Beam

****Manually created, passively constrained******Fixed VE Elastic Modulus (E+04 instead of E+03)******Non-reduced integration elements******Constant VE properties, add bulk modulus properties************For writing out the piezoelectric stiffness matrices***********NODE**

1,	0.0,	0.0,	0.0
5,	4.0,	0.0,	0.0
405,	284.0,	0.0,	0.0
406,	0.0,	0.62,	0.0
410,	4.0,	0.62,	0.0
810,	284.0,	0.62,	0.0
811,	0.0,	1.24,	0.0
815,	4.0,	1.24,	0.0
1215,	284.0,	1.24,	0.0
1216,	4.0,	1.254,	0.0
1616,	284.0,	1.254,	0.0
1617,	4.0,	1.268,	0.0
2017,	284.0,	1.268,	0.0
2018,	4.0,	1.522,	0.0
2418,	284.0,	1.522,	0.0
2419,	4.0,	1.776,	0.0
2819,	284.0,	1.776,	0.0
2820,	4.0,	1.79,	0.0
3220,	284.0,	1.79,	0.0
3221,	4.0,	1.804,	0.0
3621,	284.0,	1.804,	0.0

***NGEN**

1,5,1

5,405,1

406,410,2

410,810,2

811,815,1

2018,2418,2

***NGEN,NSET=SENSBOT**

815,1215,1

***NGEN,NSET=SENSMID**

1216,1616,2

***NGEN,NSET=SENSTOP**

1617,2017,1

***NGEN,NSET=ACTUBOT**

2419,2819,1

***NGEN,NSET=ACTUMID**

```

2820,3220,2
*NGEN,NSET=ACTUTOP
3221,3621,1
*ELEMENT,TYPE=CPS8
401,1,3,813,811,2,408,812,406
*ELGEN,ELSET=BEAM
401,202,2
*ELEMENT,TYPE=CPS8E
1,815,817,1619,1617,816,1218,1618,1216
201,2419,2421,3223,3221,2420,2822,3222,2820
*ELGEN,ELSET=PIEZO
1,200,2
201,200,2
*ELEMENT,TYPE=CPS8
603,1617,1619,2421,2419,1618,2020,2420,2018
*ELGEN,ELSET=VISCO
603,200,2
*SOLID SECTION,ELSET=BEAM,MATERIAL=PMMA
3.080E+01
*MATERIAL,NAME=PMMA
*ELASTIC,TYPE=ISOTROPIC
4.250E+06 2.900E-01
**DAMPING,BETA=0.00114
*DENSITY
1.240E-06
*SOLID SECTION,ELSET=PIEZO,MATERIAL=PVDF
3.080E+01
*MATERIAL,NAME=PVDF
*ELASTIC,TYPE=ISOTROPIC
2.250E+06 2.900E-01
*PIEZOELECTRIC,TYPE=S
0.0,0.0,0.0,0.0,0.0,0.0,0.0518E-06,0.0
0.0,0.0,0.0,0.0,0.0,0.0,0.0,0.0
0.0,0.0
*DIELECTRIC,TYPE=ISO
1.041E-11
*DENSITY
1.800E-06
*SOLID SECTION,ELSET=VISCO,MATERIAL=DYAD-606
3.080E+01
*MATERIAL,NAME=DYAD-606
*ELASTIC,TYPE=ISOTROPIC
6.647E+04 4.000E-01
*VISCOELASTIC,FREQUENCY=TABULAR
1.177,0.0,1.177,0.0,1.E-6
1.177,0.0,1.177,0.0,1.E+6
*DENSITY

```



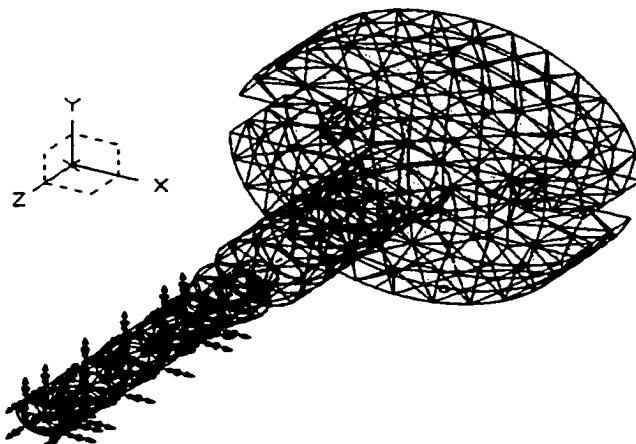
```
1.104E-06
*STEP,AMPLITUDE=STEP,PERTURBATION
*FREQUENCY
10,10.
*RESTART,WRITE,FREQUENCY=      1
*BOUNDARY,OP=NEW
1,1,2
406,1
811,1
ACTUBOT,9
SENSBOT,9
*NODE FILE,FREQUENCY=          1,GLOBAL=YES
U
EPOT
*NODE PRINT
U
EPOT
CECHG
*EL FILE
S,E,PHS,PHE
EPG,EFLX,PHEPG,PHEFL
*EL PRINT
EPG1,EPG2,EFLX2
PHEPG,PHEFL
S
E
*ELEMENT MATRIX
OUTPUT,ELSET=PIEZO,ELSET=BEAM,ELSET=VISCO,OUTPUT FILE=USER
DEFINED,
STIFFNESS=YES,MASS=YES,FILE NAME=asmematrix10
**ELEMENT MATRIX OUTPUT,ELSET=PIEZO,STIFFNESS=YES,MASS=YES
*END STEP
```

APPENDIX C
IDEAS FEA RESULTS FOR IMPLANT MODEL

LIST OF FILE NAMES

Page	IDEAS Model File Names	Comments	Figure
43	Newloading10test15.mfl	Changing Boundary Conditions (Final Fixture Design Includes the implant)	2-10
44	Newloading10test1.mfl	Testing theory results	2-2
45	Newloading10test10.mfl	Testing geometry of Fixture model	2-2
46	Newloading10test15.mfl	Varying Boundary Conditions	2-10
47	Newloading10test15AA.mfl	Changing Material Properties Al to Ti	2-10

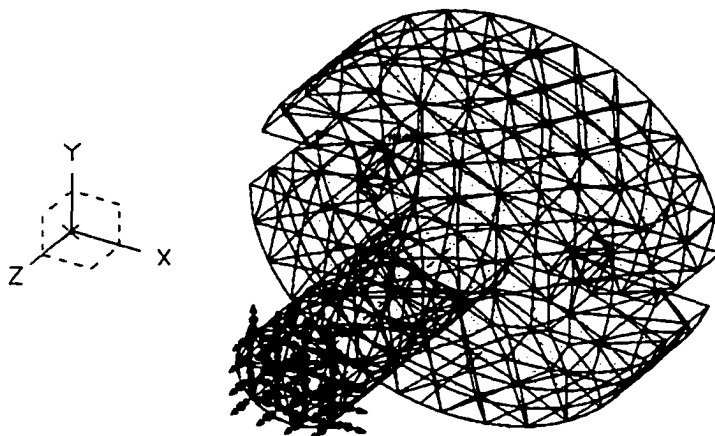
MODEL FILE : /home/ddelgado/newloading10test15.mf1



NUMBER OF NODES : 2815
NUMBER OF ELEMENTS : 1417

MODE	FREQUENCY	MODAL MASS	RESIDUAL
1	586.8267	2.66813E-02	-4.54E-09
2	598.0080	2.63100E-02	-8.79E-09
3	1384.5524	1.53376E-02	-1.06E-09
4	9495.9675	1.16959E-02	-5.45E-12
5	10488.7851	9.33128E-03	1.22E-11
6	14342.6758	3.00655E-02	3.29E-11
7	36261.5184	2.62645E-03	1.82E-12
8	36501.4180	2.76403E-03	1.14E-11
9	42774.2096	6.52030E-03	-3.55E-11
10	56904.5190	6.86889E-03	-1.47E-10

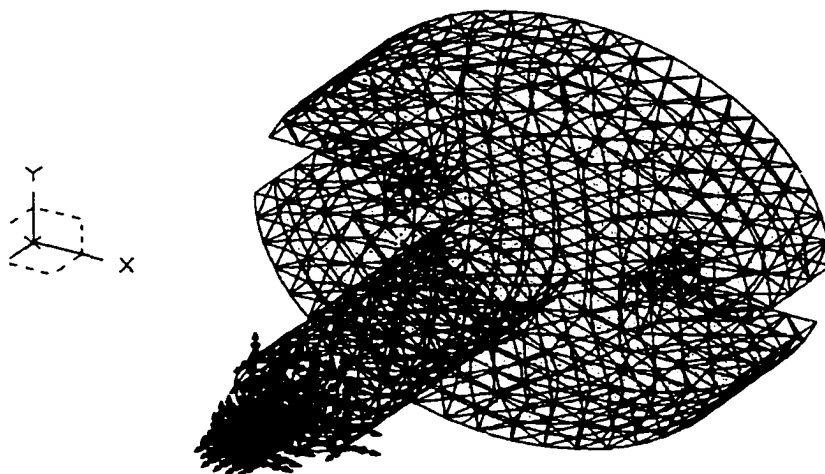
MODEL FILE : /home/ddelgado/newloading10test1.mf1



NUMBER OF NODES : 2072
NUMBER OF ELEMENTS : 1050

MODE	FREQUENCY	MODAL MASS	RESIDUAL
1	3351.5753	2.67074E-02	-2.06E-10
2	3429.7605	2.55344E-02	-1.03E-10
3	4665.9611	1.51915E-02	-2.02E-11
4	15604.7144	1.21046E-02	1.03E-11
5	16961.4060	9.12605E-03	2.05E-12
6	24974.2903	2.13314E-02	3.14E-12
7	43108.4226	6.50120E-03	2.79E-12
8	58642.0477	5.40799E-03	-1.94E-12
9	59617.3409	4.62228E-03	1.96E-13
10	72315.4874	2.80207E-03	-2.38E-11

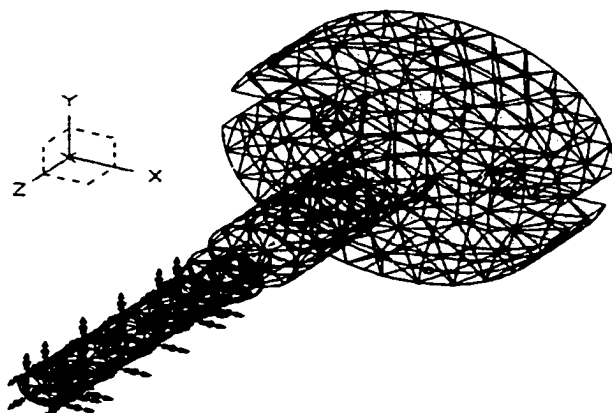
MODEL FILE : /home/ddelgado/newloading10test10.mfl



NUMBER OF NODES : 6699
NUMBER OF ELEMENTS : 3802

MODE	FREQUENCY	MODAL MASS	RESIDUAL
1	2989.5365	2.65809E-02	-3.03E-10
2	3058.8493	2.54647E-02	-2.39E-10
3	4240.3763	1.51293E-02	8.15E-11
4	14121.1510	1.19219E-02	-2.47E-11
5	15431.1458	8.99552E-03	2.90E-11
6	23683.9946	2.18706E-02	1.21E-13
7	42467.4439	6.39247E-03	6.24E-12
8	58462.2336	5.45390E-03	6.23E-12
9	59023.4491	4.72629E-03	1.70E-11
10	72173.0539	2.76617E-03	-1.62E-10

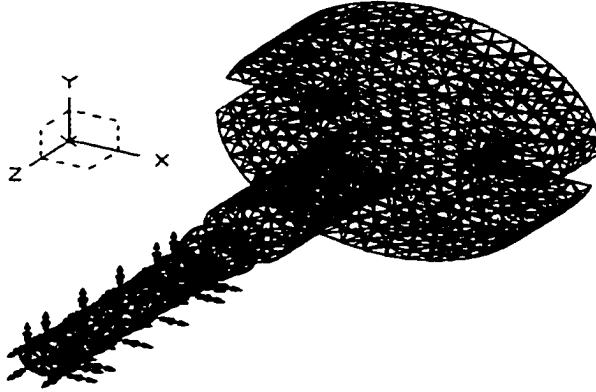
MODEL FILE : /home/ddelgado/newloading10test15.mf1



NUMBER OF NODES : 2815
 NUMBER OF ELEMENTS : 1417

MODE	FREQUENCY	MODAL MASS	RESIDUAL
1	622.2883	2.65700E-02	-1.14E-09
2	635.5787	2.61934E-02	-4.10E-09
3	1447.3904	1.53299E-02	9.20E-10
4	10145.6983	1.13761E-02	-1.66E-11
5	11228.6423	9.00694E-03	-3.33E-12
6	15165.9528	2.93387E-02	-1.43E-11
7	42285.4285	5.19896E-03	1.00E-10
8	42551.6756	5.55008E-03	8.98E-11
9	42785.1466	7.02963E-03	4.41E-11
10	57019.3019	6.90697E-03	1.98E-10

MODEL FILE : /home/ddelgado/newloading10test15AA.mf1

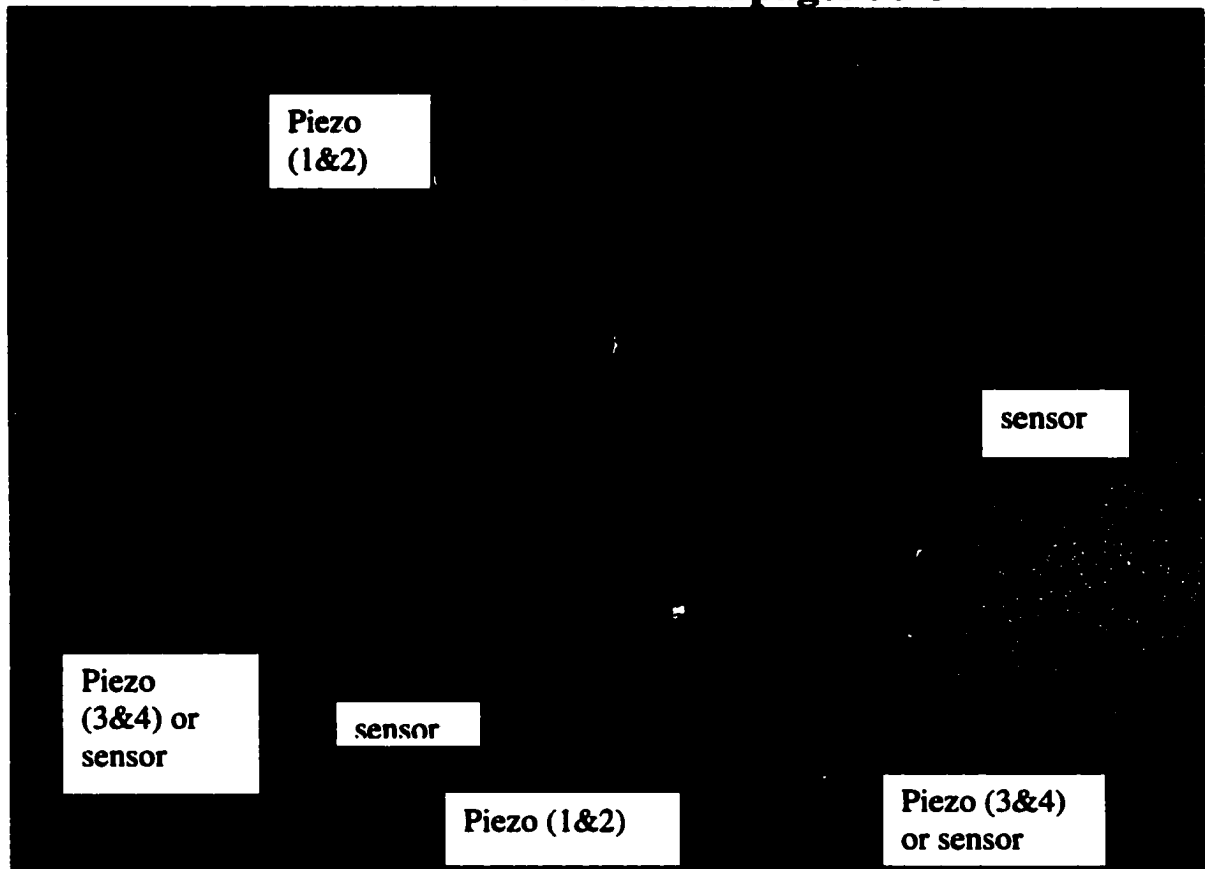


NUMBER OF NODES : 7322
 NUMBER OF ELEMENTS : 4075

ACTIVE UNITS SYSTEM : Inch (pound f)
 TEMPERATURE MODE : Relative Temperatures

MODE	FREQUENCY	MODAL MASS	RESIDUAL
1	564.6779	3.19995E-02	-7.13E-09
2	574.9463	3.13295E-02	1.54E-08
3	1340.0367	1.52960E-02	1.11E-09
4	9168.8393	1.15805E-02	-3.12E-11
5	10127.4471	9.20404E-03	-4.05E-11
6	13872.2753	2.99357E-02	-5.47E-12
7	34765.6681	4.67591E-03	6.59E-11
8	34912.3474	5.00870E-03	4.77E-11
9	41255.6014	6.39187E-03	1.30E-10
10	55409.4789	6.76534E-03	1.62E-10

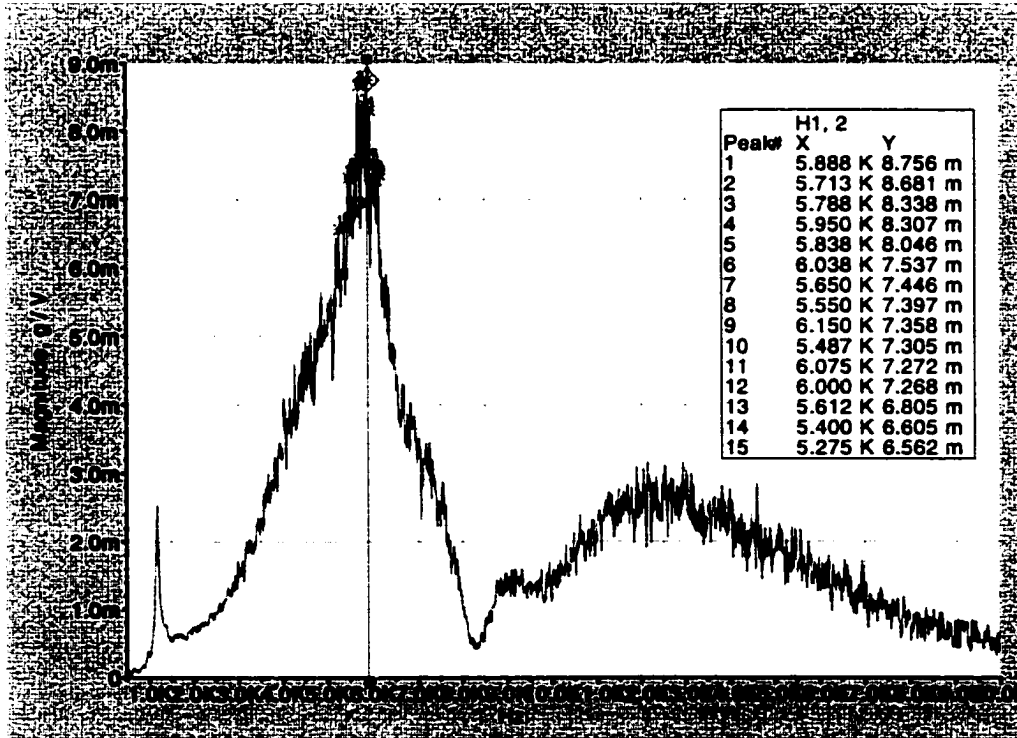
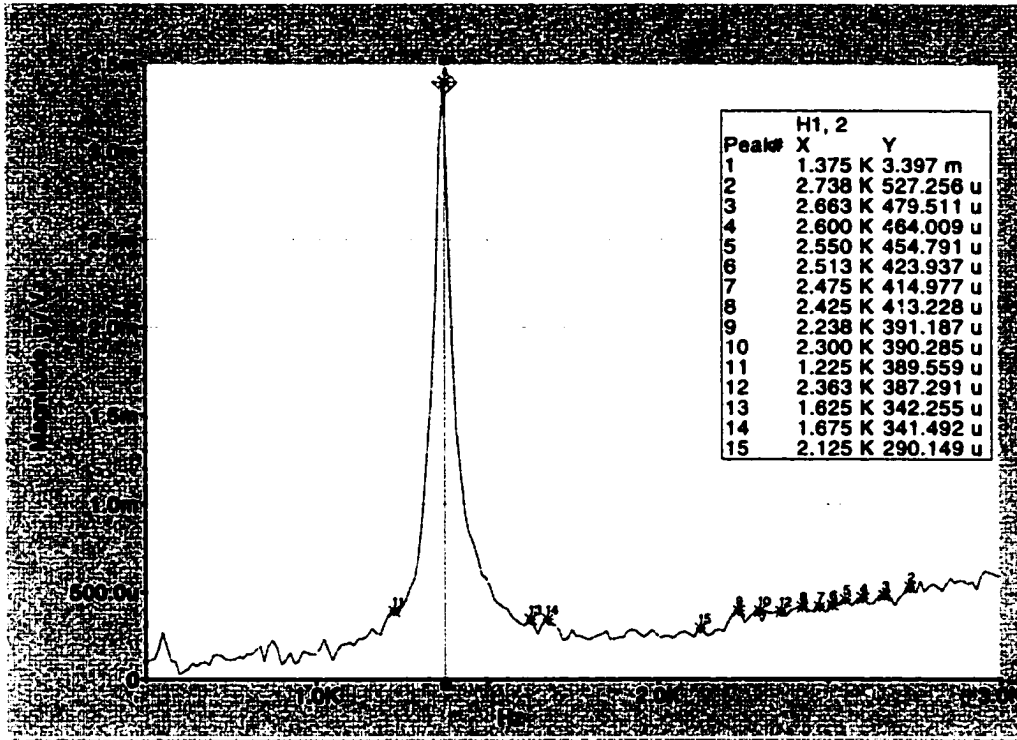
APPENDIX D
SIGNAL CAL ACE SOFTWARE GRAPH RESULTS

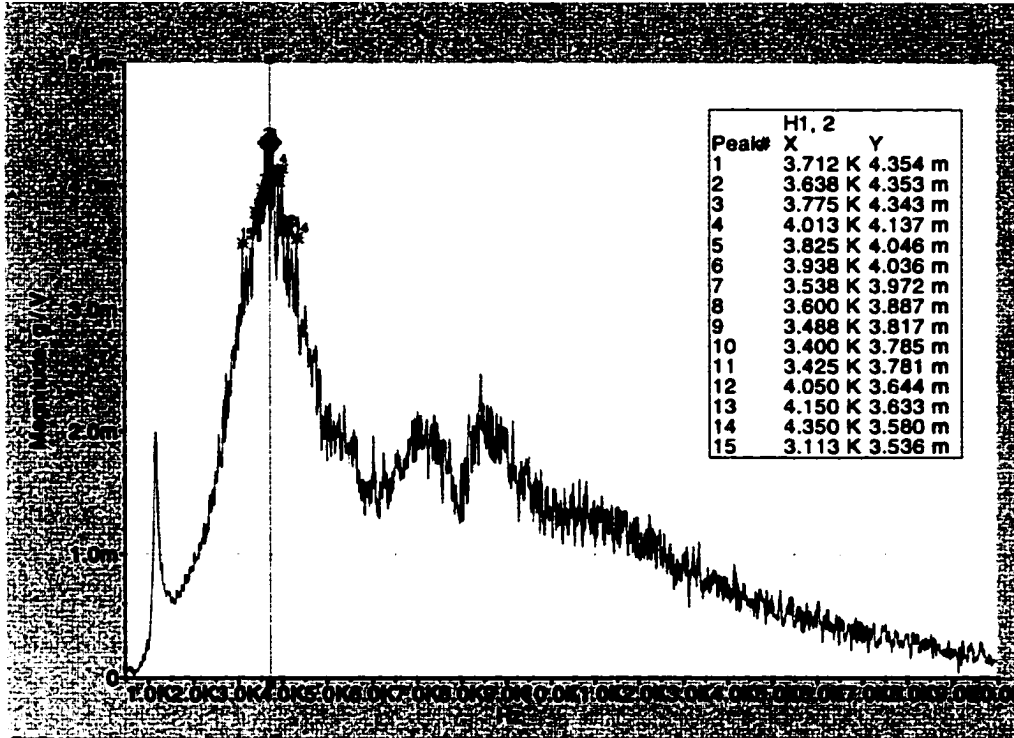
Sensor Placements Results pages 50-64

RED arrows indicate all the location the sensor and piezos were placed.

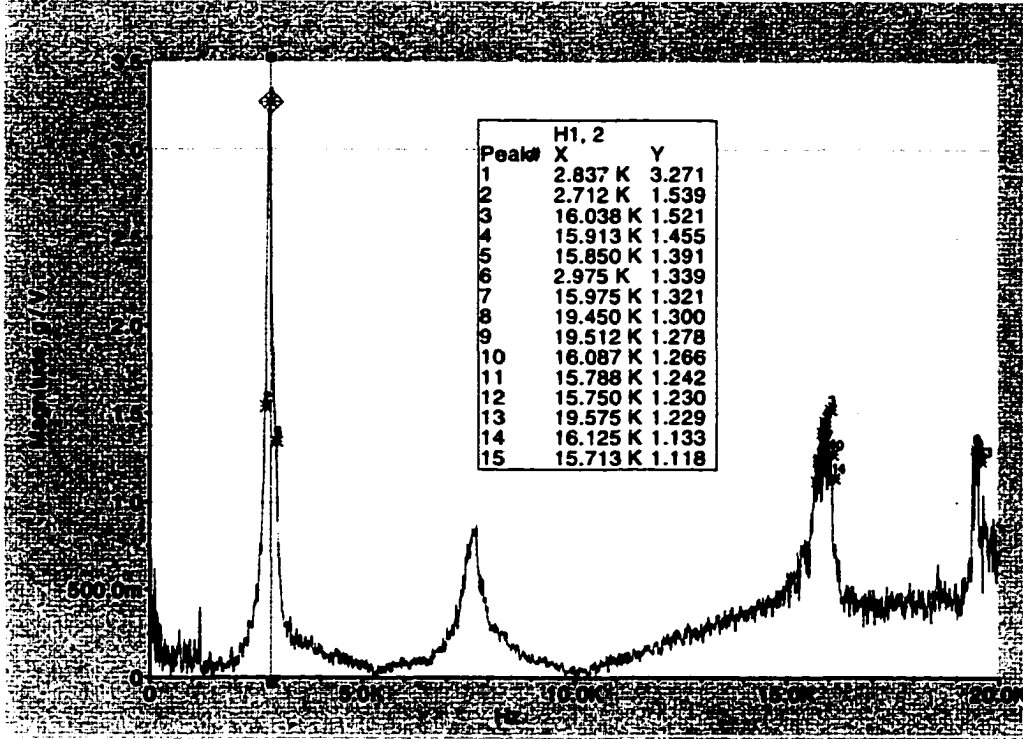
Brass mount

In the middle of the implant place the sensors.

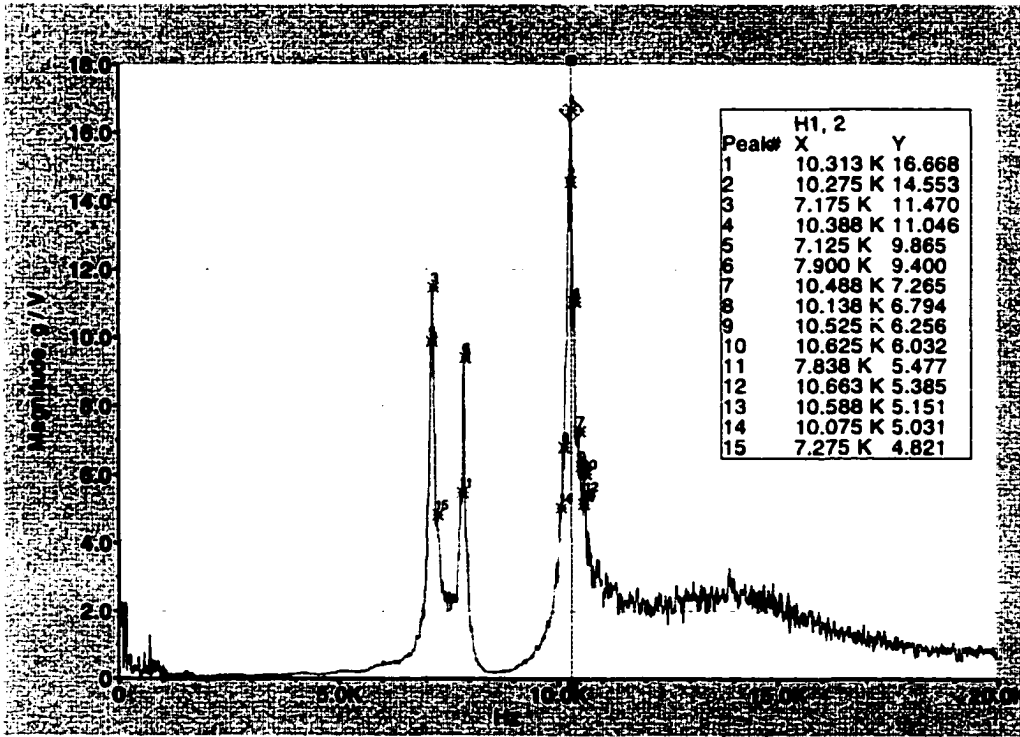




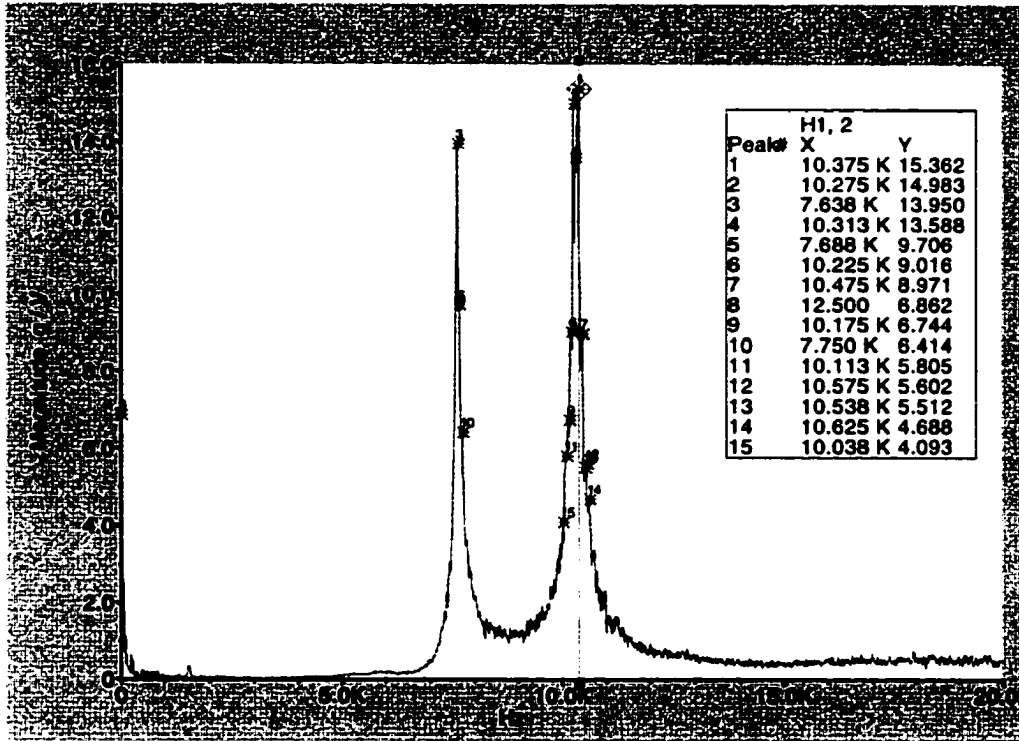
Unthreaded Case



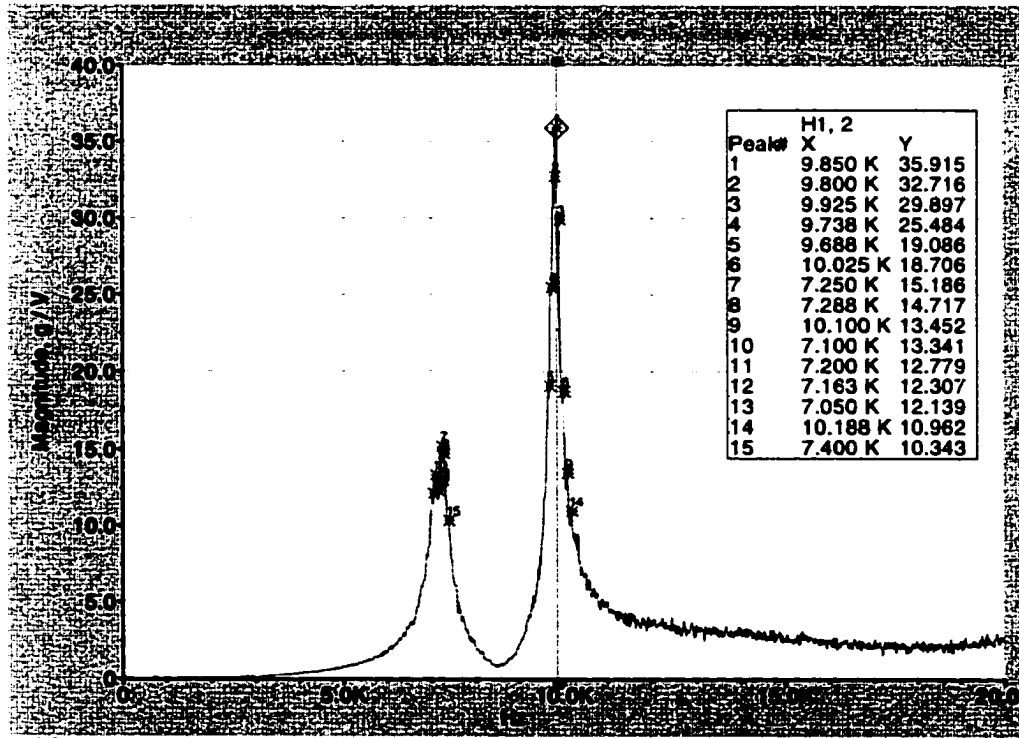
Threaded Case moving sensor closer to the one side of the piezos.



Threaded Case moving sensor to the original position.

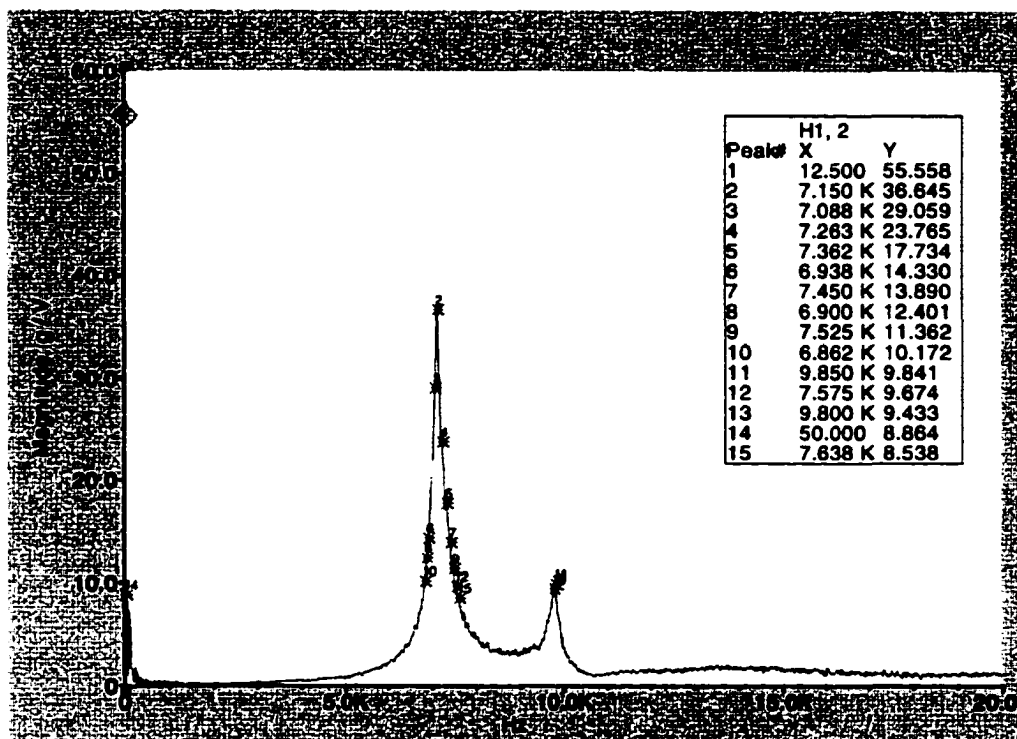


Threaded Case With only one piezo on the left sided tape.



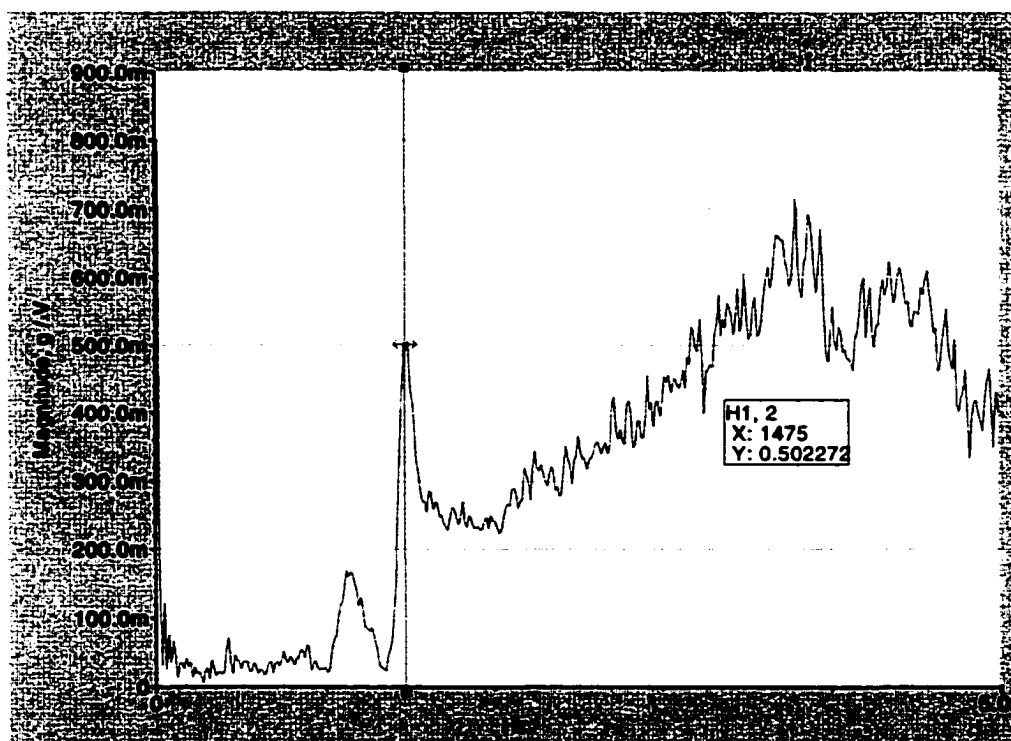
threaded Case

With the one sided piezo on only.



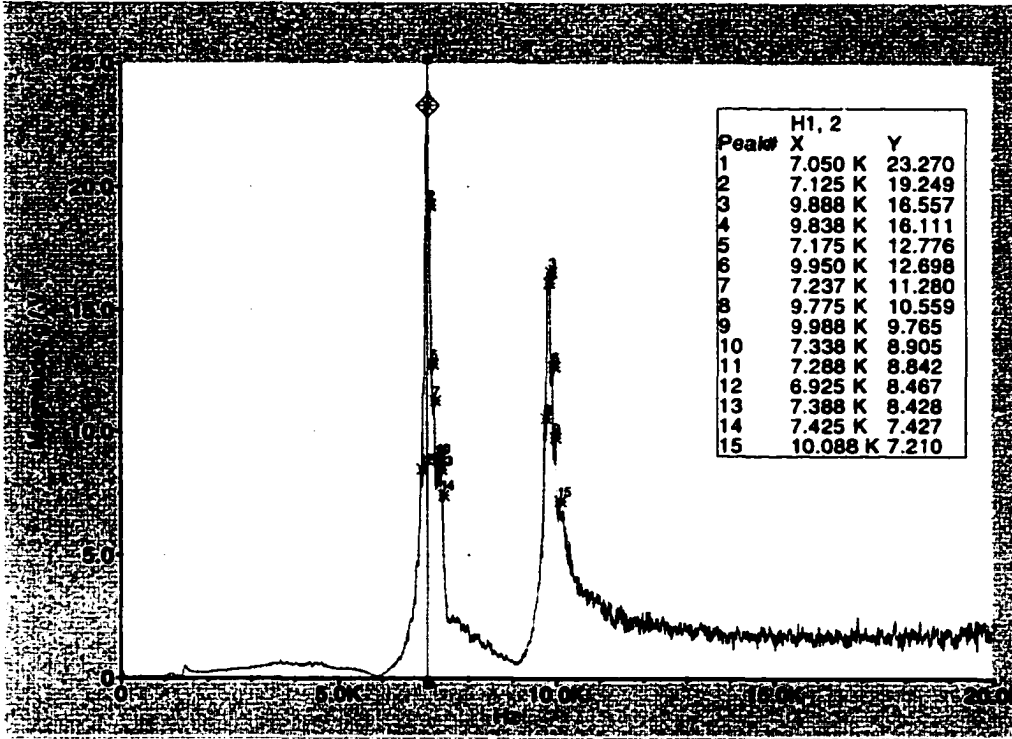
Threaded Case

Closer look at the small peak at 0-5KHz.



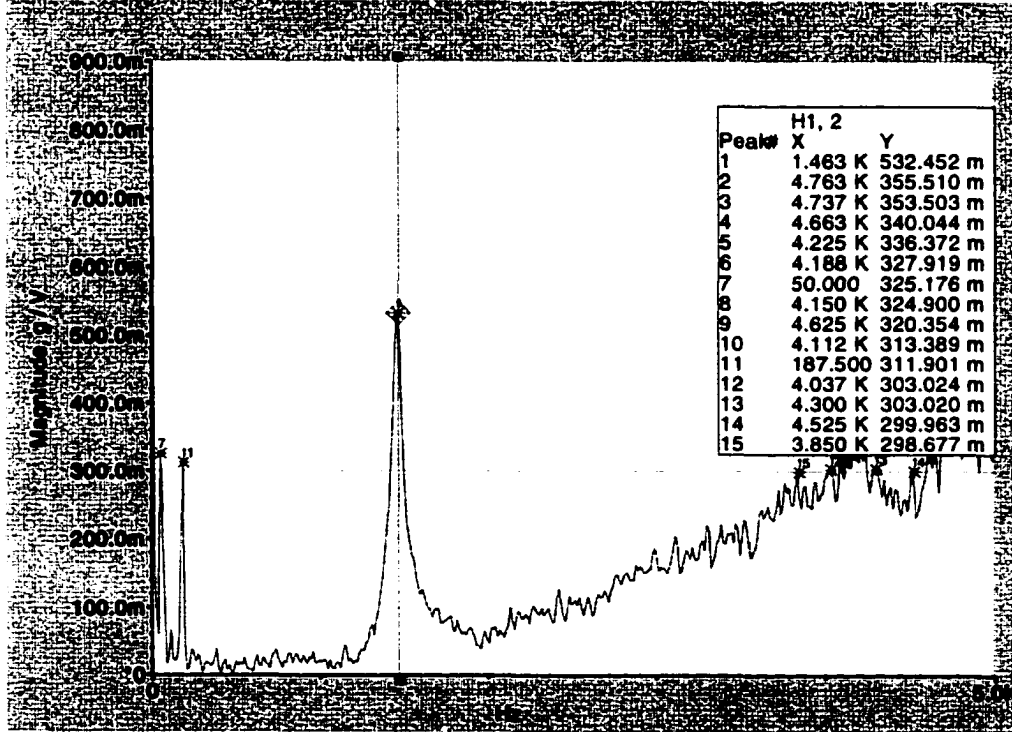
Threaded Case

With the sensor changes direction of measures.

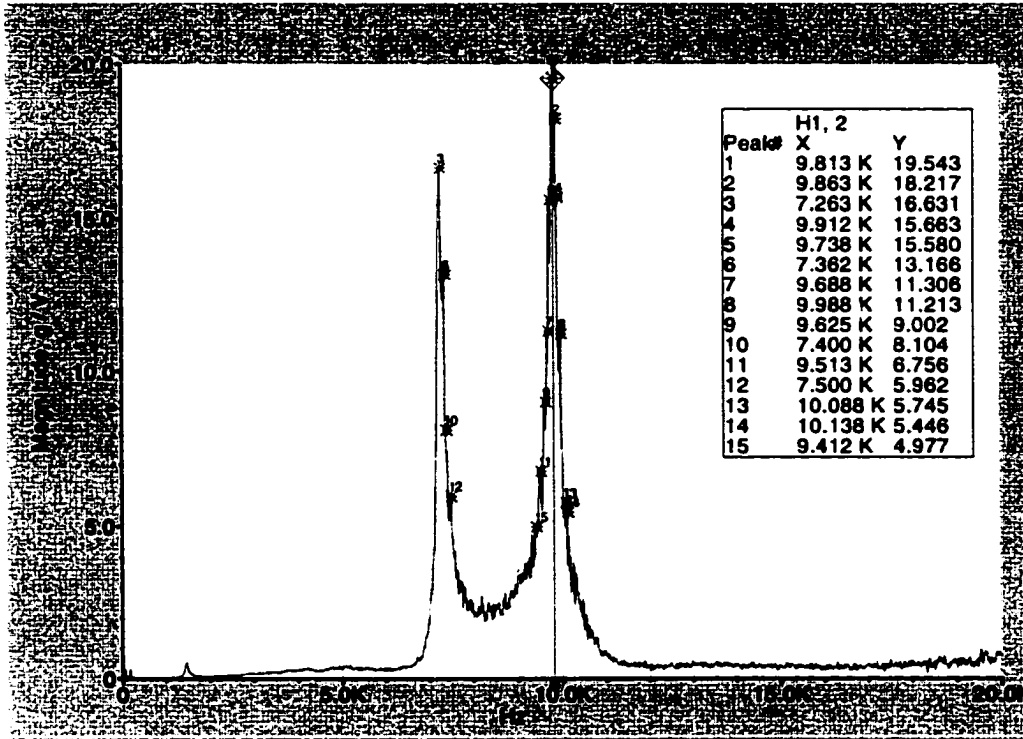


Threaded Case

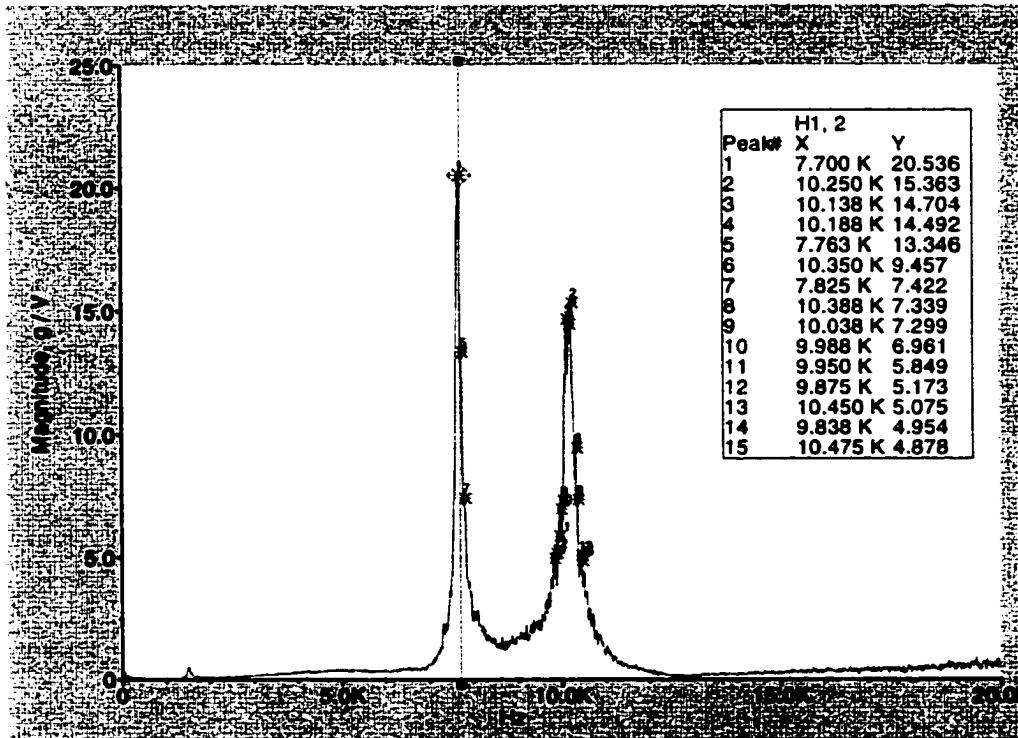
with the sensor change direction.



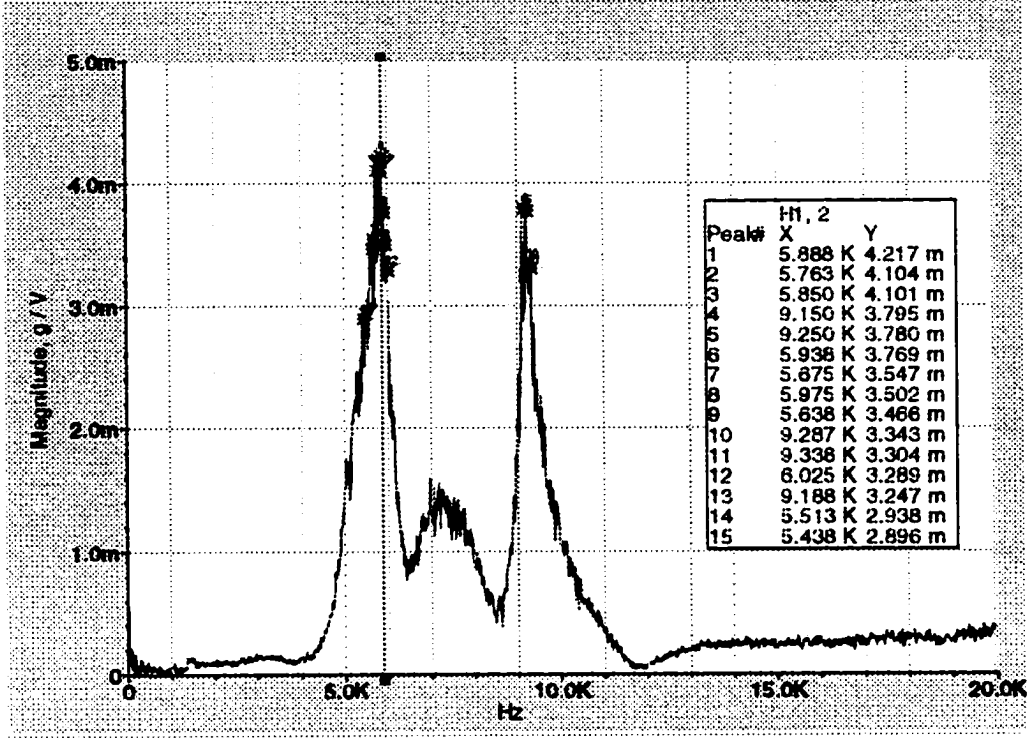
Threaded Case With the sensor change direction.



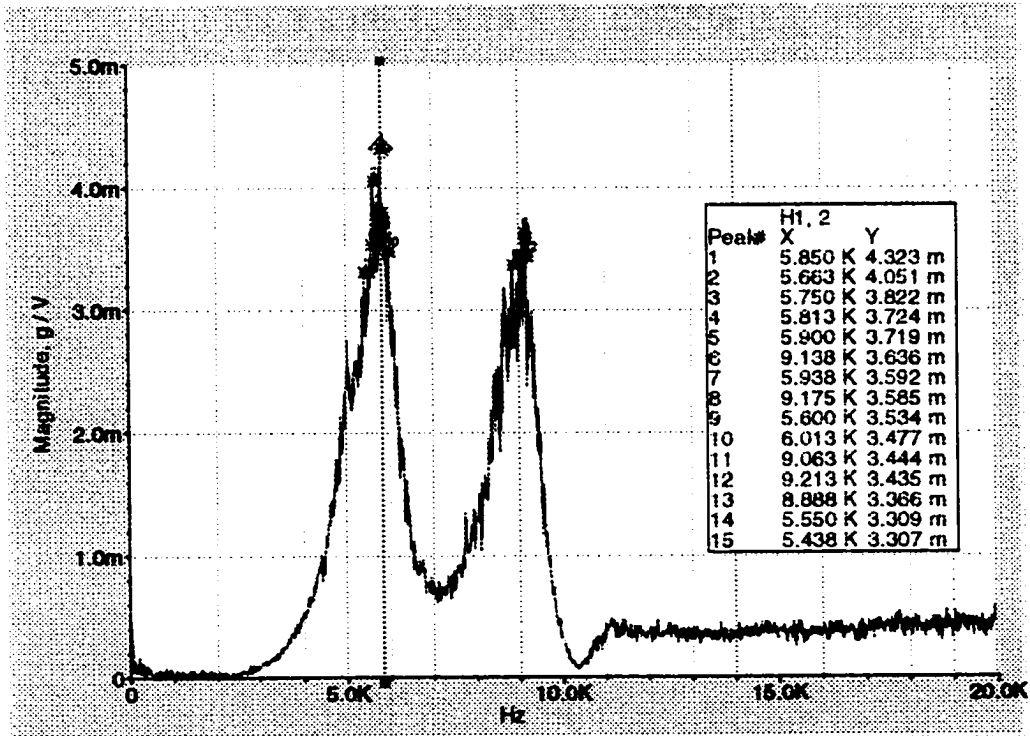
Threaded Case Unbalanced mass Same as above



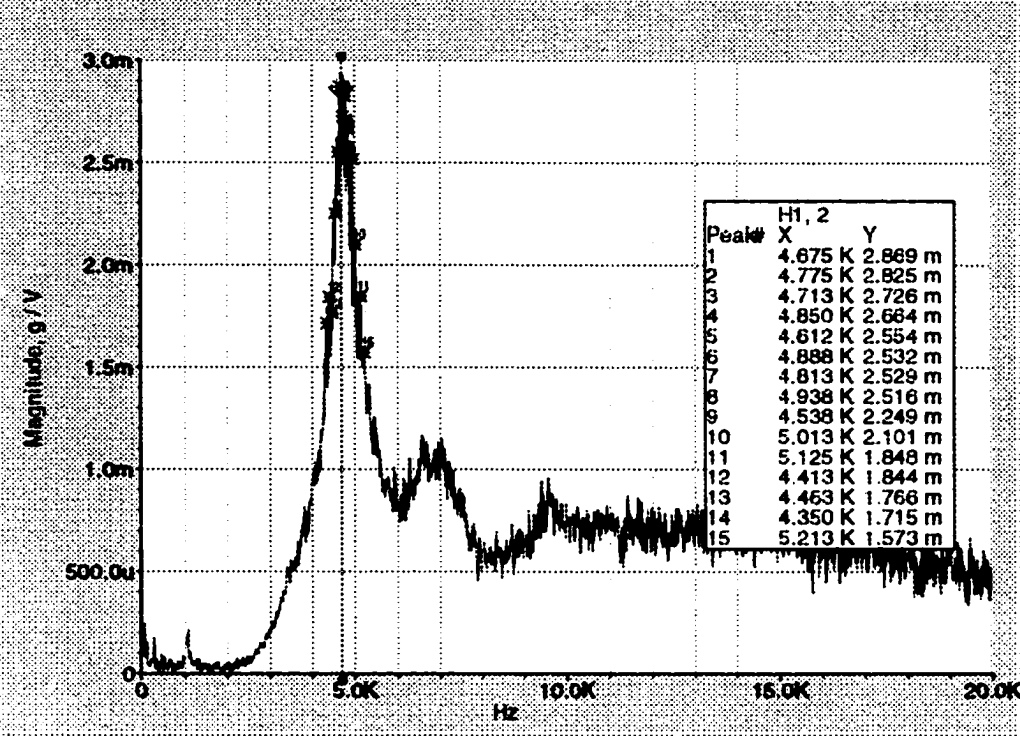
Threaded Case



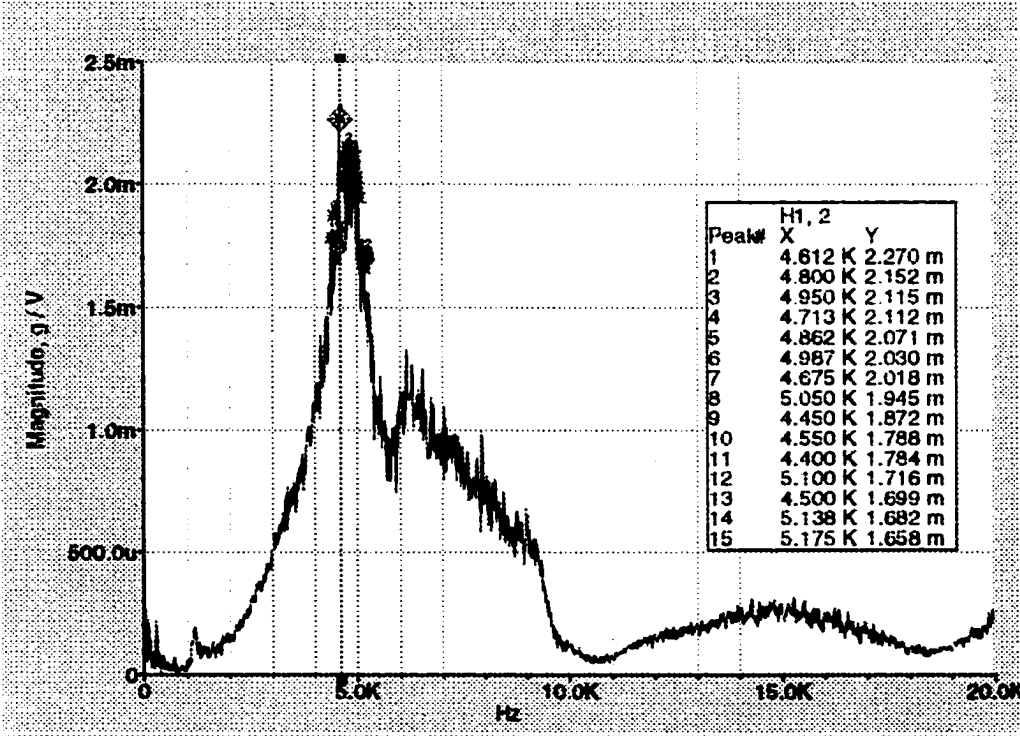
Threaded Case



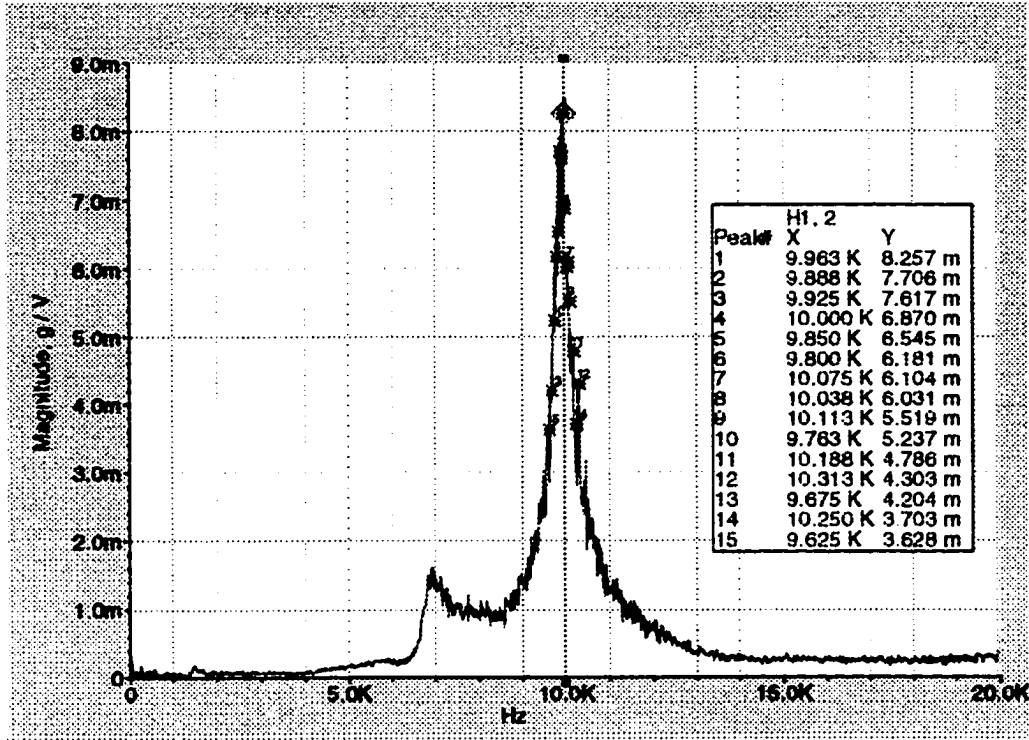
Threaded Case



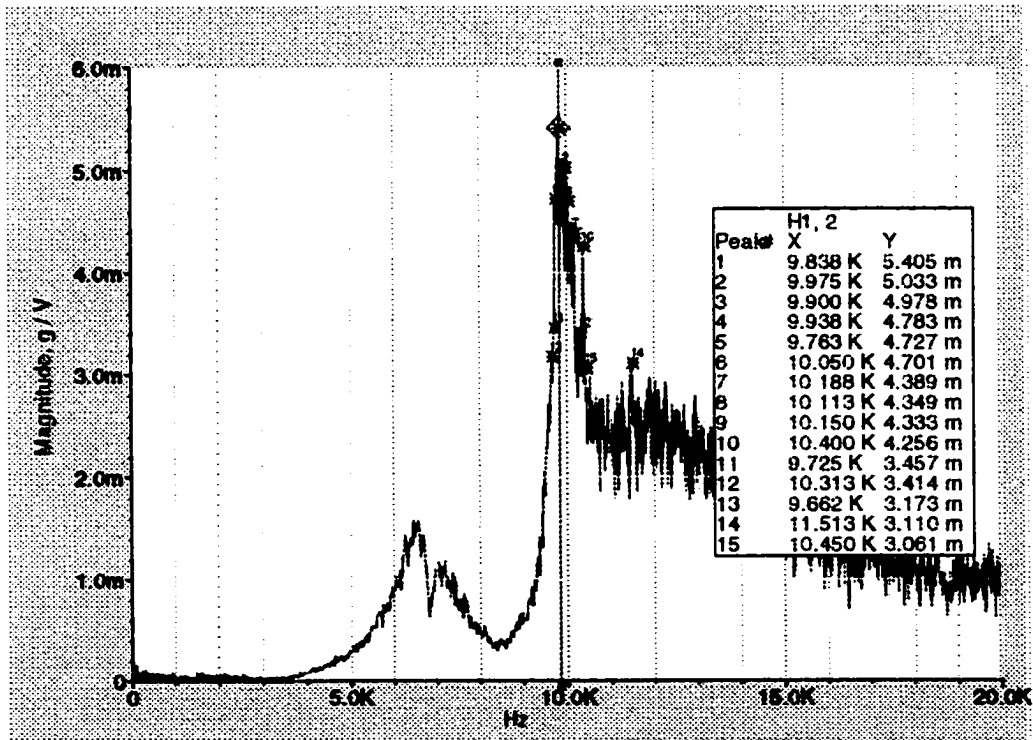
Threaded Case



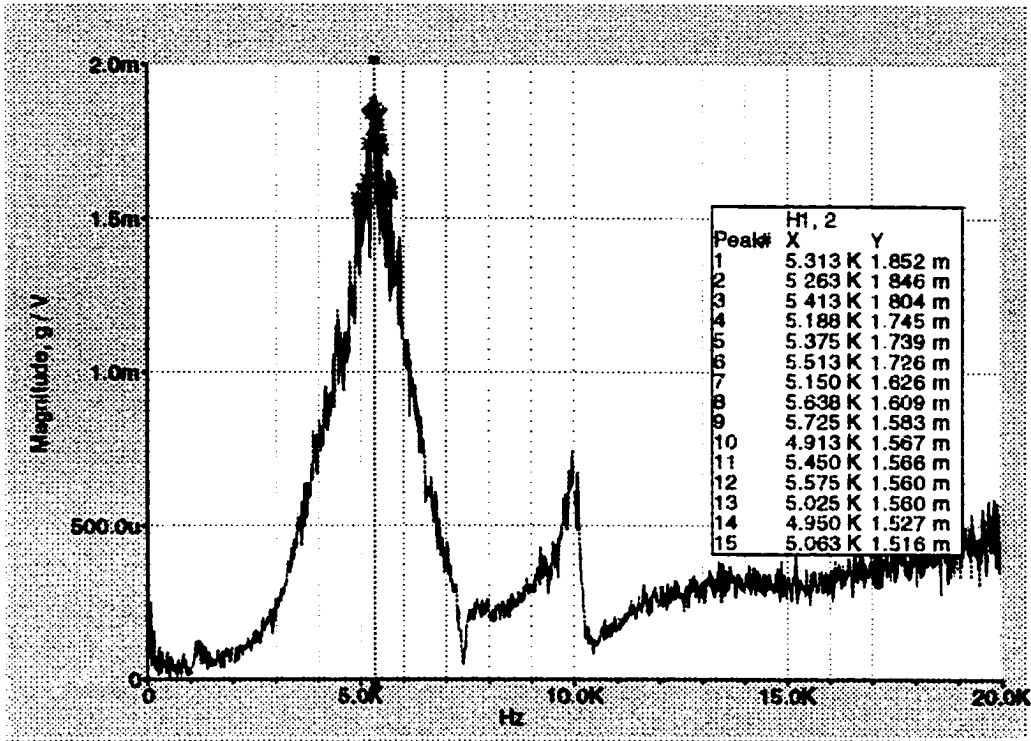
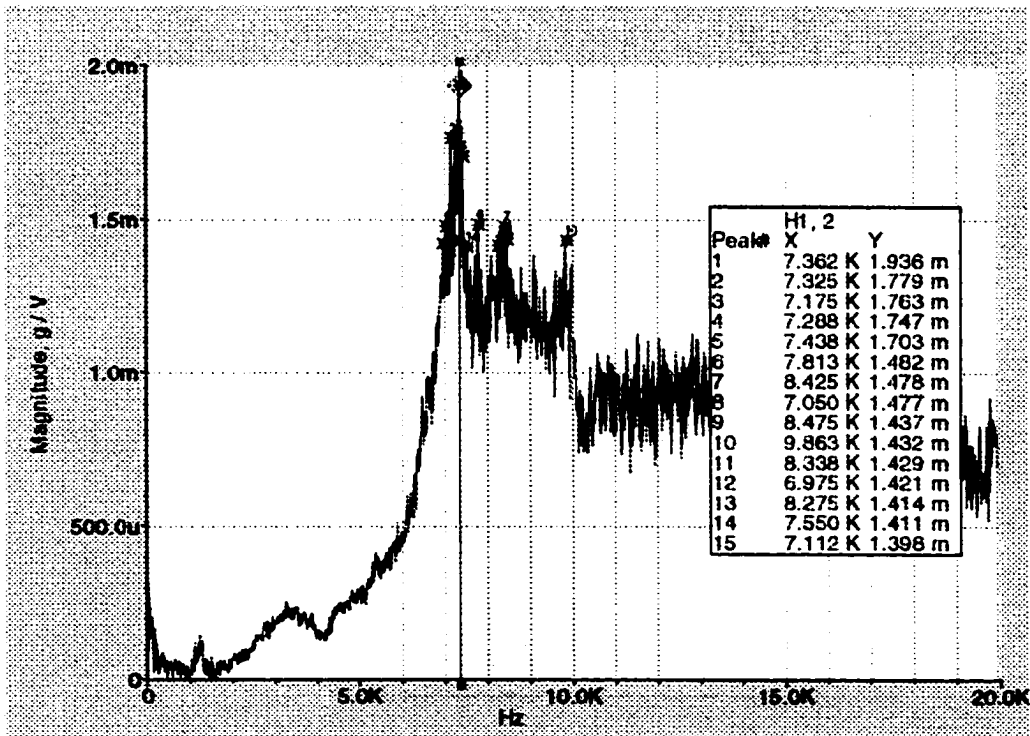
Threaded Case
Unbalanced masses of sensors



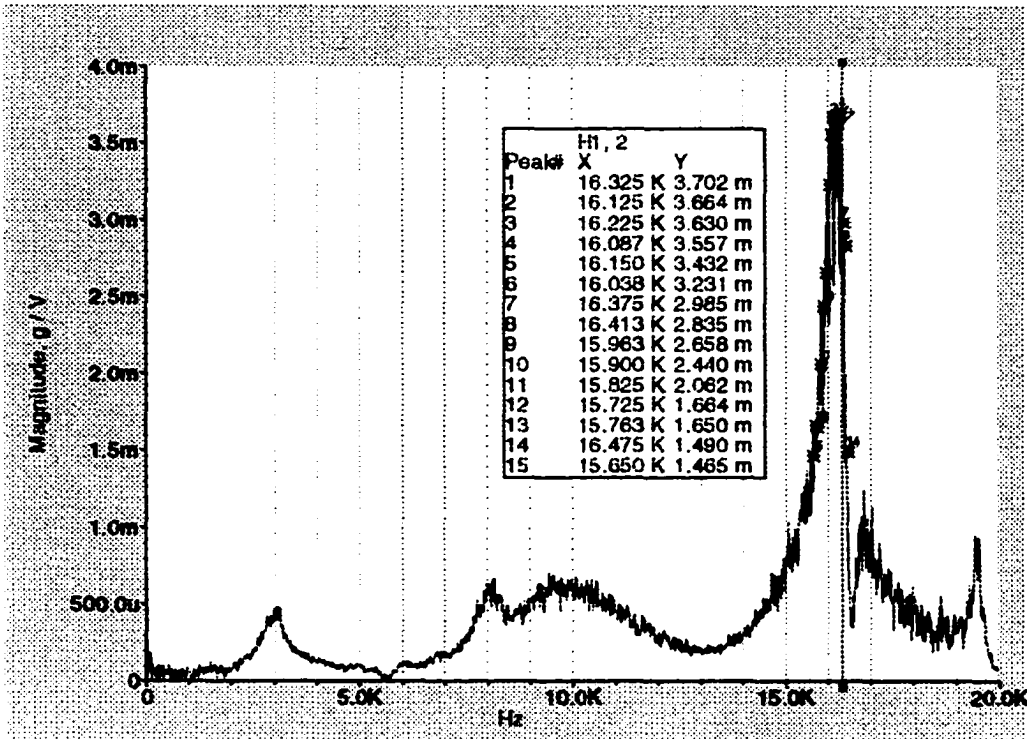
Threaded Case
Unbalanced



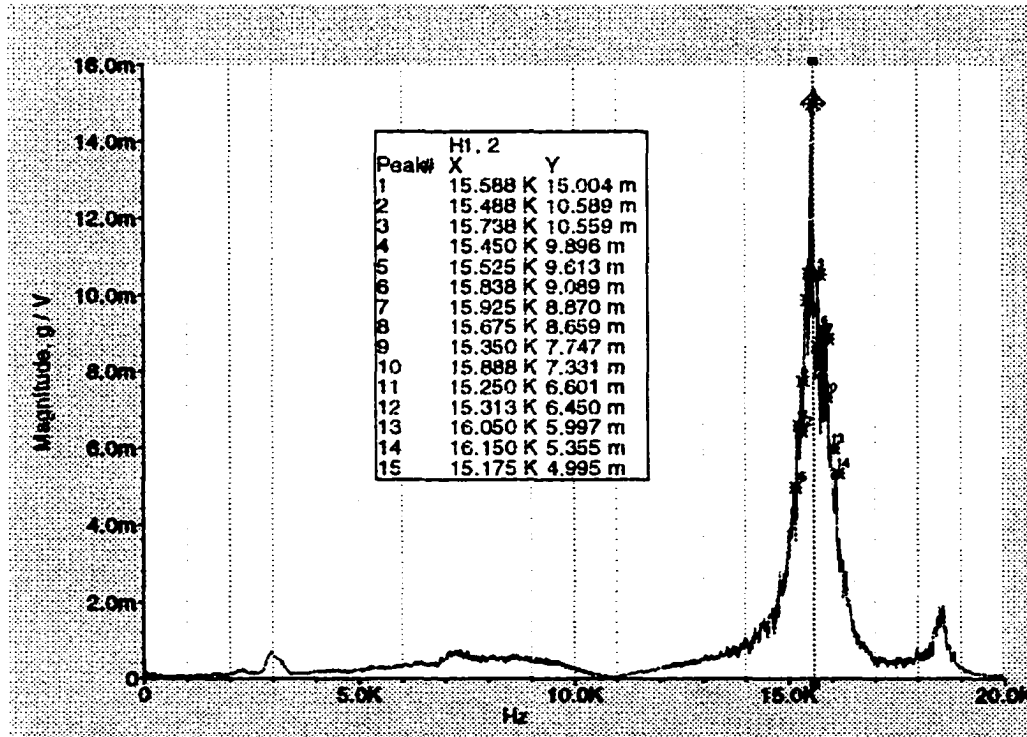
Threaded Case

Threaded Case
unbalanced masses of sensors

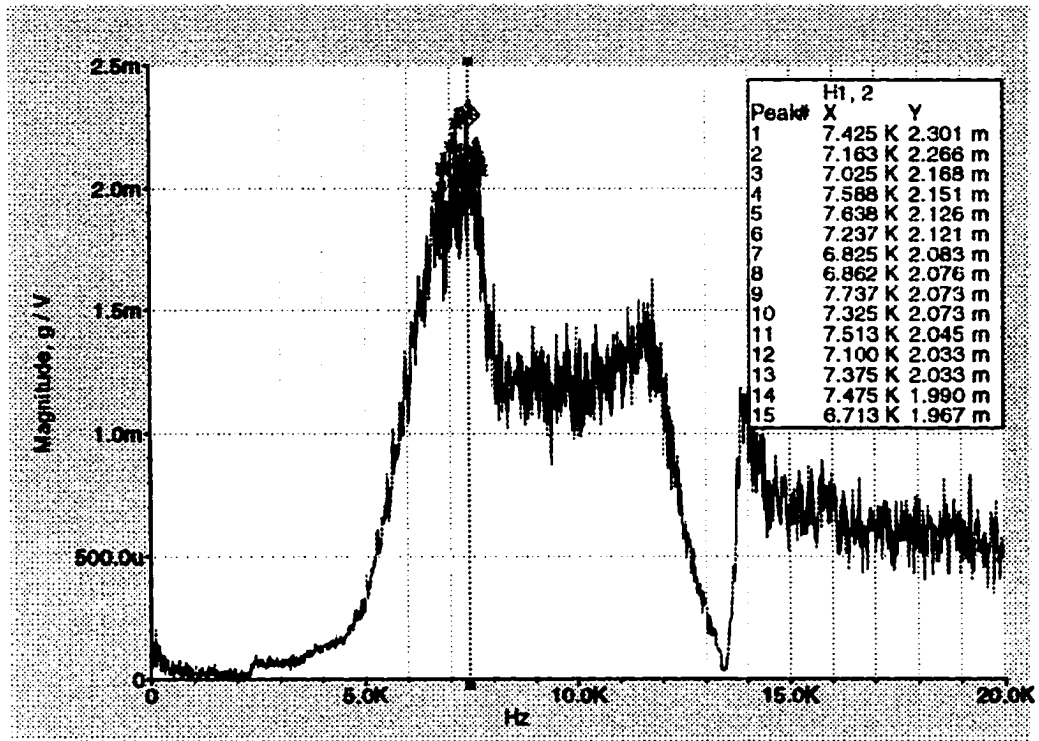
Unthreaded Case



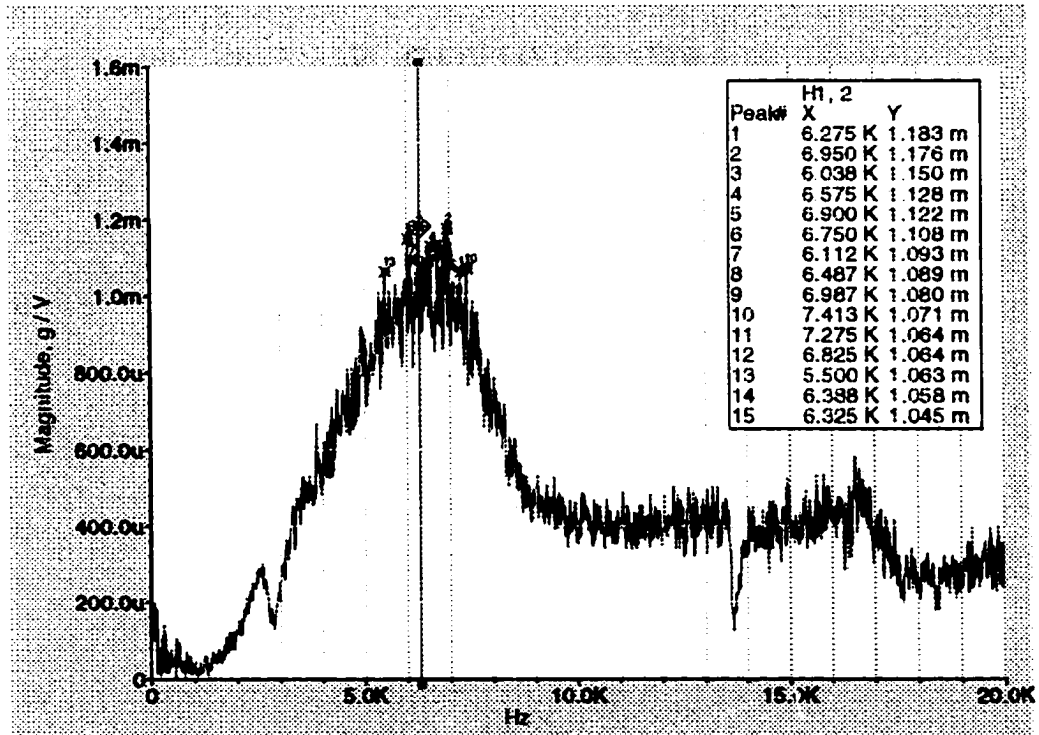
Unthreaded Case



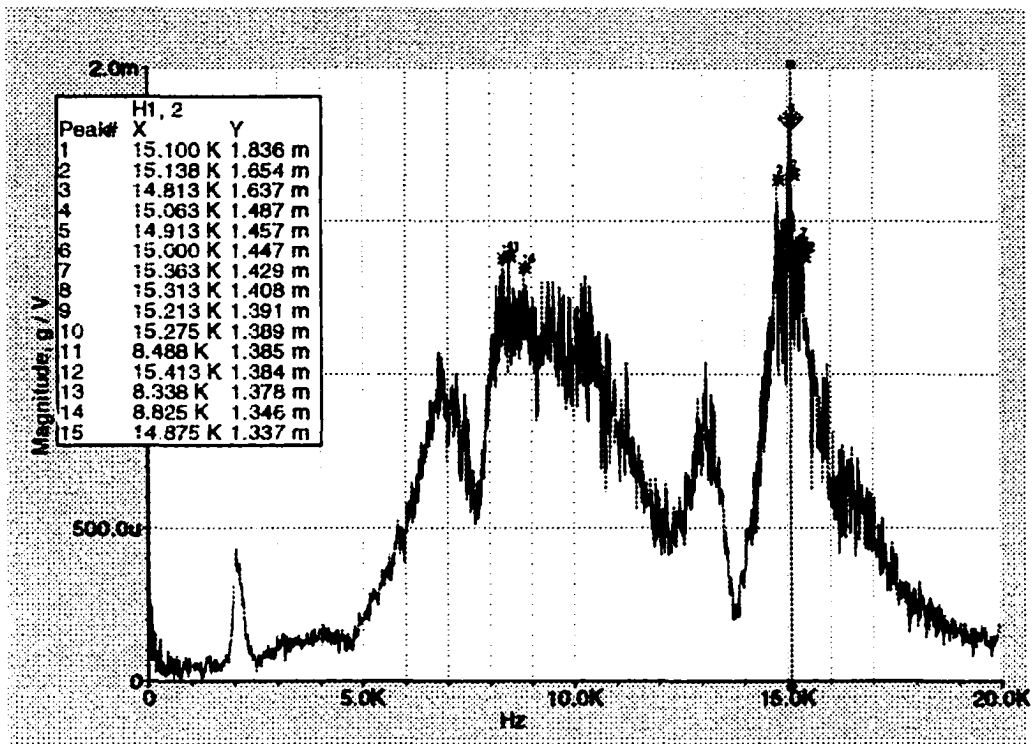
Unthreaded Case



Unthreaded Case



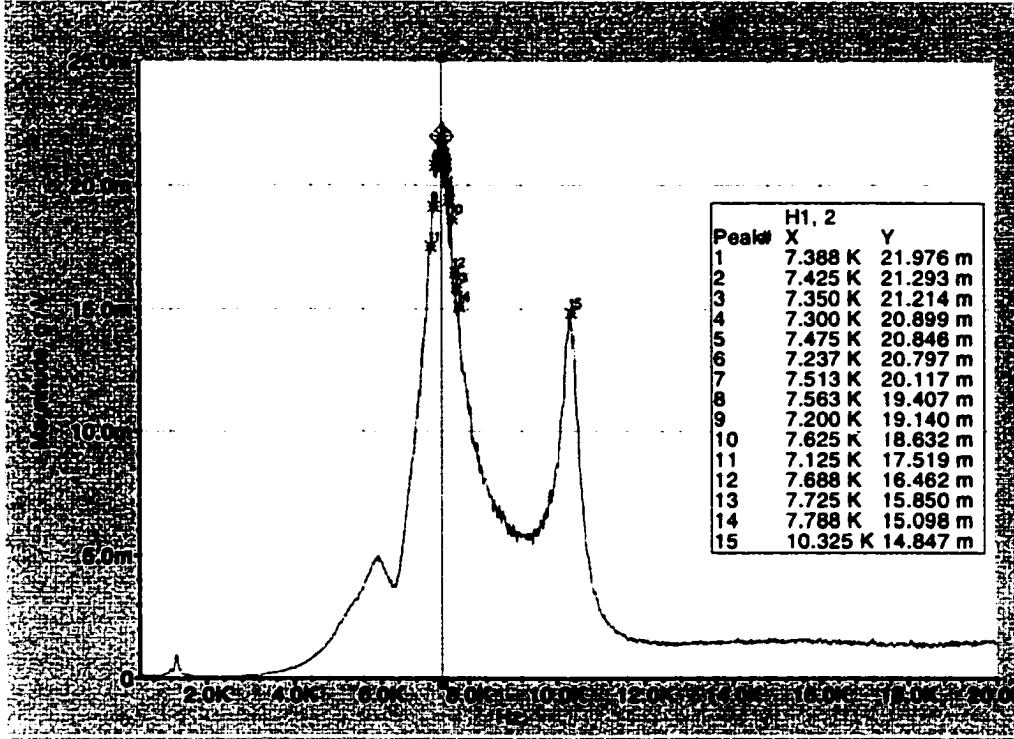
Unthreaded Case
Balanced masses of sensors



Brass mount

piezo 1&2 on

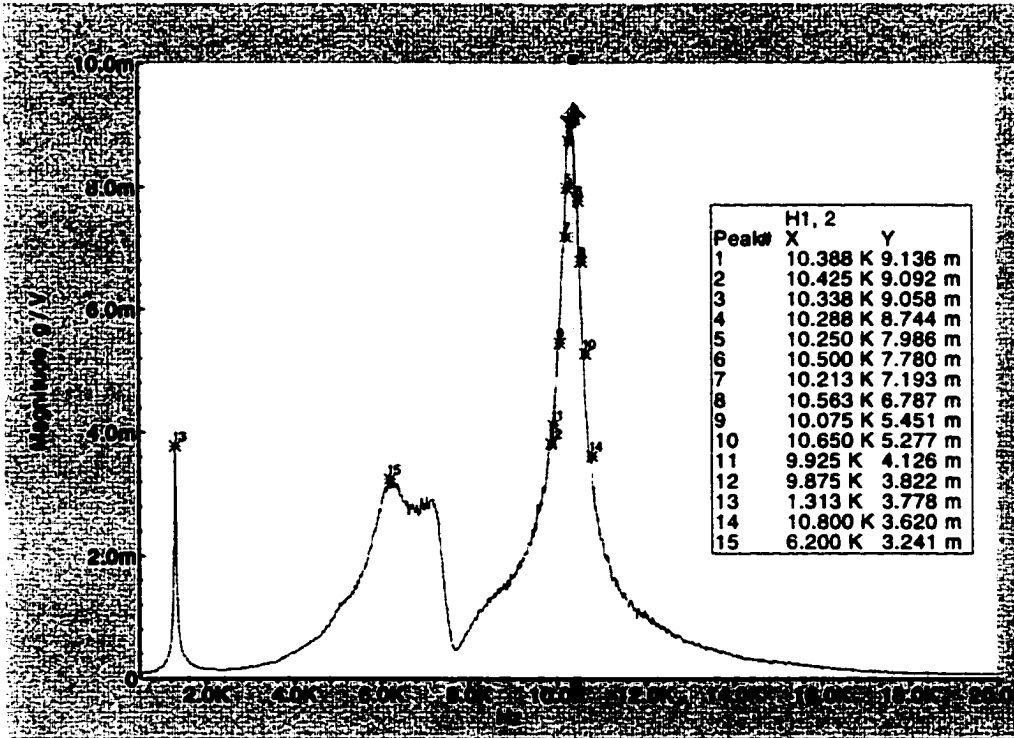
Torsional Vibration

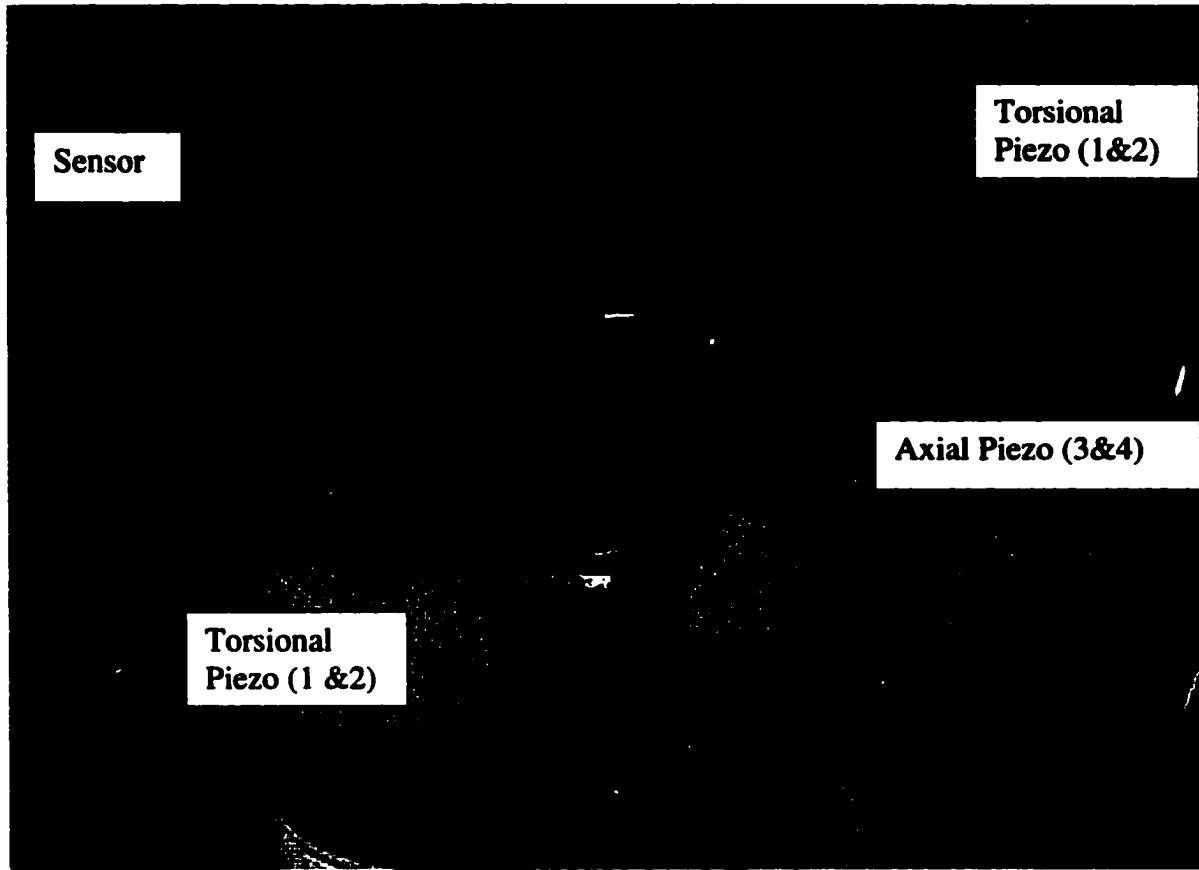


Brass mount

piezo 3&4 on

Axial Vibration



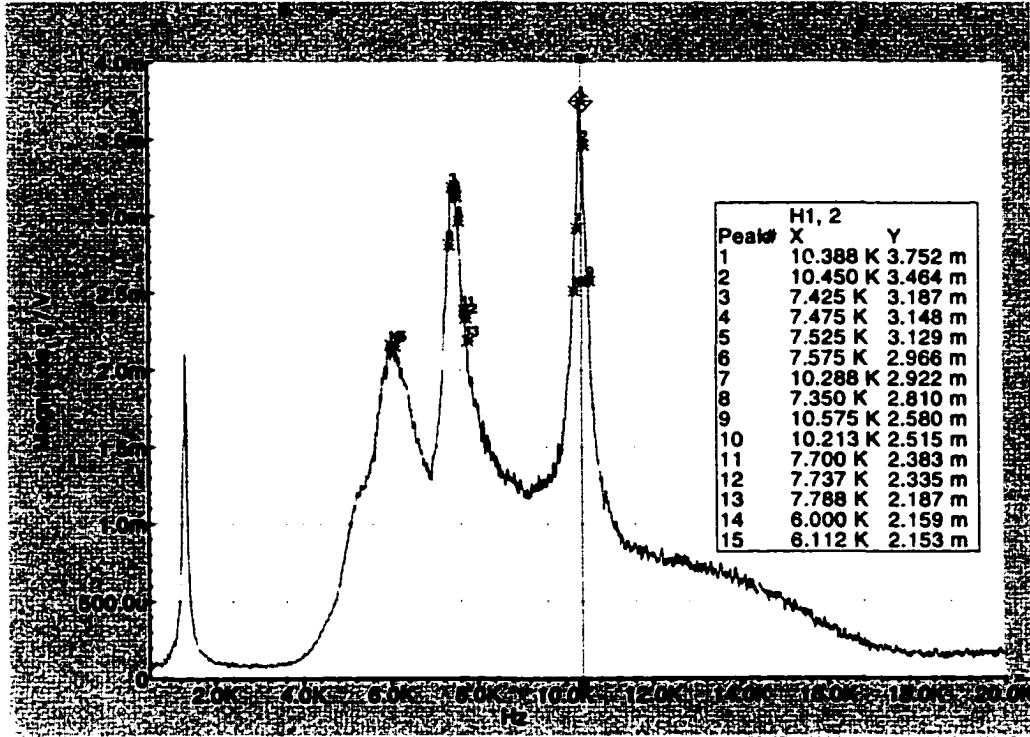
FINAL PLACEMENT OF SENSOR AND PIEZOS PAGES 66-76

PAGES 77-88 shows the testing results for Table 2-7.

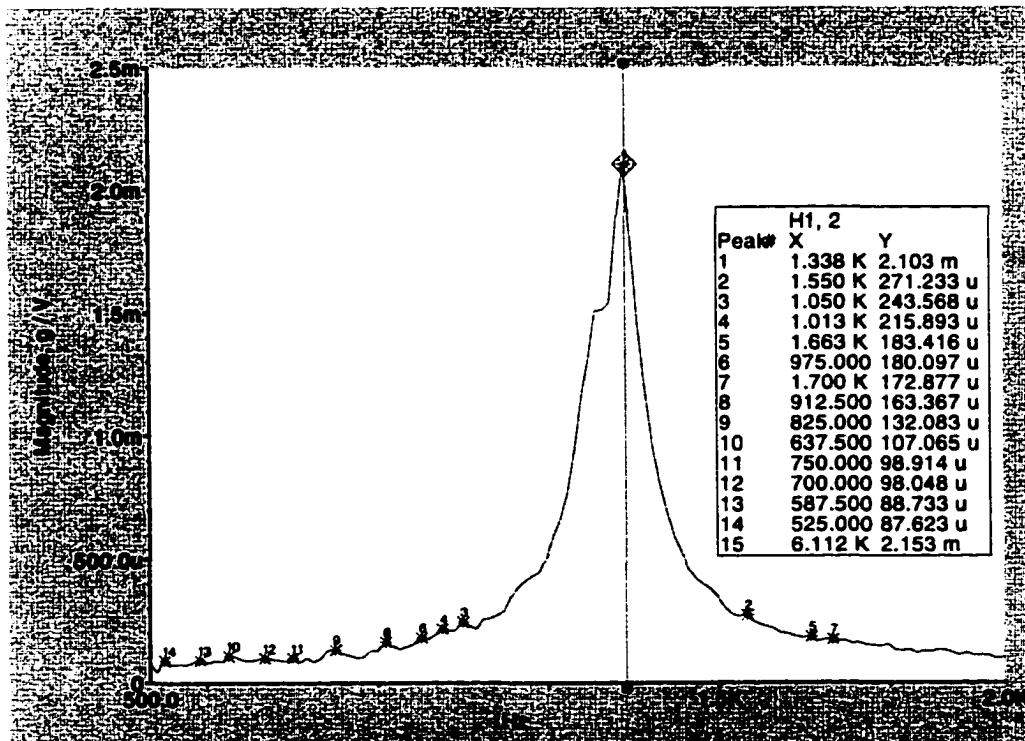
PAGES 89-104 shows the testing results for Table 2-6.

PAGES 105-153 shows the testing results for Table 2-8,2-9,2-10,2-11

Brass mount vibration with axial piezo 3&4

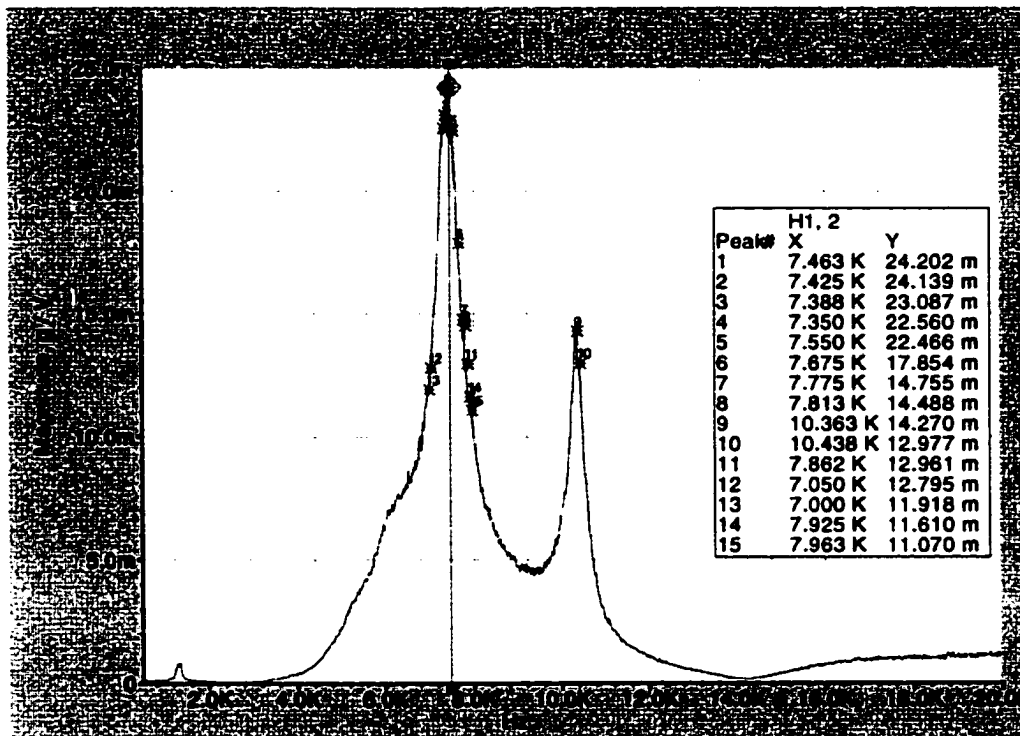


Close up of Torsion vibration

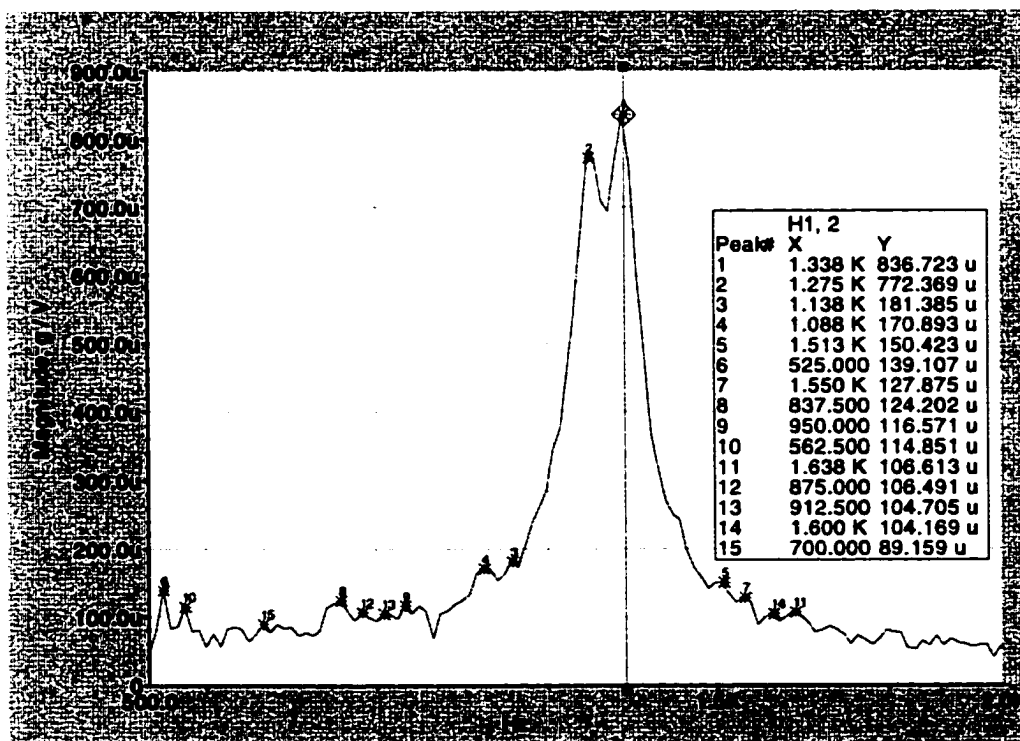


Brass Mount

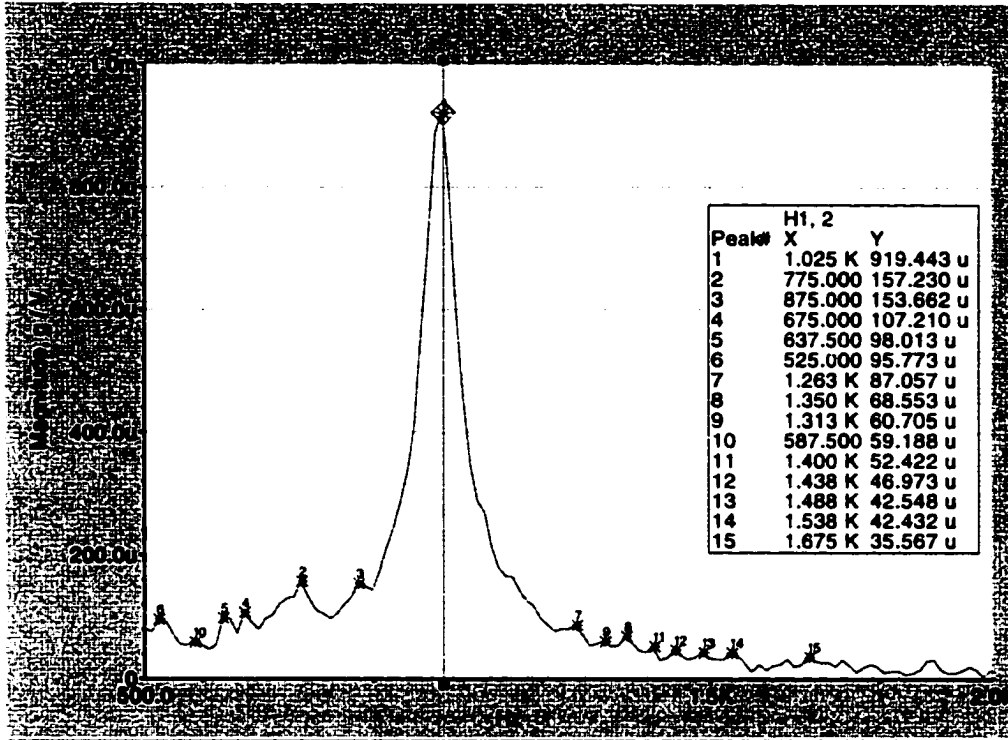
Torsion vibration Piezo 1 & 2



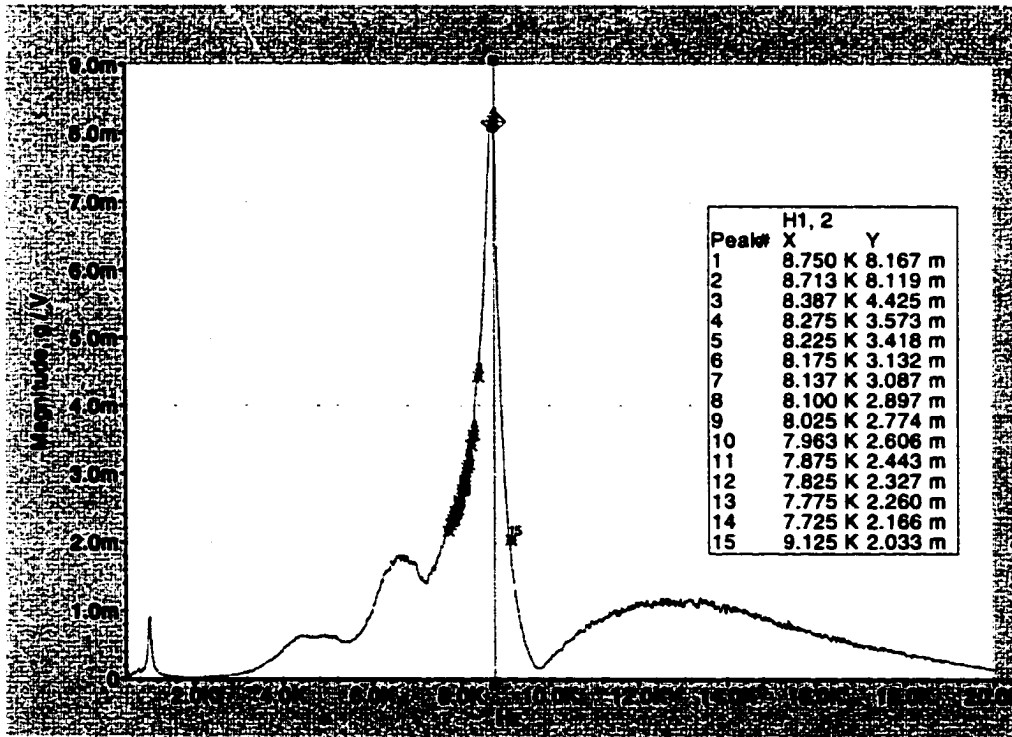
Torsion close up



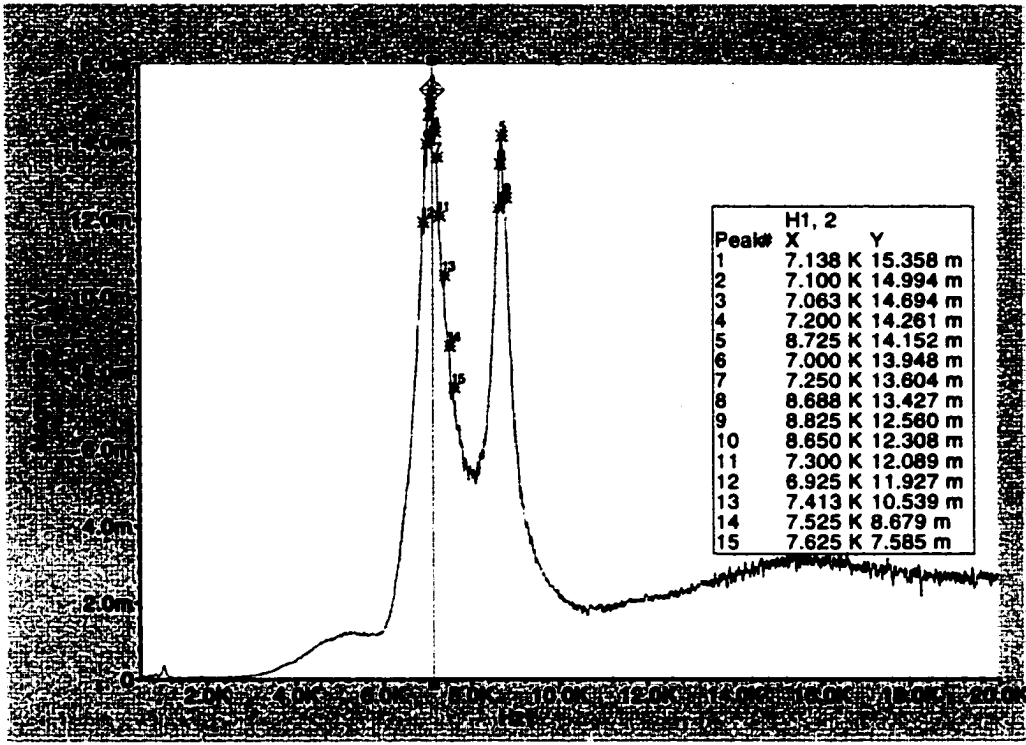
Acrylic mount Threaded Axial vibration
P3&P4



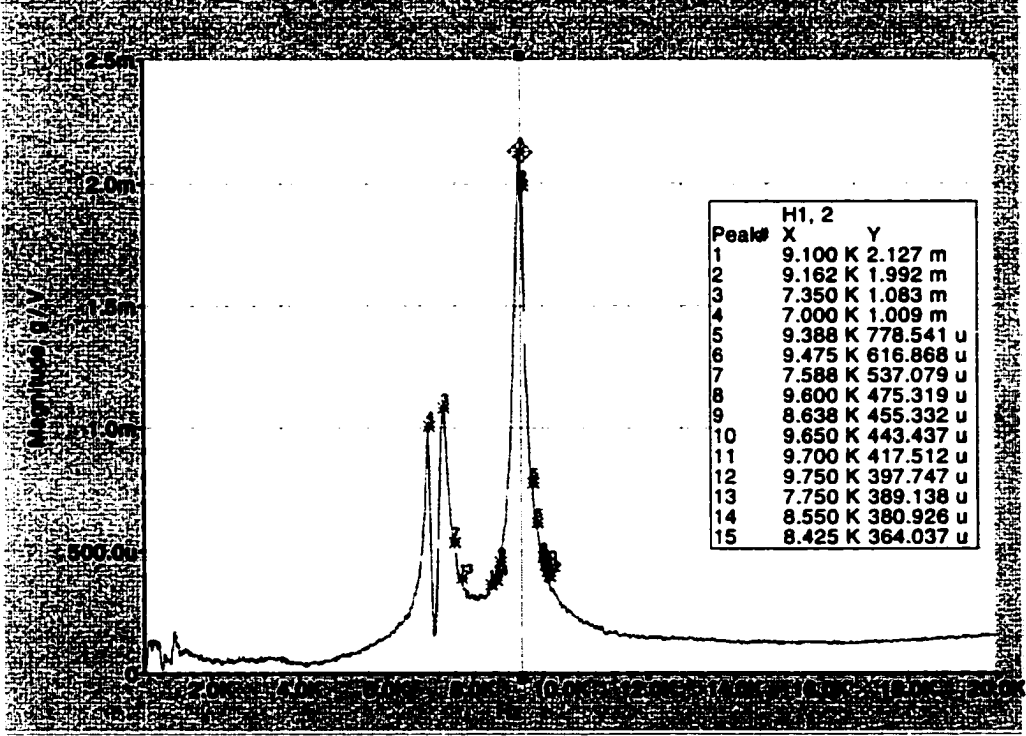
Axial max value



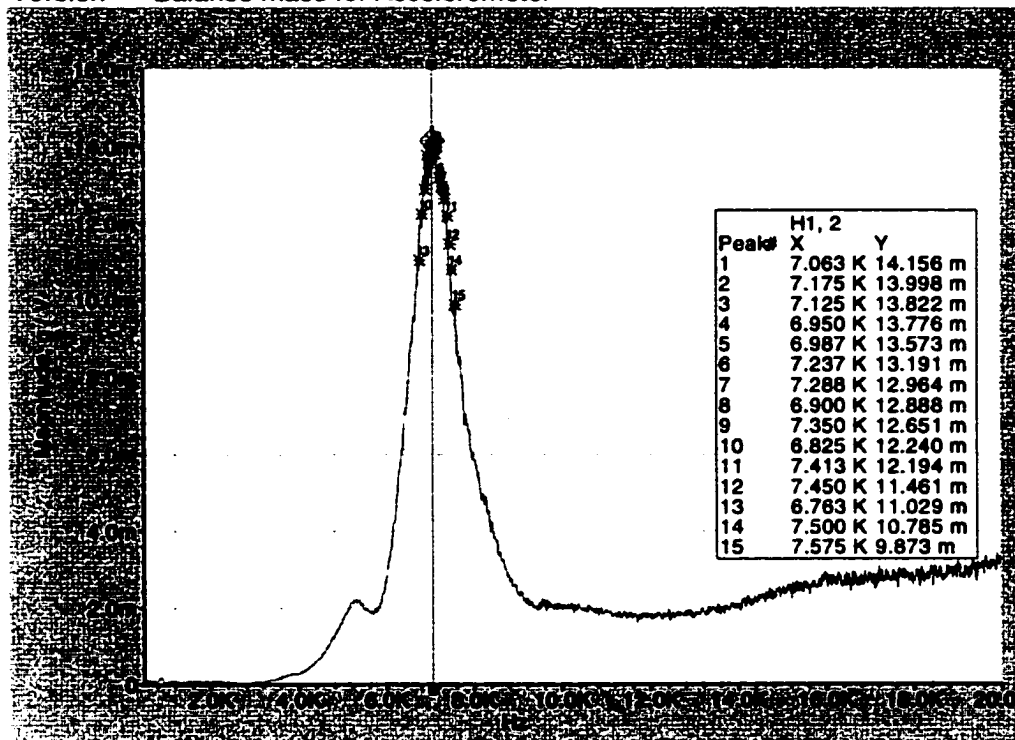
Torsion Vibration



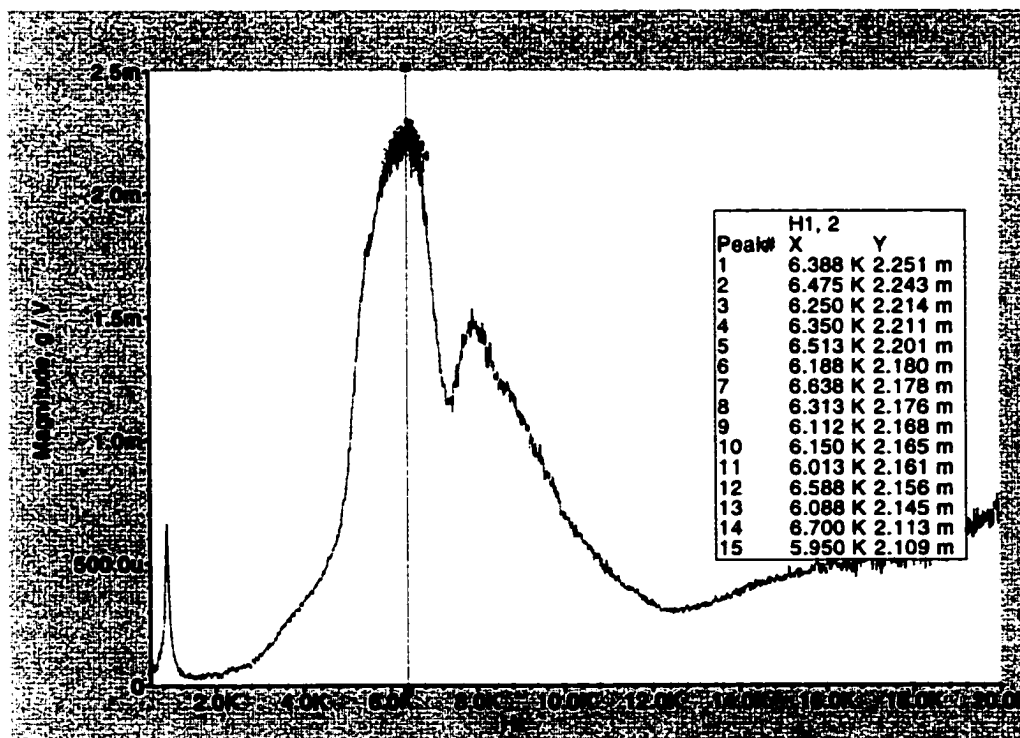
Better response



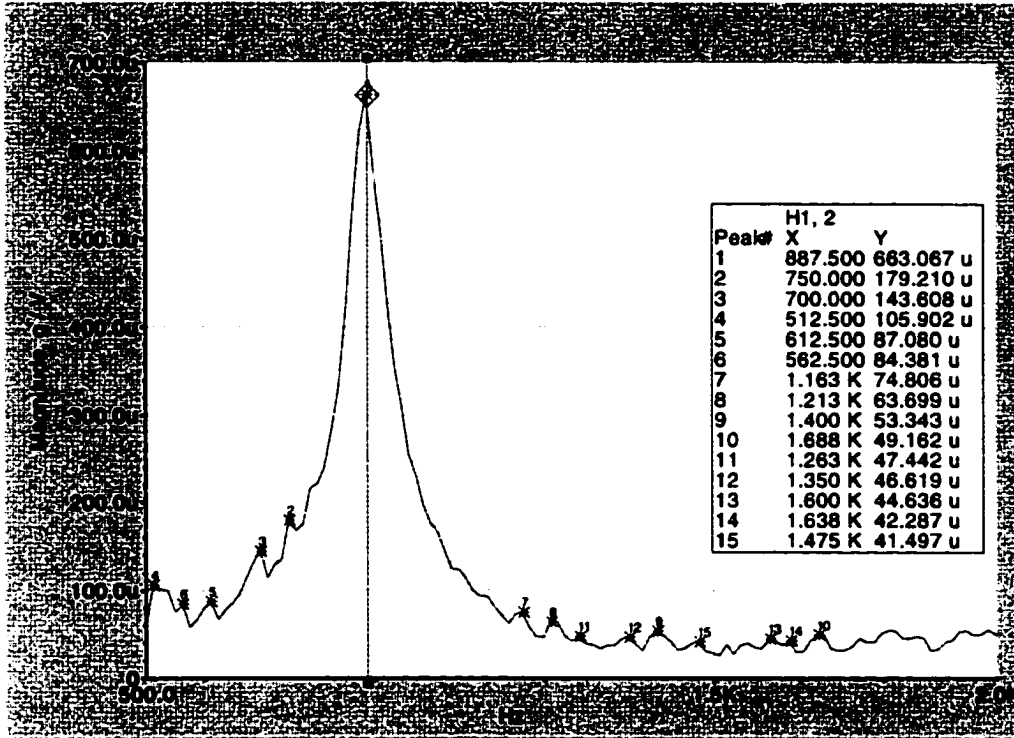
Torsion Balance mass for Accelerometer



Axial Balance mass



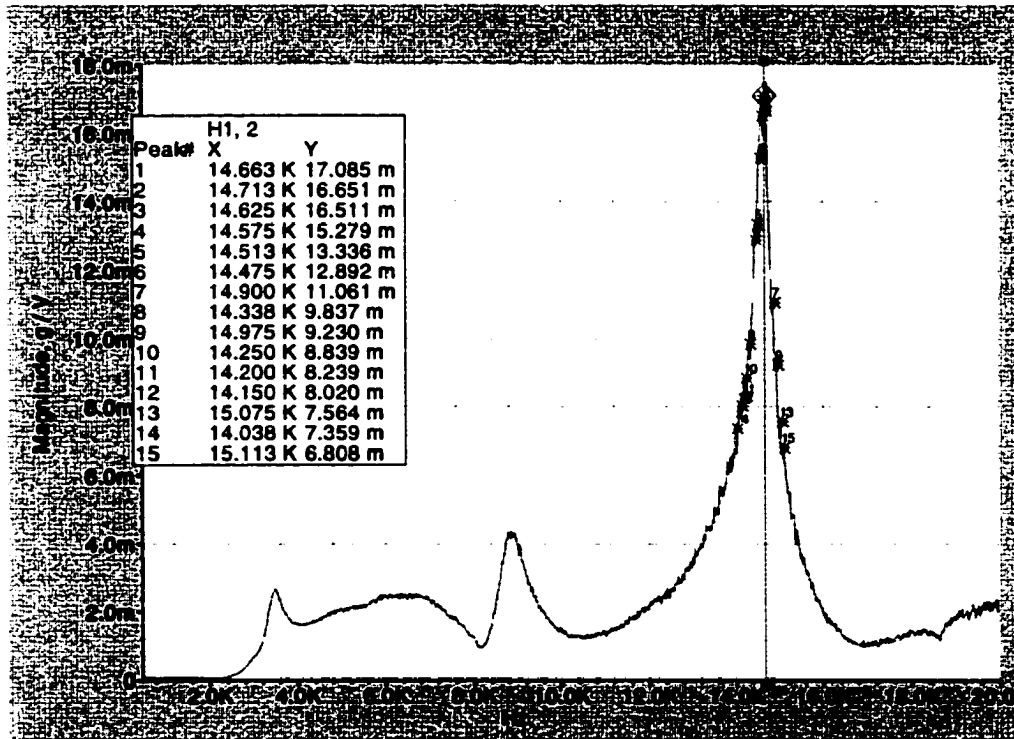
Close up of torsion



Unthreaded acrylic mount

Torsion vibration

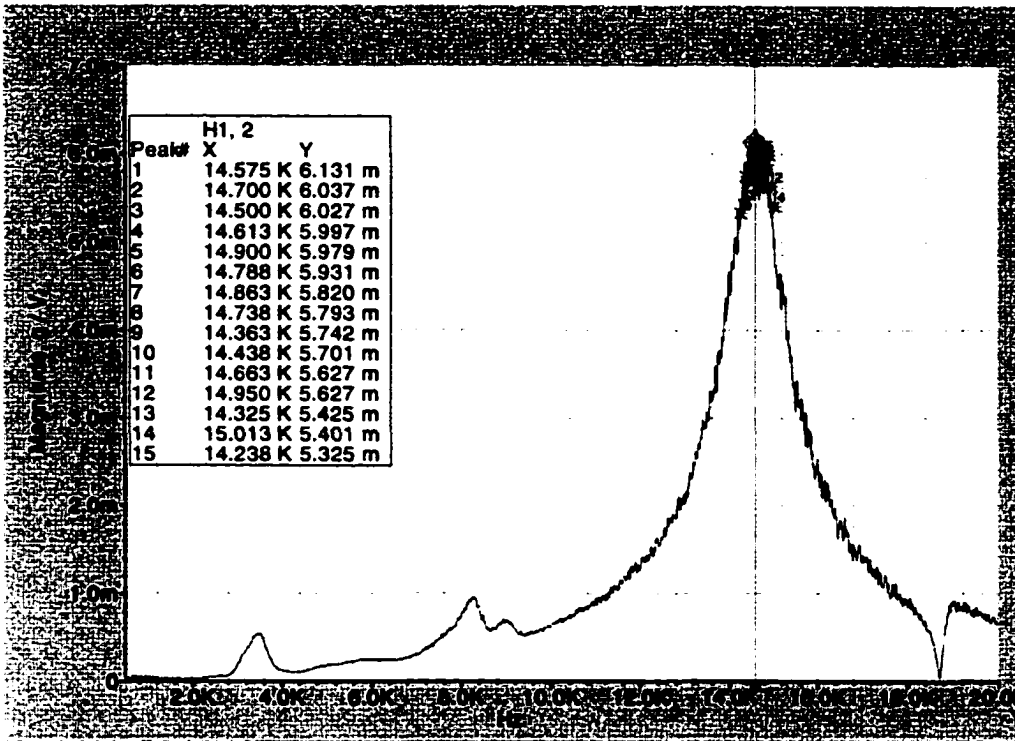
Balance masses



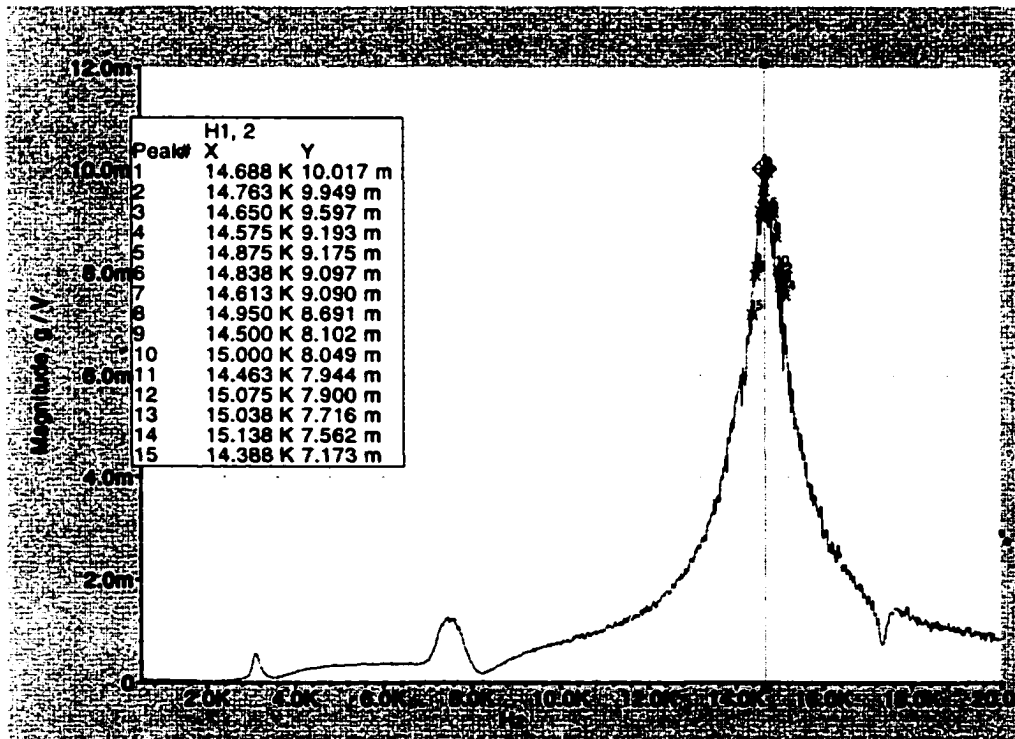
Unthreaded

Axial vibration

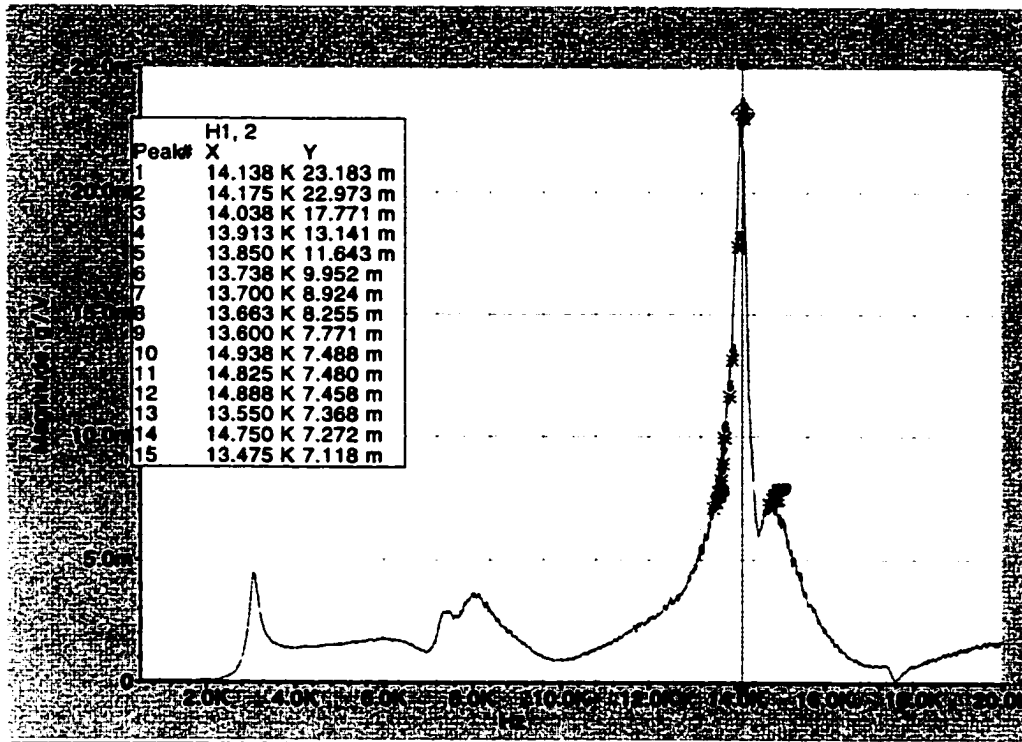
Balance mass

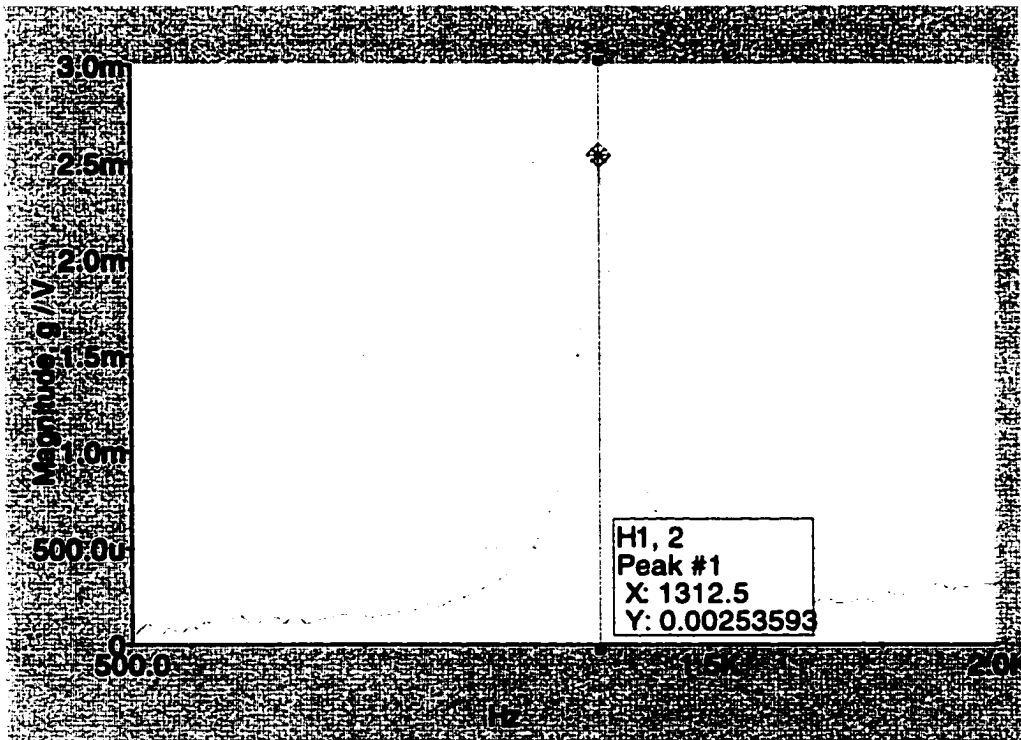
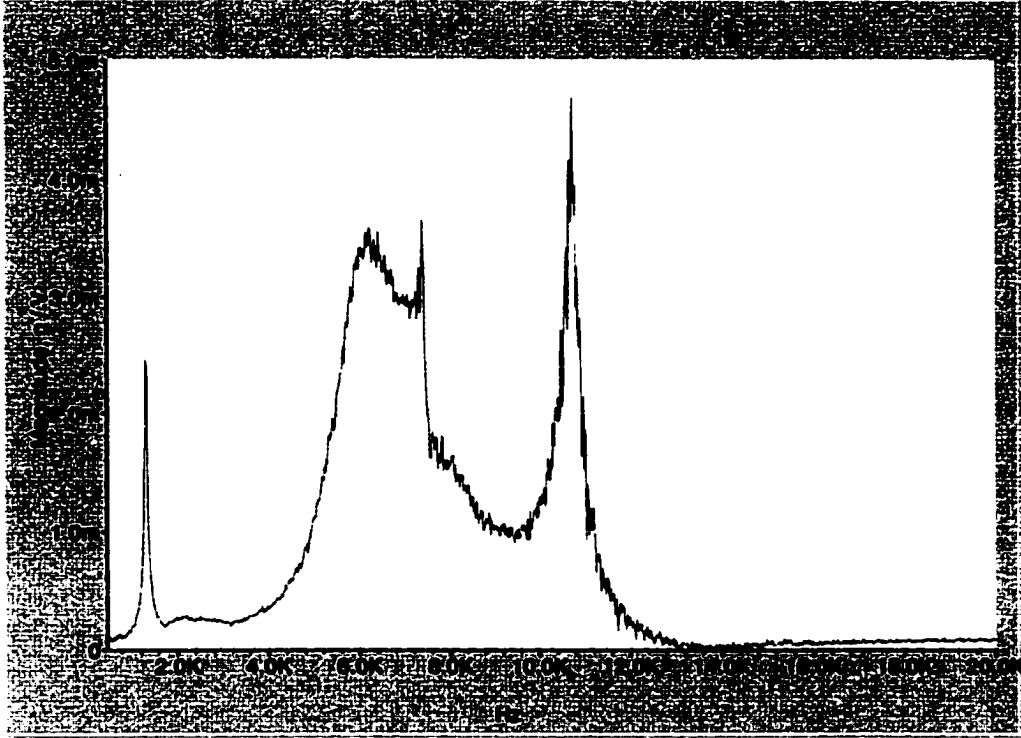


Unthreaded masses
axial vibration



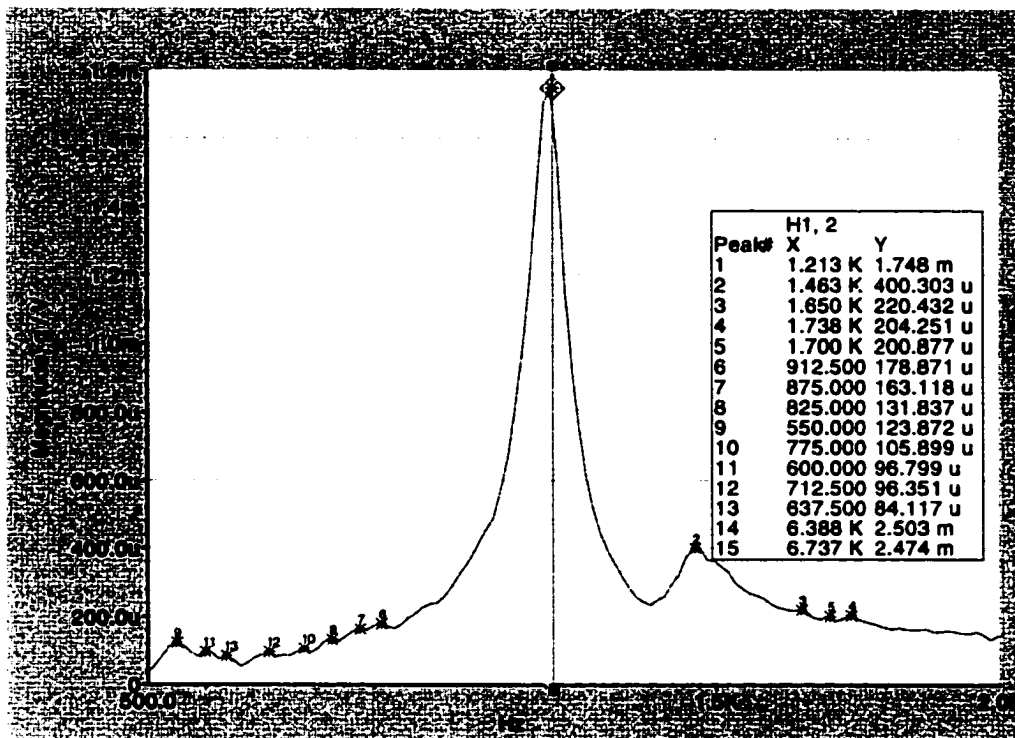
Unbalance masses
Torsion vibration



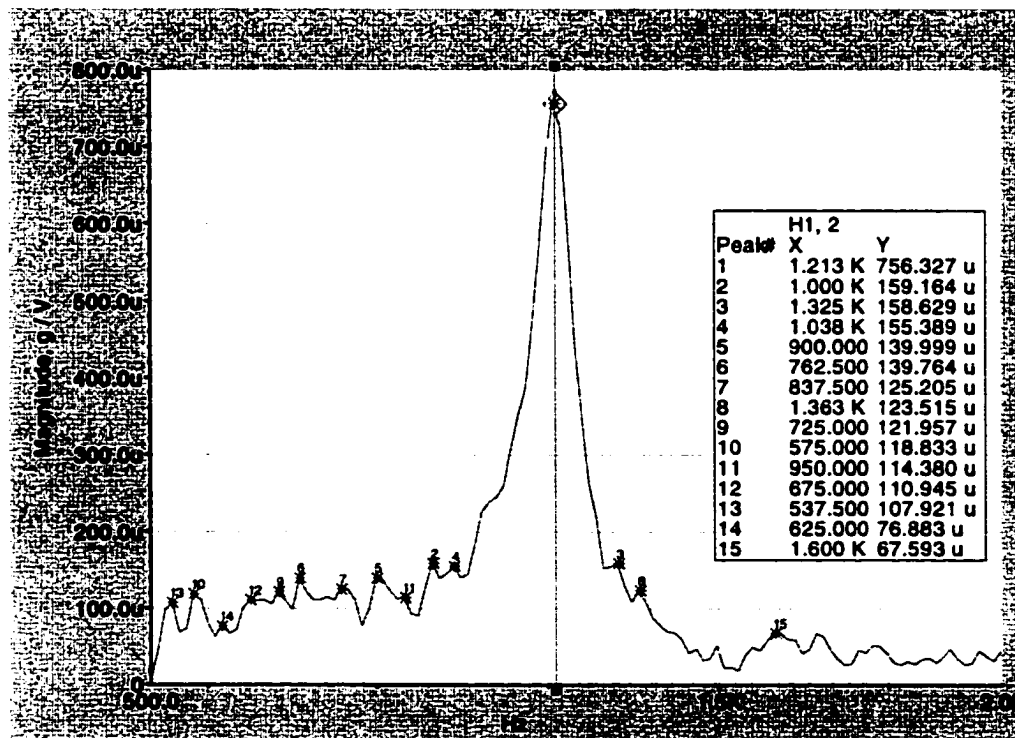


new mount little oversized by .144in

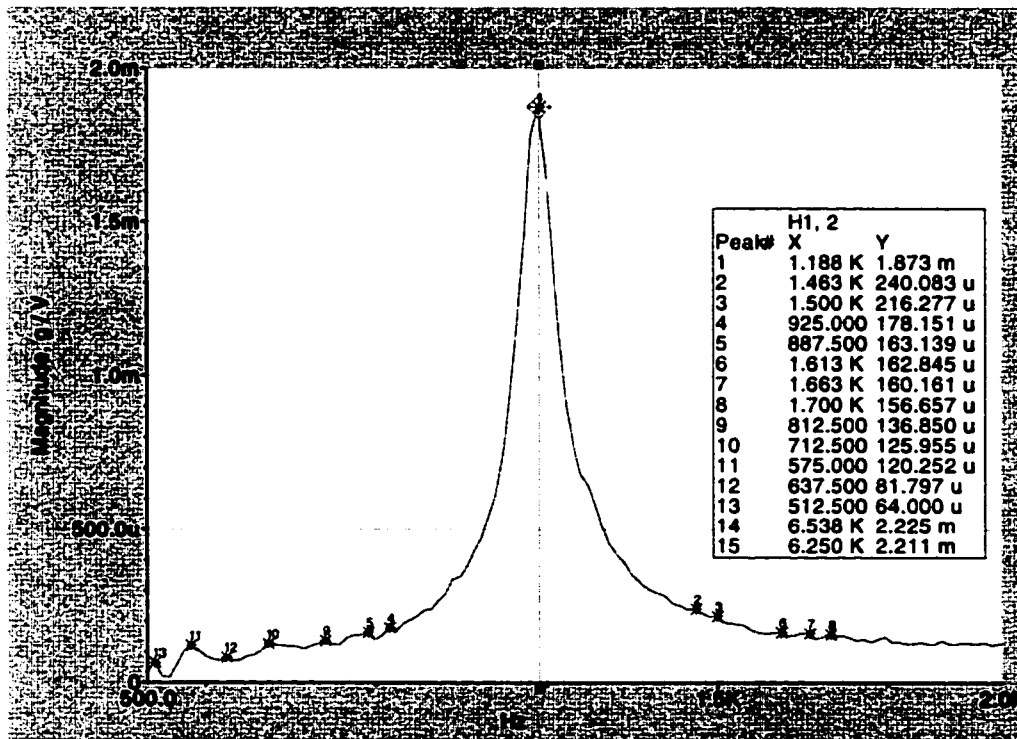
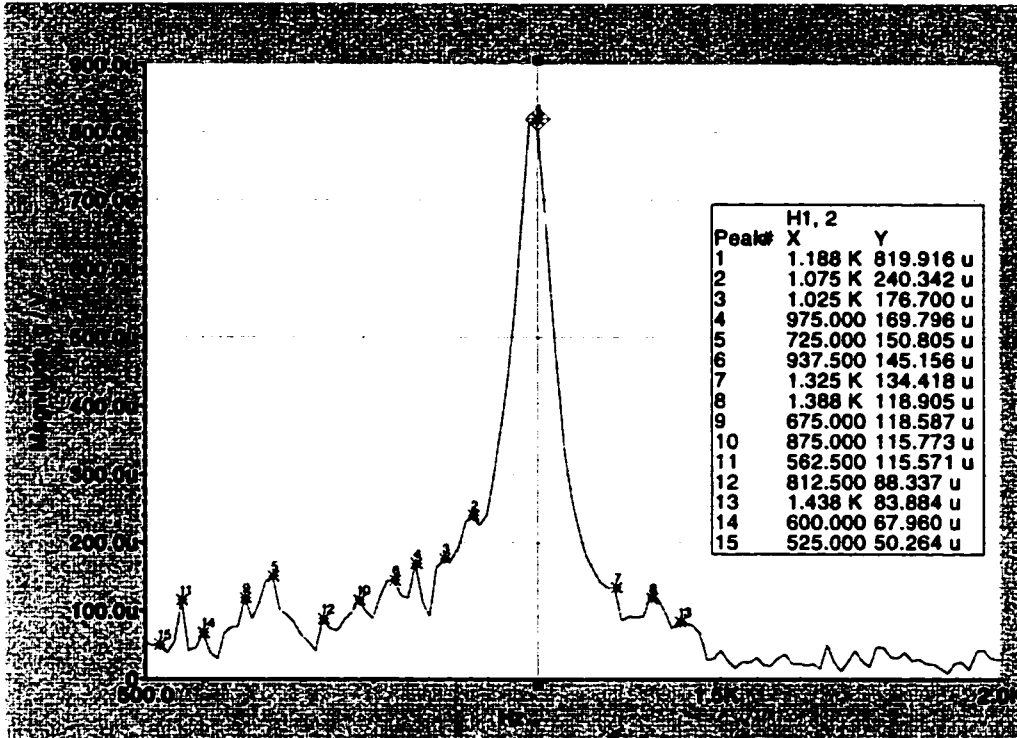
mount#3 Axial vibration



mount #3 torsion vibration

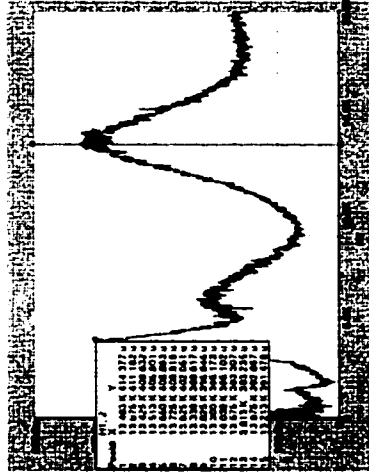


mount #4 torsion vibration unbalance masses size .153

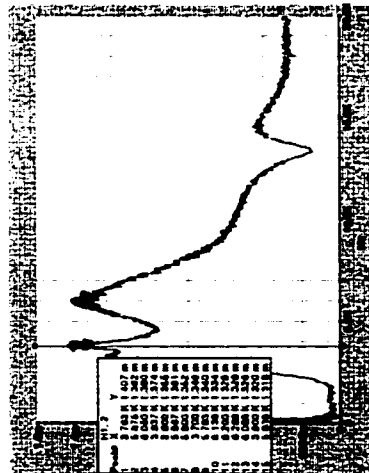


CLOSE UP ON TORSION

AXIAL VIBRATION



TORSION VIBRATION

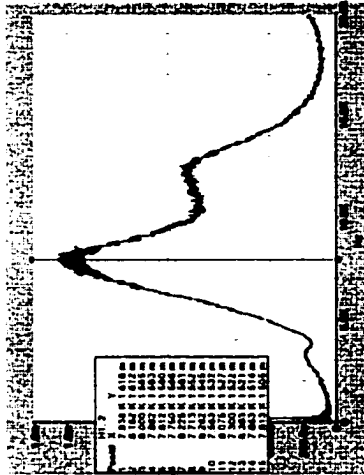


5 mm

CLOSE UP ON TORSION

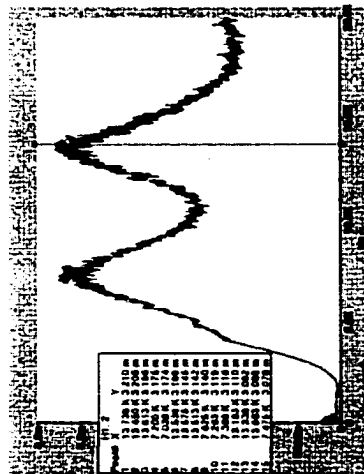


AXIAL VIBRATION

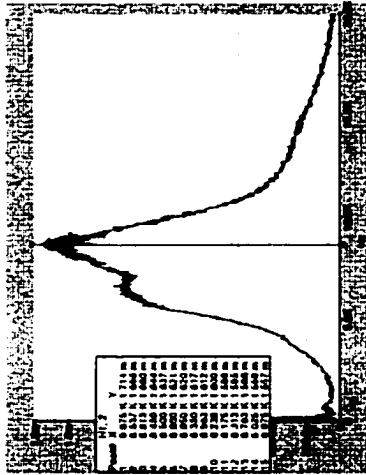


TORSION VIBRATION

10 mmh

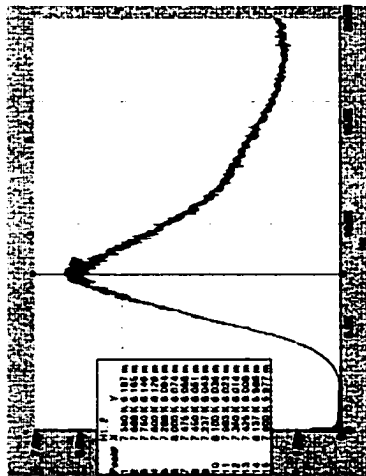


AXIAL VIBRATION

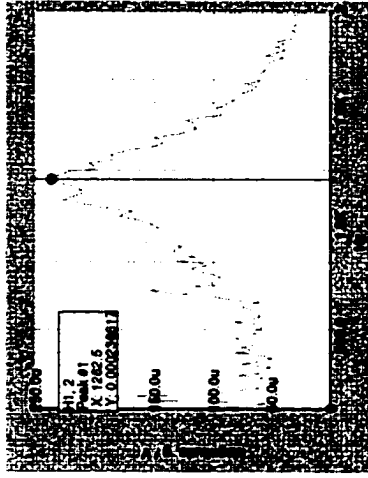


TORSION VIBRATION

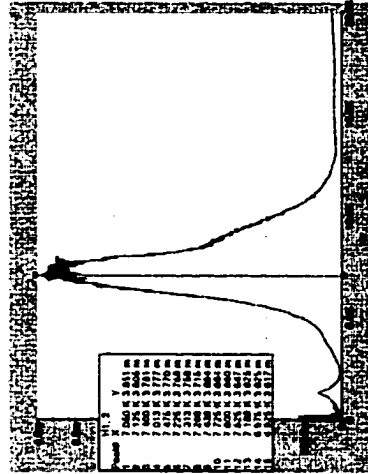
15 mm



CLOSE UP ON TORSION

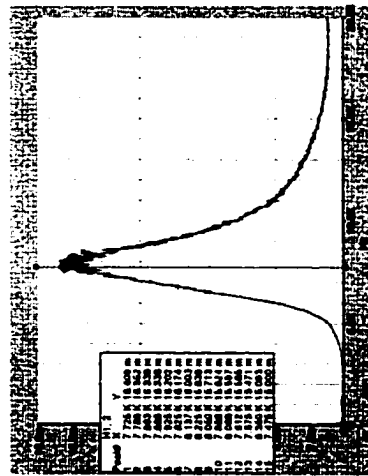


AXIAL VIBRATION

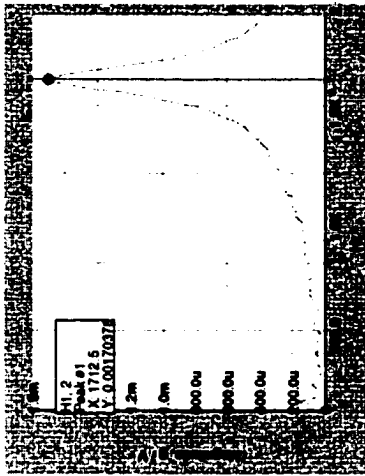


TORSION VIBRATION

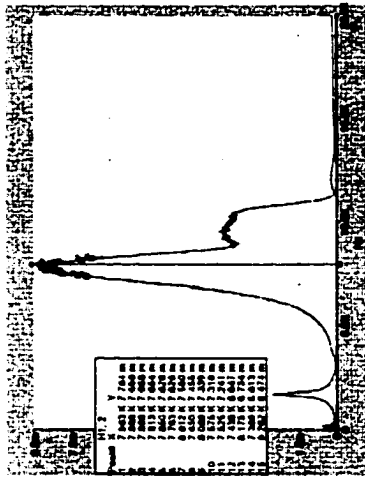
20 in/s



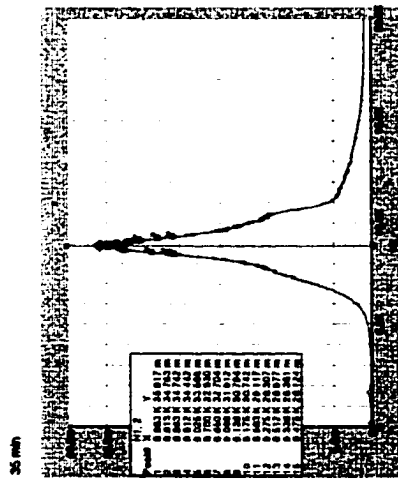
CLOSE UP ON TORSION



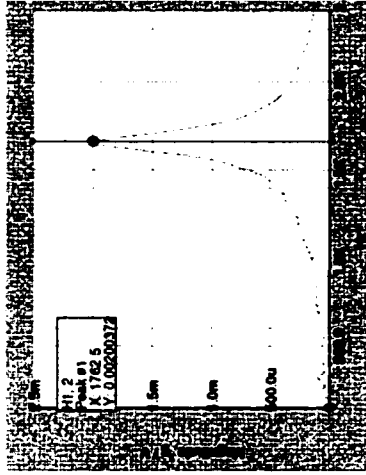
AXIAL VIBRATION



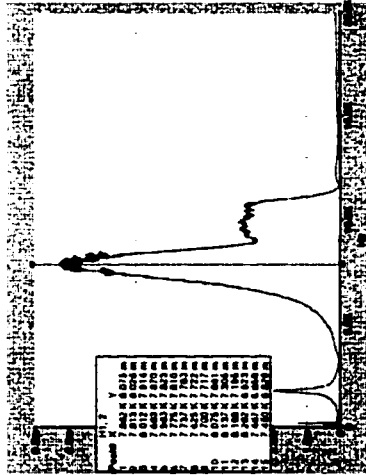
TORSION VIBRATION



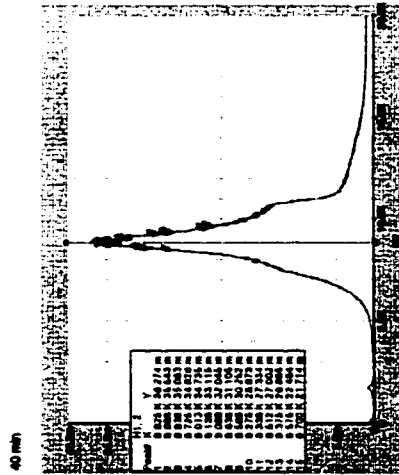
CLOSE UP ON TORSION



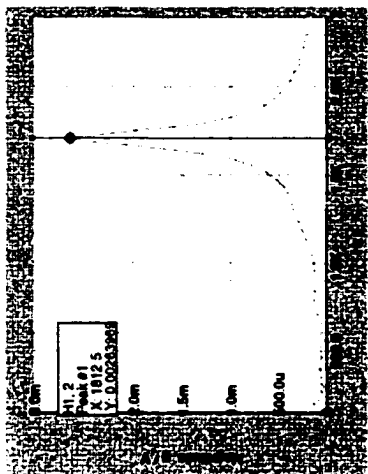
AXIAL VIBRATION



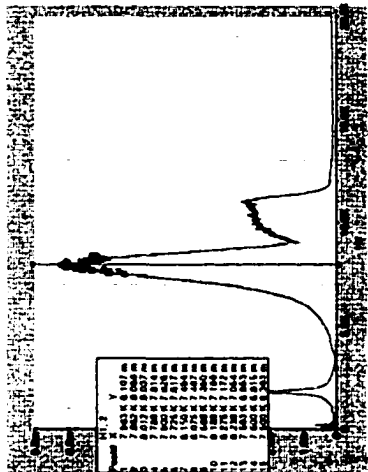
TORSION VIBRATION



CLOSE UP ON TORSION

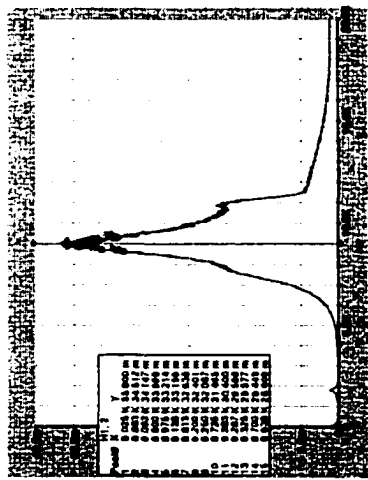


AXIAL VIBRATION

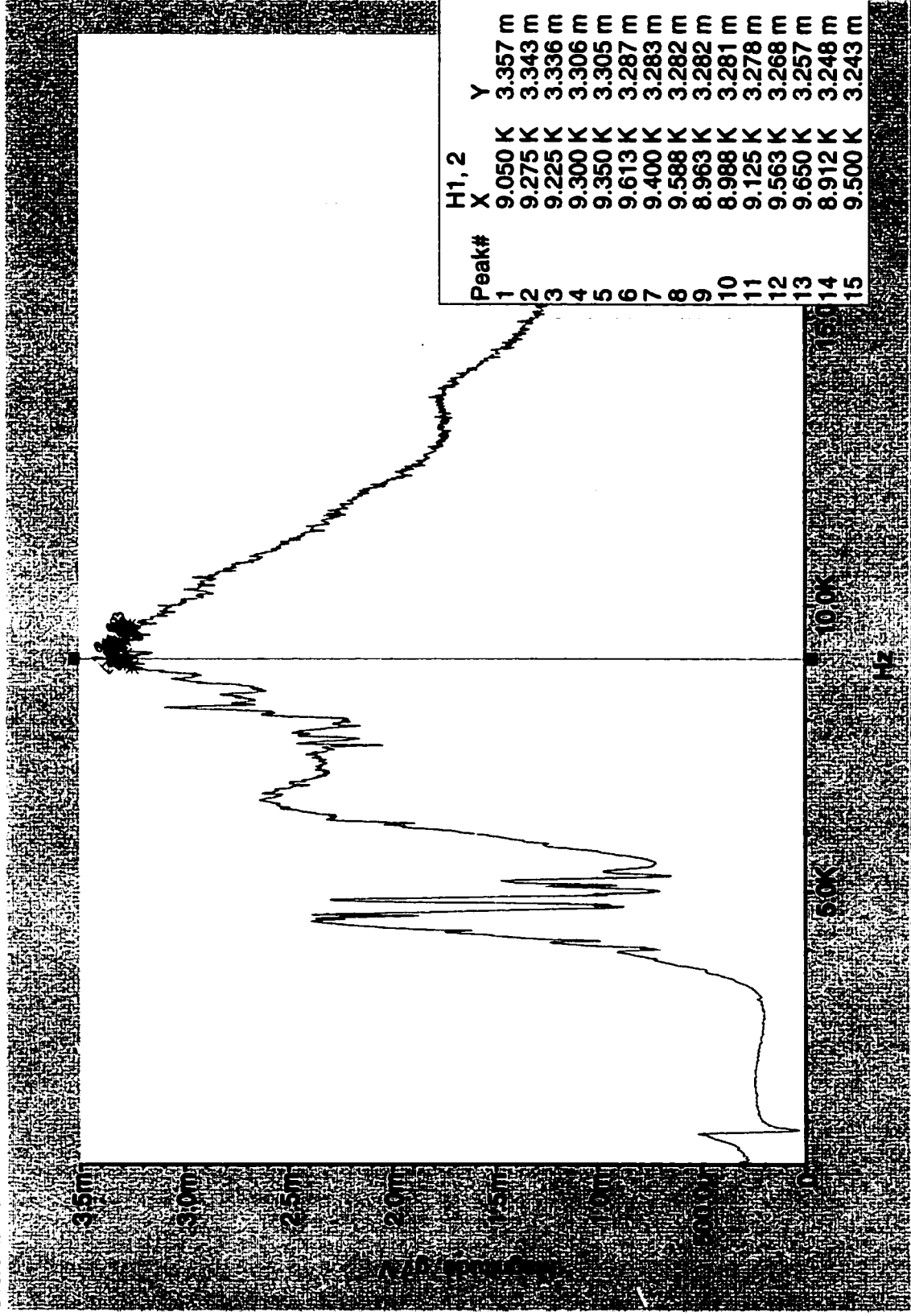


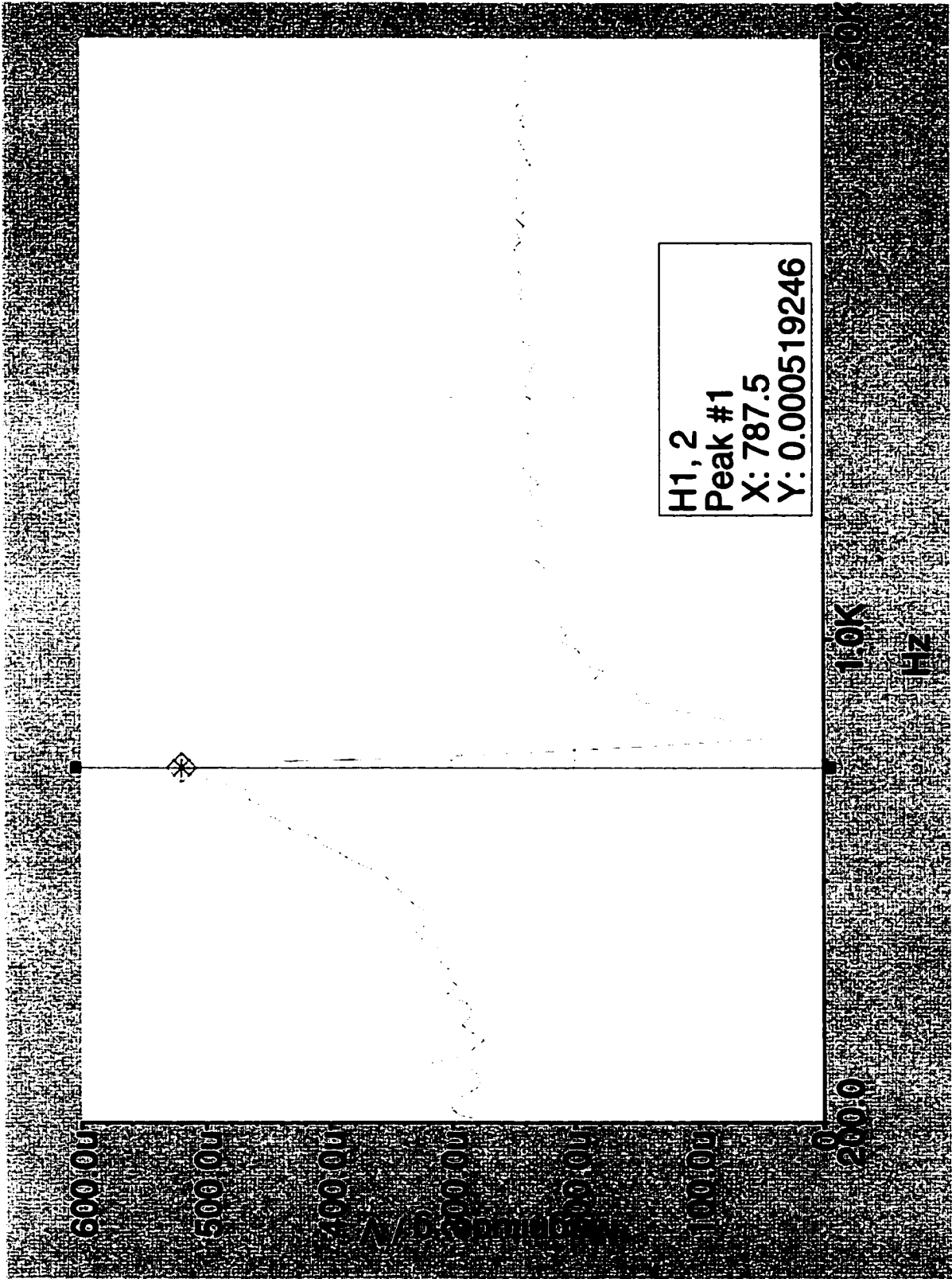
TORSION VIBRATION

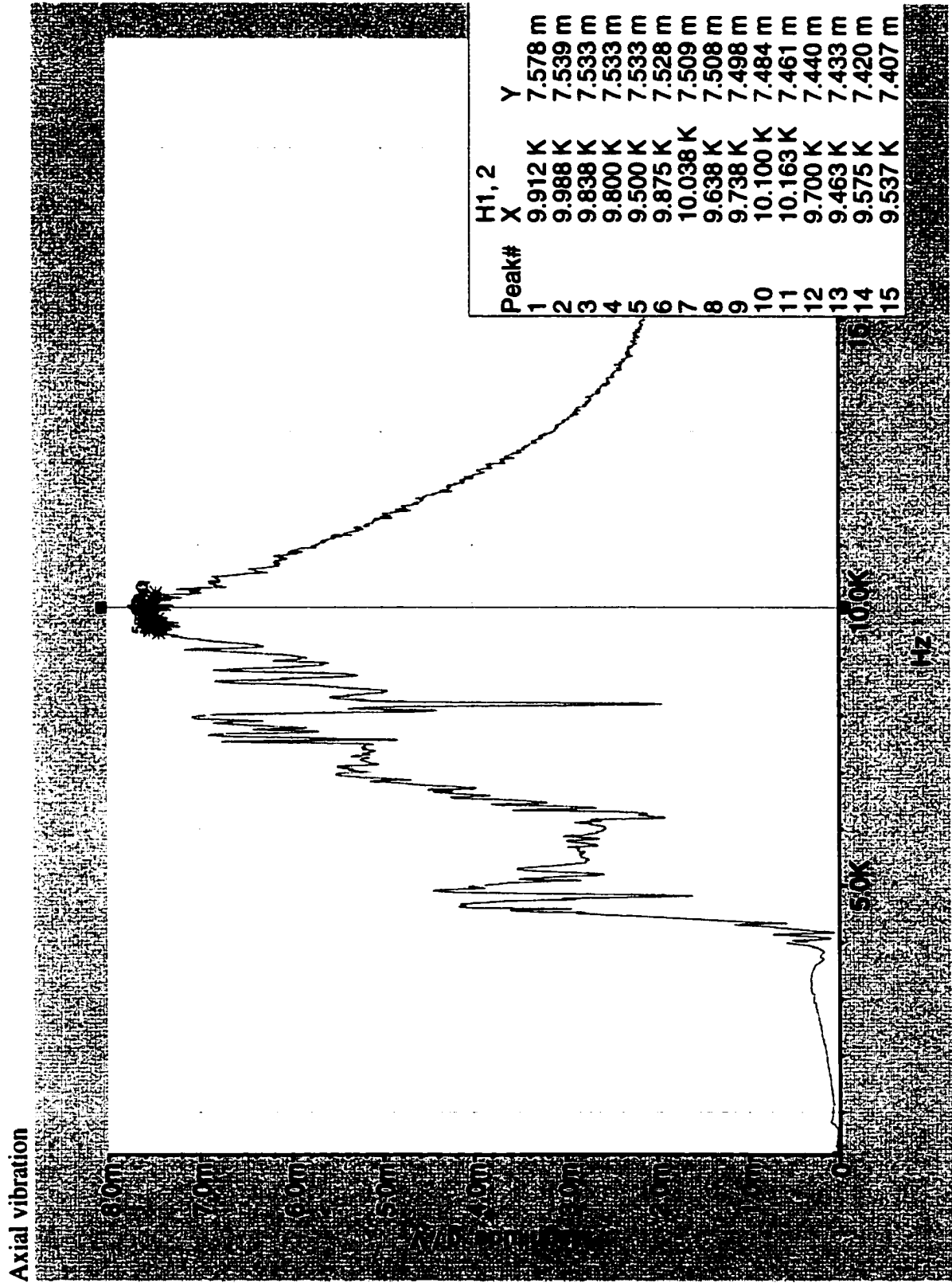
5.6 mm

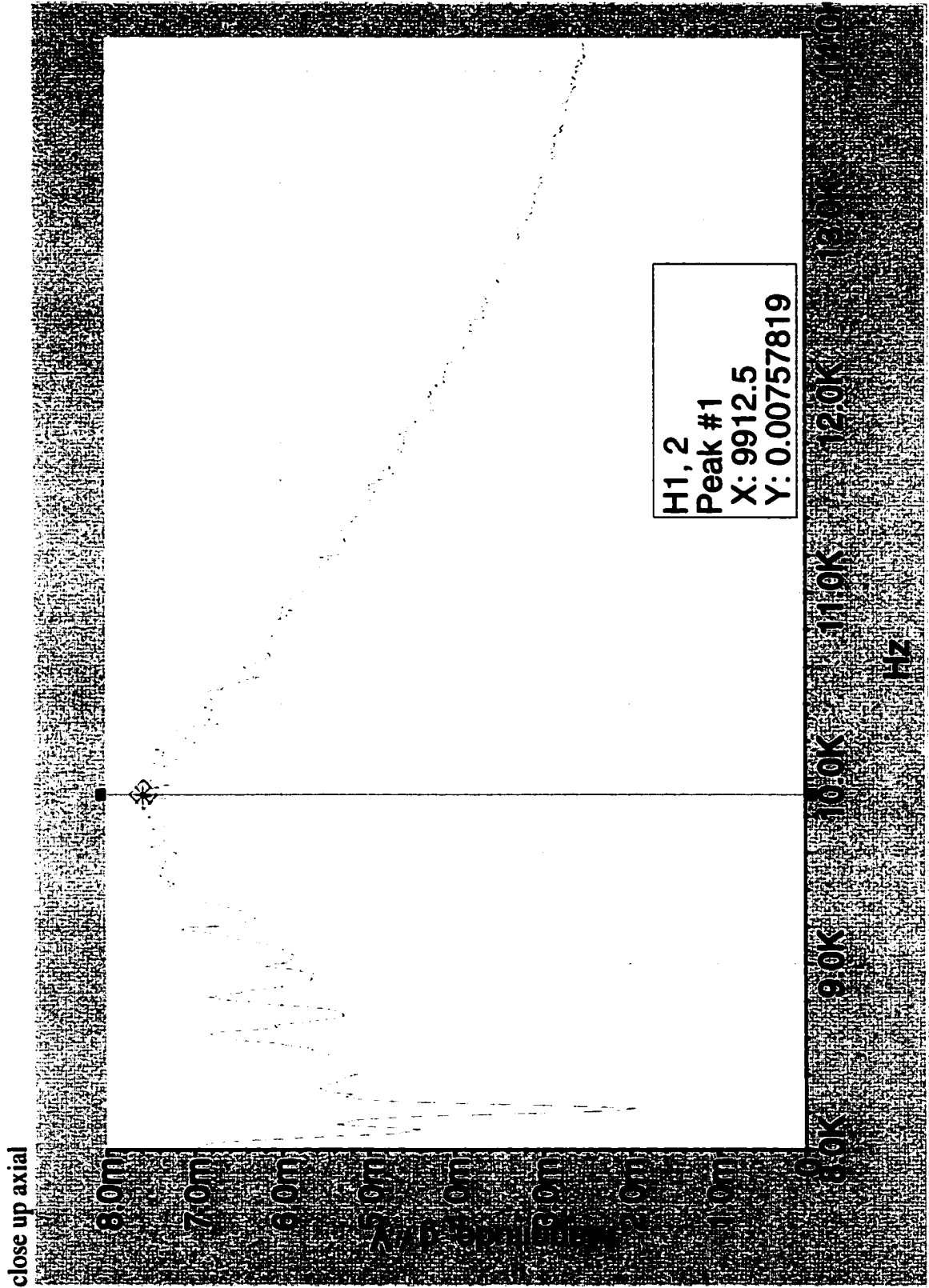


Torsion Vibration of Mount A Full Threaded

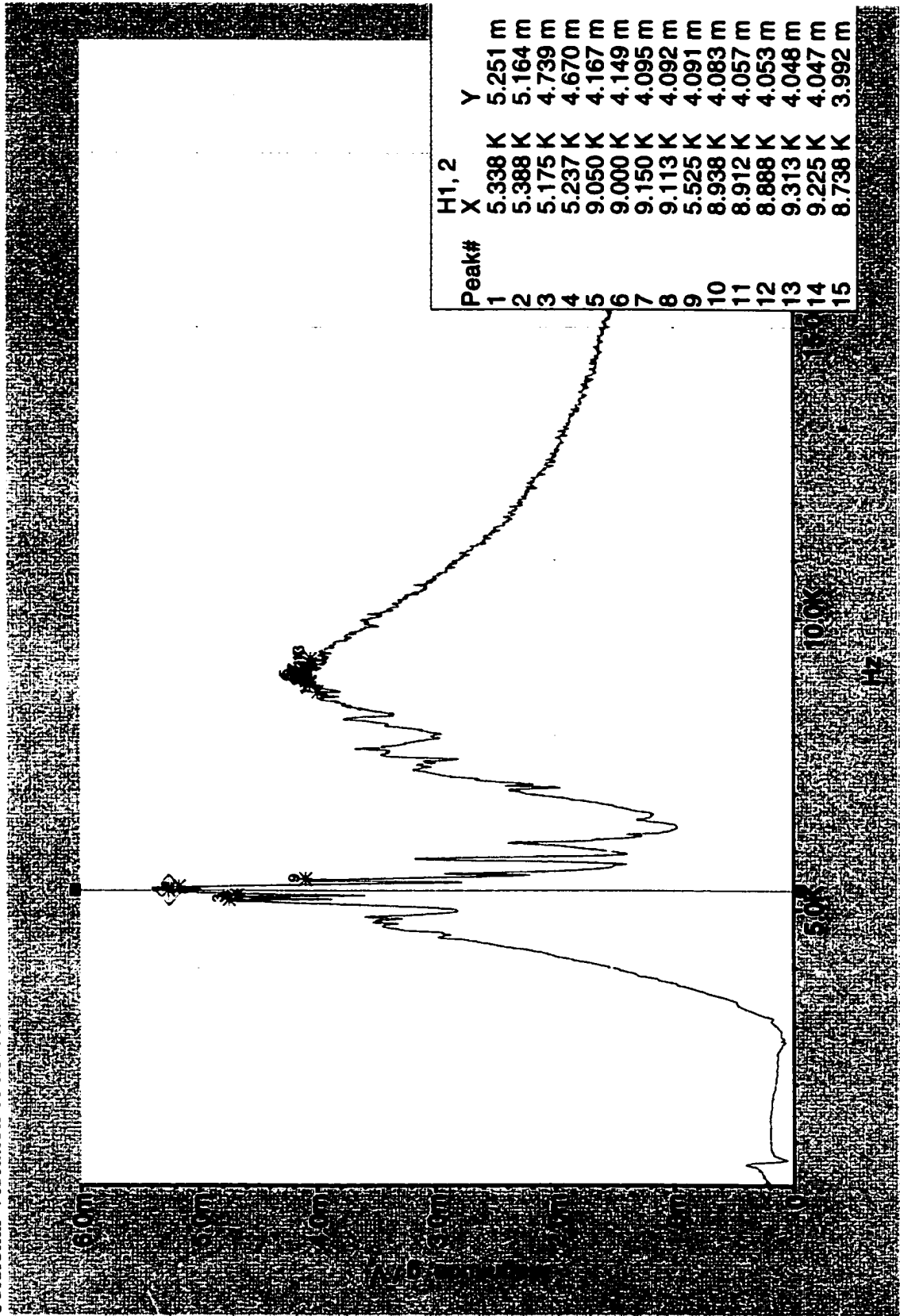




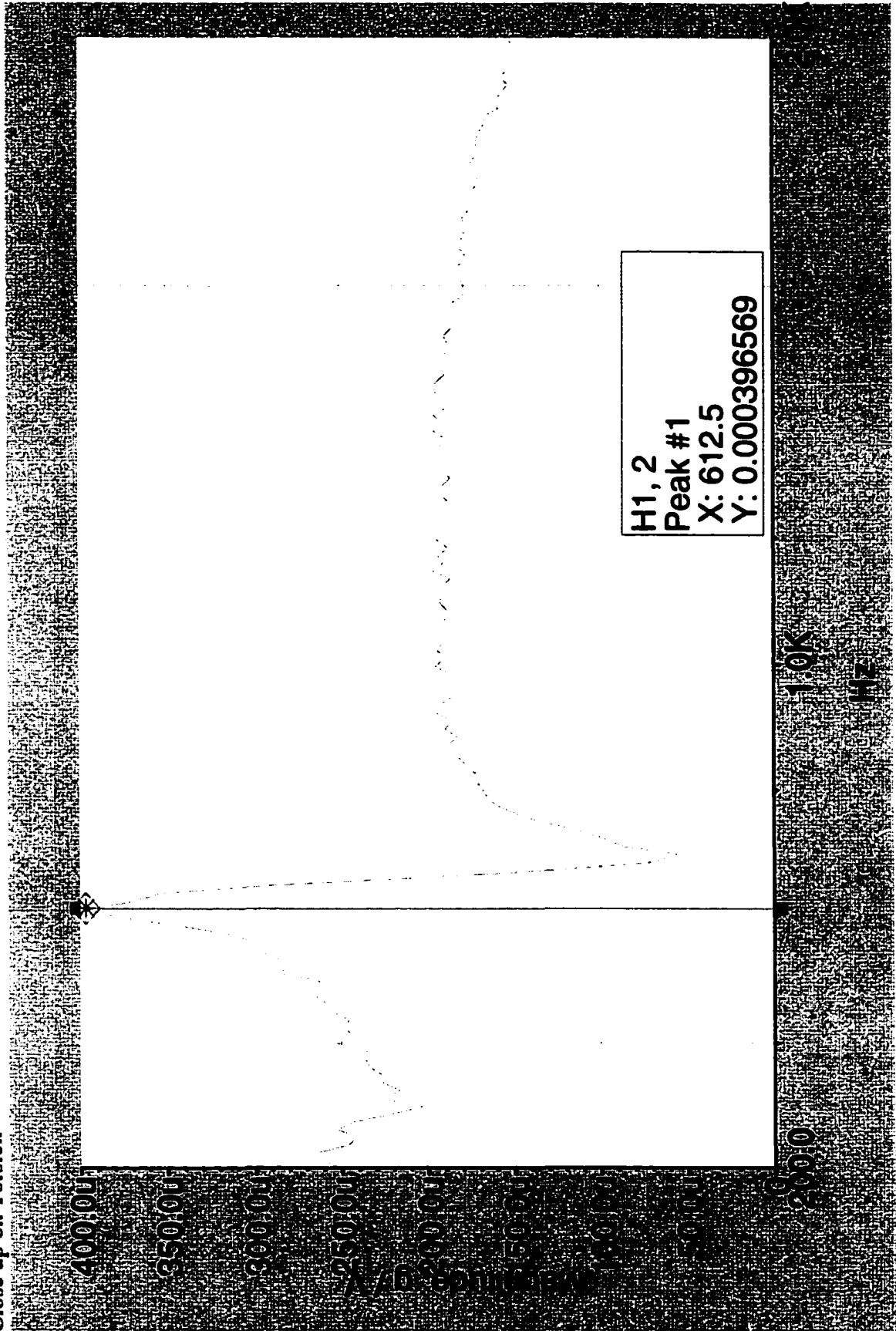


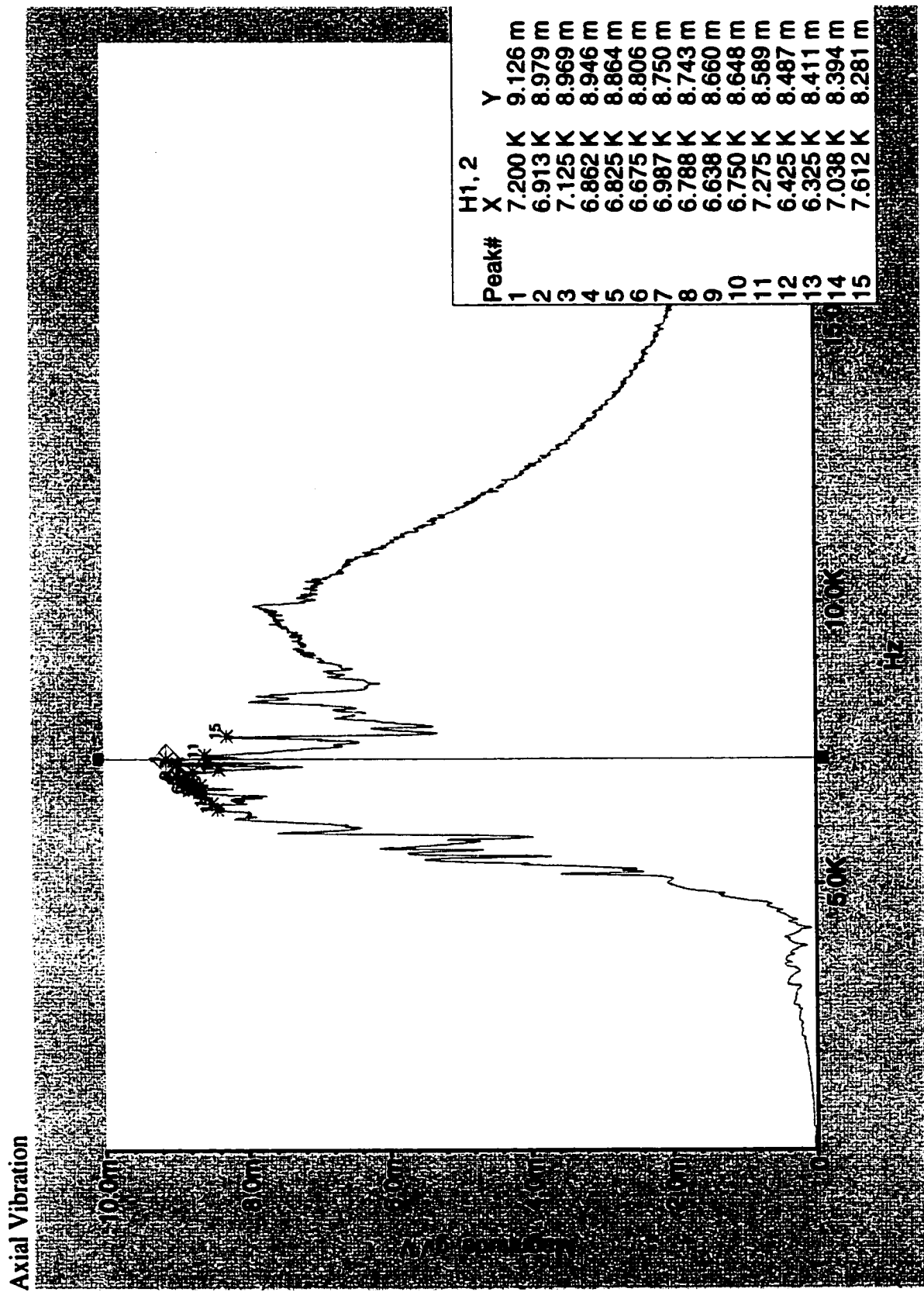


Torsional Vibration of Mount B.

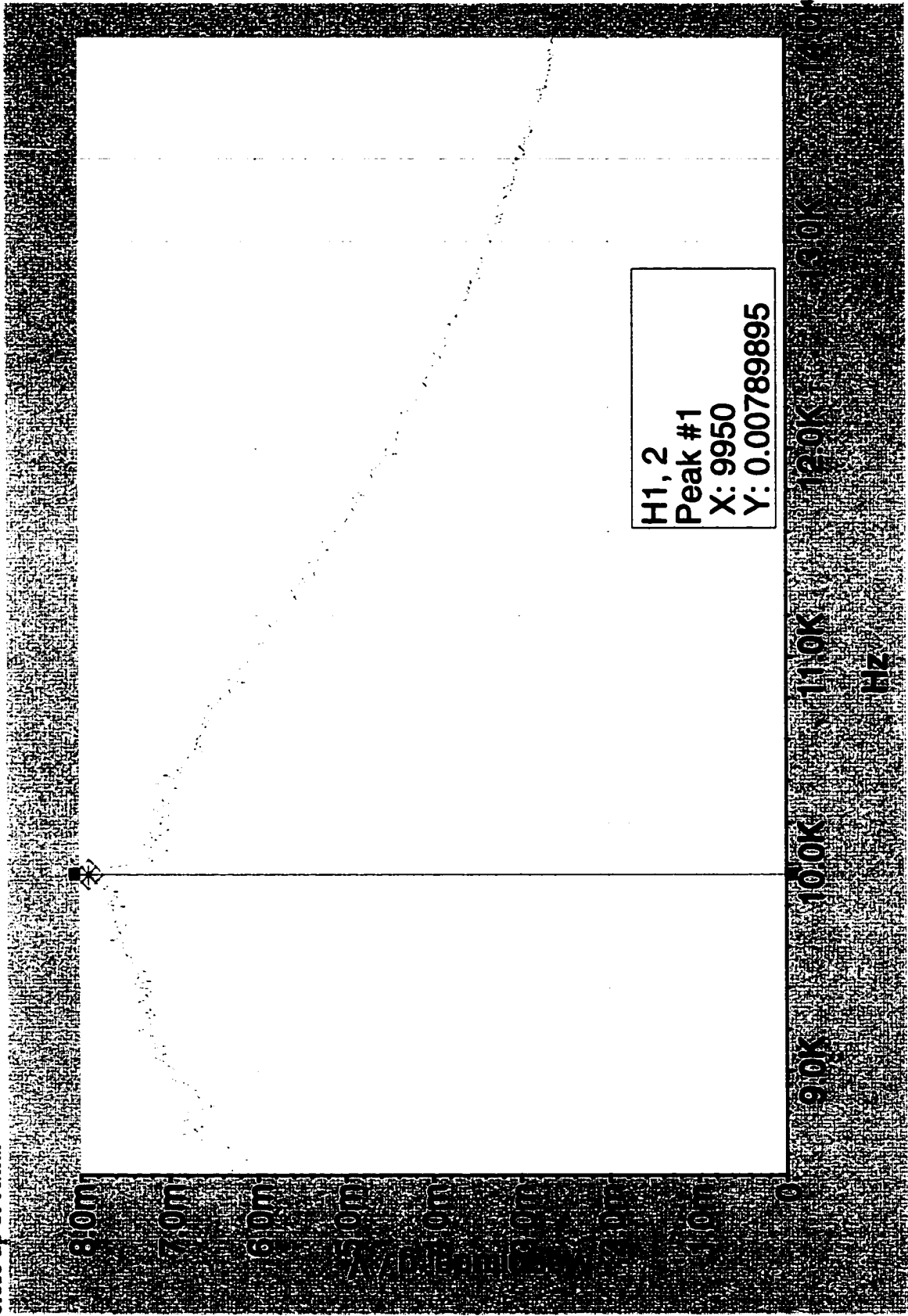


Close up on Torsion

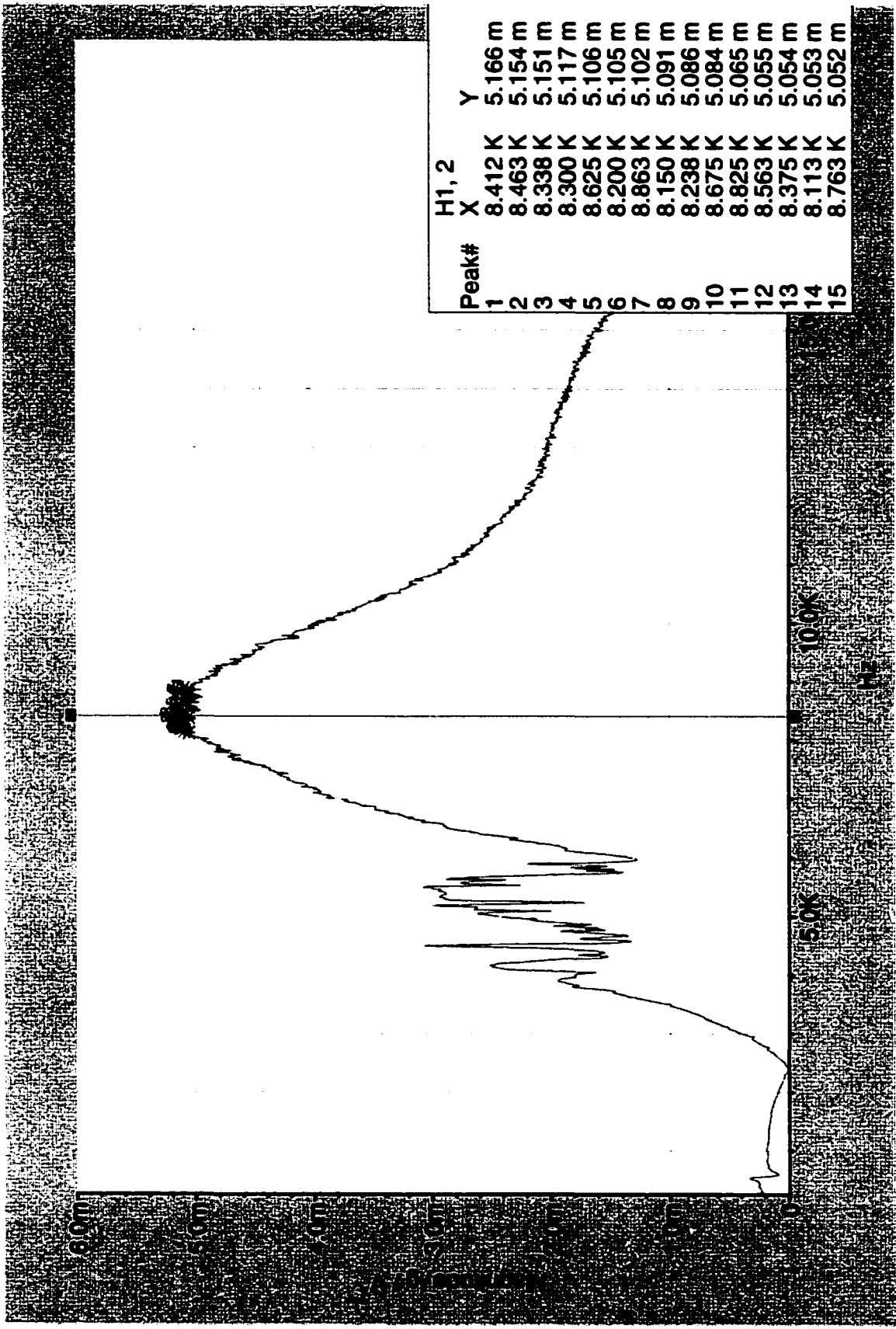


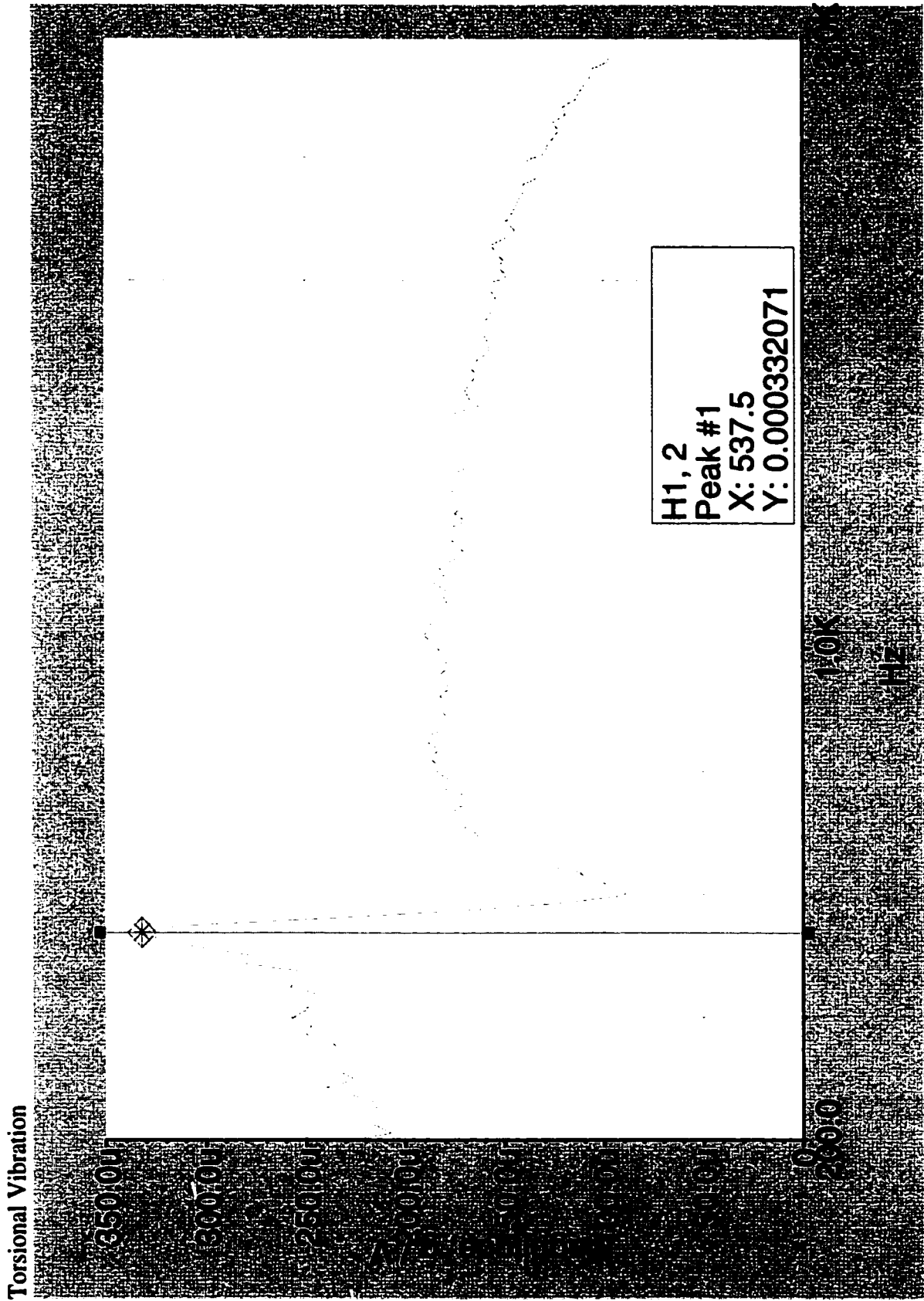


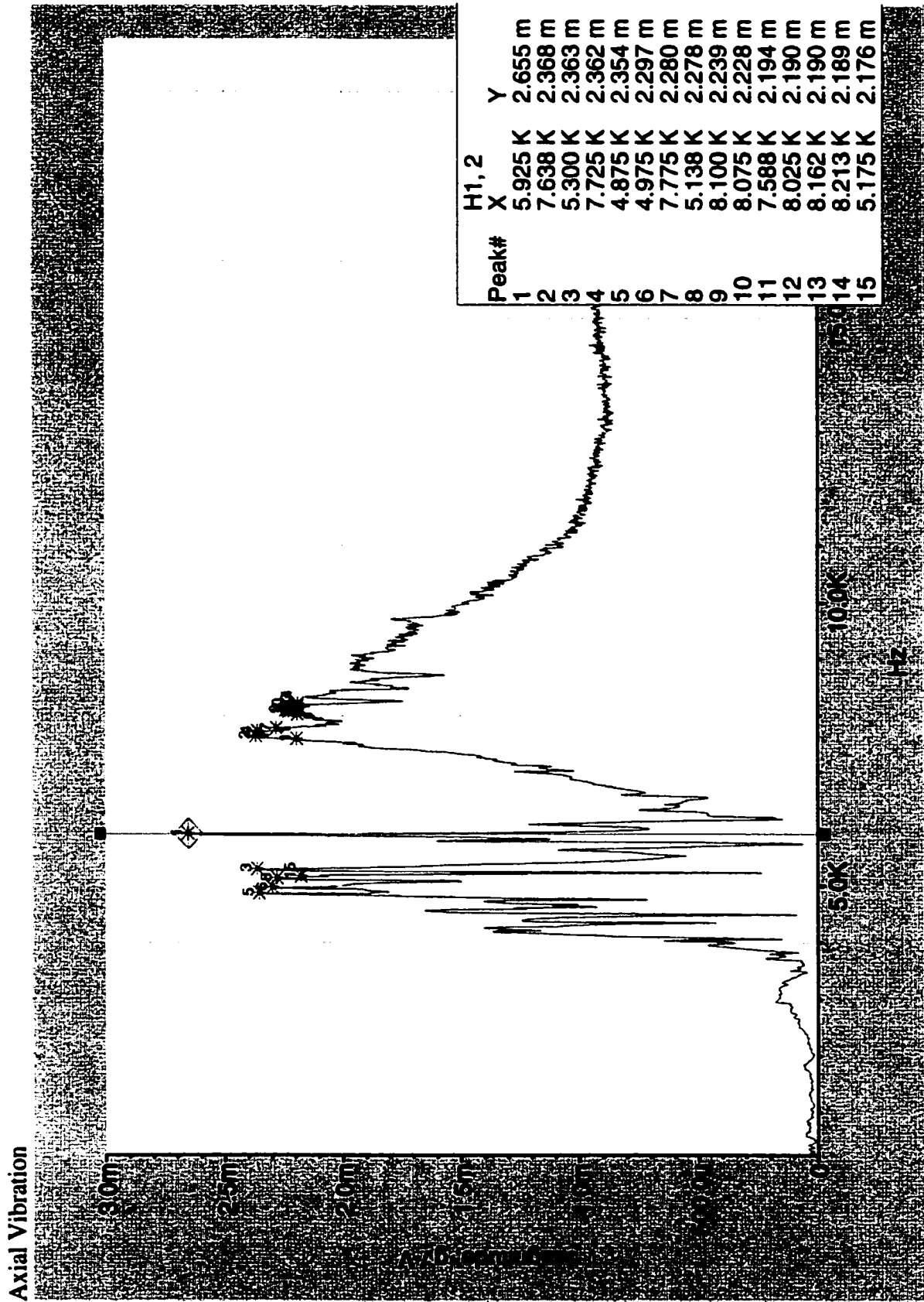
close up of Axial



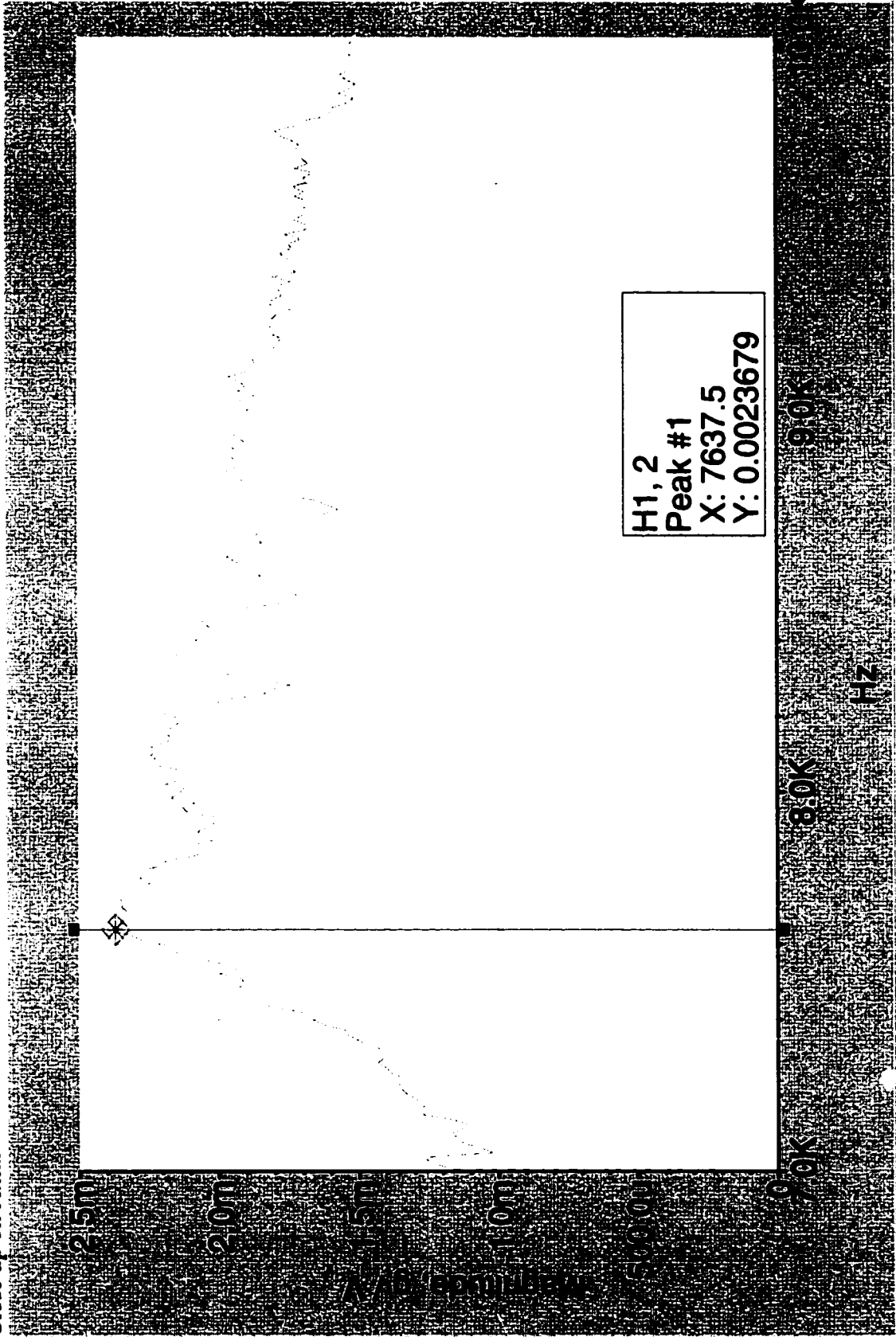
Mount A Lower half Threaded



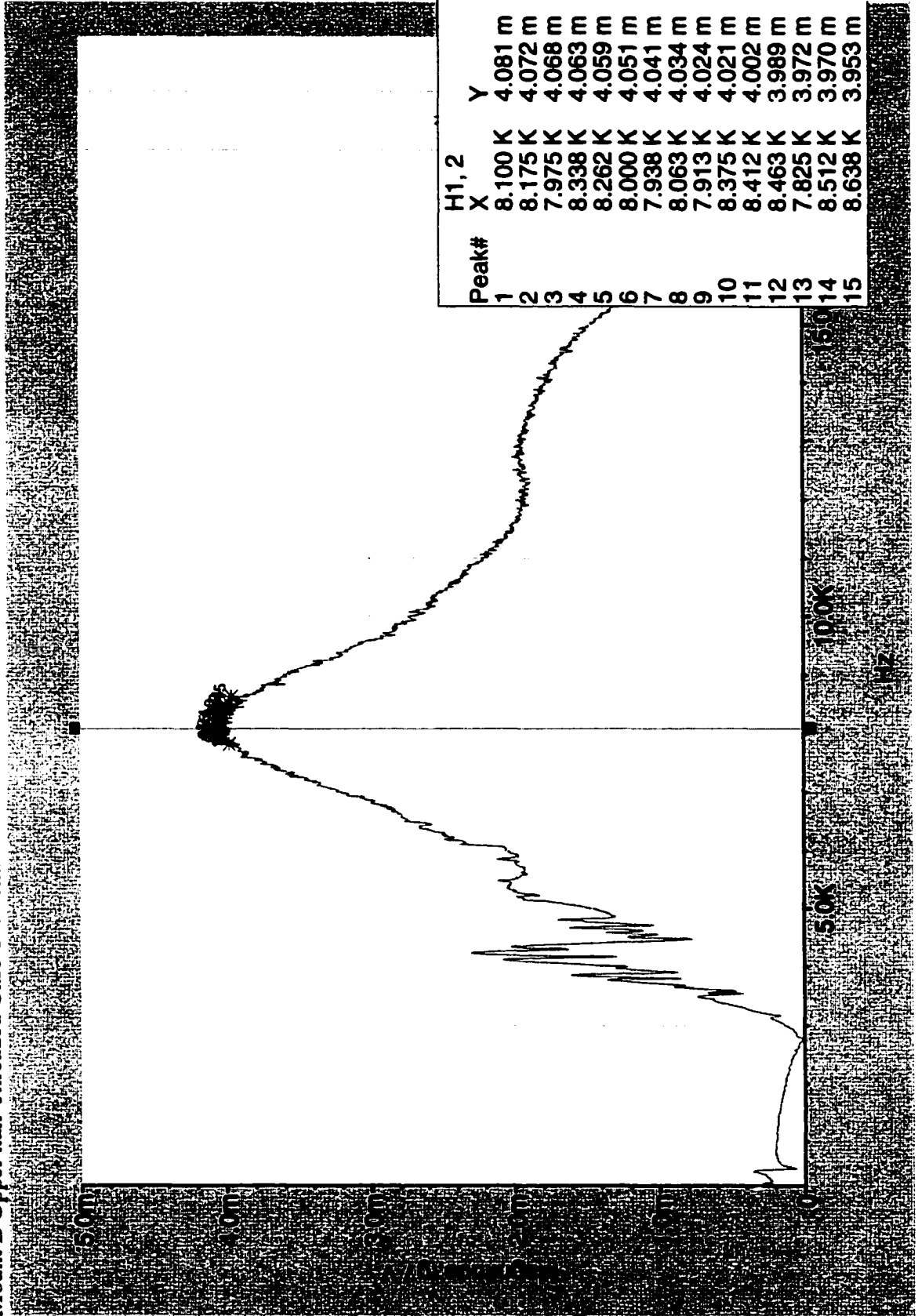


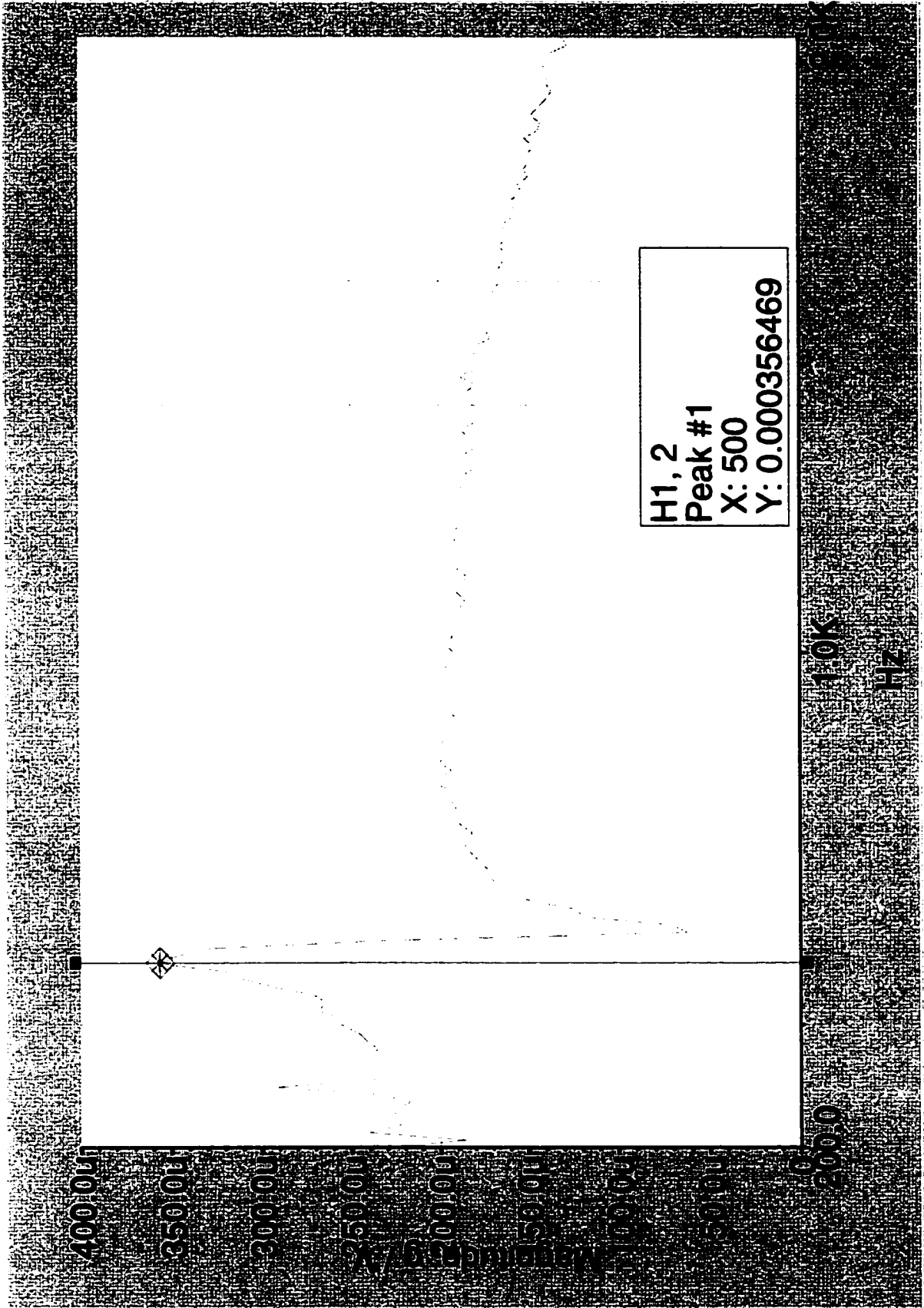


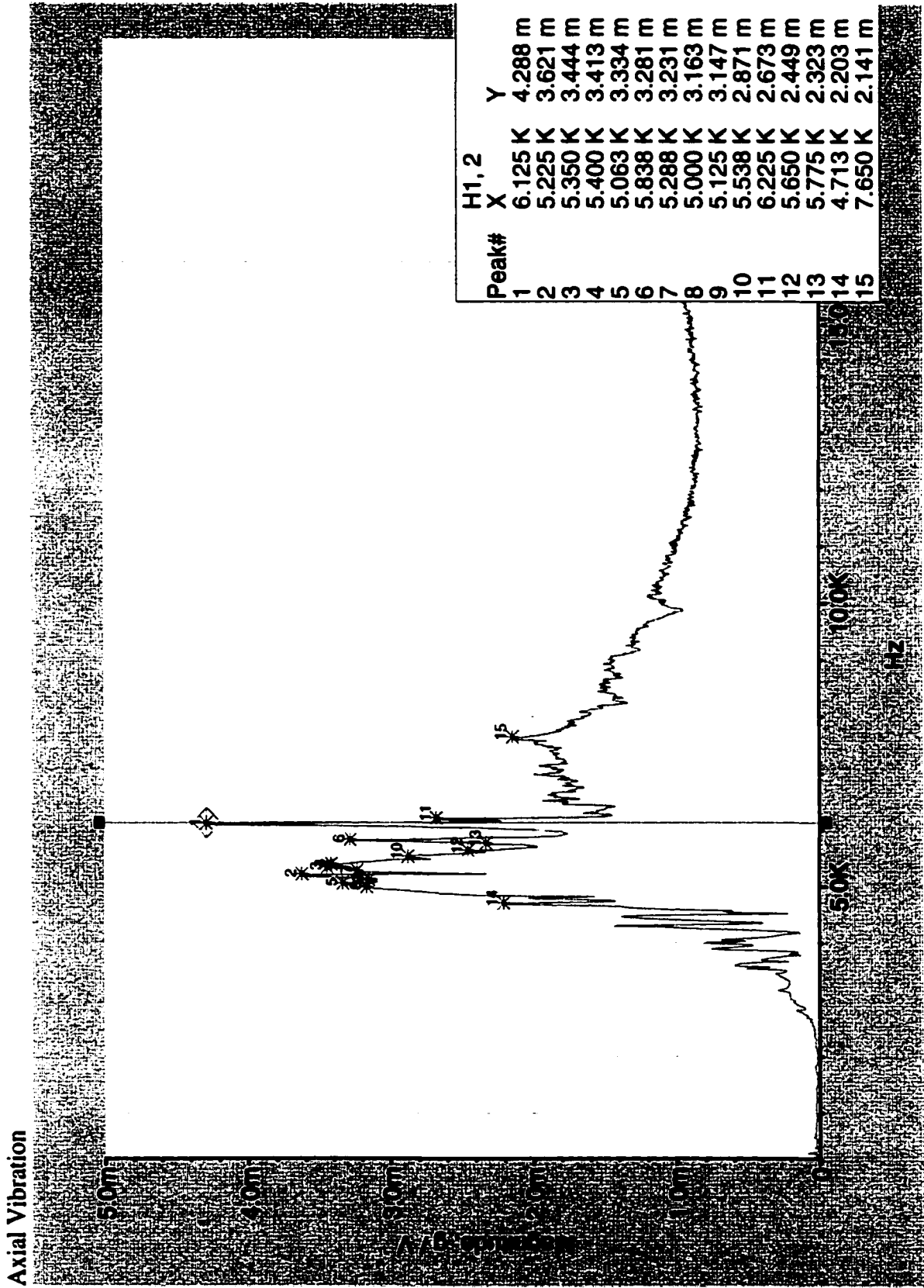
Close up on Axial

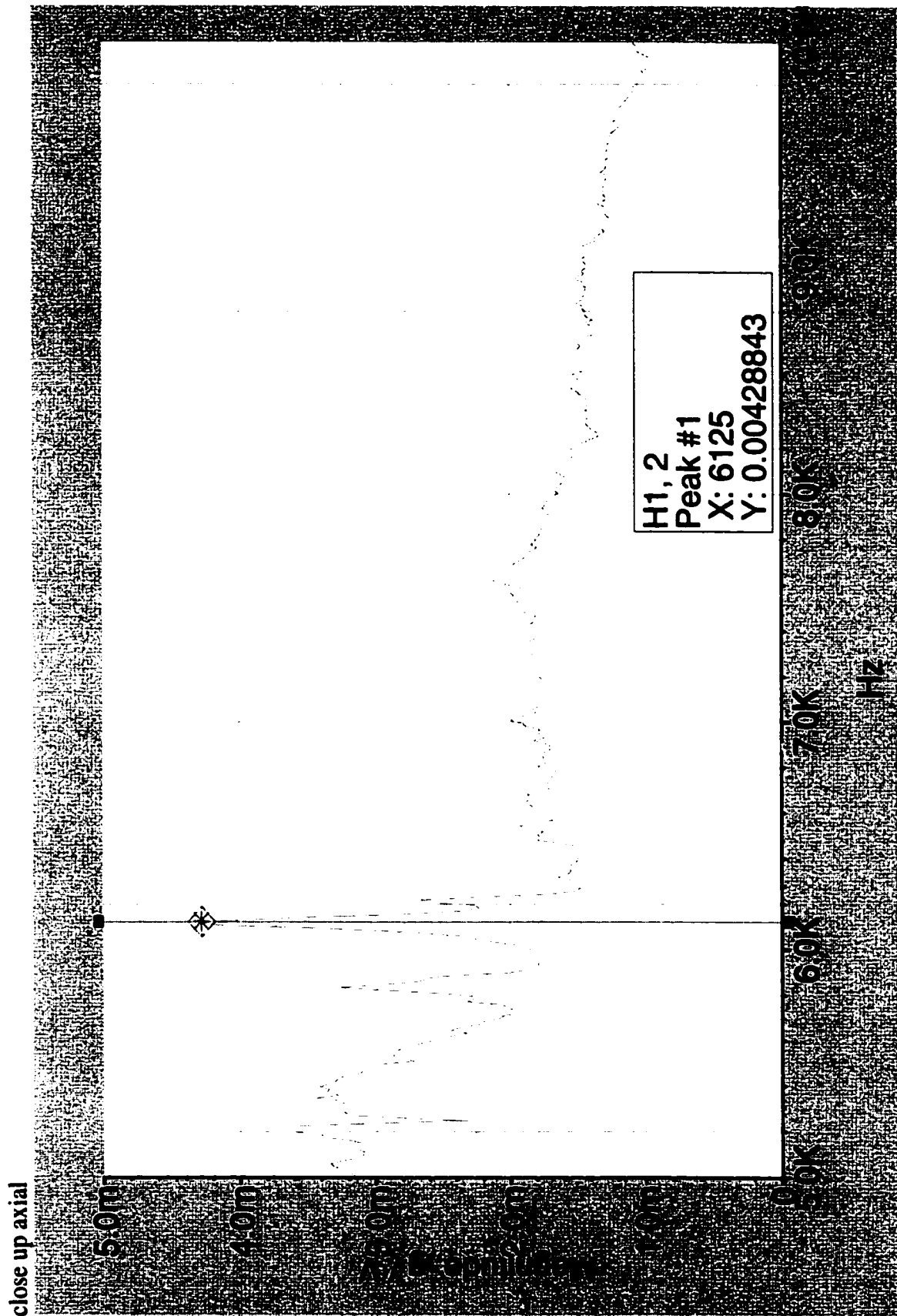


Mount B Upper half Threaded Case Torsional Vibration

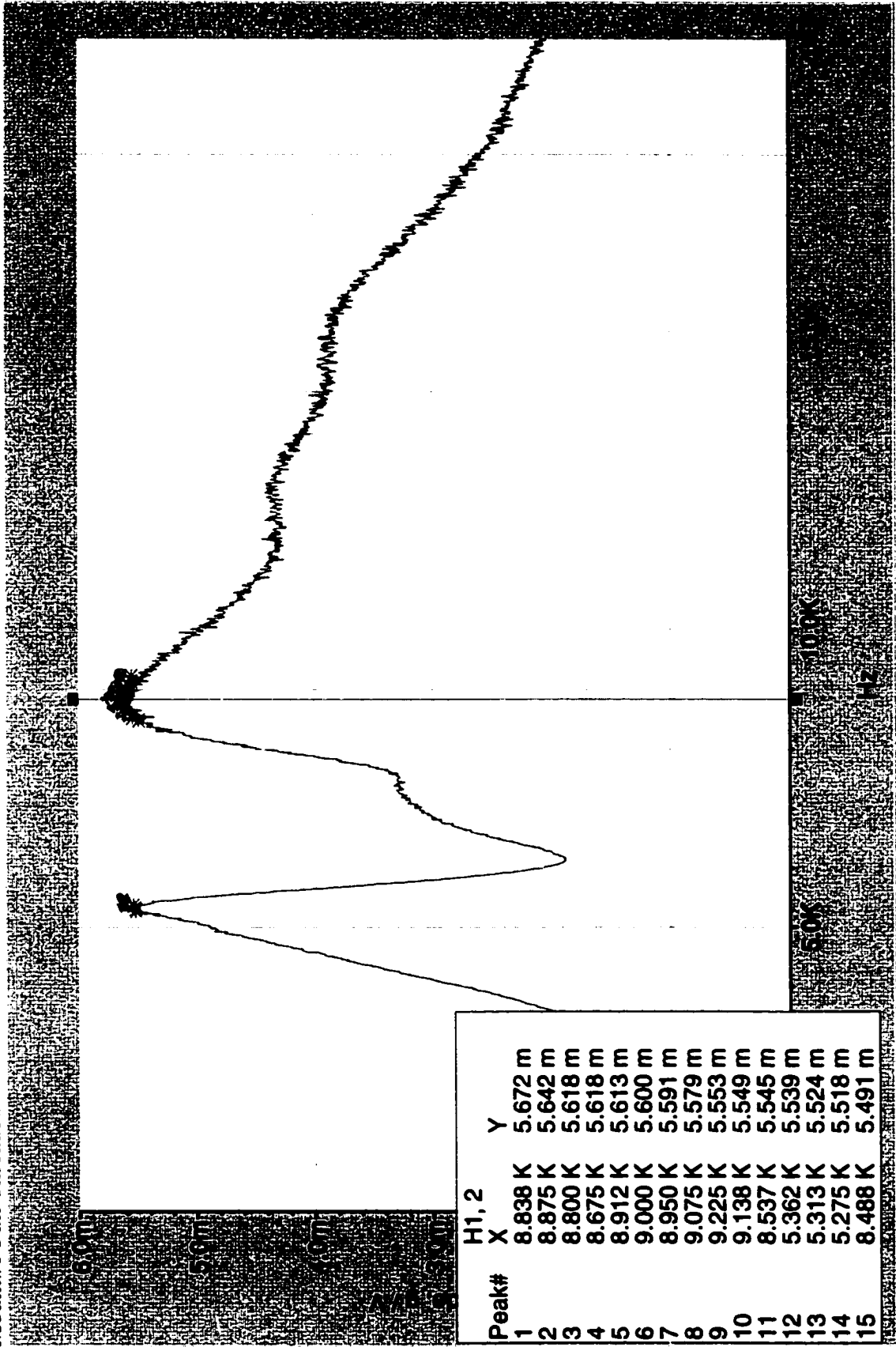


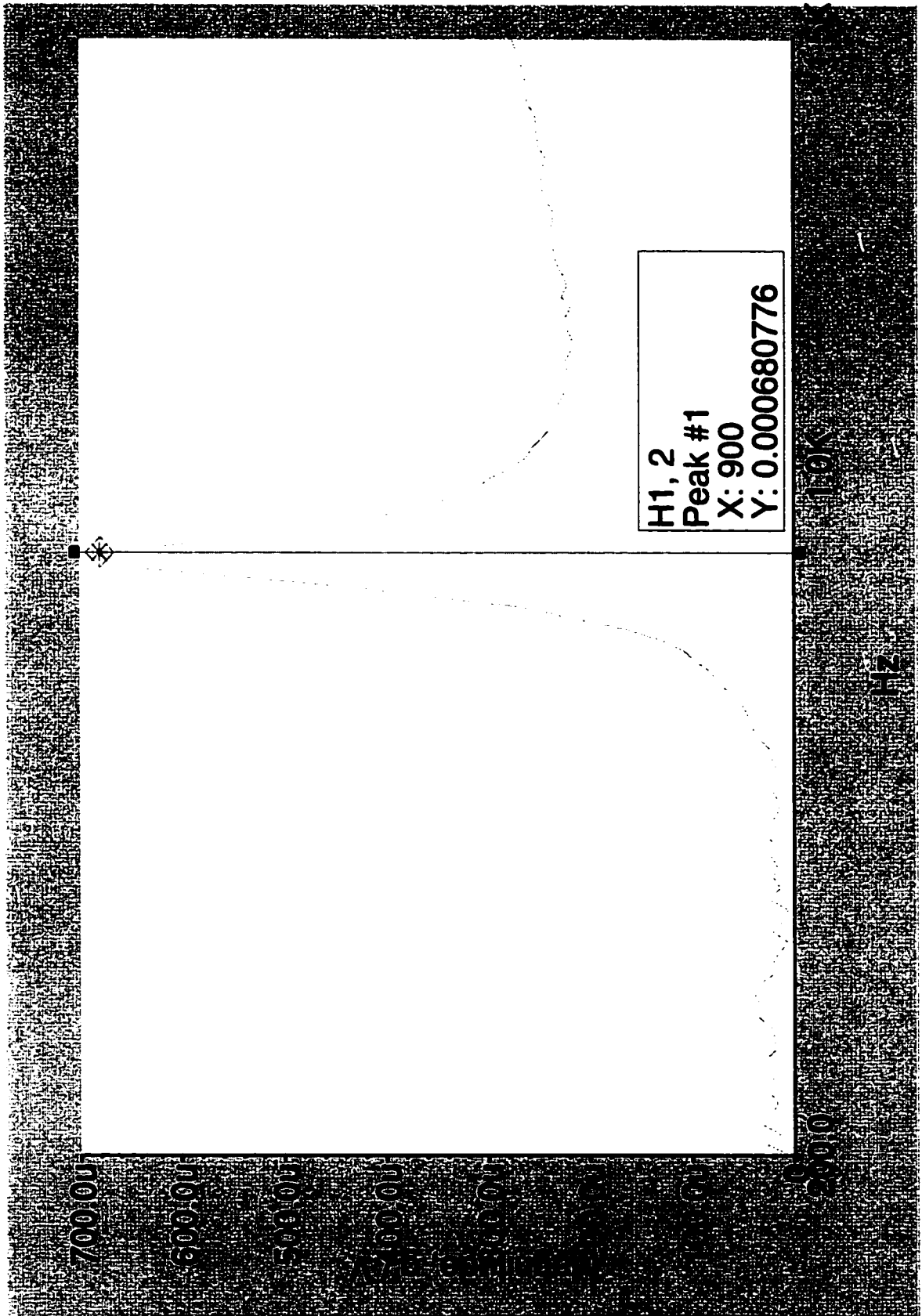


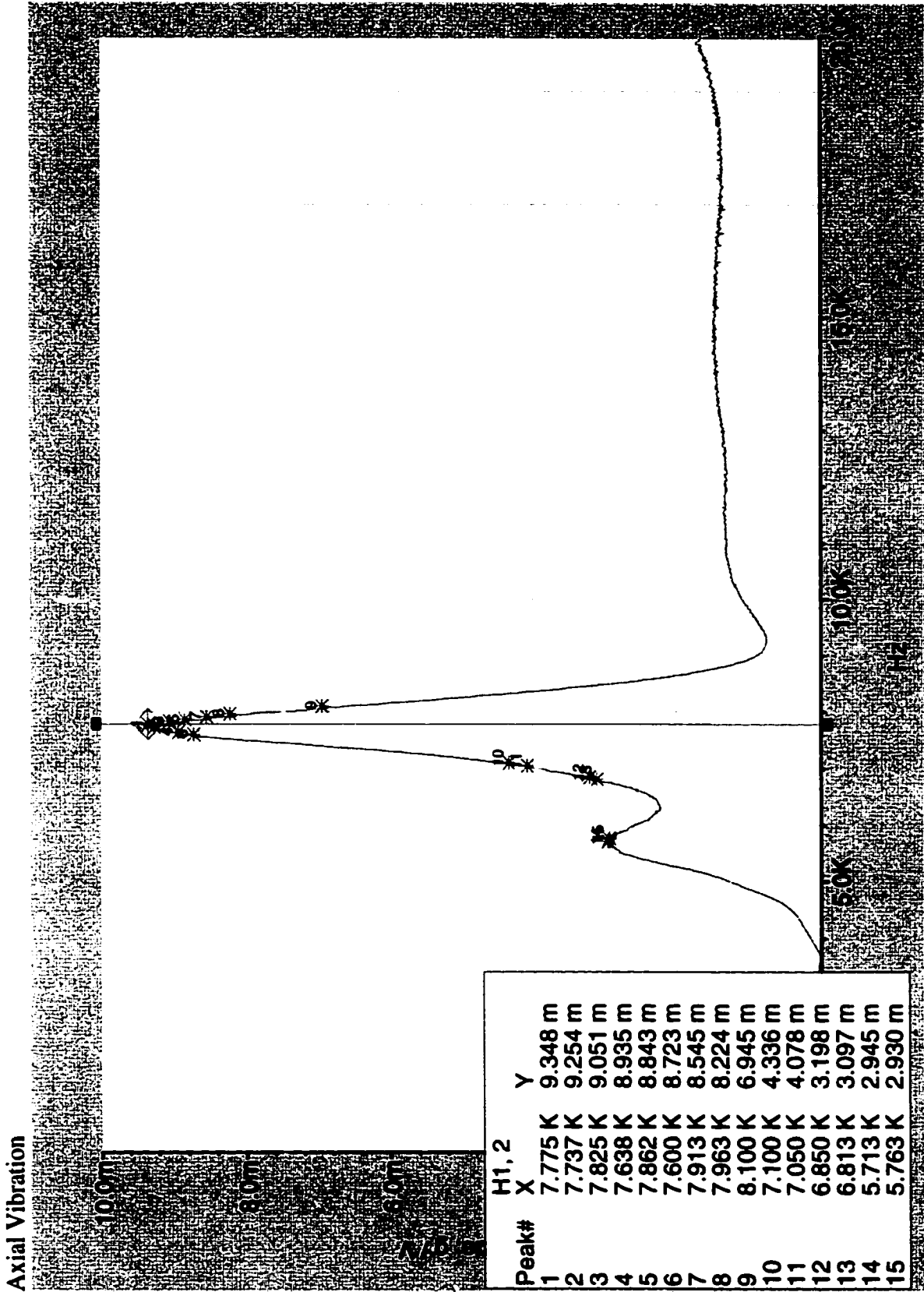


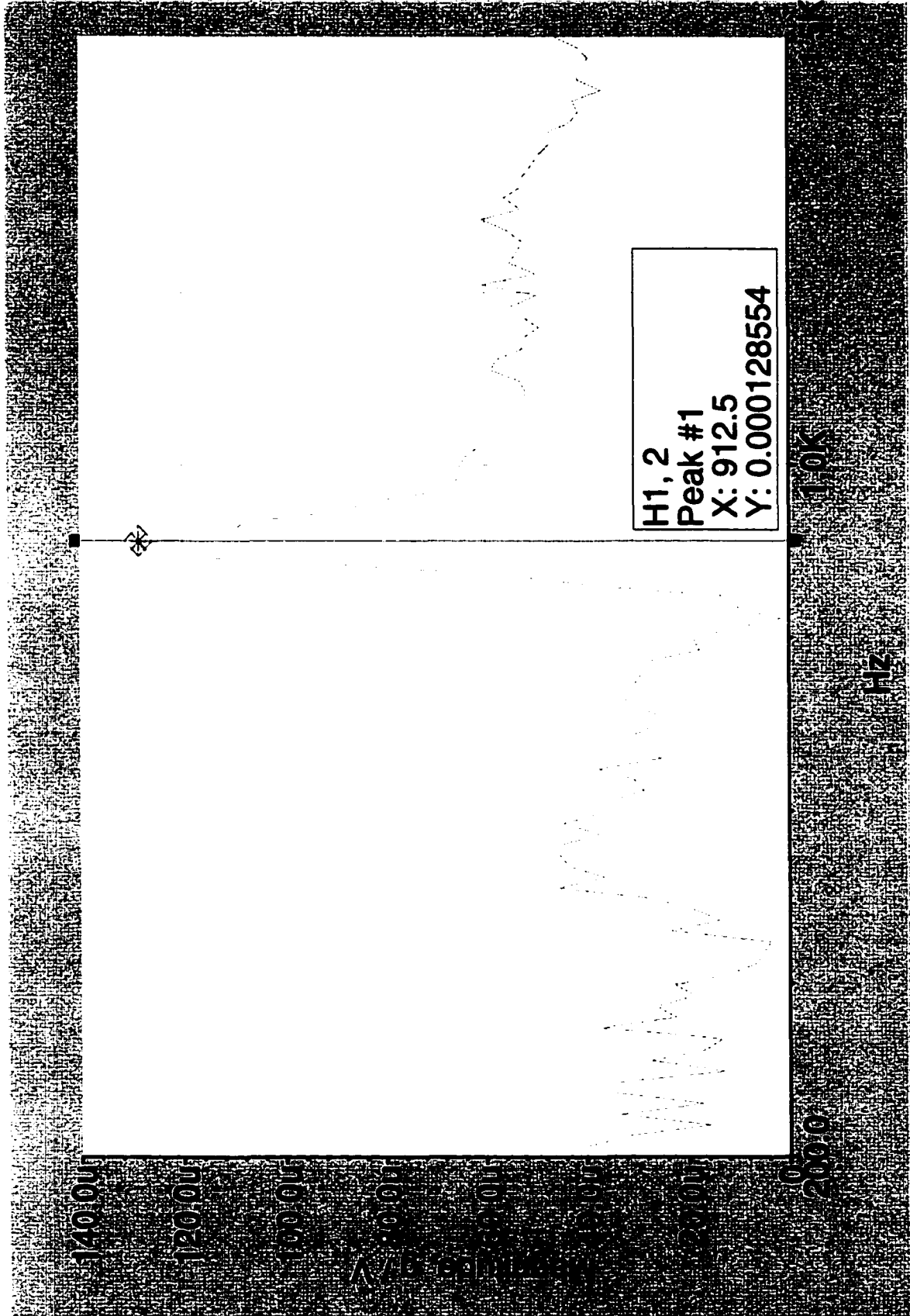


Mount#1 Full Threaded Case Torsional Vibration

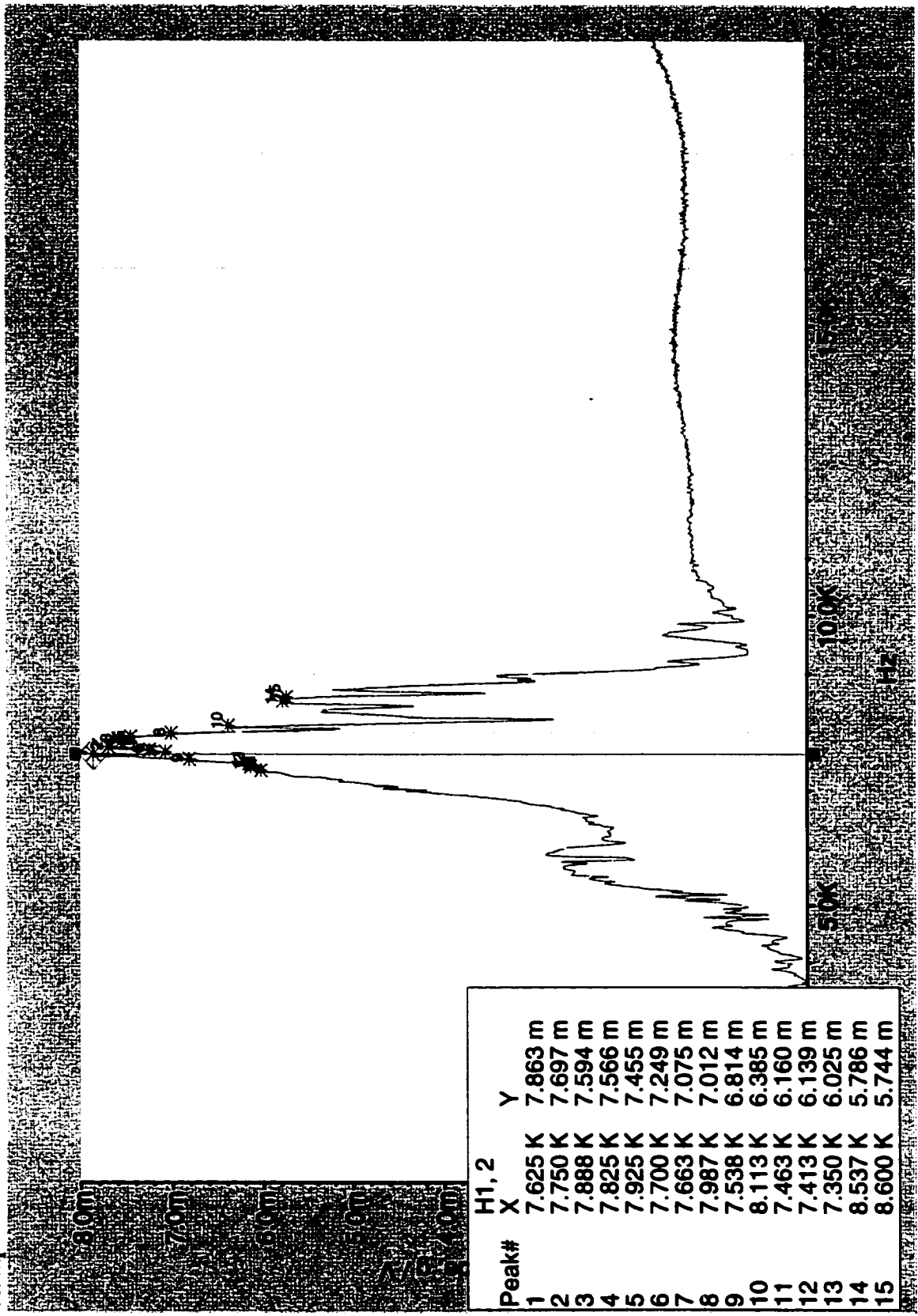


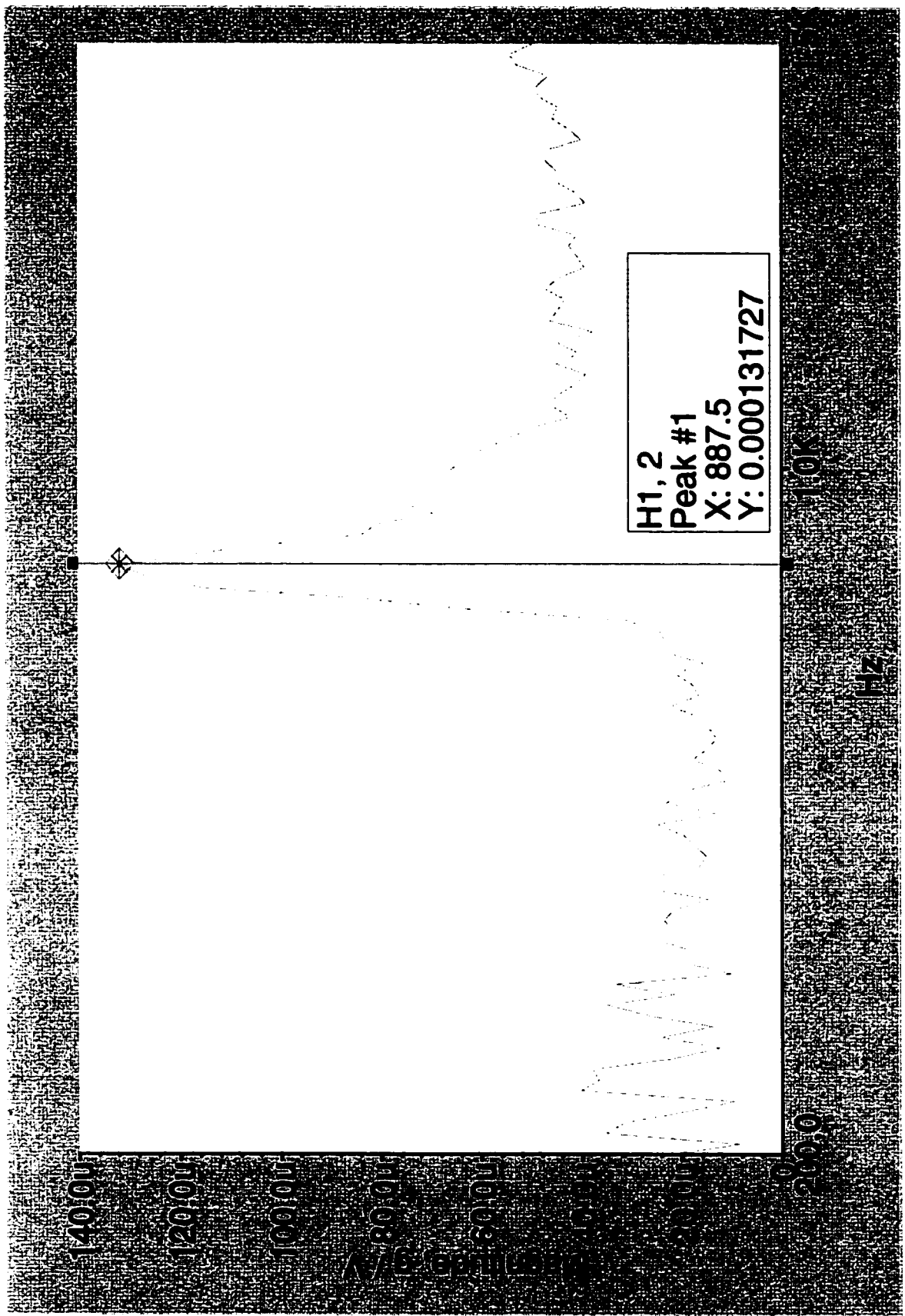




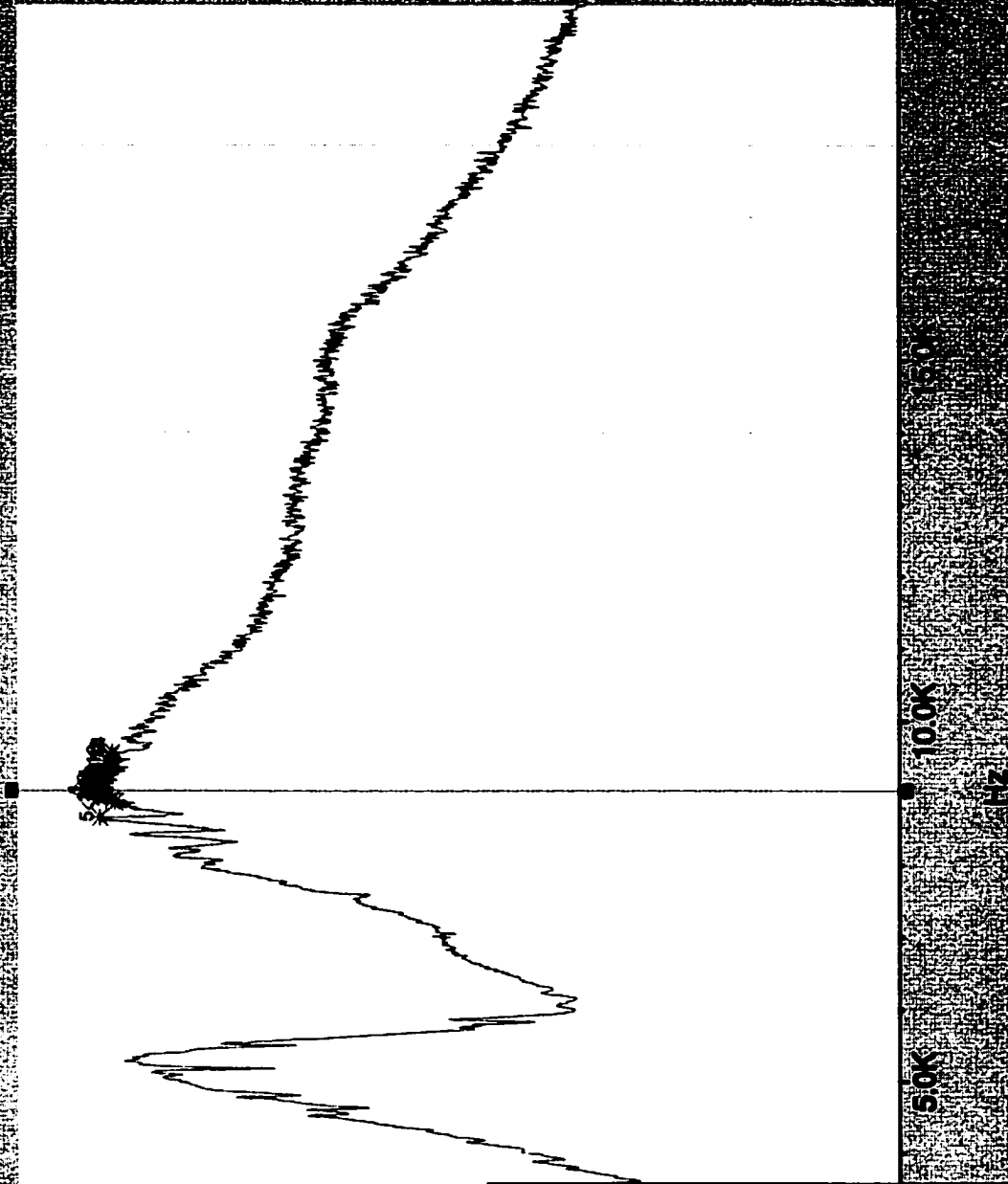


Clamped Results Axial

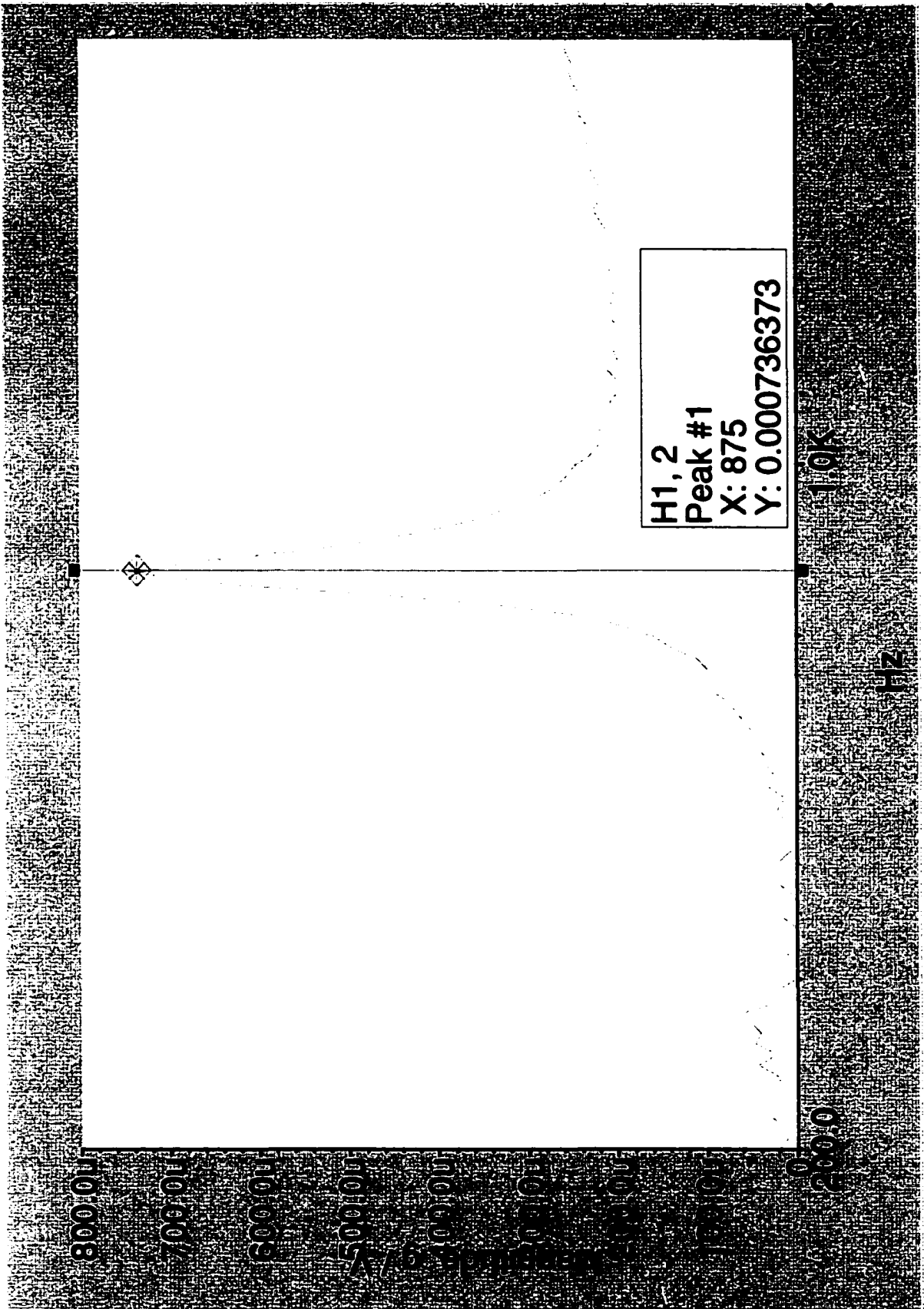




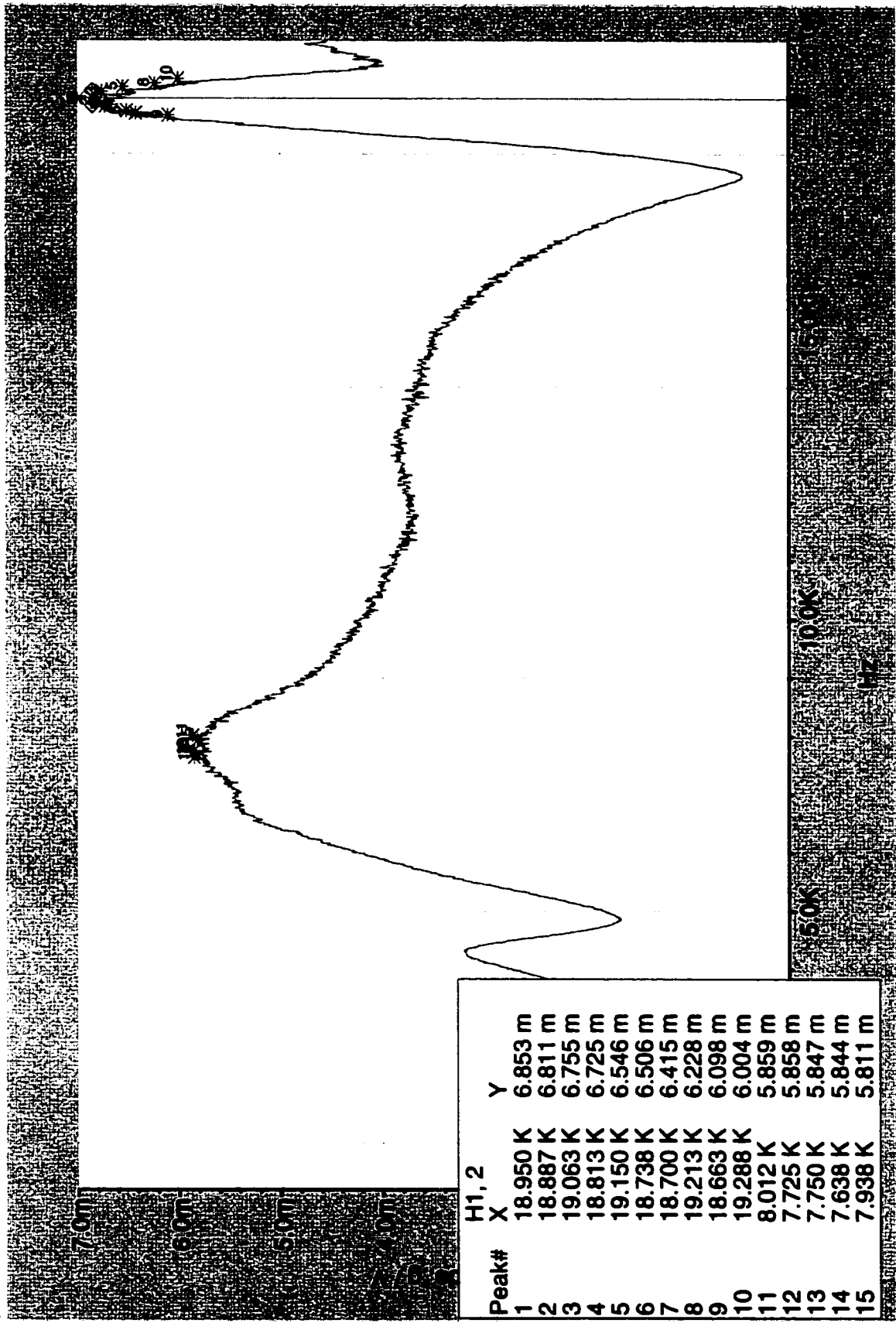
Torsional

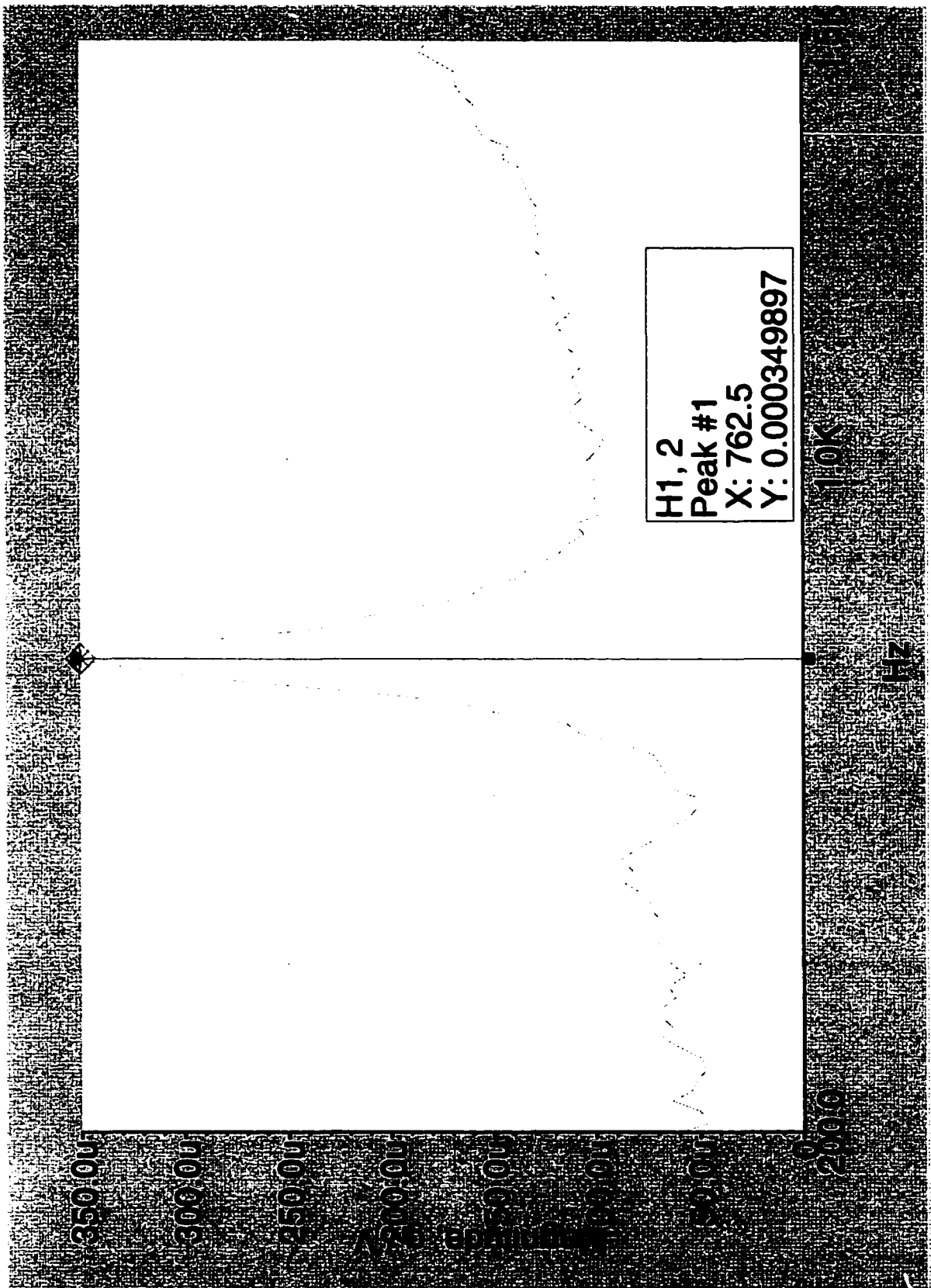


Peak#	H1,2	X	Y
1		9.050 K	5.525 m
2		9.200 K	5.459 m
3		8.950 K	5.455 m
4		9.263 K	5.449 m
5		8.675 K	5.446 m
6		9.138 K	5.445 m
7		9.100 K	5.428 m
8		8.975 K	5.412 m
9		9.313 K	5.410 m
10		9.450 K	5.394 m
11		9.375 K	5.373 m
12		9.513 K	5.371 m
13		8.912 K	5.363 m
14		9.563 K	5.361 m
15		8.888 K	5.341 m

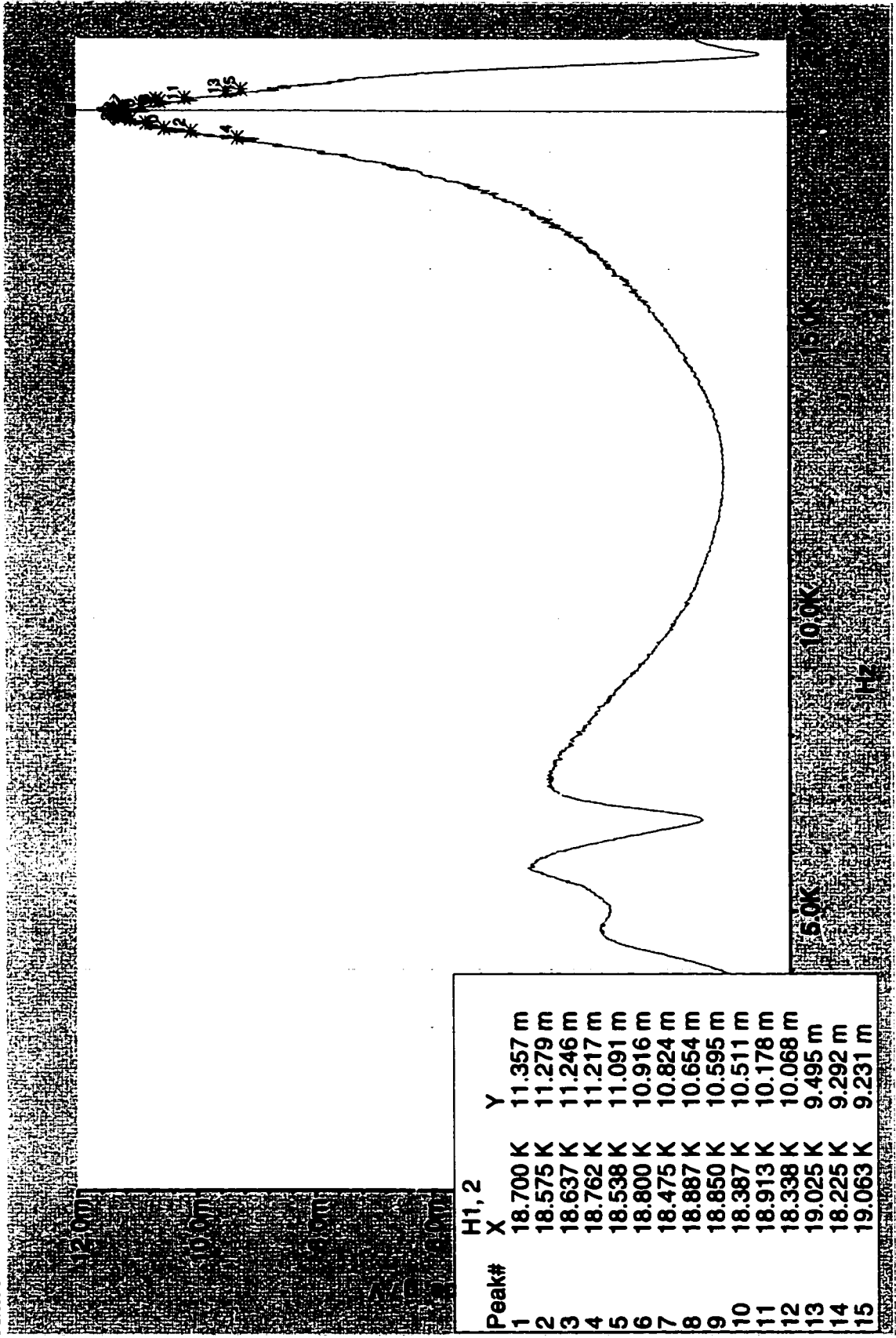


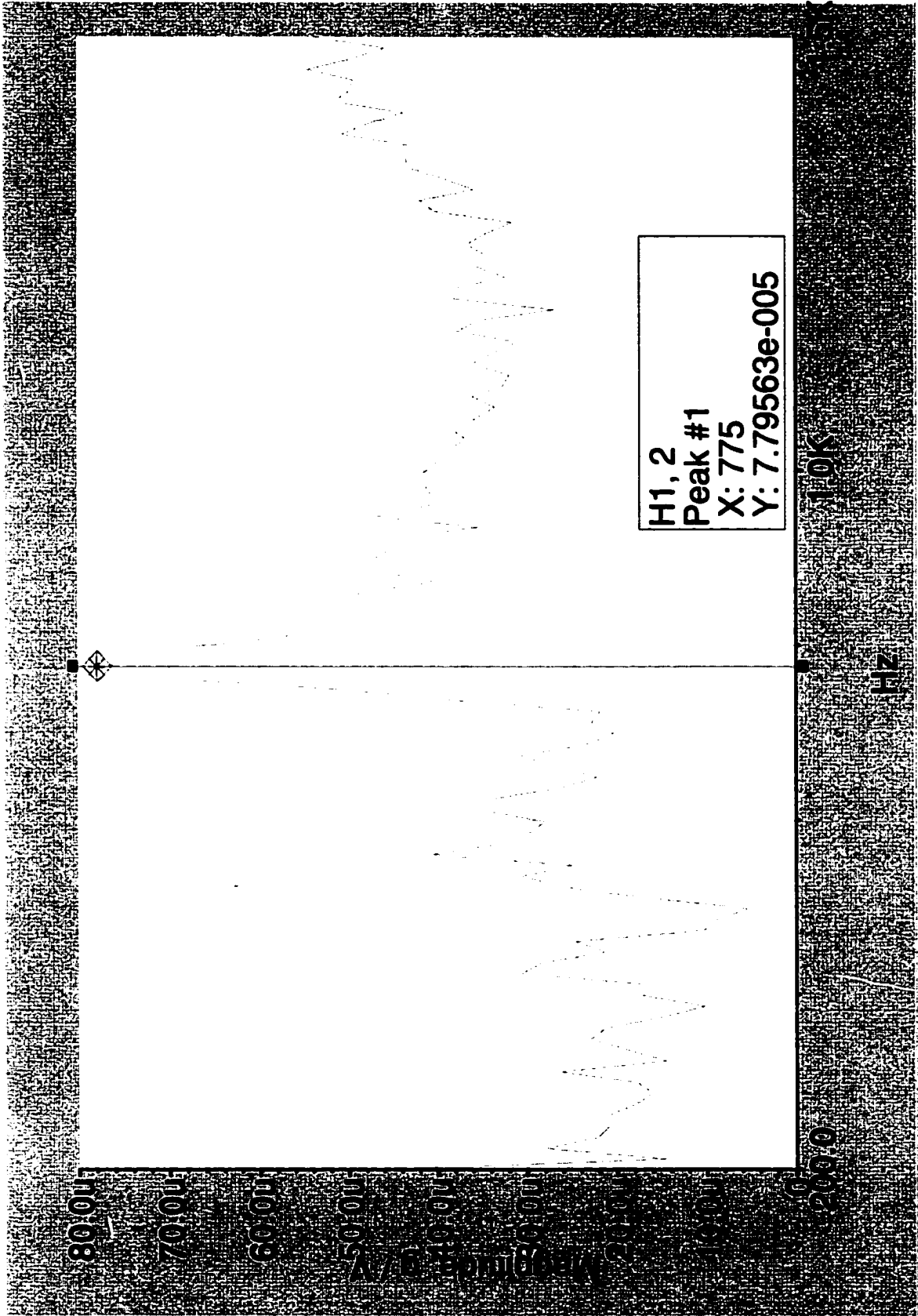
Half Threaded Case



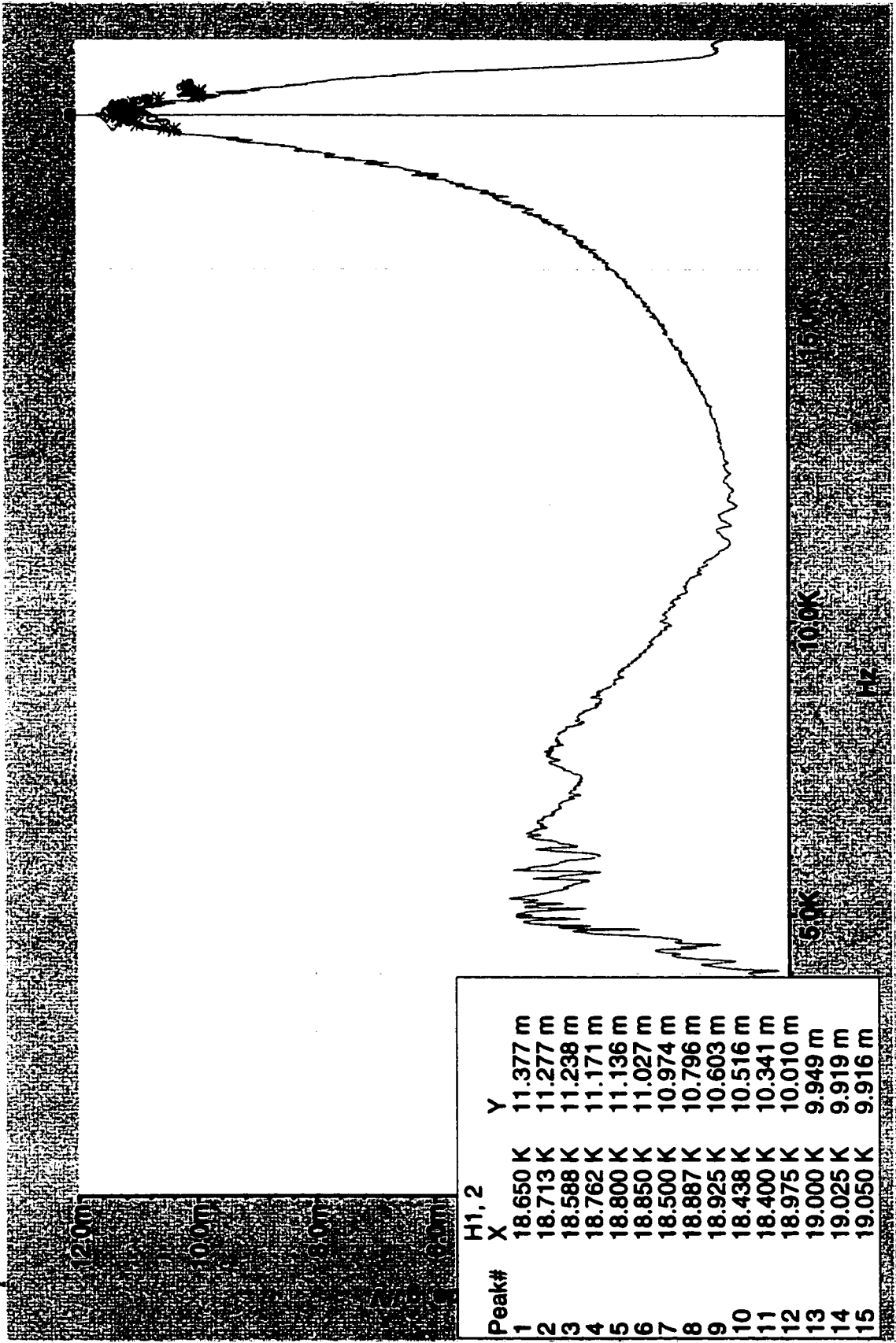


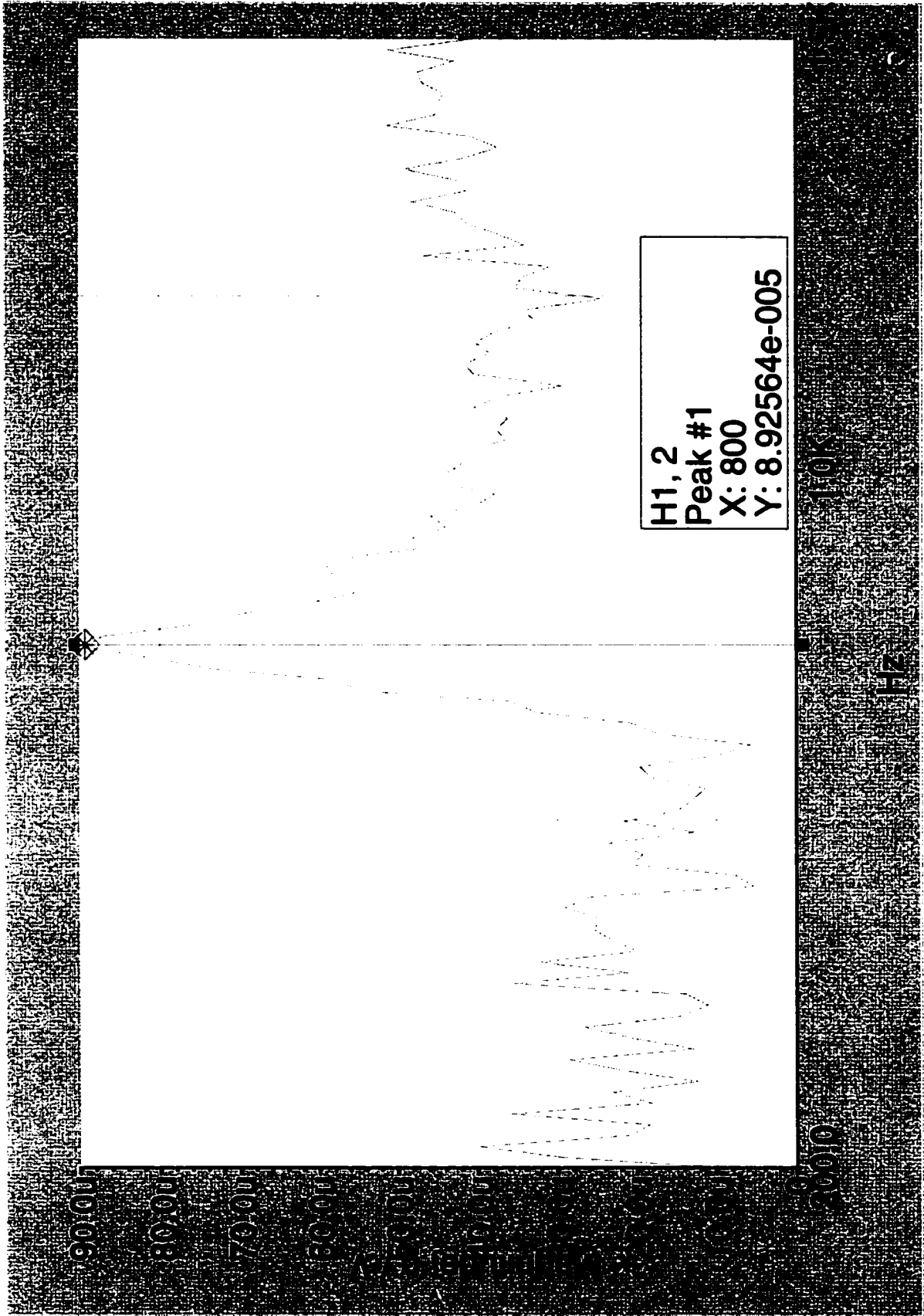
Axial



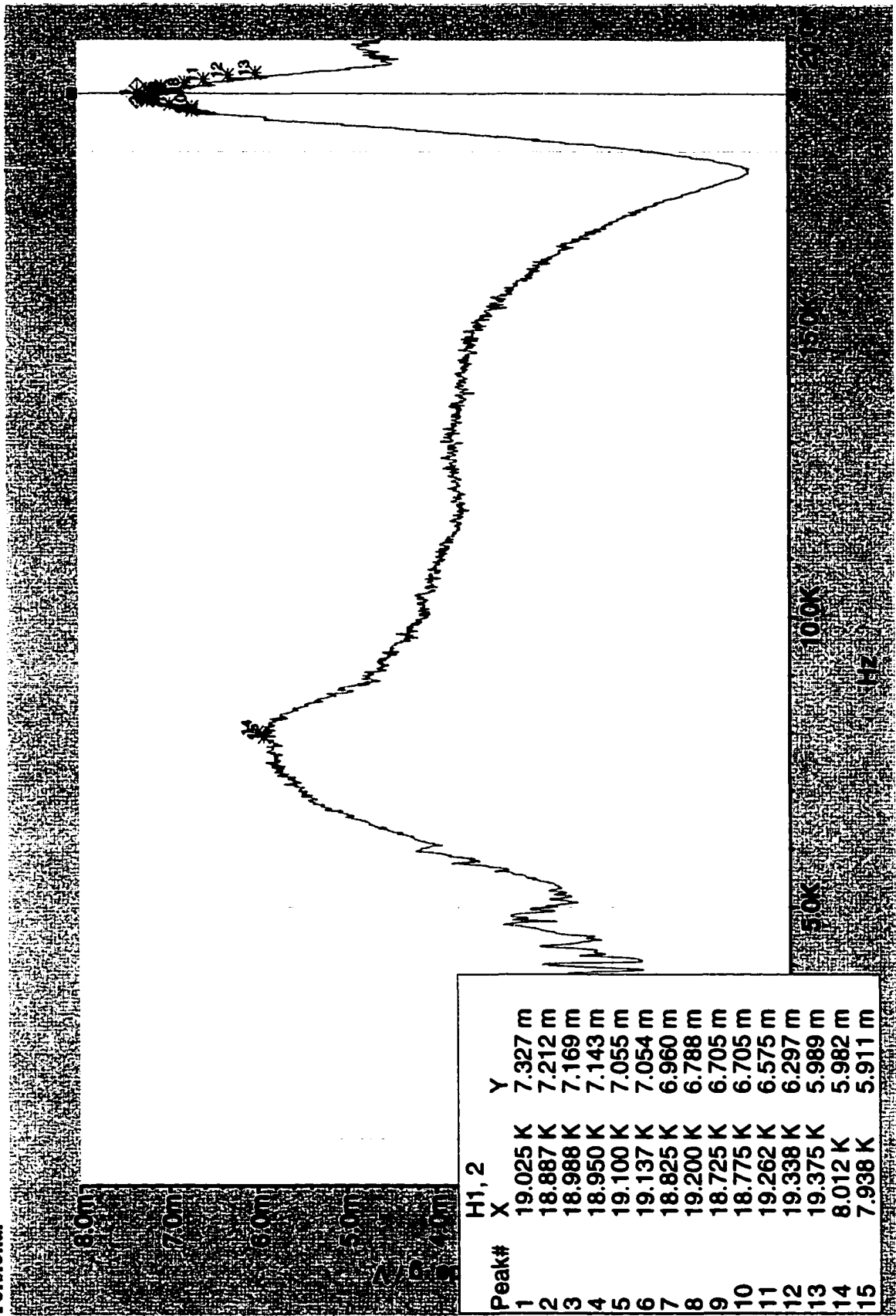


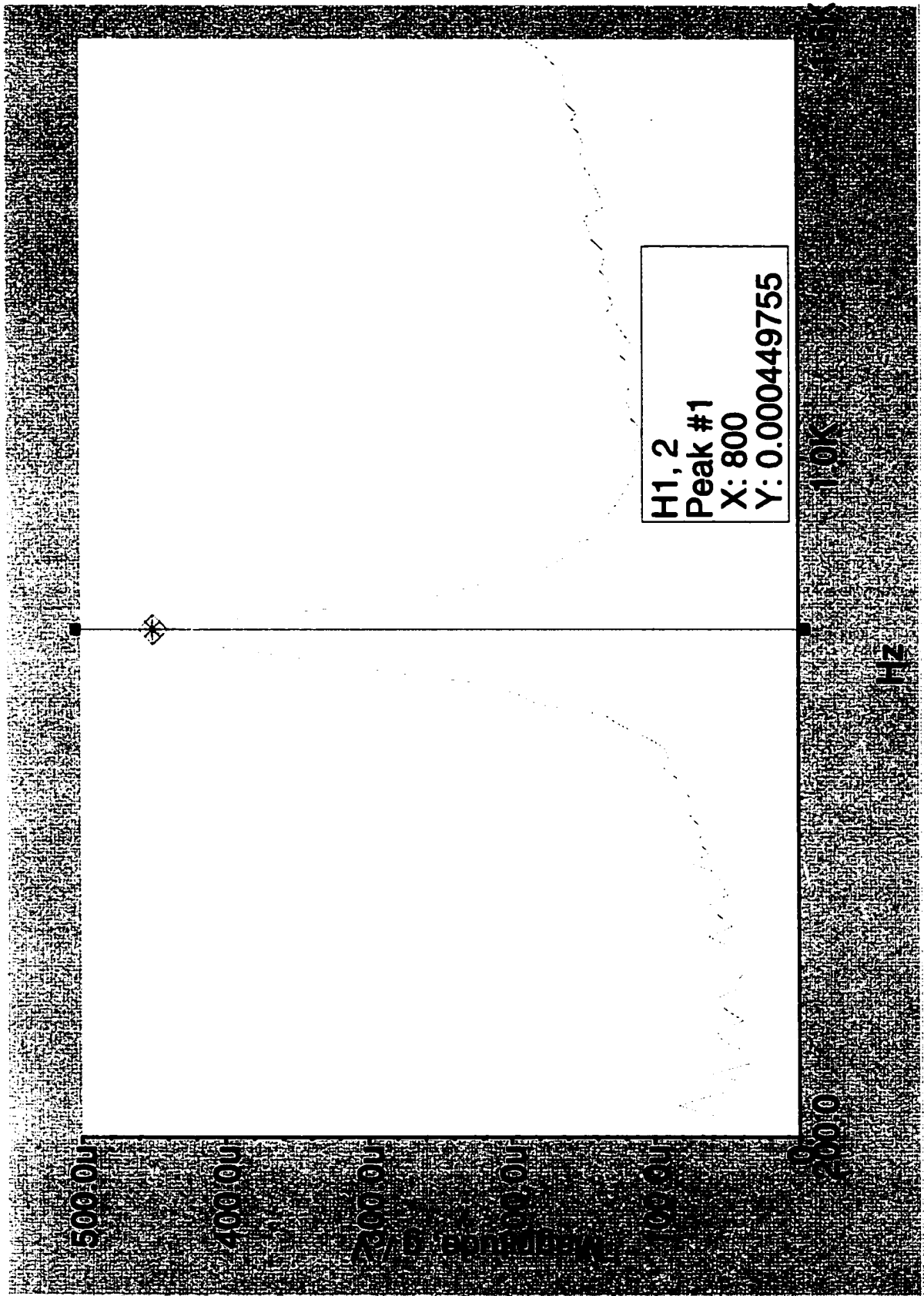
Clamped Results Axial



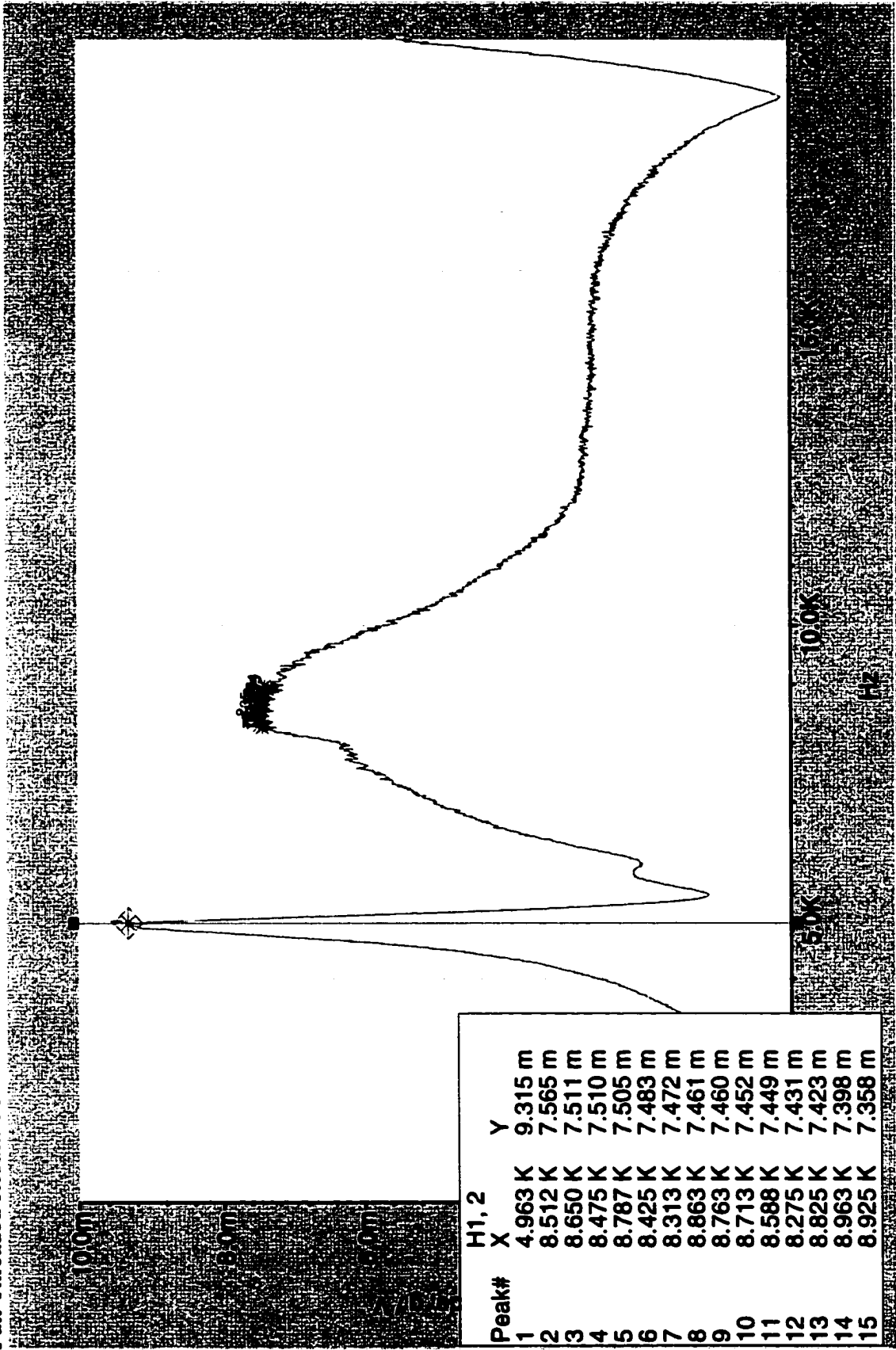


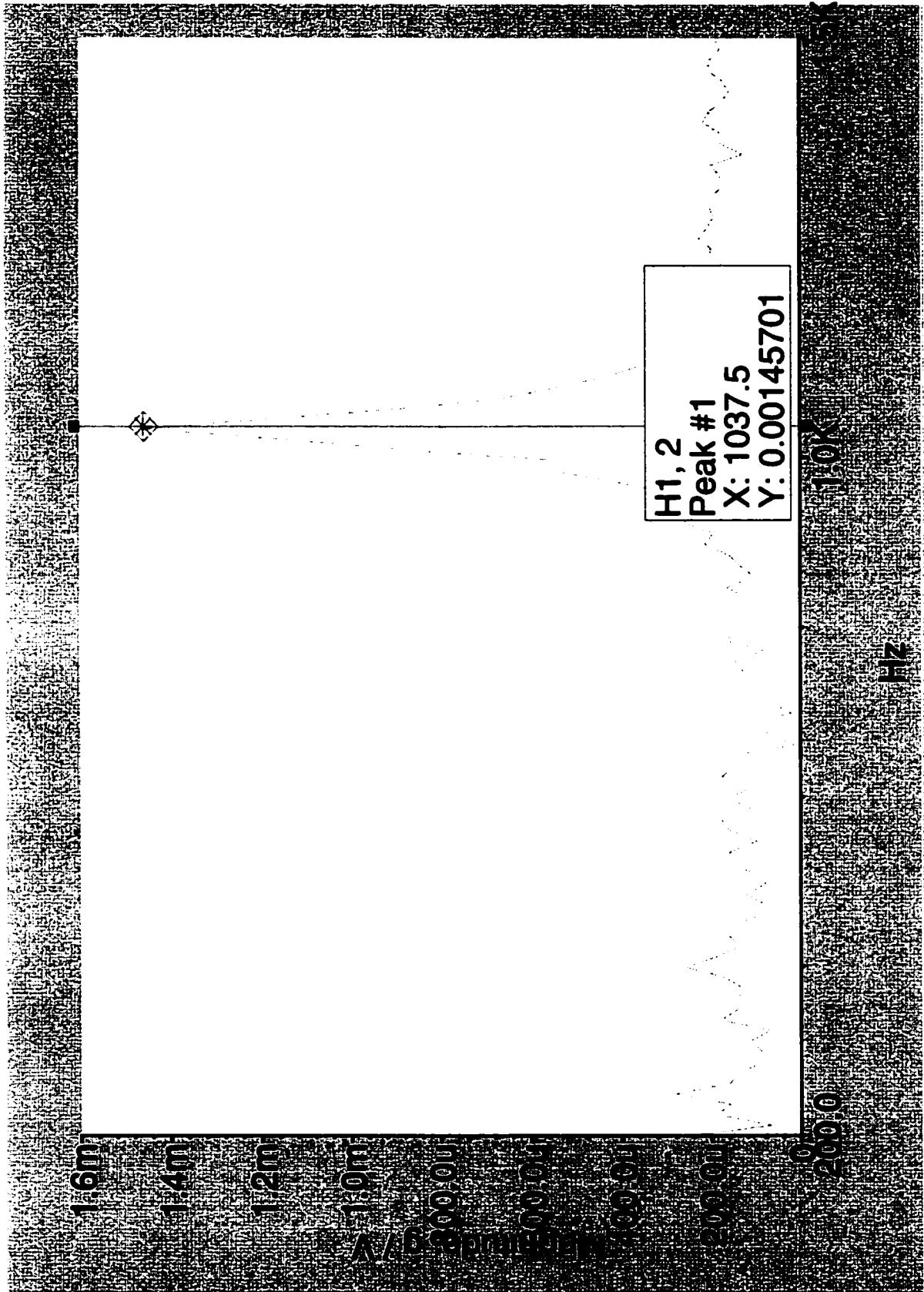
Torsional



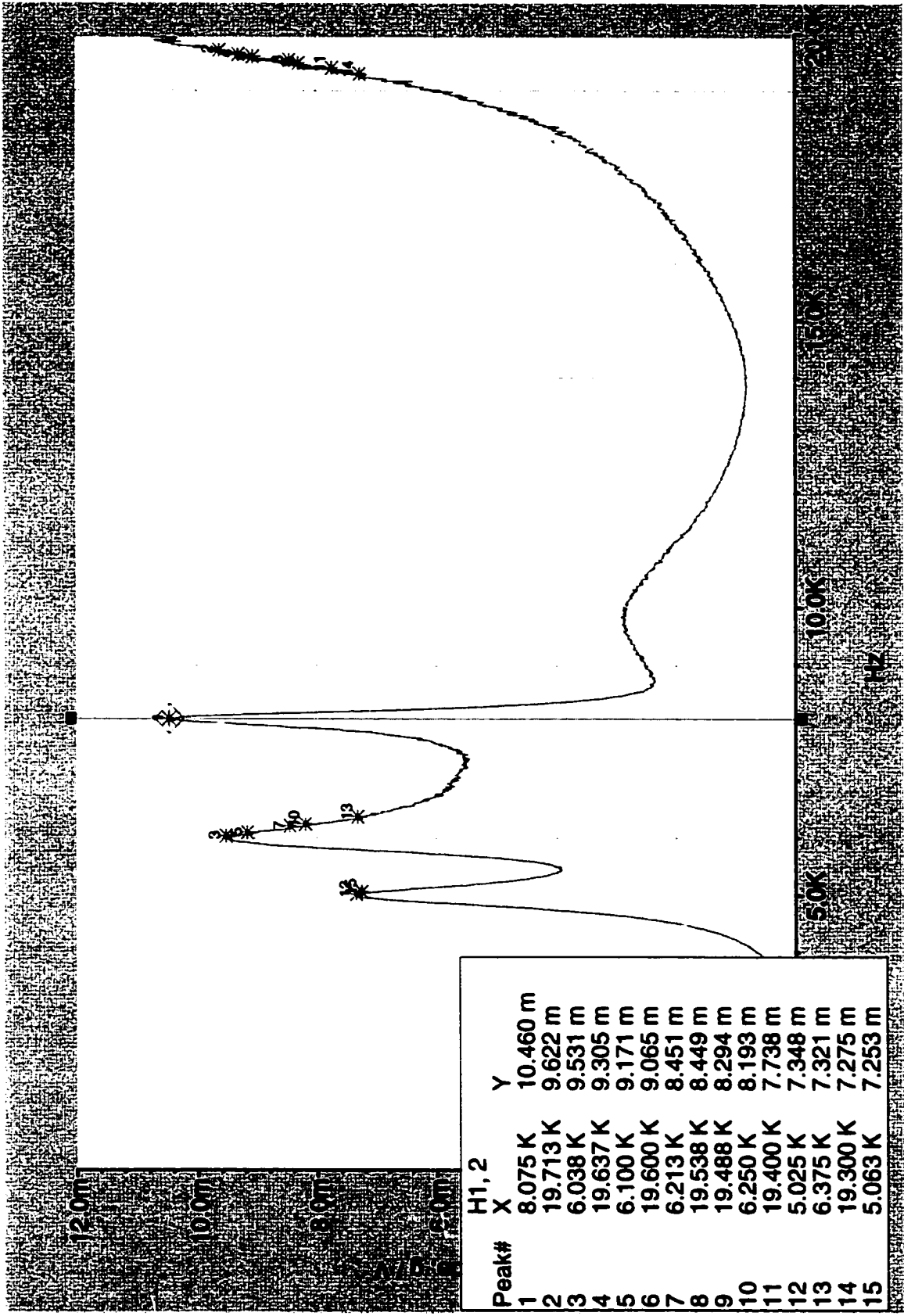


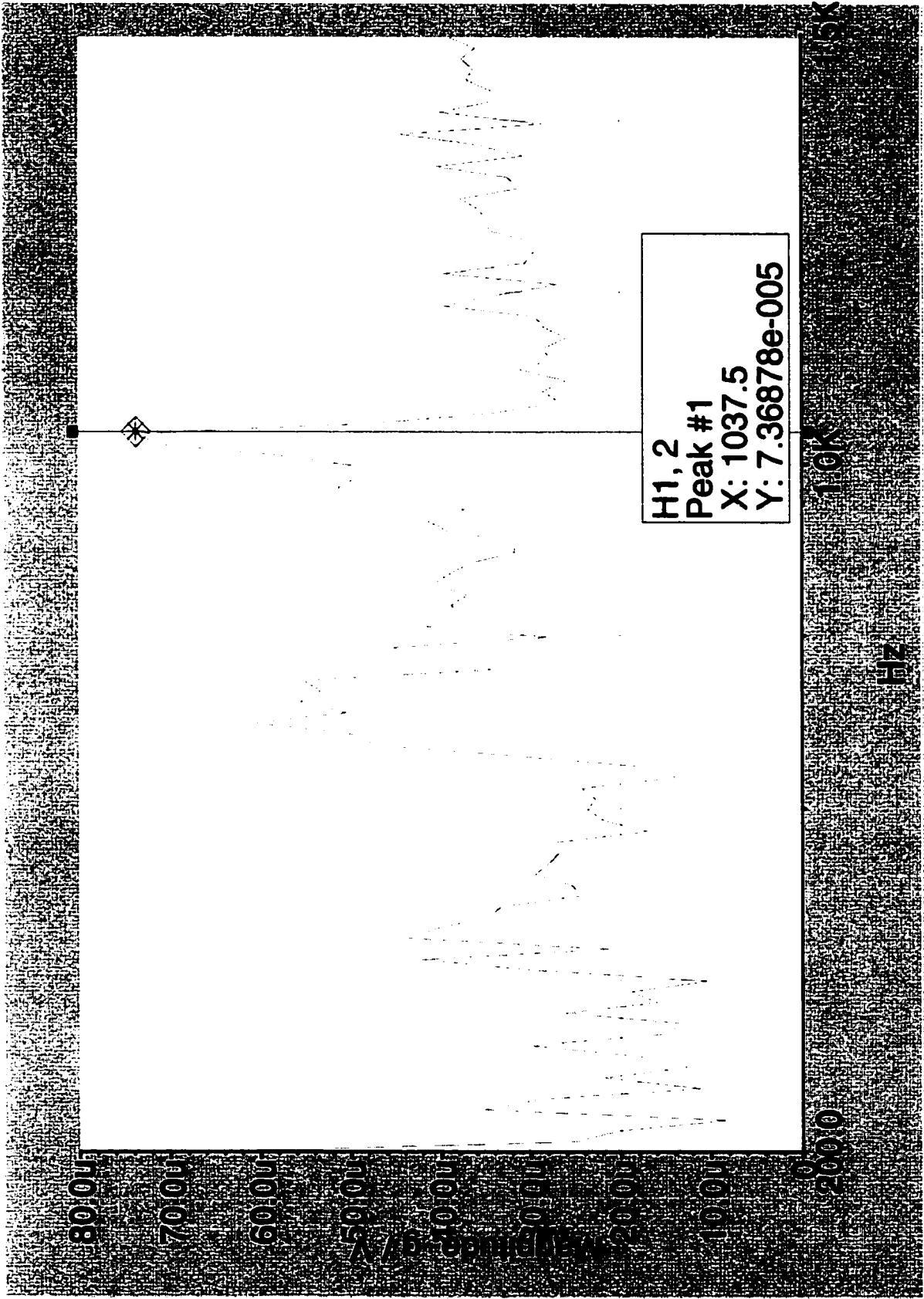
Full Threaded Results Mount #2 Torsional



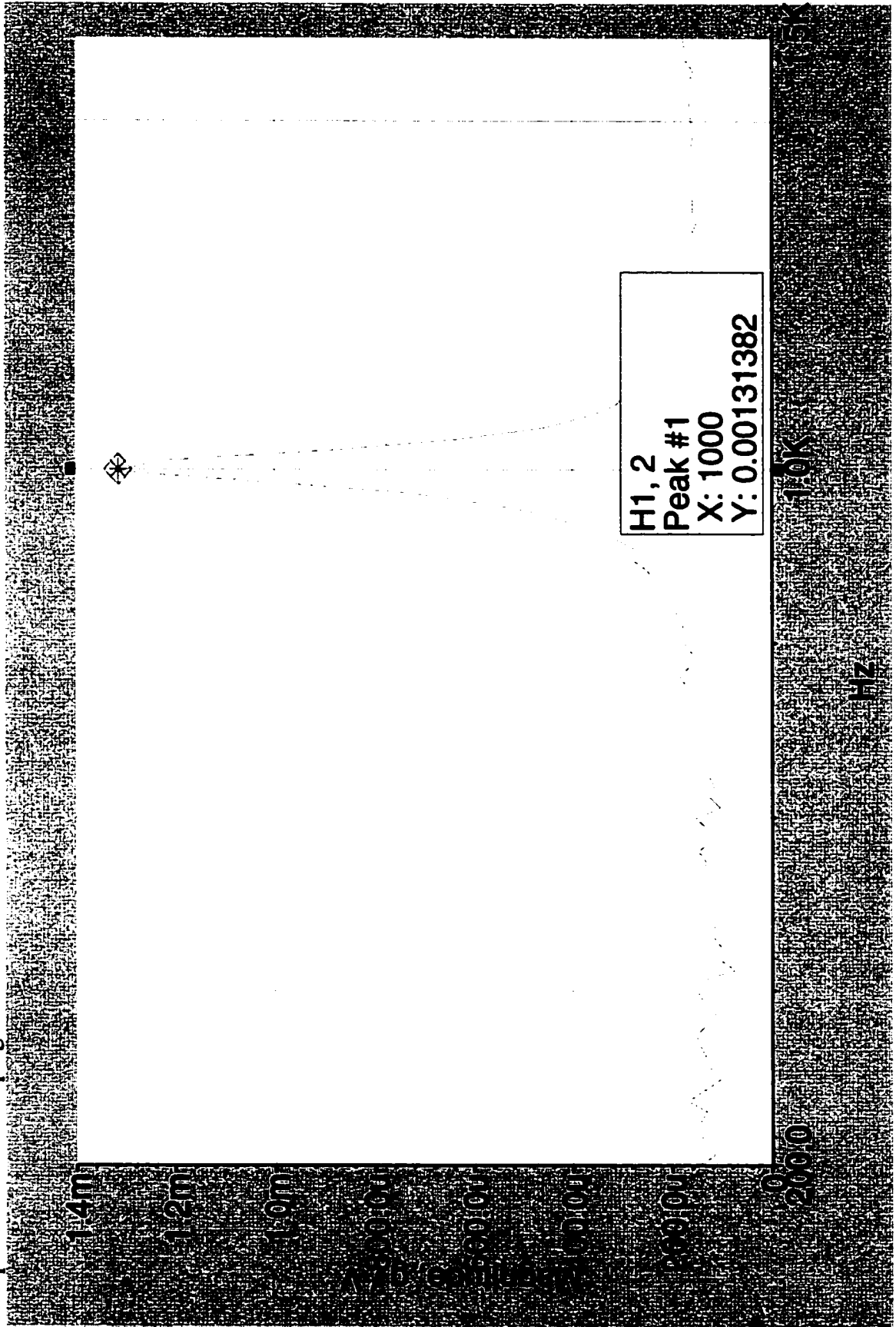


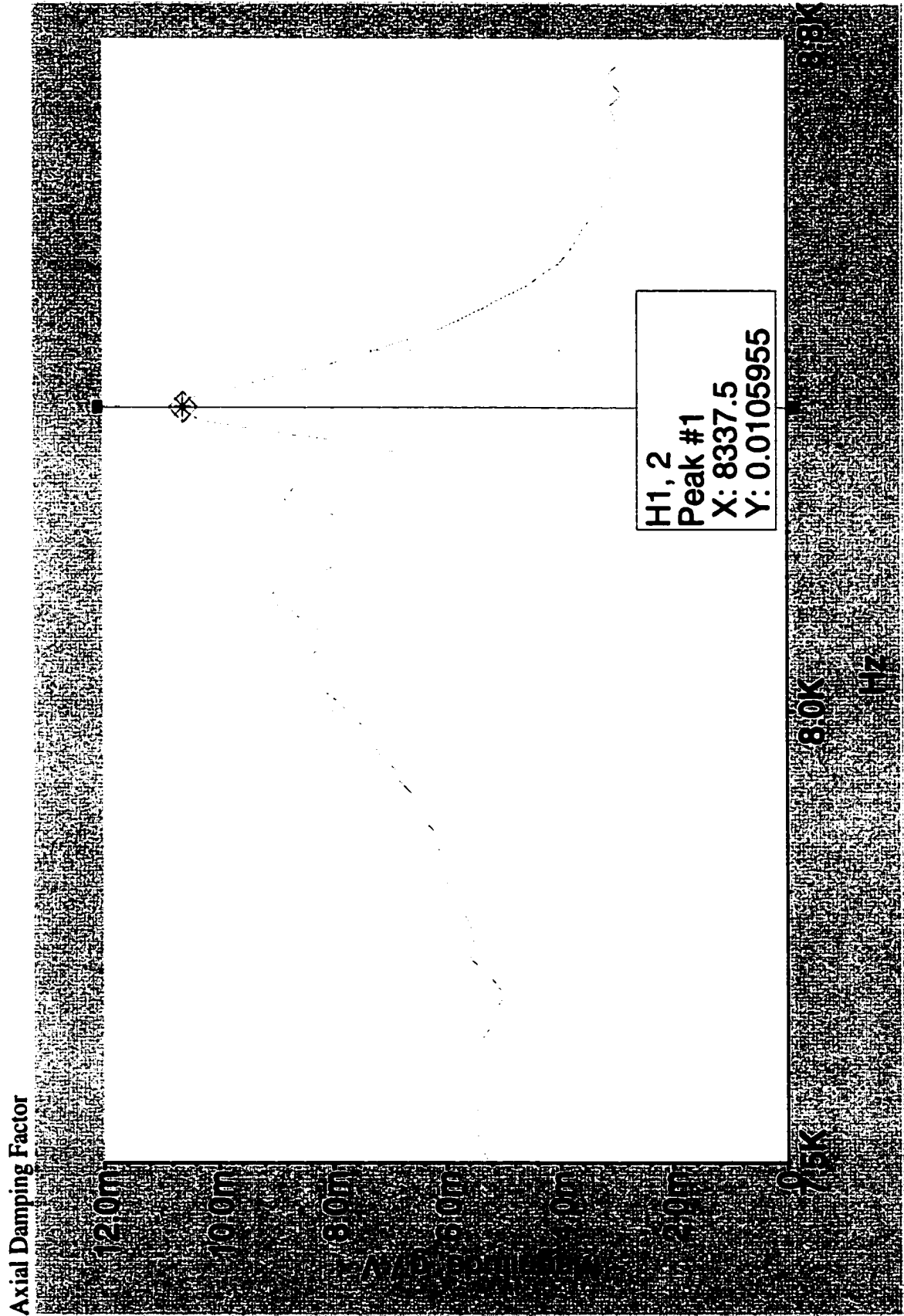
Axial



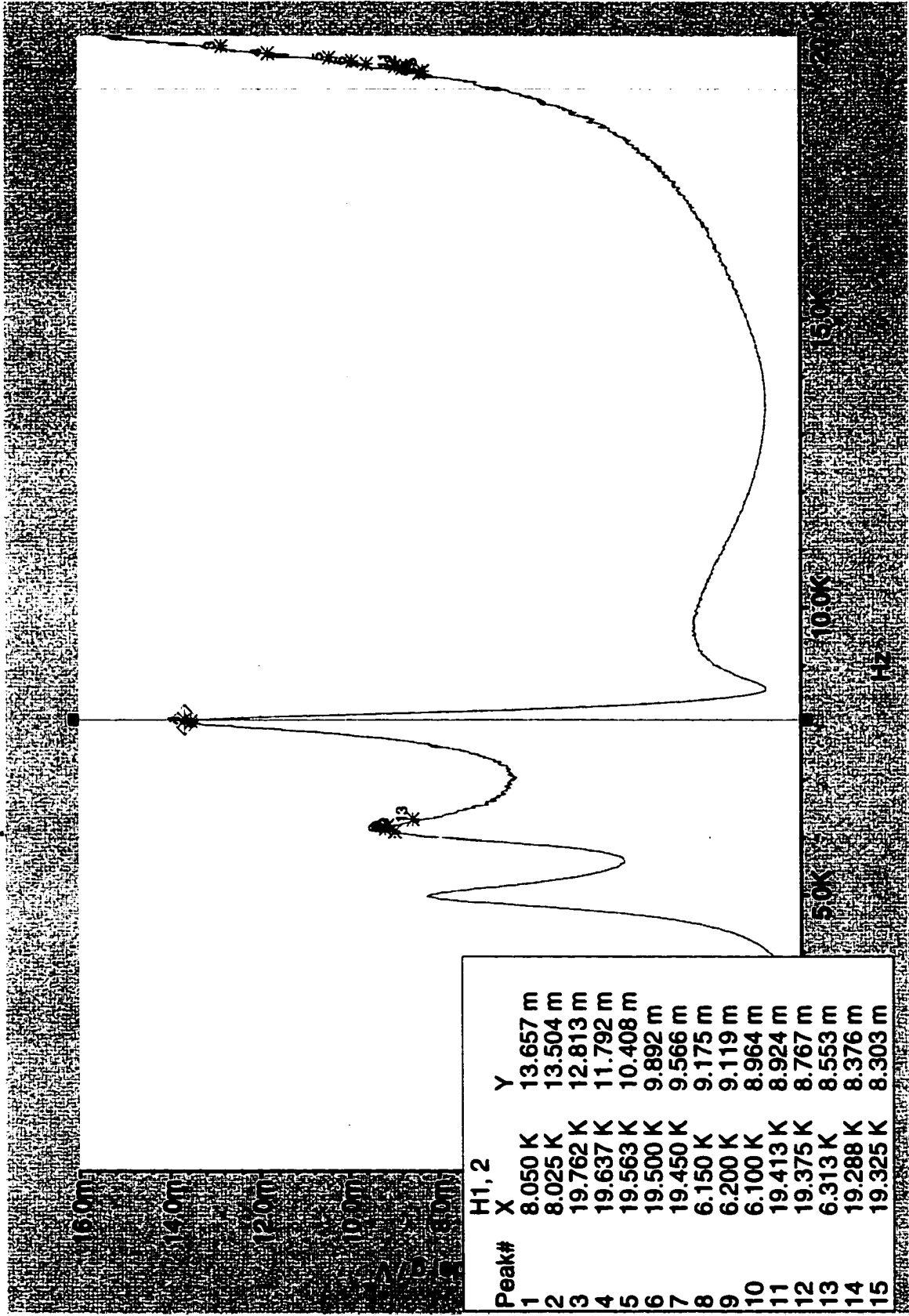


Clamped Result for Damping Factor

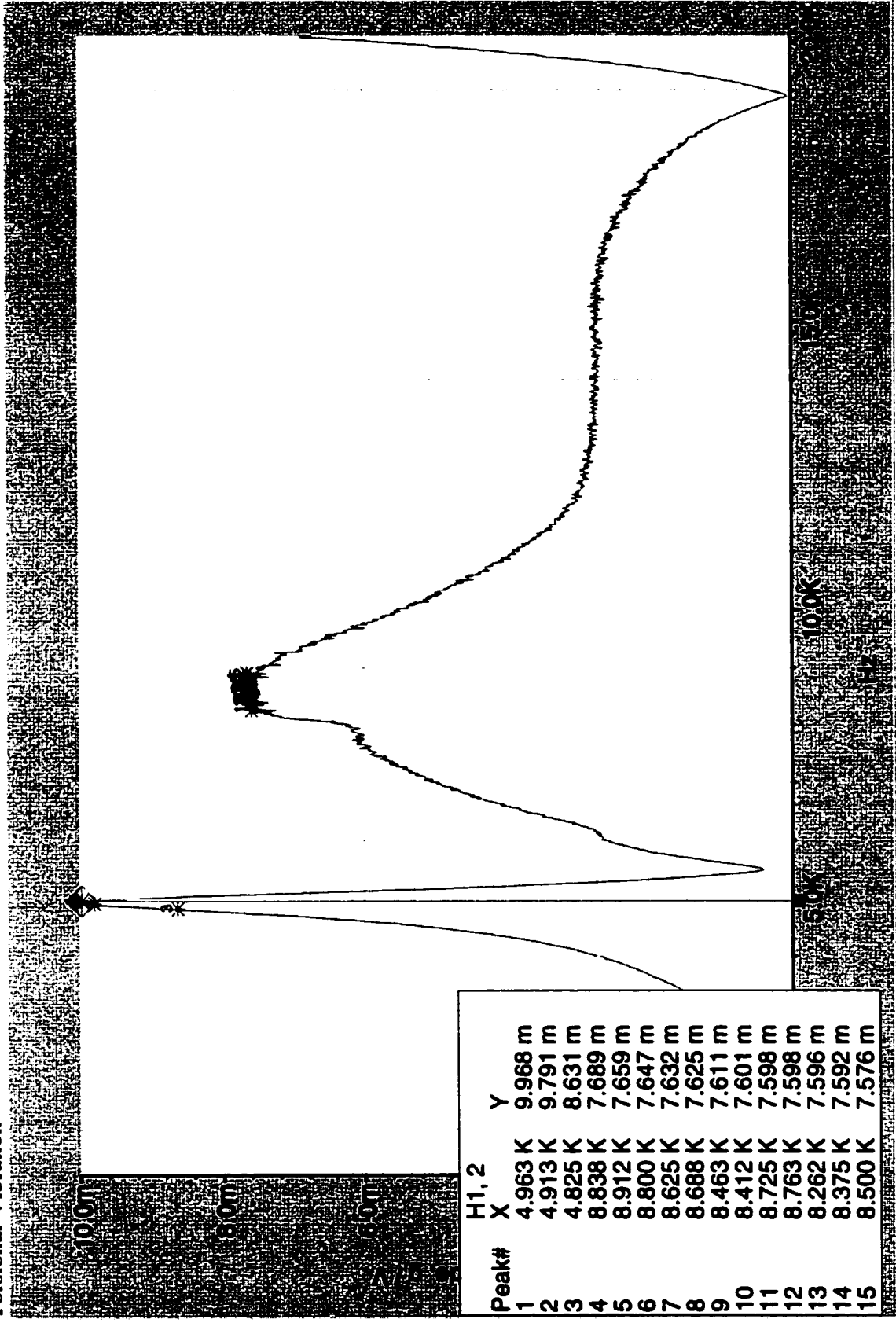


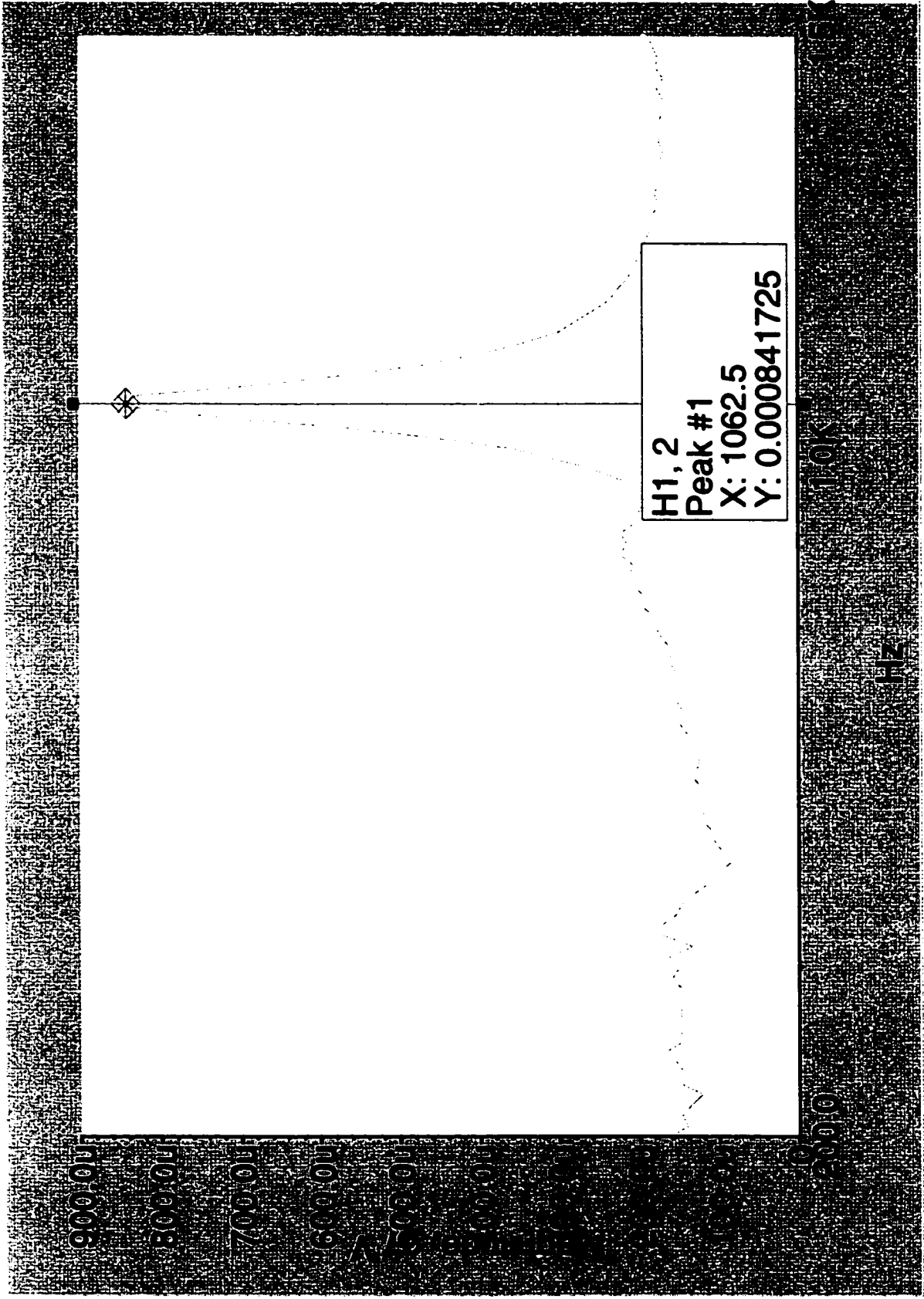


Axial for Mount #2 with a hole on one side see picture

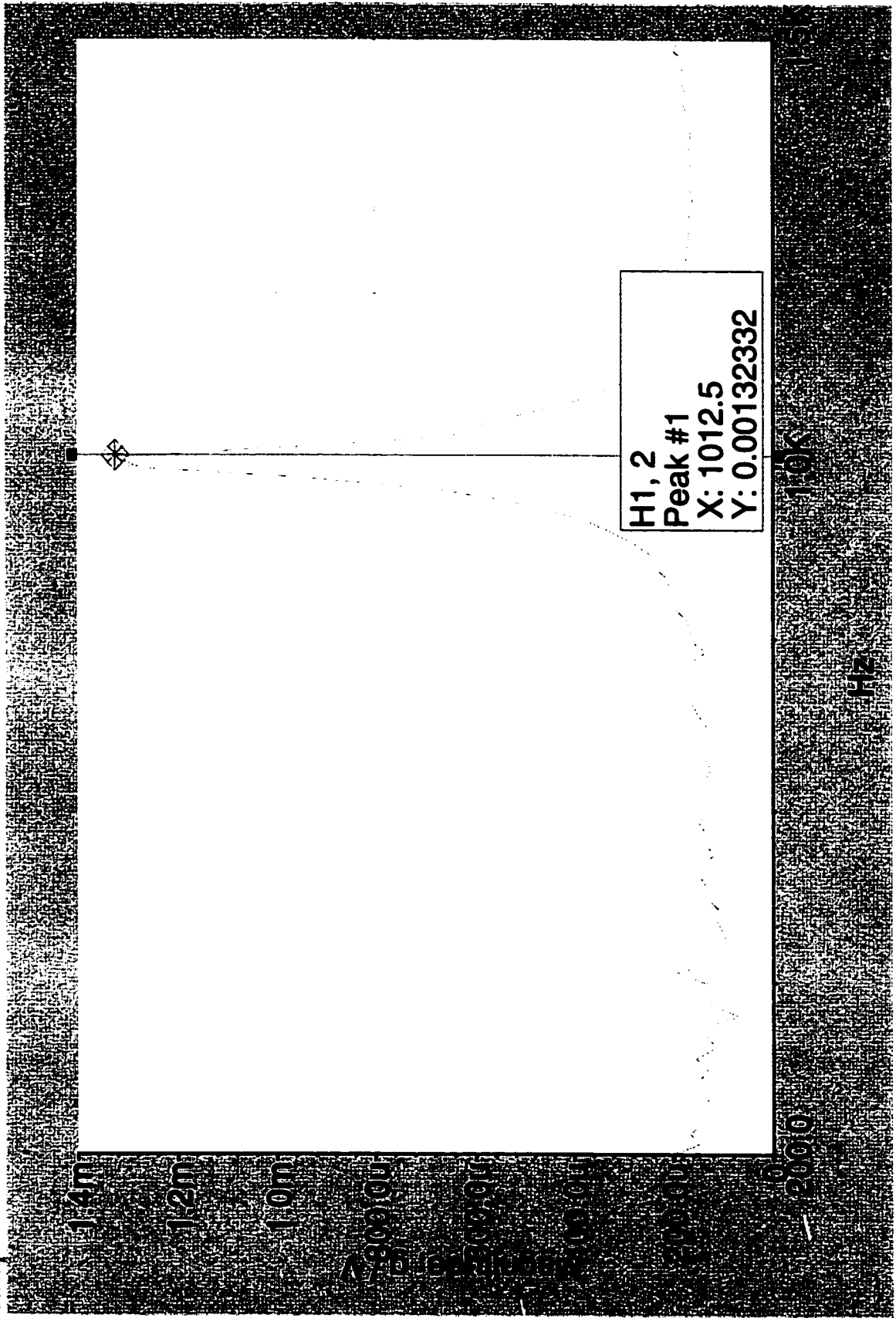


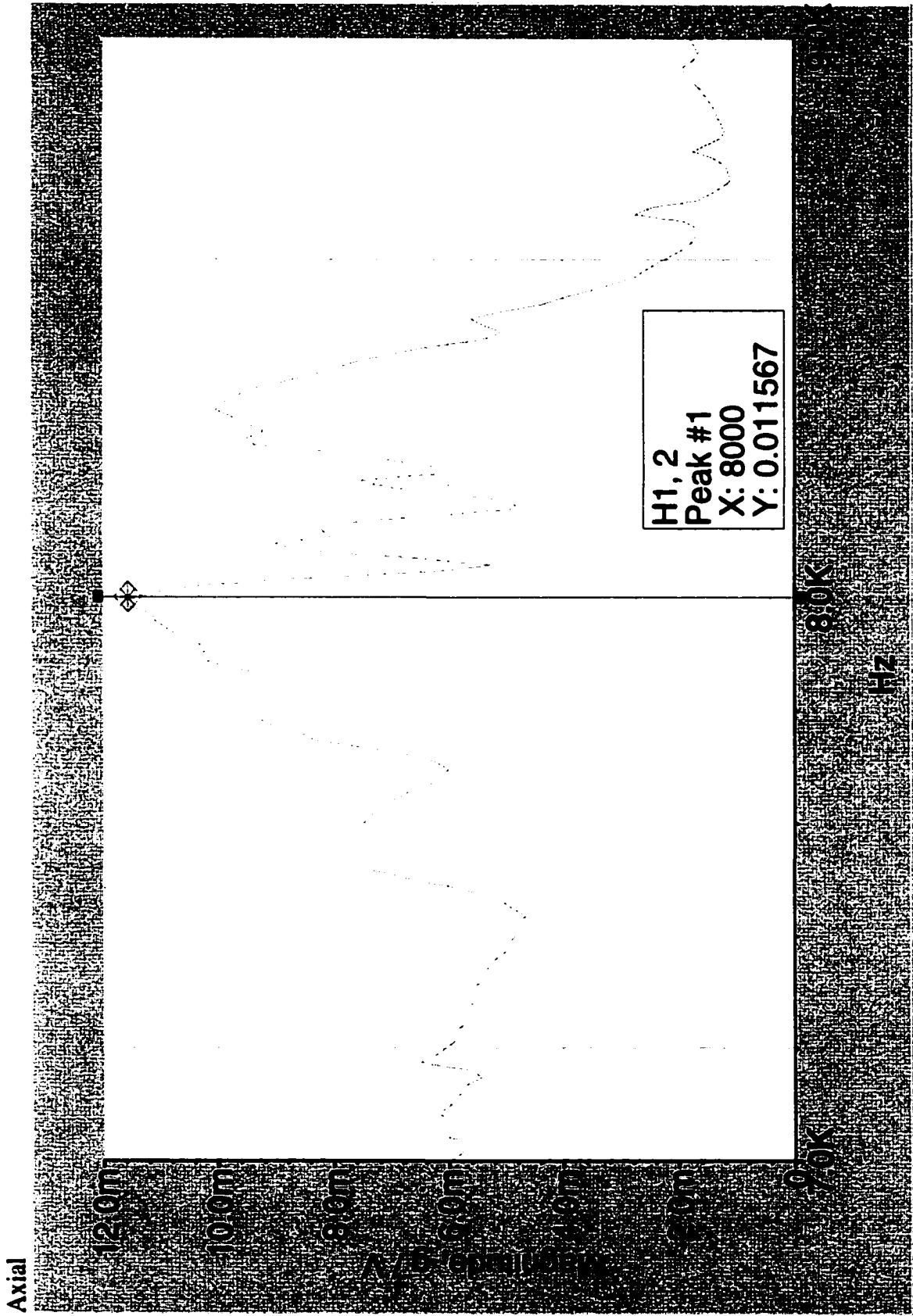
Torsional Vibration



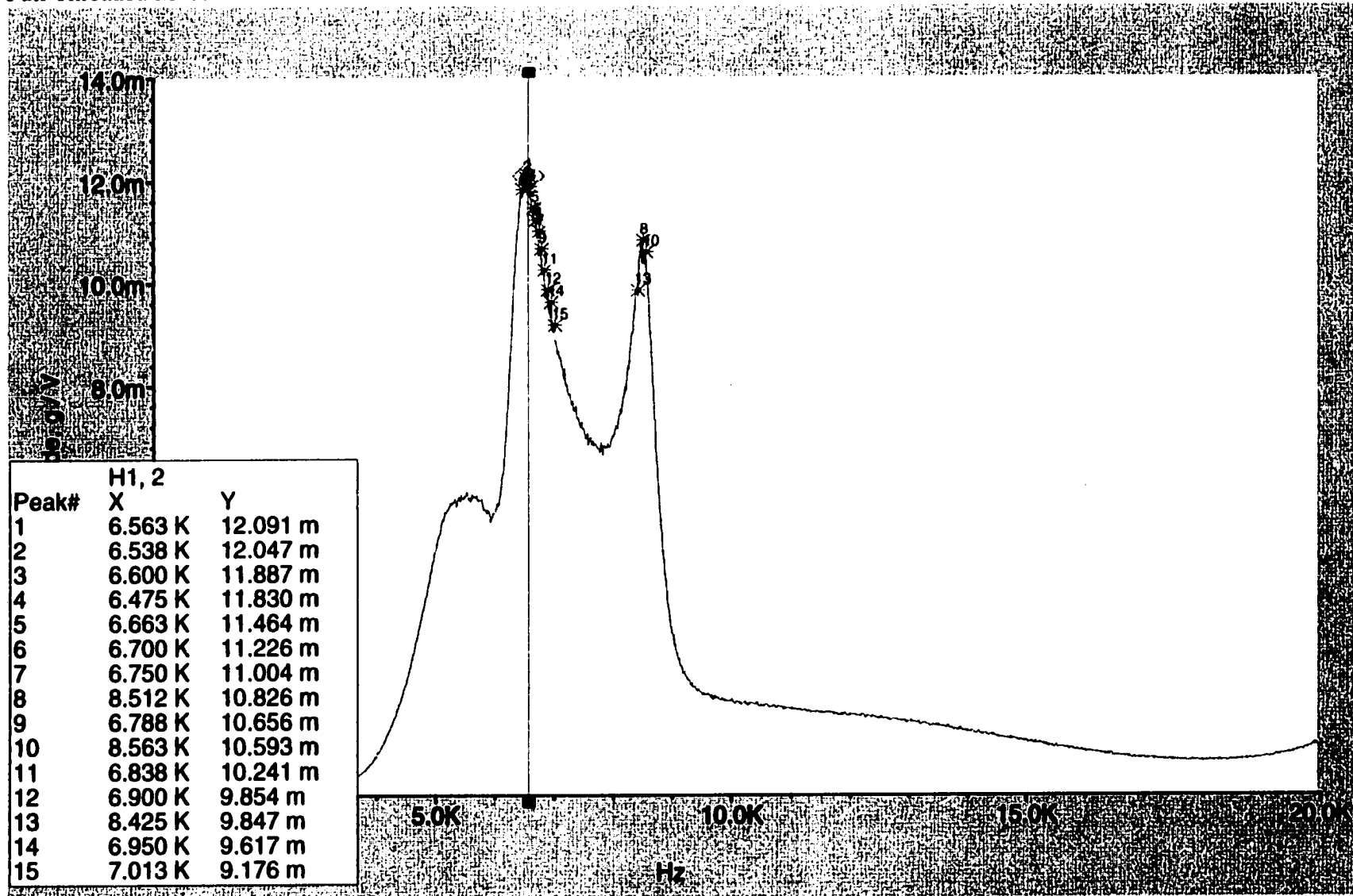


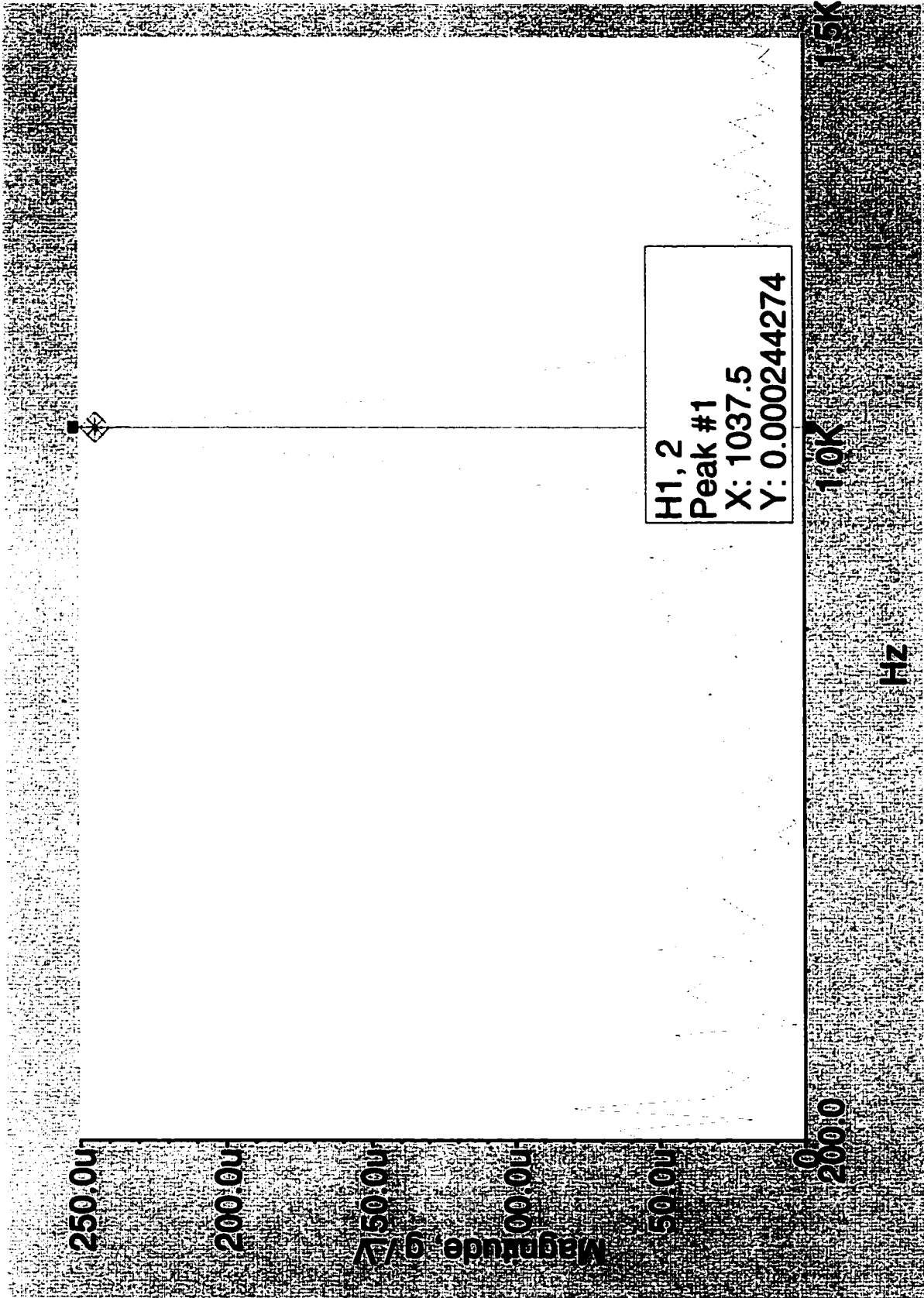
Clamped Torsional

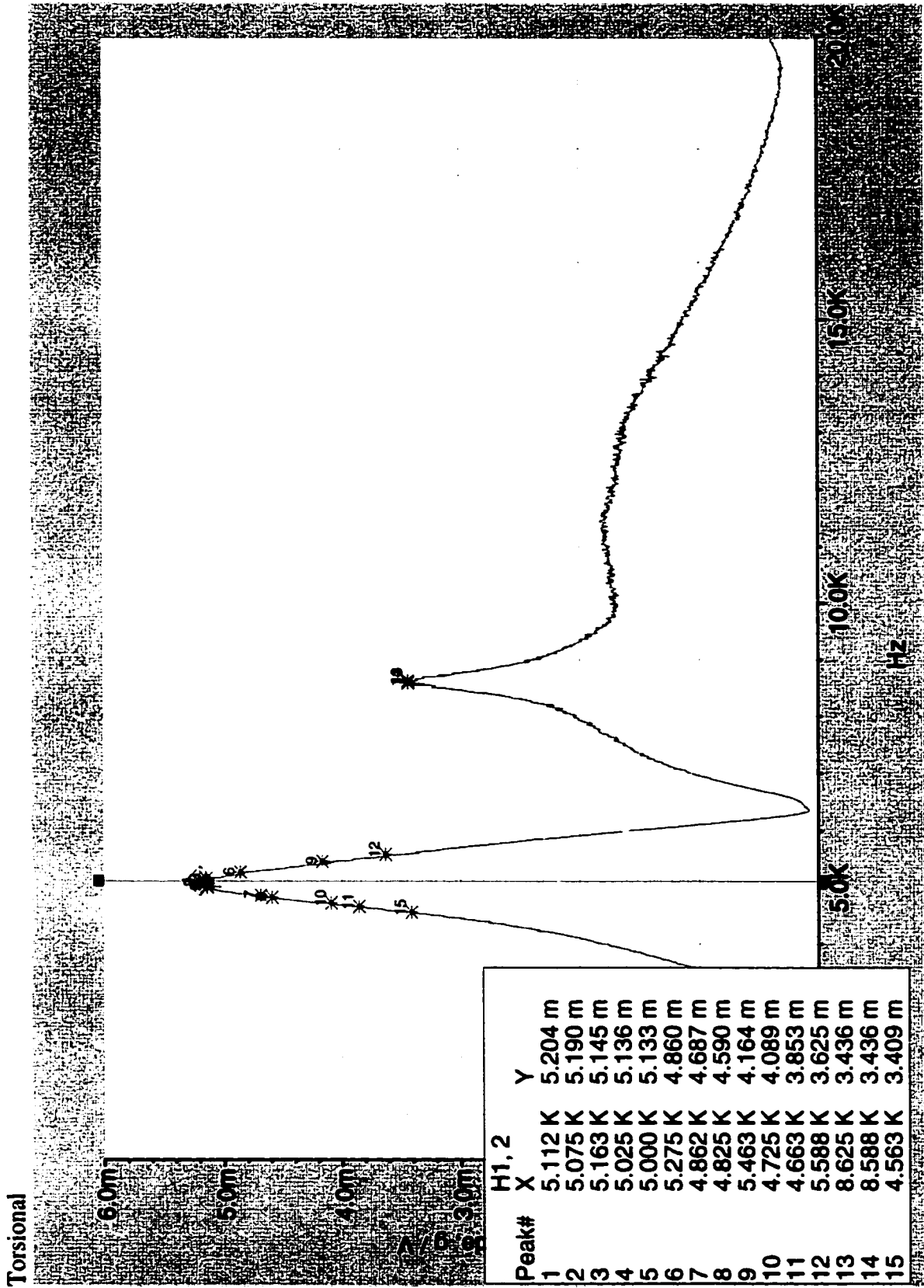


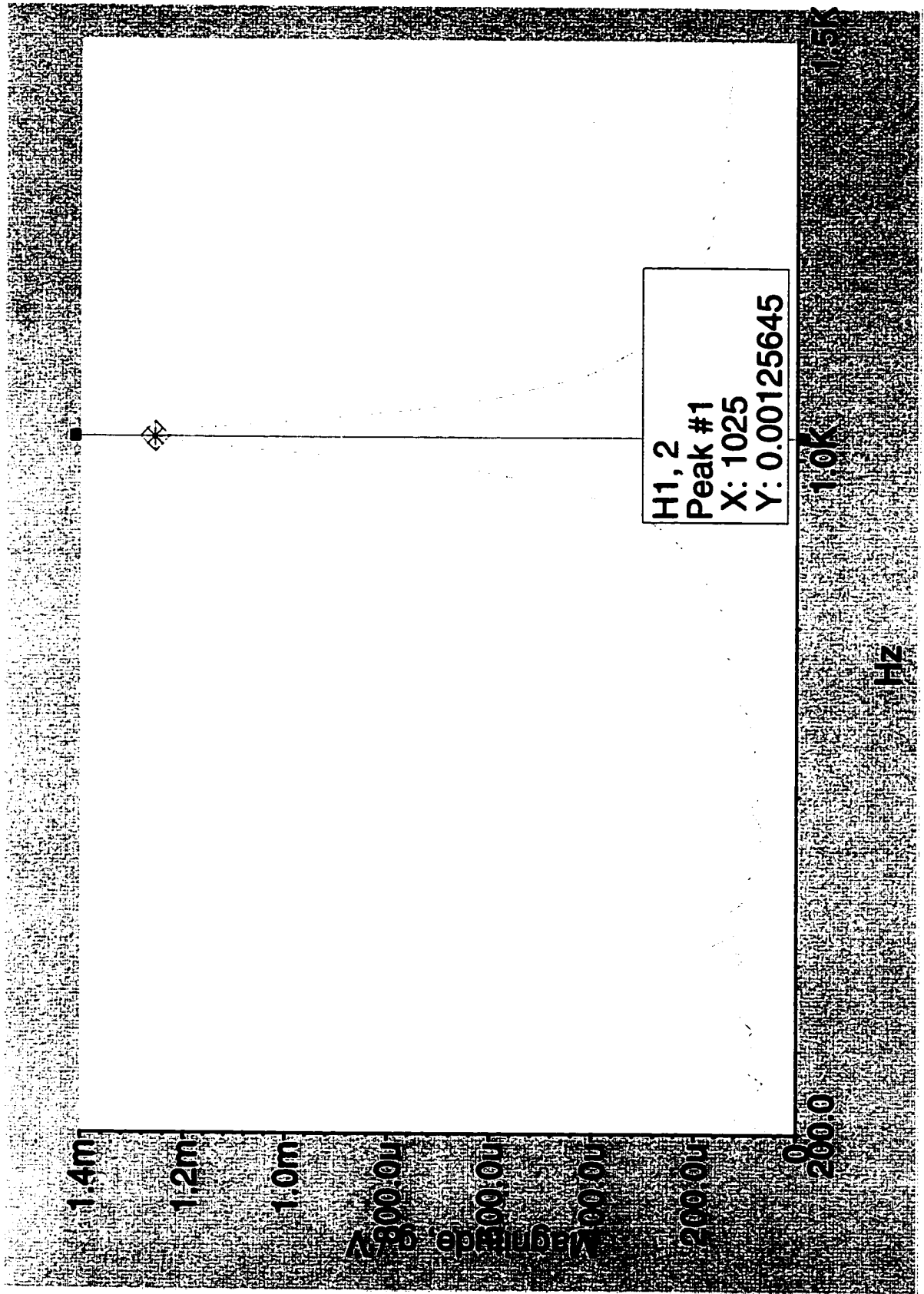


Full Threaded Mount #3 Axial

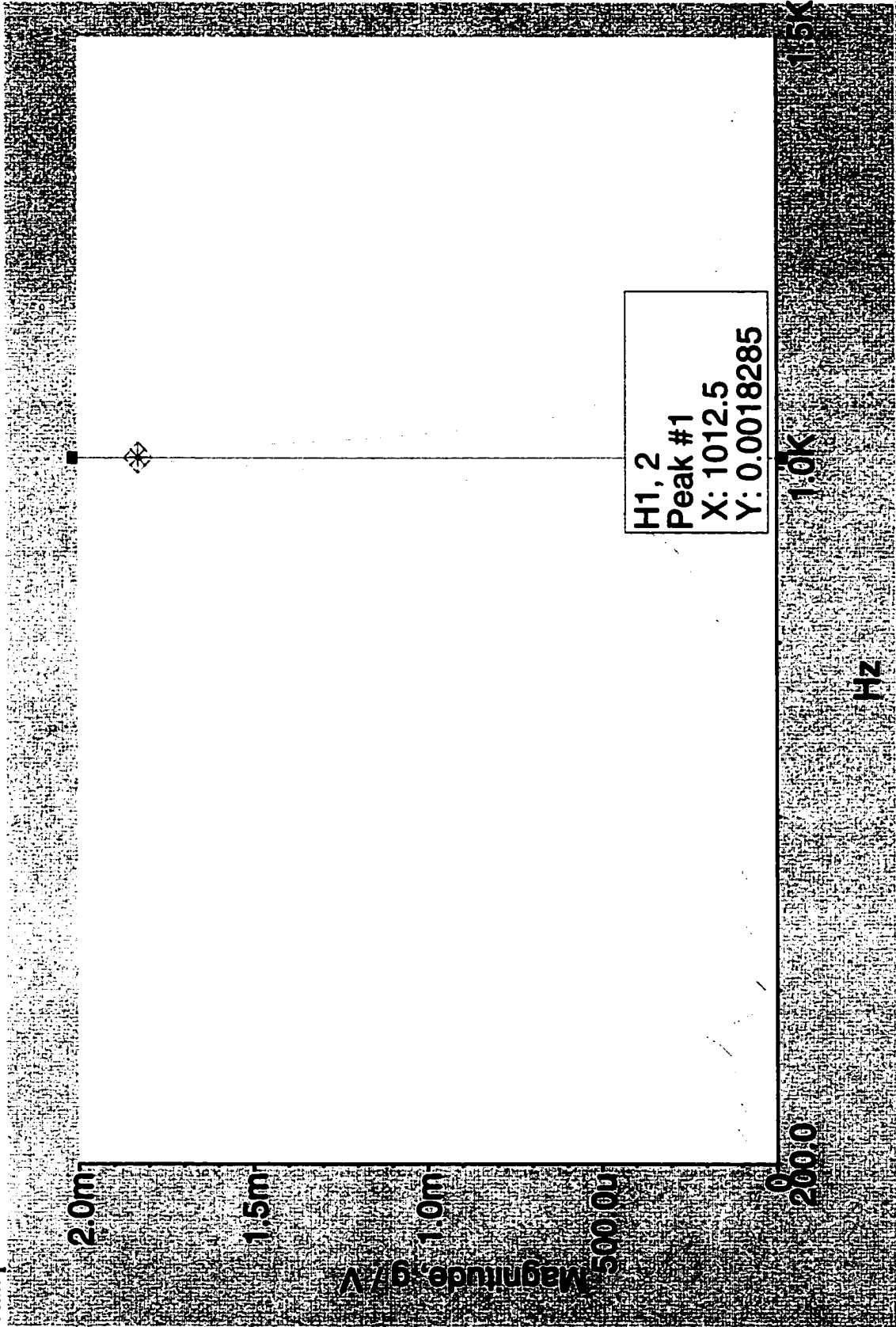


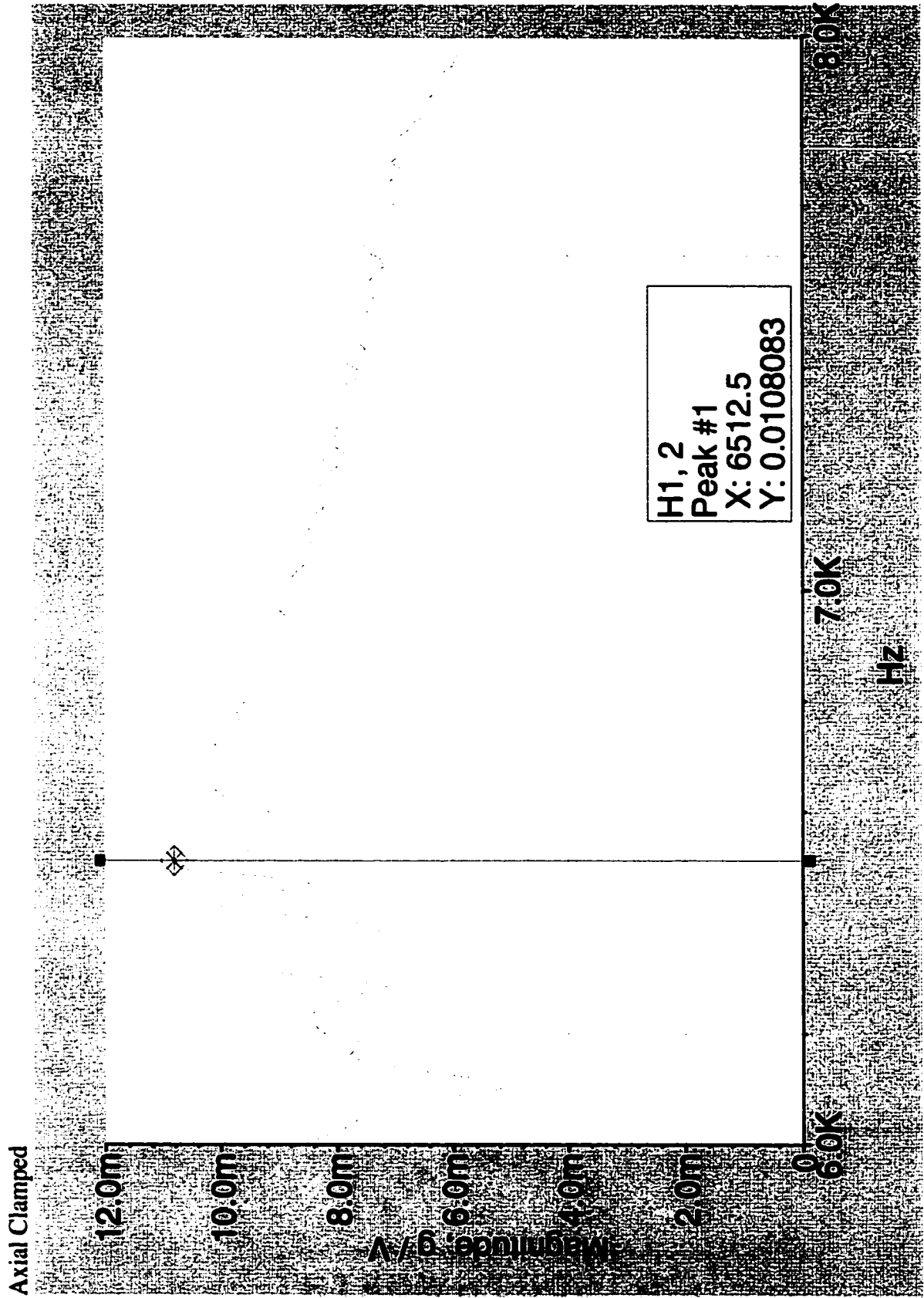




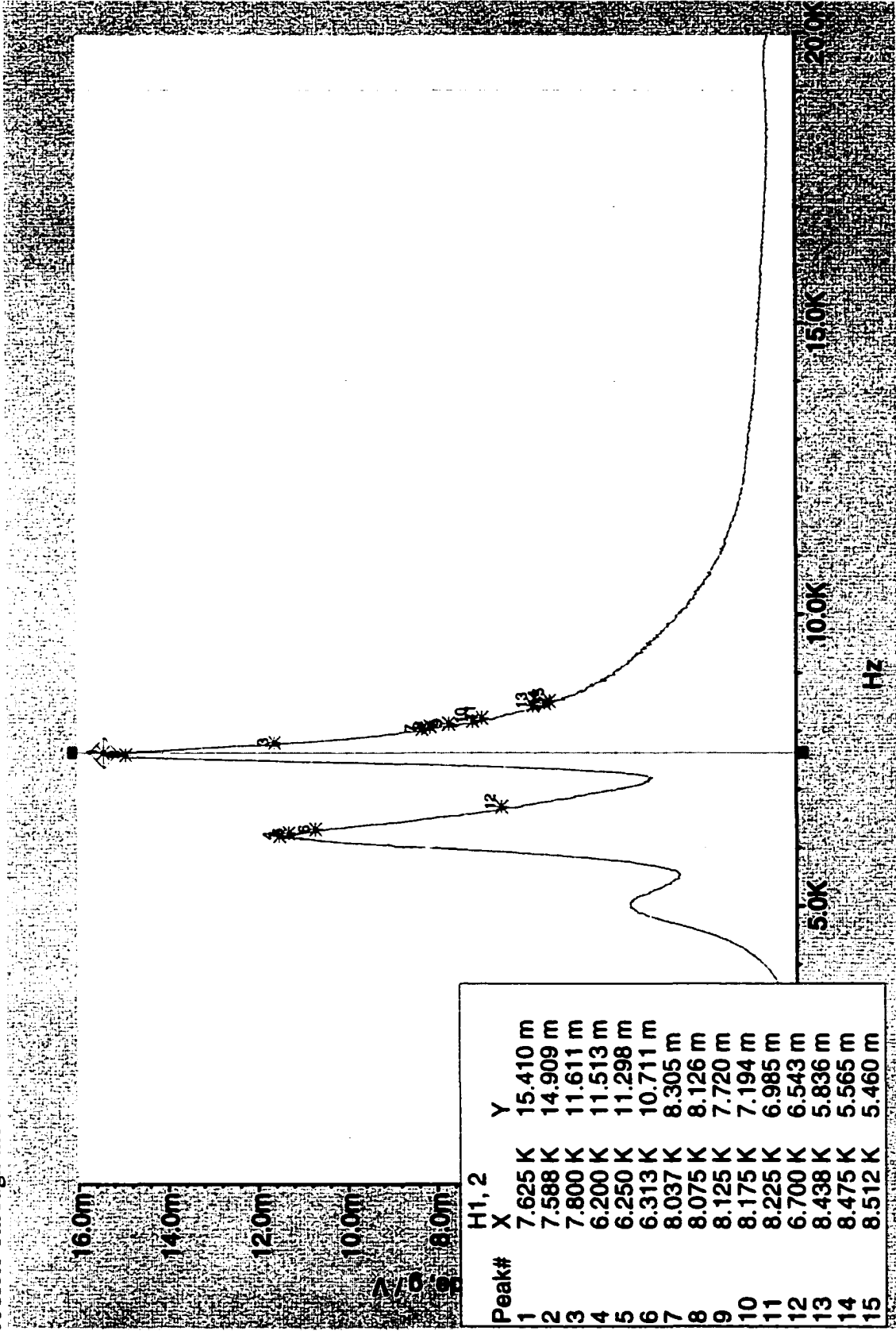


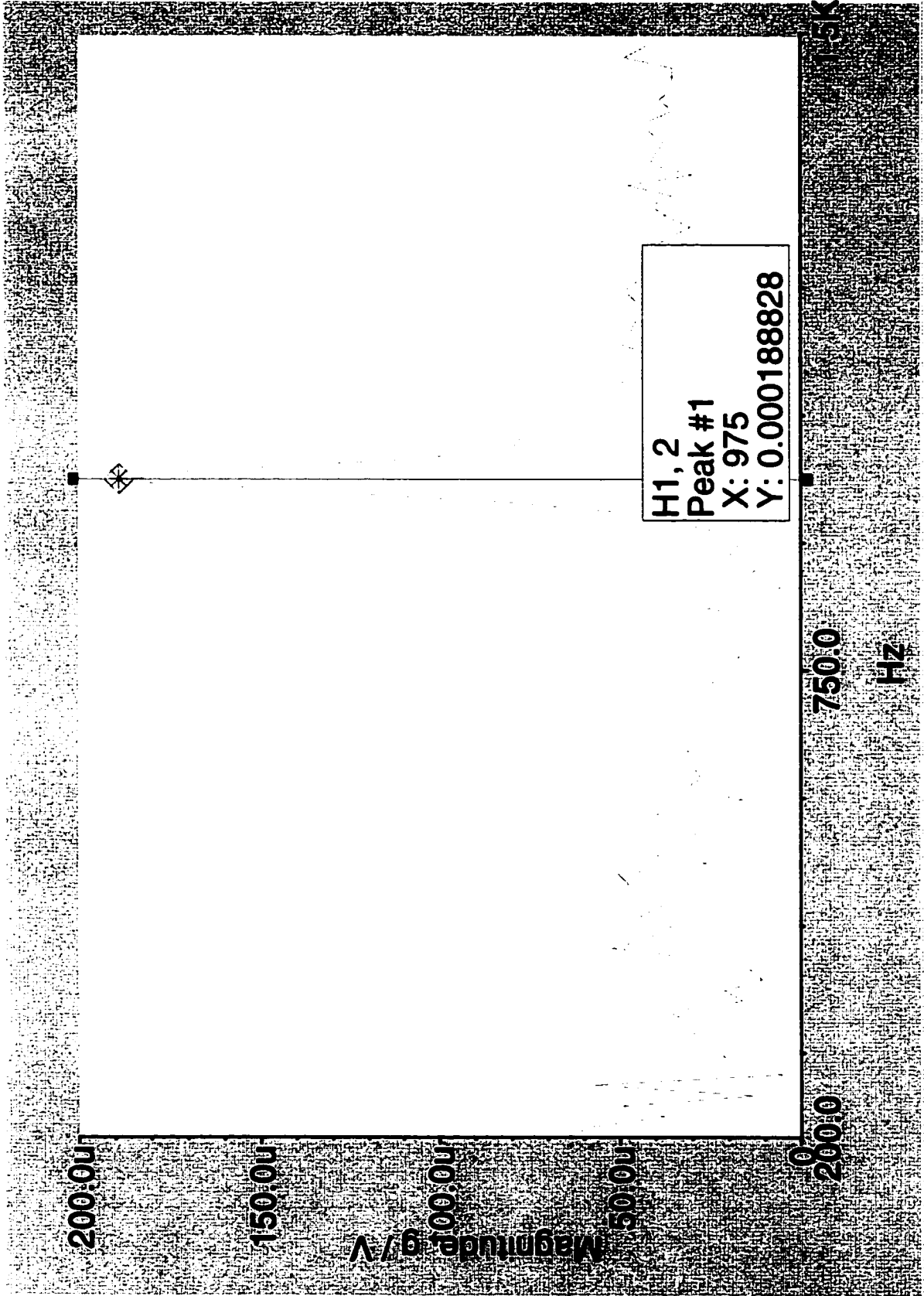
Clamped Torsional Results

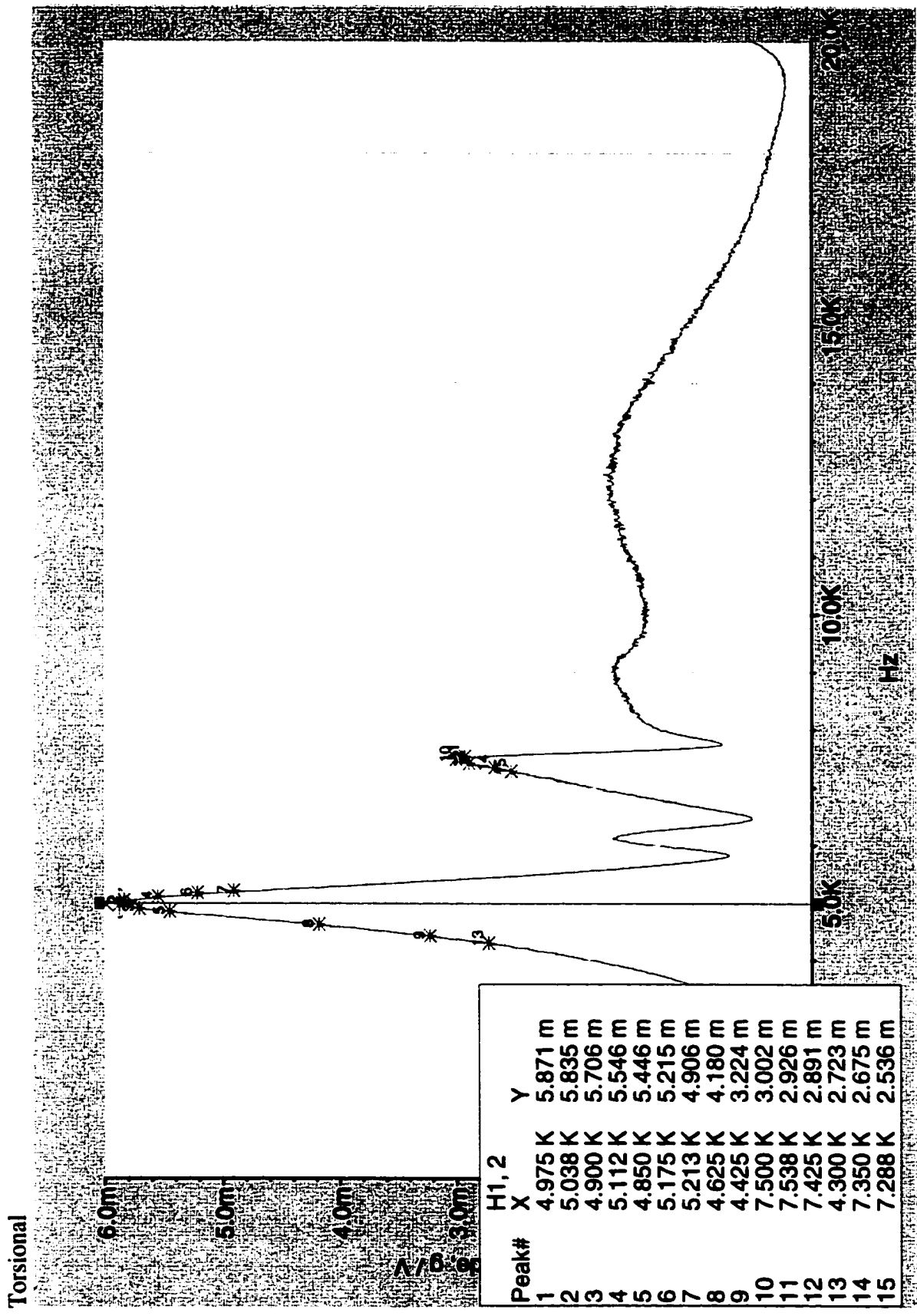


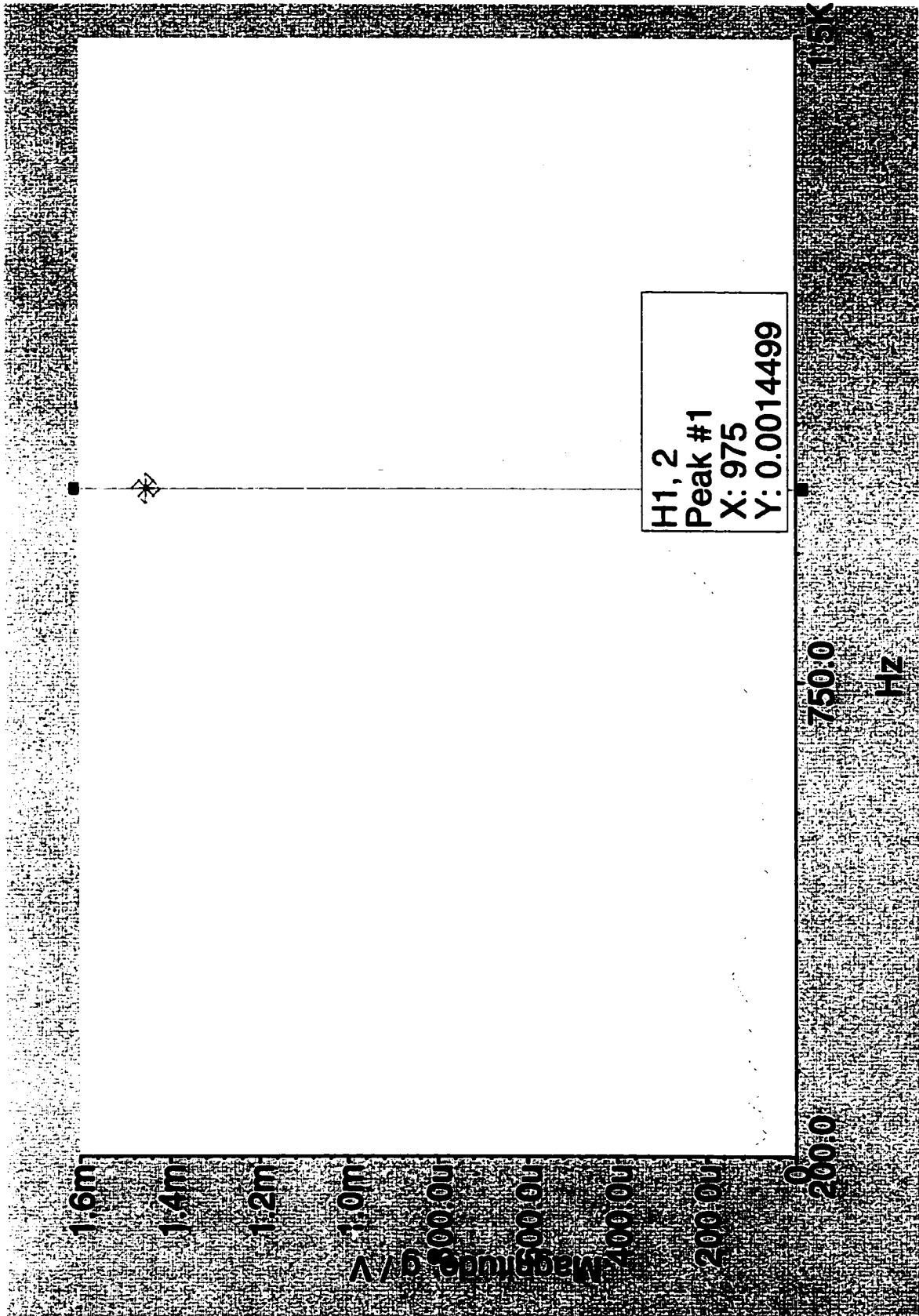


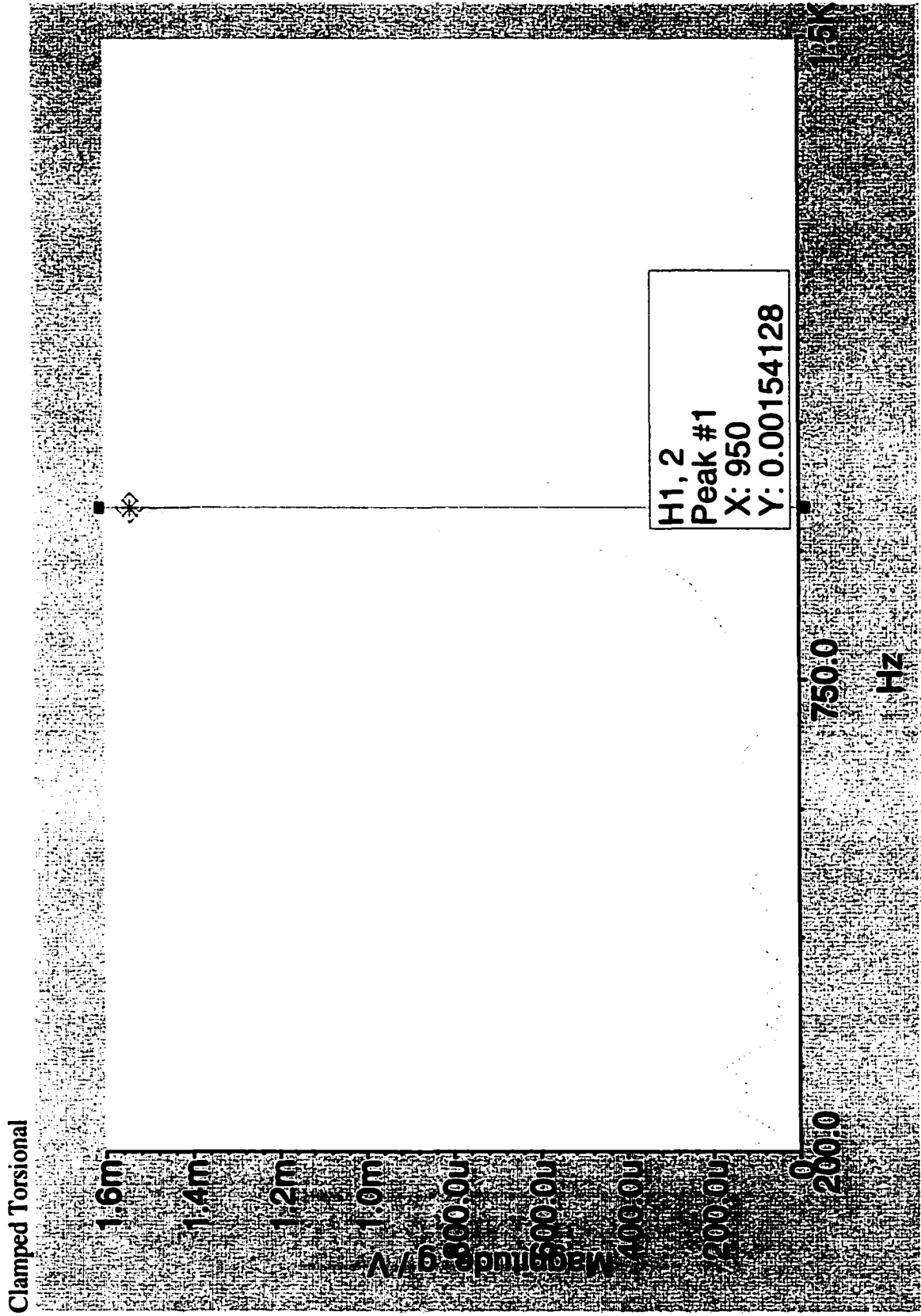
A Hole Through the Mount on both sides. Axial



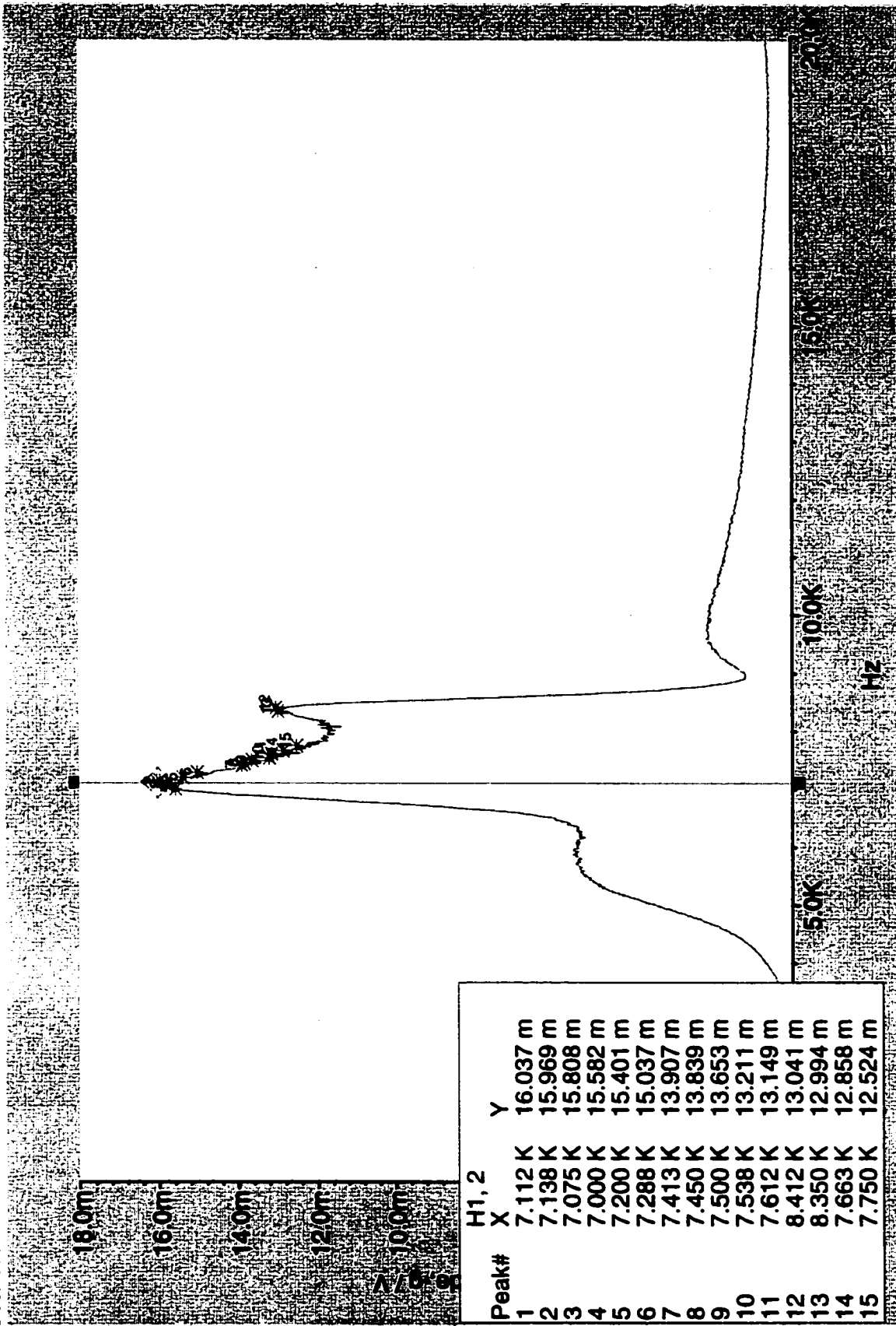


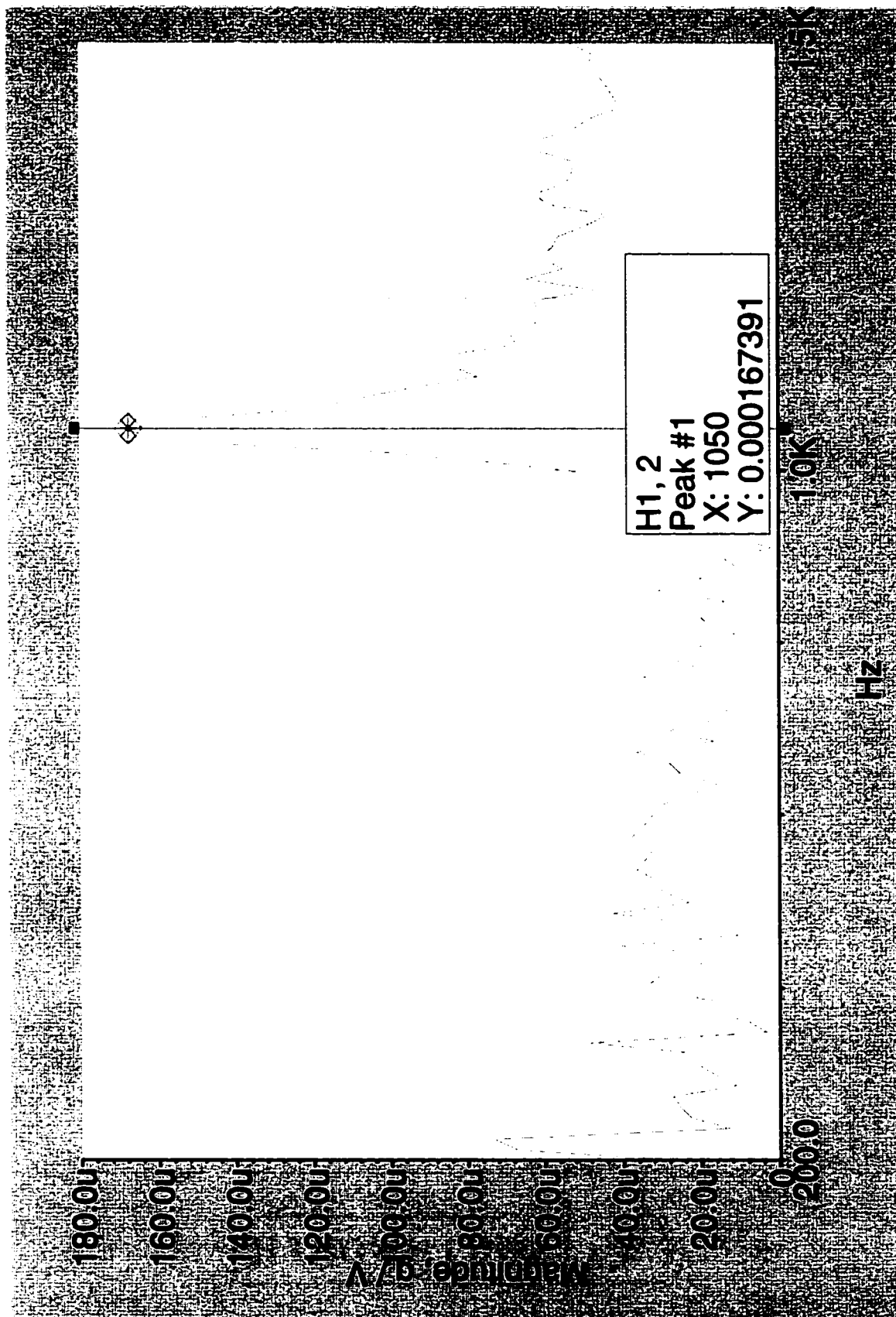


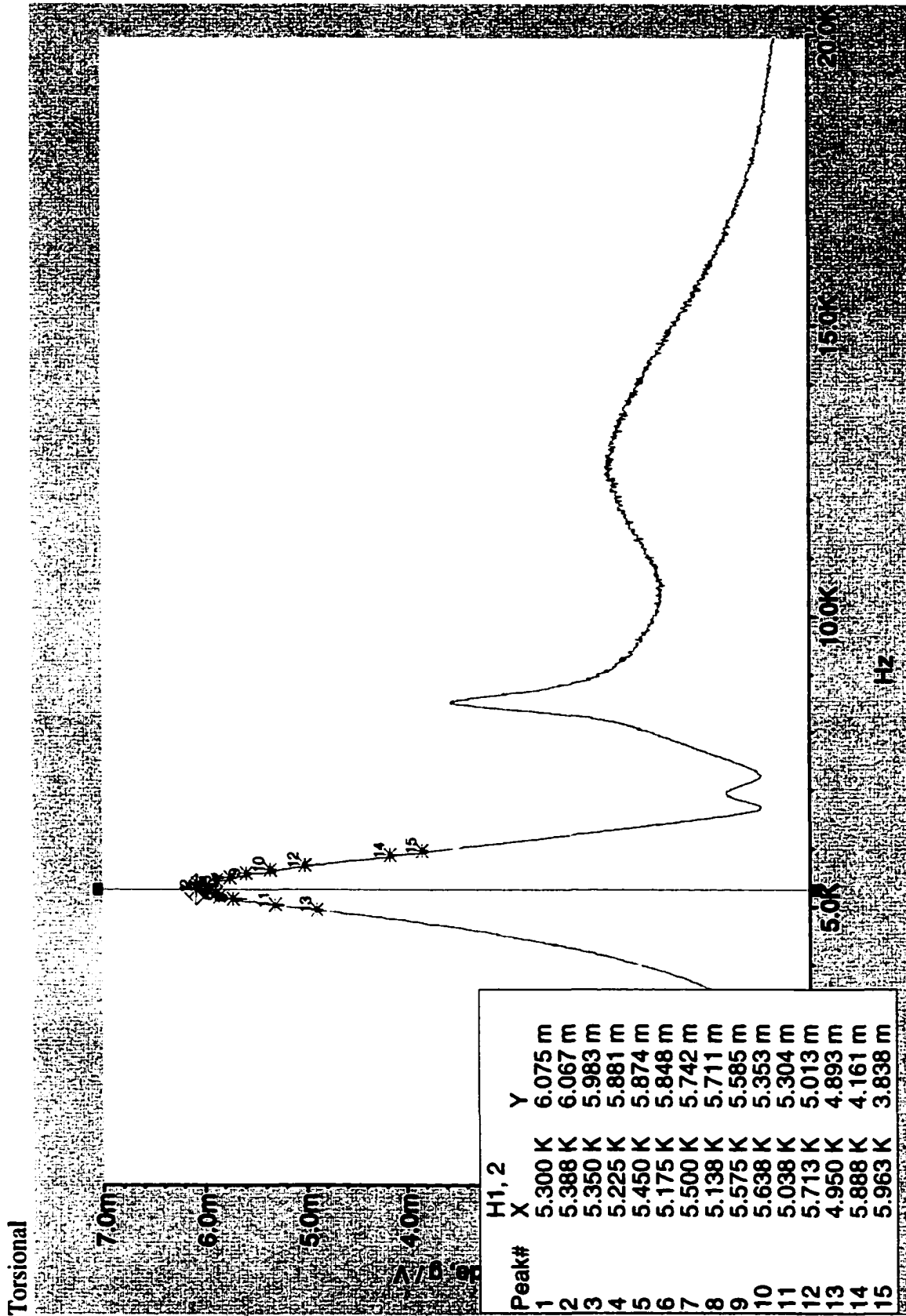


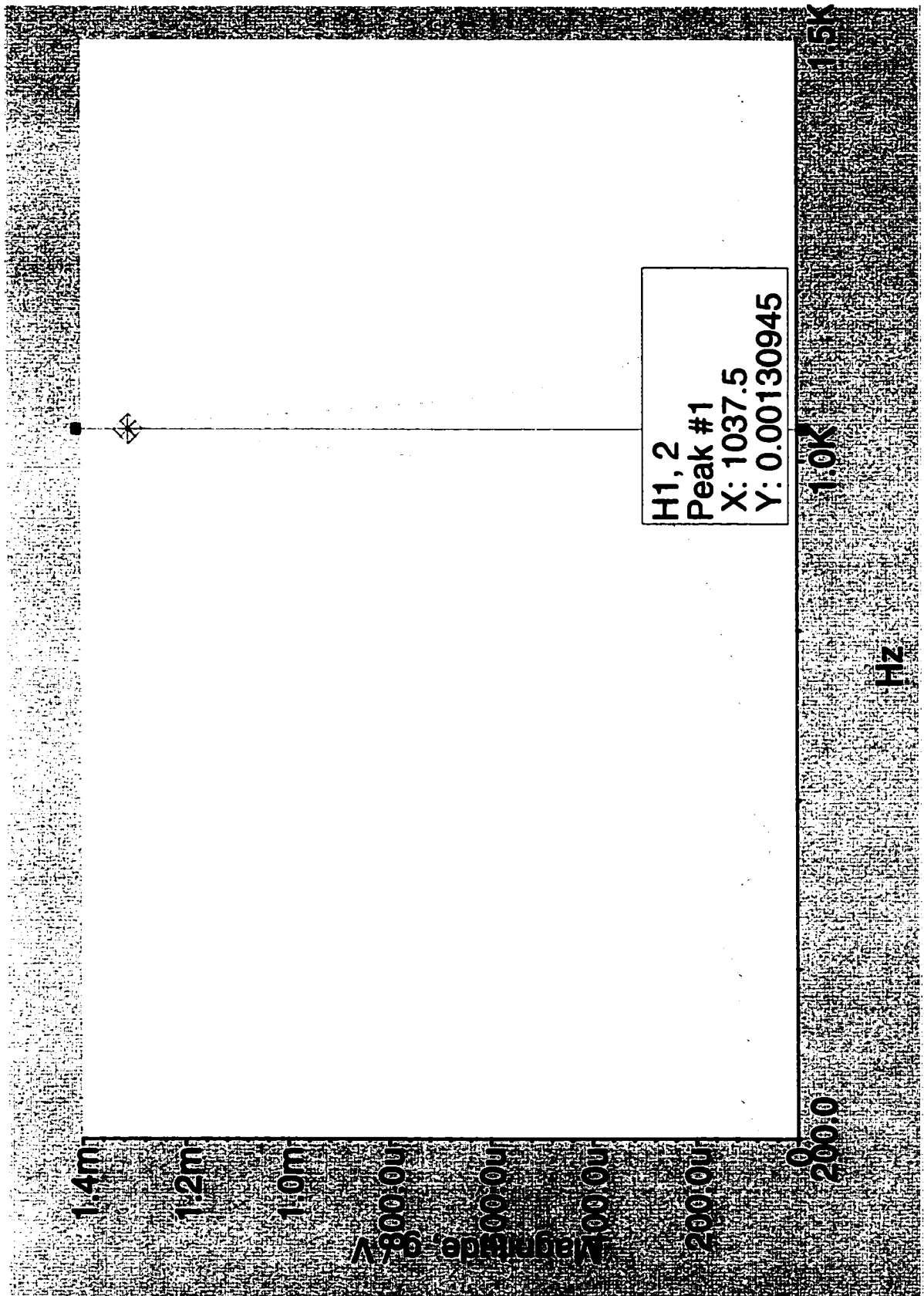


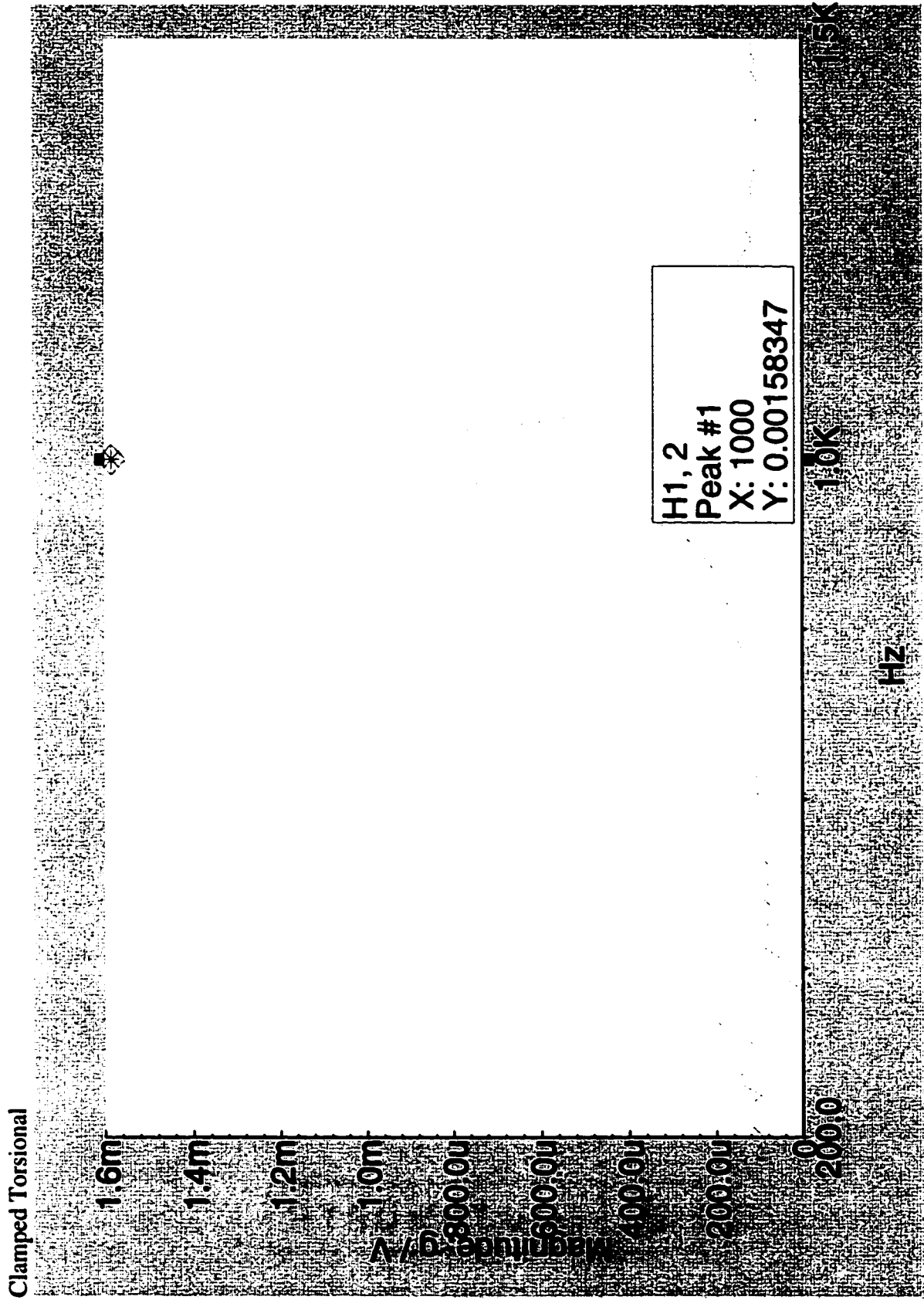
Full Threaded Mount #4 Axial

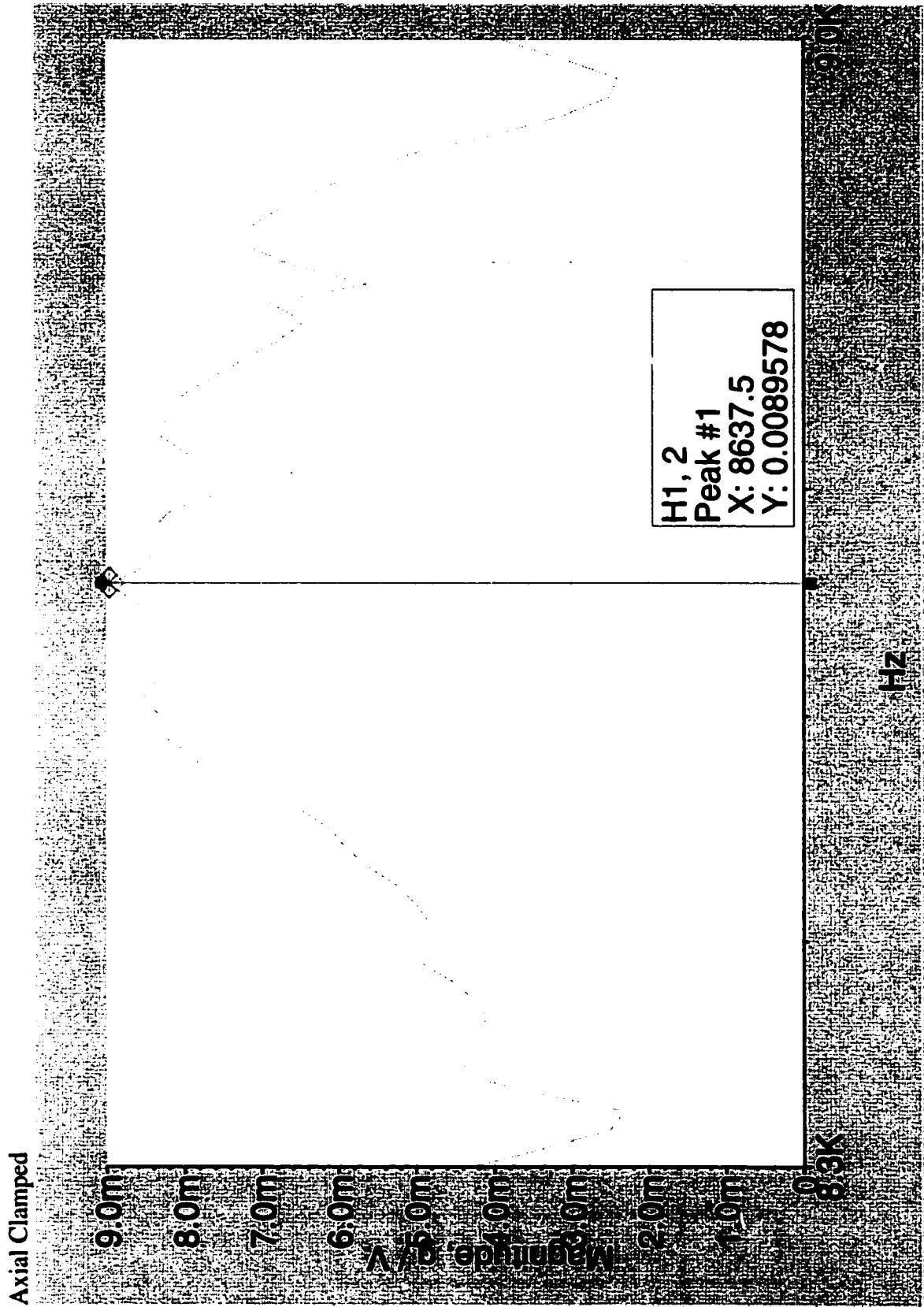




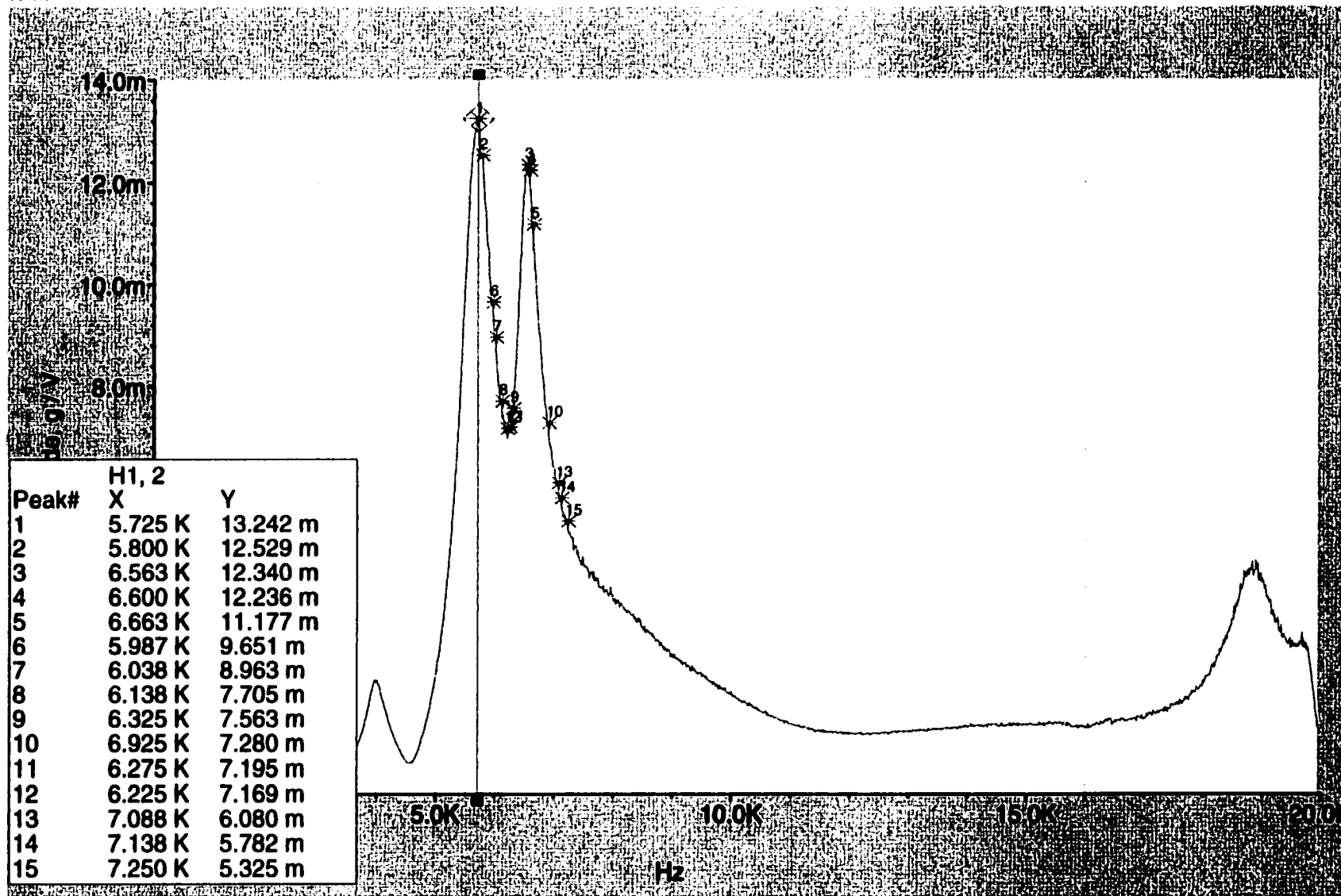


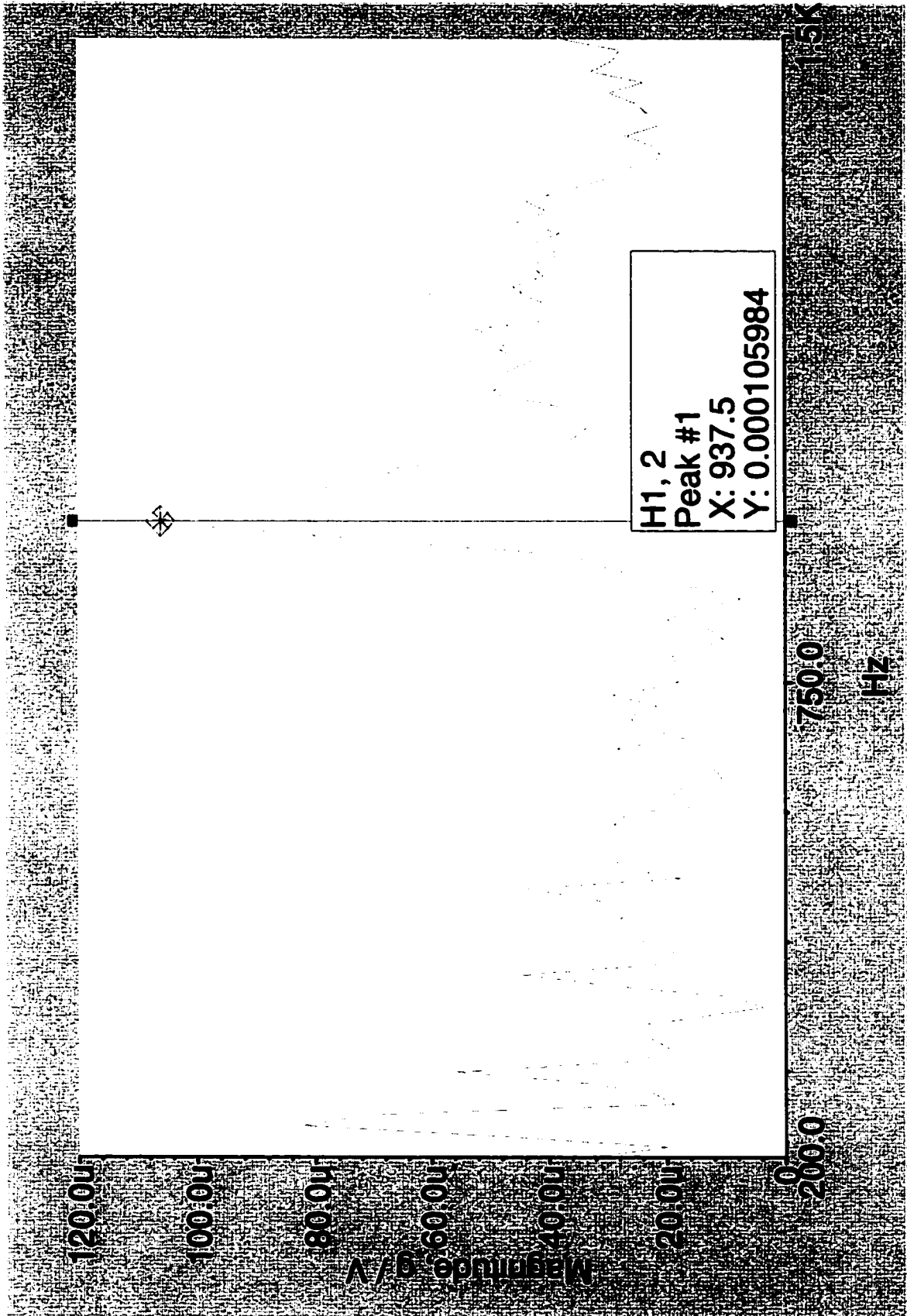




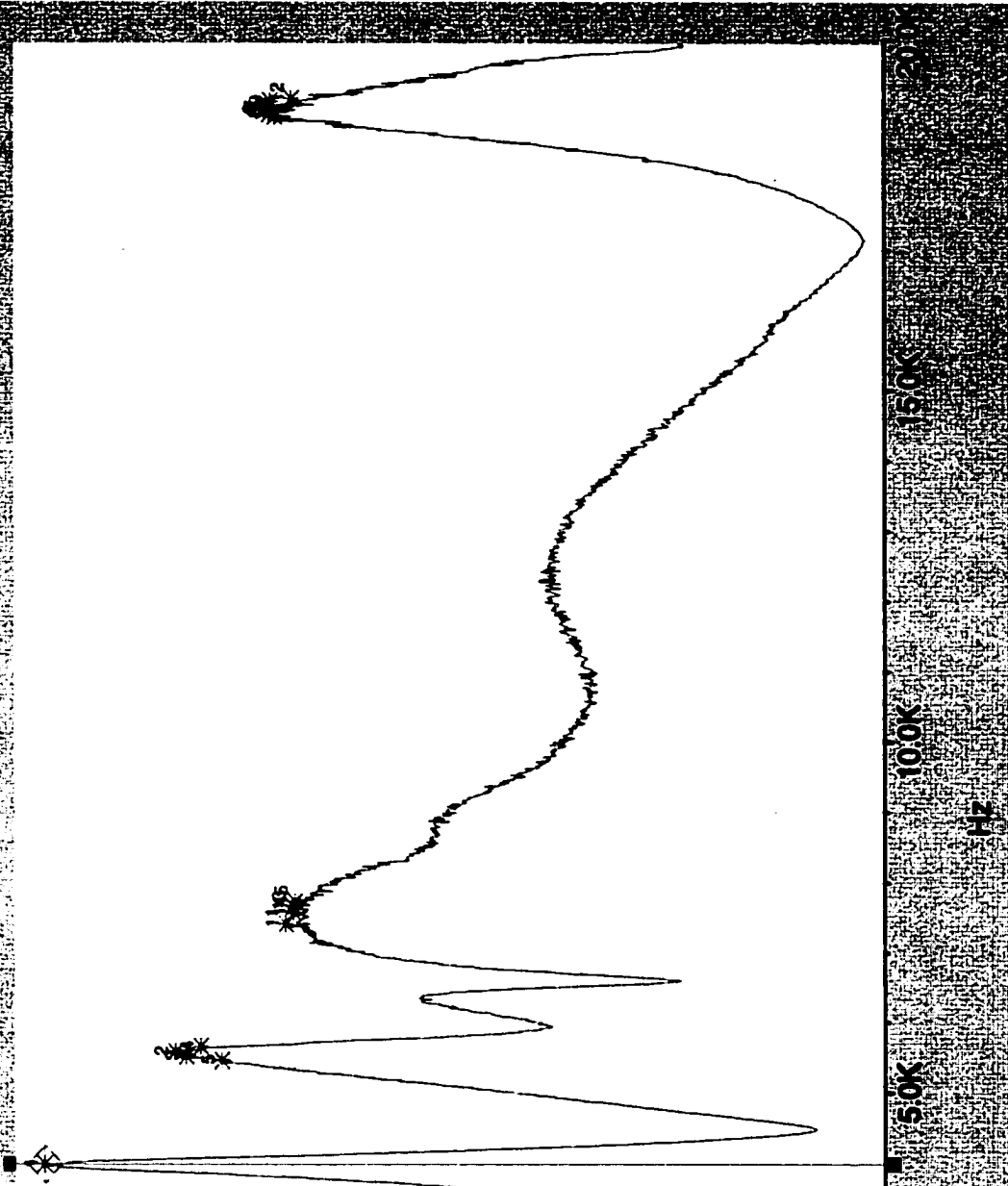


Half Threaded Case See Picture for details. Axial

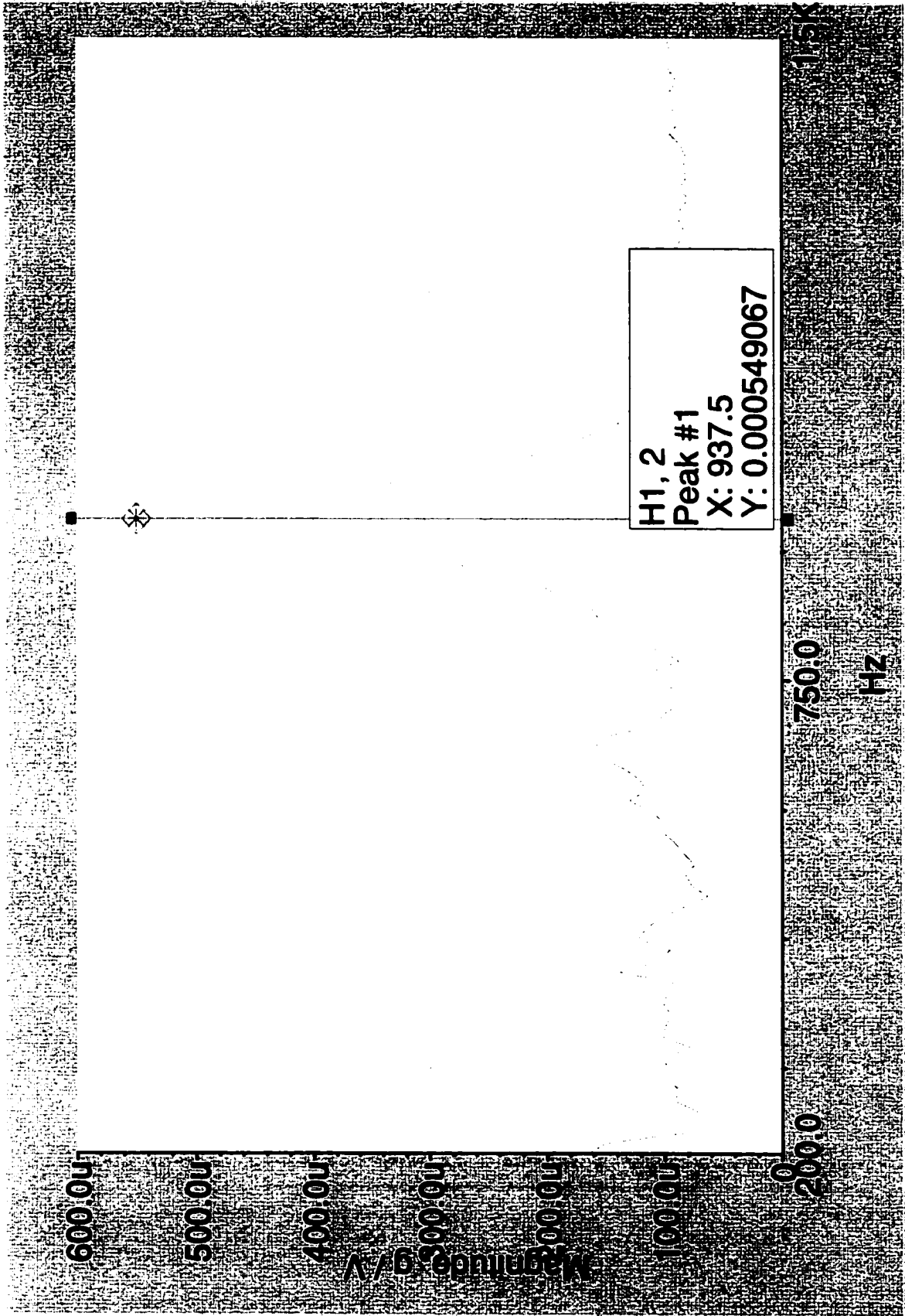


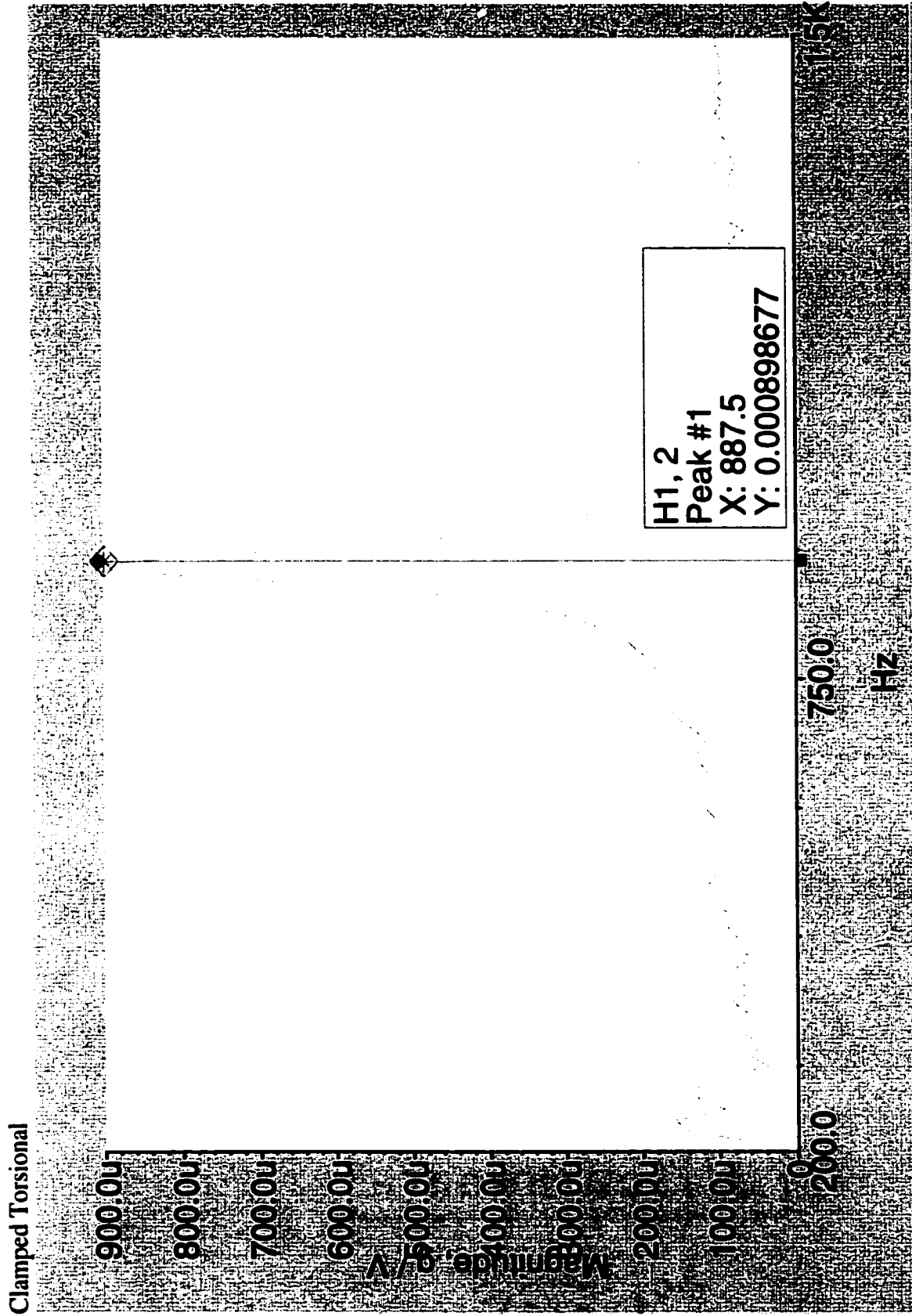


Torsional



Peak#	H1, 2	X	Y
1	3.988 K	3.865 m	
2	5.575 K	3.269 m	
3	5.513 K	3.220 m	
4	5.650 K	3.151 m	
5	5.450 K	3.052 m	
6	18.988 K	2.854 m	
7	19.038 K	2.846 m	
8	18.938 K	2.828 m	
9	19.113 K	2.823 m	
10	18.900 K	2.802 m	
11	7.413 K	2.755 m	
12	19.150 K	2.726 m	
13	7.663 K	2.723 m	
14	7.575 K	2.718 m	
15	7.737 K	2.712 m	





APPENDIX E

MATHCAD SOLUTION FOR THEORETICAL VALUES

Torsional Vibration Theoretical Calculation

Material Properties of the Aluminum

$$G_a := 26 \cdot 10^9 \cdot \text{Pa} \quad \rho_a := 2700 \cdot \frac{\text{kg}}{\text{m}^3}$$

$$L := 0.515 \text{ in}$$

$$L_1 := .2 \cdot \text{in}$$

$$r_o := .096 \cdot \text{in} \text{ The radius of the beam.}$$

$$R_{1o} := .375 \cdot \text{in} \text{ The radius of the disk.}$$

$$J_o := \left[\frac{1}{2} \cdot \pi \cdot (r_o^4) \cdot L \right]$$

$$J_{o1} := \frac{1}{2} \cdot \pi \cdot (R_{1o}^4) \cdot L_1$$

$$J_o = 7.264 \times 10^{-13} \text{ m}^5$$

$$J_{o1} = 6.568 \times 10^{-11} \text{ m}^5$$

$$c_a := \sqrt{\frac{G_a}{\rho_a}} \quad c_a = 3.103 \times 10^3 \frac{\text{m}}{\text{s}}$$

$$\beta := \frac{J_o}{J_{o1}}$$

$$\alpha_2 := 3.1448$$

$$\alpha_1 := .1$$

$$\beta = 0.011$$

$$\text{1 mode} \quad \omega_n := \frac{1}{2 \cdot \pi} \frac{c_a}{L} \cdot \sqrt{\frac{J_o}{J_{o1}}}$$

$$\omega_n = 3.971 \times 10^3 \text{ Hz}$$

$$\text{2 mode} \quad \omega_n := \frac{\alpha_2}{2 \cdot \pi} \frac{c_a}{L}$$

$$\omega_n = 1.187 \times 10^5 \text{ Hz}$$

Transverse Vibration Theoretical Calculation

Material properties of Aluminum

$$G_a := 26 \cdot 10^9 \text{ Pa} \quad \rho_a := 2700 \cdot \frac{\text{kg}}{\text{m}^3} \quad \nu := 0.33$$

$$E_a := 69 \cdot 10^9 \cdot \text{Pa}$$

$$L := .515 \cdot \text{in} \quad r_o := .096 \cdot \text{in} \quad L_1 := .2 \cdot \text{in} \quad R_{1o} := .375 \cdot \text{in}$$

The Area of the Beam

$$A_r := \pi \cdot r_o^2$$

The Area of the Disk

$$A_d := \pi \cdot R_{1o}^2 - (0.179 \cdot \text{in} \cdot 0.125 \text{in}) - (0.174 \cdot \text{in} \cdot 0.125 \cdot \text{in})$$

$$A_{df} := A_d - \left[\frac{1}{2} \cdot (0.021 \cdot \text{in} \cdot 0.125 \cdot \text{in}) \right] - \frac{1}{2} \cdot (0.034 \cdot \text{in} \cdot 0.125 \cdot \text{in})$$

$$I := \frac{1}{4} \cdot \pi \cdot r_o^4$$

$$M := \rho_a \cdot A_{df} \cdot L_1$$

$$M_b := \rho_a \cdot A_r \cdot L$$

$$M = 3.488 \times 10^{-3} \text{ kg}$$

$$M_b = 6.597 \times 10^{-4} \text{ kg}$$

$$\beta := \frac{M}{\rho_a \cdot A_r \cdot L} \quad \beta = 5.288$$

The Longtitude Vibration

$$c := \sqrt{\frac{E_a}{\rho_a}} \quad L_2 := .515 \cdot \text{in}$$

$$\beta_2 := \frac{M_b}{M} \quad \beta_2 = 0.189$$

$$\omega_1 := \frac{1}{2 \cdot \pi} \cdot \frac{c}{L_2} \cdot \sqrt{\beta_2}$$

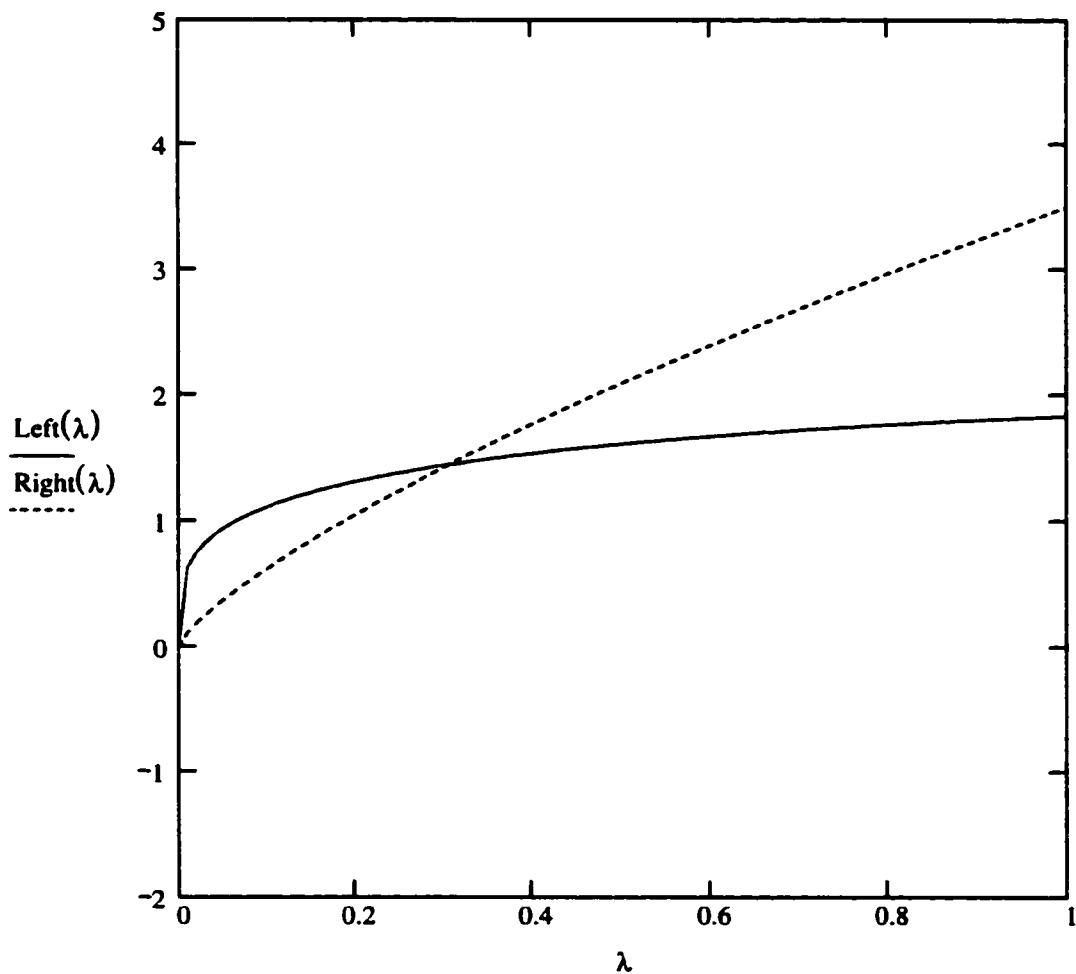
$$\omega_1 = 2.675 \times 10^4 \text{ Hz}$$

Solving for λ for $\beta=5.288$.

$$\lambda := 0, 0.01 .. 1000$$

$$\text{Left}(\lambda) := \sqrt[4]{\lambda} \cdot (\cos(\sqrt[4]{\lambda}) \cdot \cosh(\sqrt[4]{\lambda}) + 1)$$

$$\text{Right}(\lambda) := -\beta \cdot [(\cos(\sqrt[4]{\lambda})) \sinh(\sqrt[4]{\lambda}) - \cosh(\sqrt[4]{\lambda}) \cdot \sin(\sqrt[4]{\lambda})]$$



A graph of the first λ_1 of bending Vibration

**Beams with Concentrated Mass
Bending Vibration**

$$\lambda_1 := 0.306 \quad \lambda_3 := 3099.483 \quad \lambda_5 := 36985.658$$

$$\lambda_2 := 308.74 \quad \lambda_4 := 12989.139$$

$$\omega_1 := \frac{\sqrt{\lambda_1}}{2 \cdot \pi} \cdot \sqrt{\frac{Ea \cdot I}{\rho a \cdot A r \cdot L^4}} \quad \boxed{\omega_1 = 3.171 \times 10^3 \text{ Hz}}$$

$$\omega_2 := \frac{\sqrt{\lambda_2}}{2 \cdot \pi} \cdot \sqrt{\frac{Ea \cdot I}{\rho a \cdot A r \cdot L^4}} \quad \boxed{\omega_2 = 1.007 \times 10^5 \text{ Hz}}$$

$$\omega_3 := \frac{\sqrt{\lambda_3}}{2 \cdot \pi} \cdot \sqrt{\frac{Ea \cdot I}{\rho a \cdot A r \cdot L^4}} \quad \boxed{\omega_3 = 3.192 \times 10^5 \text{ Hz}}$$

$$\omega_4 := \frac{\sqrt{\lambda_4}}{2 \cdot \pi} \cdot \sqrt{\frac{Ea \cdot I}{\rho a \cdot A r \cdot L^4}} \quad \boxed{\omega_4 = 6.534 \times 10^5 \text{ Hz}}$$

$$\omega_5 := \frac{\sqrt{\lambda_5}}{2 \cdot \pi} \cdot \sqrt{\frac{Ea \cdot I}{\rho a \cdot A r \cdot L^4}} \quad \boxed{\omega_5 = 1.102 \times 10^6 \text{ Hz}}$$

WORKS CITED

1. Baz, A., "Optimization of Energy Dissipation Characteristics of Active Constrained Layer Damping," Smart Materials and Structures, Vol. 6, pp. 380-368, 1977.
2. Baz, A., and Ro, J., "Performance Characteristics of Active Constrained Layer Damping," Symposium of Smart Structures and Materials: Passive Damping, pp. 98-114, 1994.
3. Cawley, P., Pavlakovic, B., Alleyne D.N., George, R., Back, T., Meredith, N., "The design of a vibration transducer to monitor the integrity of dental implants." Proc. Instn. Mech. Engrs., Vol. 212, pp. 265-272, 1998.
4. Chantalakhana, C., and Stanway, R., "Active Constrained Layer Damping of Clamped-Clamped Plate Vibrations," Journal of Sound and Vibration, Vol. 241, pp. 755-777, 2001
5. Chen, T., and Baz, A., "Performance Characteristics of Active Constrained Layer Damping Versus Passive Constrained Layer Damping with Active Control," Proceedings of SPIE-The International Society for Optical Engineering Smart Structures and Materials, pp. 256-268, San Diego, CA, 1996.
6. Ewins, D.J., Modal Testing: Theory and Practice 2nd Edition, Research Studies Press, Ltd., England, 2000.
7. Gabbert, Ulrich, Koppe, H., Trajkov, T. N., "Controller Design for Engineering Smart Structures Based on Finite Elements Models." SPIE's 9th Annual International Symposium on Smart Structures and Materials in San Diego, CA, #4693-47, 2002.
8. Heo, S.J., Sennerby, L., Odersjo, M., Granstrom, G, Tjellstrom A, Meredith, N., "Stability measurements of craniofacial implants by means of resonance frequency analysis. A clinical pilot study." J Laryngol Otol, Vol. 112, pp. 537-542, 1998.
9. Huang, S.C., Inman, D.J., and Austin, E.M., "Some Design Considerations for Active and Passive Constrained Layer Damping Treatments," Smart Materials and Structures. Vol. 5, pp.301-313, 1996.
10. Kelly, S. Graham, Fundamentals of Mechanical Vibrations, McGraw-Hill, Boston, 2000.
11. Liu, Y., and Wang, K.W., "Active-Passive Hybrid Constrained Layer for Structural Damping Augmentation," Journal of Vibration and Acoustics, Vol. 122, pp. 254-262, 2000.
12. Lumsdaine, Arnold, "Modeling of Active constrained Layer Damping Structures Using a Commercial Finite Element Code," Proceedings of the ASME International Mechanical Engineering Congress and Exposition, 2001 ASME International Mechanical Engineering Congress and Exposition, New York, NY 001.
13. Meredith, N., "The Application of Modal Vibration Analysis to Study Bone Healing in Vivo." Journal of Dental Research, Vol. 793, pp.73-74, 1994.
14. Meredith, N., Alleyne D, Cawley P., "Quantitative determination of the Stability of the Implant-Tissue interface using resonance Frequency Analysis." Clinical Oral Implants Research, Vol. 7, pp. 261-267 1996.

15. Meredith, N., Rasmussen, I., Sennerby L., Alleyne D., "Mapping implant stability by resonance Frequency analysis." Med Sci. Res., Vol. 24, pp. 191-193 1996.
16. Meredith, N., Shagaldi F., Alleyne D., Sennerby L., Cawley, P., "The Application of Resonance Frequency Measurement to Study the Stability of Titanium Implants During Healing in the Rabbit Tibia." Clinical Oral Implants Research, Vol. 8, pp. 234-243 1997.
17. Meredith, N., Book K., Friberg B., Jemt T., Sennerby L. "Resonance Frequency Measurements of Implant Stability in Vivo." Clinical Oral Implants Research, Vol. 8, pp. 226-233, 1997.
18. Meredith, N., "On the Clinical Measurement of Implant Stability and osseointegration." PhD-Thesis at the University of Gothenburg, 1997.
19. Meredith, N., "A review of nondestructive test methods and their application to measure the stability and osseointegration of bone anchored endosseous implants." Crit. Rev. Biomed. Eng., vol.24-26, pp. 275-291,1998.
20. Meredith N., "Assessment of implants stability as a prognostic determinant." Int. Journal Prosthodont, Vol. 11, pp. 491-501,1998.
21. Rasmussen, L., Meredith N., Sennerby L., "Measurements of stability changes of titanium implants with exposed threads subjected to barrier membrane induced bone augmentation." Clinical Oral Implants Research, Vol. 8, pp. 316-322, 1997.
22. Ray, M.C., and Baz, A., "Optimization of Energy Dissipation of Active Constrained Layer Damping Treatments of Plates," Journal of Sound and Vibration, Vol. 208, pp. 391-406,1997.
23. Sennerby, L., Meredith, N., "Resonance Frequency analysis: measuring implant stability and osseointegration." Compend Contin Educ. Dent., Vol. 19, pp. 493-498, 1998.
24. Tomlinson, G., "Overview of Active/Passive Damping Techniques Employing Viscoelastic Materials," Proceedings of SPIE-International Society for Optical Engineering 3rd International Conference on intelligent Materials, pp. 656-669, Lyon, France, 1996.
25. Varadan, V.V., Lim, Y., Varadan, V.K., "Closed Loop Finite Element Modeling of Active/Passive Damping in Structural Vibration Control," Smart Materials and Structures, Vol. 5, pp. 685-694, 1996.
26. Velez, D.E., Rao, S.S., "Comparison of Active, Passive, and Hybrid Damping in Structural Design," Smart Materials and Structures, Vol. 5, pp. 660-671, 1996.

VITA

Daniel Delgado Jr. was born on May 14, 1974 in Harlingen, Texas. He lived in the Rio Grande Valley all his life. He attended the University of Texas Pan American at Edinburg, where he received a Bachelor of Science degree in Mechanical Engineering in August 1999. After receiving his degree, he worked for Datacom Custom Manufacturing Inc. from May 1999 to May 2001. He return to University of Texas Pan American to join the Mechanical Engineering graduate program in August 2000, he started working on a research project with Dr. Arnold Lumsdaine and Dr. Bob Jones. This research will lead to the thesis presented.